Experimental thermal performance study on heat storage unit using beeswax and graphite

Ph.D Thesis

Abhay Dinker
(2013RCH9067)

DEPARTMENT OF CHEMICAL ENGINEERING
MALAVIYA NATIONAL INSTITUTE OF TECHNOLOGY JAIPUR
August, 2017

Experimental thermal performance study on heat storage unit using beeswax and graphite

This thesis is submitted as a partial fulfillment of the Ph.D. programme in Chemical Engineering

Abhay Dinker
(2013RCH9067)

DEPARTMENT OF CHEMICAL ENGINEERING
MALAVIYA NATIONAL INSTITUTE OF TECHNOLOGY JAIPUR
August, 2017

MALAVIYA NATIONAL INSTITUTE OF TECHNOLOGY
JAIPUR

DEPARTMENT OF CHEMICAL ENGINEERING

DECLARATION

I hereby declare that the work presented in this thesis entitled "**Experimental thermal performance study on heat storage unit using beeswax and graphite**" in partial fulfillment of the requirement for the award of degree of Ph.D. in Chemical Engineering submitted to the Department of Chemical Engineering, Malaviya National Institute of Technology Jaipur is an authentic record of my own work carried out from July, 2013 to April, 2017 under the supervision and guidance of Dr. Madhu Agarwal, Assistant Professor, Department of Chemical Engineering, MNIT Jaipur and Dr. Ghanshyam Das Agarwal, Associate Professor, Department of Mechanical Engineering, MNIT Jaipur. Information used from literature and other sources in the present thesis has been duly acknowledged by citing references at appropriate places. In case any type of pilagiarism found, I will be solely and completely responsible for it. I have checked plagiarism through software "turnitin". The report showed 96% original and 4% plagrism has been completed by Mr. Abhay Dinker (Student ID: 2013RCH9067) under our supervision.

Date: **(Abhay Dinker)**
2013RCH9067

Ph.D Viva voce Examination of Mr. Abhay Dinker (ID No. 2013RCH9067) was held on 22nd August 2017. Thesis was examined and approved for the award of Ph.D degree.

(Mithilesh Kumar Jha)	**(Madhu Agarwal)**	**(Dr. Ghanshyam Das Agarwal)**
External Examiner	Supervisor	Co-Supervisor
Professor	Assistant Professor	Associate Professor
Deptt. of Chemical Engg.	Deptt. of Chemical Engg.	Deptt. of Mechanical Engg.

Date :

ACKNOWLEDGEMENT

Mere words shall not be sufficient to express my sincere gratitude and thankfulness for my respected supervisors **Dr. Madhu Agarwal** and **Dr. Ghanshyam Das Agarwal** for their consistent guidance, motivation and valuable advice at every stage of this research work. I feel in debt to them for not only teaching me each and every aspect of the art of doing research, but also other aspects of life. Their kind support and patience have given me courage and their friendliness has given me hope during the difficult time of my research work.

I am happy to express my thanks to doctoral guidance committee members, Prof. S.P. Chaurasia, Dr. Kailash Singh and Dr. Prabhat Pandit for their valuable suggestions.

I am thankful to Dr. Manisha Sharma for providing her valuable suggestion whenever needed during my Ph.D thesis.

I wish to express my deepest gratitude to my father Mr. Ramavtar Dinker and my mother Mrs. Madhu Dinker for their blessings, affection and all their prayers, without which I would not be able to endure hard time and carry on.

My words fail to express my gratitude and appreciation to my wife Mrs. Nisha Sharma for all that she silently endured during the difficult times and way she always supported me and stood by my side. I also wish to thank my daughter Ani Sharma for her love, affection and unending patience during the duration of this work.

I am thankful to Jharna Gupta, Swati Dubey, Shruti Chakraborty and all the Ph.D students of chemical engineering department for their support and joy spent during the Ph.D tenure.

I would like to thank Mr. Ramesh Sharma, our lab technician whose technical knowledge and fabrication skills resulted in the development of experimental set-up and all the faculty members, office staff of chemical engineering department for their support and encouragement during my Ph.D tenure in MNIT.

Abhay Dinker

ABSTRACT

Energy crisis has been the most important global agenda in the last few decades due to the depletion of conventional sources of energy, increasing environmental pollution and rise in population. To reduce the wastage of energy and to balance the energy demand and supply, various researches have been performed on the storage of energy from the renewable energy sources and waste heat from flue gases and other industrial processes. Different researchers have worked on the identification, development and application of various types of heat storage materials and heat storage units to store the energy trapped by solar water heater, solar air heater etc. However, these studies show that most of the energy storage materials are synthetic, costlier and have poor thermal properties which restrict their use for wide range of applications. Looking to the limitations of energy storage materials and systems researchers are trying to identify new, natural and green energy storage materials.

In the present study pure beeswax and its composite with expanded graphite (EG) (2-10 wt. %) has been tried as new phase change materials (PCMs) along with natural graphite as sensible heat storage material. Two thermal storage units, one small scale of capacity 2.5 kg and second large size of capacity 18-22 kg were developed and used in the study to evaluate heat storage potential of beeswax and its composite with expanded graphite. The performance in terms of efficiency has also been evaluated for both the developed units.

Physical, chemical and thermal characterization of beeswax and synthesized composite were performed using X-ray diffraction (XRD), scanning electron microscope (SEM), fourier transform infrared (FTIR), differential scanning calorimetry (DSC) and thermogravimetric analysis (TGA). Initially plain water has been used as Heat Transfer Fluid (HTF) at four different flow rates (0.25 LPM, 0.5 LPM, LPM and 1.0 LPM) and four fluid inlet temperatures (60 ºC, 70 ºC, 80 ºC, 90 ℃) to study the time required for charging the unit (charging time) with beeswax, its composite and natural graphite. Apart from the plain water other three heat transfer fluids such as expanded graphite/water suspension (0.05 wt. %-1.0 wt. %), Al_2O_3/water suspension (0.2 vol. %-2.0 vol. %) and exhaust gases have also been used to study the charging behavior of beeswax and its composite in large thermal storage unit.

Increase in flow rate of hot water from 0.25 LPM to 1.0 LPM reduced the charging time of beeswax and its composite by 16.39% and 13.92% respectively at 80 °C inlet fluid temperature. Also, the charging time for beeswax and its composite reduced by 10.25% and 12.94% respectively with increase in inlet fluid temperature from 60 °C to 90 °C at fixed flow rate of 0.5 LPM. Suitable results in terms of efficiency were obtained in the study at 0.5 LPM and 80°C inlet fluid temperature.

Increased concentration of EG/water suspension (0.05 wt. % -1.0 wt. %) and alumina nanofluid (0.2 vol. %-2.0 vol. %) resulted in reduction of charging time by 2.72-15.42% and 3.6% to 10.0% respectively for beeswax and 5.33% to 14.66% and 2.66 % to 13.33% respectively for composite material at 0.5 LPM and 80 °C inlet fluid temperature.

Increased fluid flow rates and inlet fluid temperatures also reduced the charging time of graphite bed (sensible heat storage) by 38.46% and 17.94% respectively and increase in concentration of nano-fluids and expanded graphite/water suspension has reduced the charging time of graphite by 7.14-14.28% and 14.28-23.82% respectively.

Modelling and simulation of PCMs and natural graphite in both thermal storage units was carried out using COMSOL Multiphysics software to study the movement of solid-liquid interface of the PCM during melting and to determine the melting time and charging time of PCM and natural graphite. Simulation results found to be in good agreement with the experimental results.

The results of this study show that beeswax, a natural PCM and its composite with expanded graphite with improved thermal properties can be used as potential thermal storage materials for low temperature applications.

TABLE OF CONTENTS

LIST OF FIGURES

LIST OF TABLES

NOMENCLATURE

Dimensional variables

d_i	inner diameter of tube (m)	L	length of tube (m)
d_o	outer diameter of tube (m)	b	pitch length (m)
C_{ps}	heat capacity of solid (J kg^{-1} K^{-1})	A_s	total surface area of tube (m^2)
C_{pl}	heat capacity of liquid (J kg^{-1} K^{-1})	A_o	outer surface area of the coil (m^2)
$C_{p_{eff}}$	effective heat capacity of HTF (J kg^{-1} K^{-1})	A_i	Inner surface area of the coil (m^2)
C_p	heat capacity of solute (J kg^{-1} K^{-1})	L	latent heat of fusion (kJ kg^{-1})
C_{p_f}	heat capacity of base fluid (J kg^{-1} K^{-1})	U_o	overall heat transfer coefficient (W m^{-2} K^{-1})
T_w	wall temperature (K)	h_i	internal heat transfer coefficient (W m^{-2} K^{-1})
T_b	bulk temperature (K)	h_o	external heat transfer coefficient (W m^{-2} K^{-1})
T_{out}	fluid outlet temperature (K)	k	thermal conductivity (W m^{-1} K^{-1})
T_{in}	fluid inlet temperature (K)	K_{eff}	effective thermal conductivity of HTF (W m^{-1} K^{-1})
T_m	melting temperature (K)	k_p	thermal conductivity of solute (W m^{-1} K^{-1})
T_i	initial temperature of PCM (K)	K_f	thermal conductivity of base fluid (W m^{-1} K^{-1})
T_f	final temperature of PCM (K)	D_c	diameter of curvature (m)
ΔT_m	least mean temperature difference (K)		**Greek Symbols**
$\dot{m}$	mass flow rate of HTF (kg s^{-1})	ρ	density of water (kg m^{-3})
m_w	mass of PCM (kg)	ρ_{eff}	Effective density of HTF (kg m^{-3})
v	velocity (m s^{-1})	ρ_f	density of base fluid (kg m^{-3})
$\dot{Q}$	instantaneous energy(kJ)	ρ_p	density of solute (kg m^{-3})
Q_a	available energy (kJ)	μ_{eff}	effective viscosity (N s m^{-2})
Q_w	energy required by wax (kJ)	ψ	Sphericity of particle
g	acceleration due to gravity (m s^{-2})	ø	volume fraction of solute

μ_f	effective viscosity of base fluid (N s m^{-2})	β	thermal expansion coefficient (K^{-1})
γ	dimensionless pitch		
φ	Liquid fraction of phase change material		

Dimensionless numbers

Nu_i	inside Nusselt number
Nu_o	outside Nusselt number
R_e	Reynolds number
D_e	Dean number
Pr	Prandlt number
Ra	Rayleigh number
Gr	Grashof number
N	total number of turns

Abbreviations

PCM	phase change material
HTF	heat transfer fluid
LPM	liter per minute
TSU	thermal storage unit
NG	natural graphite
EG	expanded graphite

LIST OF PUBLICATIONS

Journal publications:

1. A. Dinker, M. Agarwal, G.D. Agarwal, Experimental assessment on thermal storage performance of beeswax in a helical tube embedded storage unit, *Applied Thermal Engineering*, 111 (2017) 358-368.
2. A. Dinker, M. Agarwal, G.D. Agarwal, Preparation, characterization and performance study of beeswax/expanded graphite composite as thermal storage material, *Experimental Heat Transfer*, (2016).
3. A. Dinker, M. Agarwal, G.D. Agarwal, Heat storage materials, geometry and applications: A review, *Journal of the Energy Institute*, (2015).
4. A. Dinker, M. Agarwal, G.D. Agarwal, Thermal conductivity enhancement of stearic acid using expanded graphite for low temperature thermal storage, *International journal of engineering science and Innovative Technology*, 3 (2014), 531-536.
5. A. Dinker, M. Agarwal, and G.D. Agarwal, Thermal performance analysis of beeswax as thermal storage material with different types of heat transfer fluids, *International Journal of Advanced Studies of Scientific Research*, (*Accepted).*
6. A. Dinker, M. Agarwal, and G.D. Agarwal, Experimental Study on Thermal Performance of Beeswax as Thermal Storage Material, *Materials today: Proceedings (Accepted).*

Communicated papers:

1. A. Dinker, M. Agarwal, G.D. Agarwal, Performance study of beeswax/expanded graphite composite for thermal energy storage in a shell and tube unit, *Heat Transfer Engineering.*
2. A. Dinker, M. Agarwal, G.D. Agarwal, Experimental thermal performance study of natural graphite as sensible heat storage material using different heat transfer fluids, *Experimental heat transfer.*
3. A. Dinker, M. Agarwal, G.D. Agarwal, Simulation of thermal storage performance of beeswax in a shell and tube type thermal storage unit, *Applied Thermal Engineering.*

Conference publications:

1. A. Dinker, M. Agarwal, and G.D. Agarwal, “Preparation of expanded graphite and stearic acid composite for the low temperature thermal storage” *Proceedings of 67th Annual Session of IIChE and Indo-Japnese Symposium”* Jointly organized by Chandigarh Regional Center, IIChE and Dr, SSB University Institute of Chemical Engineering & Technology, Chandigarh, December 27-30, 2014.

2. A. Dinker, M. Agarwal, and G.D. Agarwal, “Experimental Study on Thermal Performance of Beeswax as Thermal Storage Material” *proceedings of International Conference On Recent Trends In Engineering And Material Sciences (ICEMS-2016)* “ Organized by Jaipur National University, Jaipur.

3. A. Dinker, M. Agarwal, and G.D. Agarwal, “Thermal performance analysis of beeswax as thermal storage material with different types of heat transfer fluids” *Proceedings of International Conference on Computational Technology (ICCT -2016)”*, Organized by Poddar International college, Jaipur.

4. A. Dinker, M. Agarwal, and G.D. Agarwal, “Preparation and application of expanded graphite/water suspension for thermal storage using graphite as heat storage material” *Proceedings of international conference on emerging technology : Micro to nano (ETMN-2015)”,* Organized by Manipal University, Jaipur.

Dedicated to
Lord Jagannath,
My Family
&
My Nation

CHAPTER 1

INTRODUCTION

Our society is presently facing energy crisis which is going to further increase due to rapidly depleting fossil fuel reserves, hike in fuel prices and environmental issues like global warming, climate change, loss of biodiversity, deforestation, ozone layer depletion etc. In one study, it was estimated that by the end of 2035, world energy demand will increase from its present value (2014) of 12.50 giga tons of oil equivalent (GTOE) to 25 giga tons of oil equivalent (GTOE) [1]. Recent studies on emission have revealed a sharp increase in greenhouse gases in environment. It is estimated that by the year 2400 about 5,000 giga tons of carbon will be released in environment starting from industrial revolution, keeping rates of fossil fuel consumption and carbon-sequestration constant [2]. It has been reported that due to enhanced emission of greenhouse gases there is average rise in global temperature at the rate of 0.15-0.20 °C per decade [3,4]. Another concern with rise in greenhouse gases in the environment is the depletion of ozone layer which led to increase in environmental and health problems [5,6]. To address these environmental issues and to tackle increased energy demand it is important to use our conventional sources wisely by saving and storing excess energy available in the form of waste heat and solar thermal energy effectively.

It was found that about 50-55% of energy produced from primary energy sources is lost as heat from various sources like flue gases, server rooms, industries, vehicle exhaust etc. In addition to primary energy sources, renewable energy sources like solar energy which is intermittent in nature, unpredictable, diffused and depend on weather conditions need to be stored for constant supply and improve energy utilization and reuse whenever required [7]. Energy storage not only saves energy but also bridges the gap between energy demand and supply and also helps in energy conservation. The key role of energy storage is to provide continuous energy supply at low cost by improving system performance and reducing energy wastage.

Properly selected energy storage materials can make energy system cost effective by efficient energy storage and discharge. Energy storage materials can be used with building materials to maintain the indoor temperature. These materials can also be applied to the wall of chimneys where it can absorb waste heat coming out with flue gases.

At present the most common form of energy storage are batteries or cells [8,9] which are quite efficient but harmful to the environment due to acid contents [10]. In last few decades other energy storage technologies such as Photo-voltaic systems [11, 12], Photovoltaic/thermal hybrid system [13], Supercapacitors [14], Hydrogen storage system [15,16], Mechanical energy storage [17,18], Chemical energy storage [19], and Thermal energy storage [20,21] have been identified, investigated and used for energy storage. Although photovoltaic systems directly convert solar energy into electricity, but are effective only during sun shine or daytime, which limit their use during off sun shine hours. Photovoltaic/thermal hybrid systems store energy in the form of heat for later use but are costlier in application due to high cost of manufacturing and large space requirement for installation of solar panels [13,22]. Industrial application of Supercapacitor has been also limited due to its high cost.

Hydrogen energy storage is expensive due to high safety requirements for its storage and handling because of high flammability of hydrogen gas. Materials with specific properties such as high permeability of hydrogen and mechanical stability of storage vessel are required for pressurized hydrogen storage [23,24]. Mechanical energy storage systems like pumped hydro power (PHP) and compressed air energy storage (CAES) are efficient in nature, but their generation and storage are limited to some geographical sites [18]. Chemical energy storage in form of conventional fuels like petrol and diesel have affected environment through pollution [25]. Thermal energy storage (TES) systems on the other hand were found to be the safest and cheaper means to store energy which have diverted the attention of whole world for its study and exploration. The TES systems are economically viable with relatively low capital cost, can store large quantities of energy without any major hazards with small (~0.05 to 1 %) daily self-discharge loss [26,27].

Thermal energy storage systems (sensible heat and latent heat) can be used to store energy from the sun and also waste heat from other sources. In solar thermal power plants integration of thermal energy storage system have reduced fluctuations between demand and supply [28]. Solar thermal energy storage systems have been used for pre-heating applications in industries [29]. For every thermal storage system there are two basic characteristics. First, the energy storage time with acceptable losses and second, energy stored per unit volume. The energy stored per unit volume not only

depends on geometry of the system but also depends on physio-chemical characteristics of energy storage materials used. An efficient thermal storage system should have high energy density that can be achieved through proper designing and selection of appropriate storage material. The application of efficient thermal storage materials not only helps in storage of direct solar energy but also useful in managing heating and cooling load to reduce fossil fuel consumption. In many cold countries heating and cooling are fundamental requirement of energy and shares a large percentage in their total energy consumption. It was estimated that about 45% of total energy in Swedish service and residential sector are used for cooling and heating [30]. Therefore, by the application of an efficient thermal energy storage system this energy requirement can be reduced.

1.1 Thermal energy storage

Thermal energy storage systems are divided into various categories based on nature of storage materials used: Sensible heat storage, Thermo-chemical heat storage, and Latent heat storage.

1.1.1 Sensible heat storage

In sensible heat storage system the amount of heat stored depends on the mass and specific heat of storage material apart from temperature change as per equation 1.1.

$$Q = m\, C_p\, dT \qquad (1.1)$$

Where, m = mass of storage material (kg), C_p = specific heat of material (kJ/kg.K), dT = temperature difference (K).

Materials used for an efficient sensible heat storage system should have high specific heat capacity, long term stability in terms of thermal cycling and should be compatible to the container material in which storage takes place [31]. A variety of materials have been used in the past for sensible heat storage such as water, rock pebbles, sand and concrete. [32]. In addition to these materials, metals like aluminium, copper, lead, iron etc. were also tried for thermal storage. Application of metals with high thermal conductivity had reduced the charging and discharging time of storage system. However, these metals have less heat capacity, high density and are expensive in terms of application [33]. Rocks pebbles and sand though cheaper but

were found to be less efficient due to their low thermal conductivity [34]. Water the most common sensible heat storage material from last few decades for solar ponds and coolant for various industrial processes [35,36] has drawback of low boiling point and dissolved impurities. From literature survey it was found that most of the sensible heat storage materials were having less heat capacity and therefore, required more mass/volume of the material which makes the system heavier and bulky. Therefore, there is a need of exploration of new materials or modification of existing ones in terms of heat storage properties. The commonly used sensible heat storage systems are solar pond [35,37], solar water heater [36,38] and solar air heater [39,40] etc.

1.1.2 Thermochemical energy storage

Thermochemical energy storage system involves either endothermic or exothermic reversible chemical reactions as per equation 1.2,

$$A + B \leftrightarrow C + Q \tag{1.2}$$

Where, A and B are the chemical species while C is the product, Q is the heat released/absorbed in the process.

Energy storage in a thermochemical storage process involves addition or liberation of another chemical species such as salt hydrate which store thermal energy with the liberation of water molecules. The stored energy can be reused latter by hydration of the chemical species [41,42]. Other than hydration and dehydration reactions, thermochemical energy can be stored at high temperature through the reduction and oxidation of metal oxide [43,44] . Thermochemical energy storage shows the promising results in terms of energy density for future applications. However, due to corrosive nature of salts, high initial cost, periodic degradation of chemical species and handling of chemicals for scale up process restrict thermochemical storage for wider range of applications and need to be investigated in detail [45].

1.1.3 Latent heat storage

Latent heat storage system stores heat using materials which undergo phase change also known as phase change materials (PCMs), and can store more heat as compared to sensible heat storage material [46]. The amount of heat stored in latent heat storage

systems depends on the mass and latent heat of the materials as expressed in equation 1.3,

$$Q = m. L \quad (1.3)$$

Where, m = mass of the material (kg), L = latent heat of phase change (kJ/kg).

The advantage of latent heat storage system is that it stores heat energy with high energy density at constant temperature and therefore these systems are compact in size as compared to the sensible heat storage systems. Based on the application and storage materials these systems store energy both in low and high temperature range. Latent heat storage system has been of great interest in last few years due to its application in waste heat recovery [29], solar energy utilization [28] and passive cooling [31].

A phase change material (PCM) used in latent heat storage unit should be non-reactive, non-toxic, should have low vapor pressure, good thermal cycling stability, good latent heat, good specific heat and a range of melting point that promotes thermal storage at wide temperature range [20,46]. Based on the chemical composition PCMs are divided as organic phase change materials and inorganic phase change materials. Organic phase change materials composed of hydrocarbons and their derivatives with good latent heat and poor thermal conductivity. These materials generally consist of low melting point range and suitable for low temperature thermal storage applications. Examples of organic phase change materials are paraffin, fatty-acids, fatty-alcohols, esters etc. [26]. Paraffin is the most commonly used organic phase change material for thermal energy storage. However, being a petroleum product its cost is high and its production process also involves carcinogenic catalyst [47]. Other organic phase change materials such as fatty acids, fatty alcohols and esters were investigated for low temperature thermal storage. However, their high production cost limited their use for wide range of thermal storage applications. Beeswax, a natural material which is used for various applications such as manufacturing of candles, sculptures and for fruit coatings is also listed as phase change material in literatures [48–50]. However, a little work is available in regarding the application of beeswax as phase change material and investigated in the present research.

Inorganic phase change materials such as nitrate salts, metals and salt hydrates having high latent heat of fusion were used for high temperature thermal storage applications like concentrated solar plant (CSP) [43]. The major drawback associated with inorganic phase change material is corrosive nature of salts which can degrade the container wall of thermal storage units [44]. Looking to these drawbacks of existing phase change materials there is a strong need to identify and explore new phase change materials having low cost, natural in occurrence, and having all the desired properties of an potential phase change material for efficient thermal energy storage.

1.2 Indian scenario on thermal storage

With the title of eleventh largest economy in the world, India stands fourth in terms of energy purchasing power within the world [51]. India receives 500,000 GWh of solar energy every year with daily radiation of 4-7 kWh per square meter per day in most of the part of the country [52,53]. However, due to intermittent nature, low energy density and lack of technical expertise only a little part of the incident solar energy (6%) is converted into the electricity by photovoltaics at present. In terms of solar thermal power production India stands at third rank in the world. Under Jawaharlal Nehru National Solar Mission (JNNSM), India set the target of 20,000 MW of grid solar power (including solar thermal systems and solar photovoltaics) and 2000 MW of off-grid capacity includes 20 million solar lightning systems and 20 million square meter of solar thermal area by 2022. In India total nine concentrated solar thermal power plants are either under construction or in operational stage with total capacity of 526 MW [51,54,55] . In addition to this, various companies like Promethean power systems, Cristopia energy systems pvt. ltd. and Calmac industries have installed thermal storage systems in different parts of the country for wider range of applications such as dairy, cooling towers etc. Promethean power systems have installed 2.5 MWh of thermal energy storage system in rural India for preservation of milk. The company is manufacturing chiller units based on PCM to store 28 kWh of energy in the form of ice [56]. Similarly thermal storage equipment of Calmac industries have been installed in cities like Bangalore, Delhi and Chennai with cooling storage capacity of 12 MW [57]. India is also focusing to reduce power consumption by regulating indoor temperature of buildings through thermal storage [58,59]. In

order to save off-peak hour energy and to supply same during peak hour Tata power enrolled a thermal storage unit of capacity over 15,000 TRH and achieved a load shift of more than 3.6 million units of energy from peak to off-peak hours [60].

Due to slow pace of thermal energy storage initiatives in India there is need to promote research and development in low temperature thermal storage area such as solar water heaters, solar air heaters, materials for temperature control of buildings etc. In the colder parts of the country like Jammu and Kashmir and Himalayan region where there is low temperature for most of the time around the year, low temperature PCM can be integrated as construction materials of building to store the thermal energy during day time and release it during evening and night [61,62].

1.3 Global scenario on thermal storage

In last few decades major share (79.3%) of the total energy was supplied from fossil fuels such as oil, coal and natural gas while a limited part (11.2%) of energy was met through renewable sources. This wide gap in energy supply and increasing environmental problem such as global warming diverted the attention of whole world towards the expansion of renewable sources of energy as well as storage of energy [63] to reduce the consumption of fossil fuels and related environment impact. It is estimated that about two third of the total energy consumed by the world by the end of 2035 will be generated from natural gas and renewable sources of the energy [64].

European OECD (Organization for Economic Co-operation and Development) countries has committed to reduce greenhouse gas emission by 20% (as compared to 1990) upto 2020 and 80% to 95% by the year 2050 [65]. At present renewable energy sources are expanding their share of power generation and with the present pace of energy generation it is estimated that renewable sources will contribute 6.5 PWh to 11.0 PWh globally in 2020 [63]. To meet these targets and to counter the limitations of renewable energy sources such as non-uniform distribution, periodic availability and unpredictable weather conditions, researchers around the world is focusing on development of efficient energy storage technologies.

At present molten salt thermal energy storage is the second largest storage method with the capacity of 2.6 GW after pumped hydroelectric storage [66]. As per the

report of Department of Energy, U.S. (DOE-US, 2013) total 1206 energy storage facilities with total capacities of 184 GW are presently available around the world. However, more than half of these facilities are under development and efforts are in place to make them operational as soon as possible. Thermal storage technology and its application was in predominant stage in USA in mid-1990 and begun to appear in Asia, Australia, Europe and South America. In USA about 1500-2000 thermal energy storage systems are installed to maintain the indoor temperature of buildings. Chilled water thermal energy storage system (9100 kWh) was installed in Texas with 1500 kW of chiller plant to meet chilling load requirement which could otherwise require a 2600 kW of energy [32].

In country like Saudi Arabia which has a daily peak load of more than 17000 MW and 30% electricity wastage, use of air conditioning systems during summer represent 60% of total energy demand of the country. To reduce this peak energy demand Saudi Consolidated Electric Companies (SCECO) proposed the use of thermal energy storage system with their HVAC installations. It is estimated that application of TES (Thermal energy storage) system in a large commercial complex can reduce the peak cooling load demand between 30-40% and peak electricity demand between 10-20%. Gas turbines are the power generating unit in Saudi Arabia and their output is dependent on ambient temperature which is usually higher in this country. It was found that integration of TES
system with gas turbine could reduce the inlet temperature by 5 °C and increase the generator output by 30% [32]. In addition to this various works related to the application of phase change materials with building materials, solar water heaters and solar air heaters are under investigation to enhance the dependency on renewable energy, reduce wastage of energy and reduce fossil fuel consumption especially in colder countries [67–69].

1.4 Origin of the problem

Thermal energy storage systems are under investigation from last few decades due to their good energy density for storage of solar thermal energy [20,46]. In addition to the solar thermal energy there are other sources which release waste heat that can be stored and use whenever required. These sources include flue gases from industrial

processes [70], hot gases from chimneys [71], exhaust gas from engines [72] and hot liquid effluent from process industries. It was found that about 50-55% of energy produced from primary energy sources is lost as heat from these sources. This waste heat can be capture by using phase change material for various pre-heating applications in industries and automobiles [73–76]. However, most of the present phase change materials are less efficient and costlier which restrict them for wide range of applications. To overcome these issues there is need to identify and investigate new, efficient and environment friendly phase change material or to modify existing material for improved thermal properties. In addition to improvement in thermal storage materials the geometries of thermal storage system has to be explored for its improved performance. In literature various geometries such as cylindrical shell and tube type, concentric type units with attached fins etc. has been reported [77–79] Some of these geometries were found to be efficient in nature but they were having less heat capacity. In order to simplify the design of thermal storage unit and to enhance its heat capacity as well as efficiency there is need to study and test some new geometries and designs using PCMs as heat storage material.

1.5 Need of the study

Various phase change materials like paraffin, fatty acids, fatty alcohols etc. were investigated for low temperature thermal storage applications [20,26,27]. However, these materials are somewhat costlier and production of paraffin generates toxic byproducts. Looking to these limitations of presently available phase change materials there is need to identify and investigate new phase change materials which are natural in origin, cheaper in cost, having good latent heat and can be used for domestic application to store thermal energy. In present work an attempt has been made to identify an efficient phase change material for low temperature thermal energy storage and to improve its thermal properties for further enhancement of its heat storage capacity. Along with PCM, geometry of a thermal storage unit (TSU) also plays significant role for an efficient thermal storage system. Various geometries of TSU such as cylindrical shell with single tube, multiple tube, concentric type etc. were investigated in literature. However, work on rectangular geometry with embedded helical coil is very limited and need to be investigated.

1.6 Scope of present research

a) Present study is focused on the identification and utilization of a new phase change material which is natural and whose thermal properties are better than that of the similar conventional PCM. Attempt has been made to improve thermal properties of identified PCM by making its composite.

b) Design and fabrication of rectangular helical coil embedded heat storage unit.

c) Performance evaluation of developed unit with sensible heat storage material and PCMs.

d) Performance evaluation and optimization of operating parameters (HTF flow rate, initial temperature of HTF etc.) with different heat transfer fluids such as plain water, expanded graphite/water suspension, Al_2O_3/water nanofluid and engine exhaust gases.

e) Simulation of thermal storage unit using COMSOL Multiphysics.

1.7 Thesis organization

For the convenience in understanding, the thesis is divided into six chapters as follows:

Chapter 1: Introduction

In chapter 1 various aspect of thermal storage technologies such as thermal storage materials, their classification, Indian and global scenario on thermal storage technique have been introduced. The origin of problem along with need and scope of present research have been highlighted.

Chapter 2: Literature review

In chapter 2 a detailed literature review related to the thermal storage technology has been presented. Studies on different types of thermal storage materials, their classification and applications are presented in this chapter. Various thermal storage Systems with their merits and demerits have been discussed. Research gap have been identified and thesis objectives have been framed.

Chapter 3: Material and methods

In chapter 3 various materials used and the experimental methodology adopted for present research is presented. In particular, this chapter elaborates methods/techniques used in preparation of expanded graphite, preparation of composite material from beeswax and their characterization. The details regarding preparation of Al_2O_3/water nanofluid, preparation of expanded graphite/water suspension and construction of experimental setup have been presented in this chapter. Parametric studies on beeswax, composite and packed bed of natural graphite have been discussed. Procedure and duration of experiments performed on different heat storage materials at different flow rates (0.25 LPM-1.0 LPM) and inlet fluid temperatures (60 °C-90 °C) have been detailed in this chapter. Detailed methodology adopted in running the setup for its performance evaluation and parameter optimization has been reported. All the analysis and characterization techniques with involved equipment information have been added in this chapter. In the design and construction of experimental set-up an effort was made to simplify and optimize the current scope of the work with available experimental resources in our lab. Details of simulation studies using COMSOL® are also incorporated in this chapter.

Chapter 4: Results and discussion

In chapter 4 results of physical, chemical and thermal characterization of phase change materials have been discussed. Results of thermal performance analysis of developed setup with different heat storage material at different parametric conditions are presented and explained. Simulation results of COMSOL® on different heat storage materials and their comparison with experimental data are presented.

Chapter 5: Conclusion

In Chapter 5 summary of work done and its conclusion are presented along with future research scope of the study.

CHAPTER 2

LITERATURE REVIEW

Energy storage is one of the major concerns in the present century due to the shortage of conventional sources of energy and non-uniform distribution of renewable energy like solar energy, wind energy, geothermal energy, energy from ocean currents etc. With increasing gap between energy demand and supply there is need to develop efficient energy storage systems for uninterrupted power supply [79,80]. At present there are varieties of energy storage systems available and being studied experimentally, numerically, and mathematically by different researchers are discussed in this chapter.

2.1 Energy storage technology

There are various types of energy storage technologies presently available to store energy from both conventional and renewable sources of energy. These technologies are broadly classified on the basis of their operation and form of the energy stored as shown in Figure 2.1.

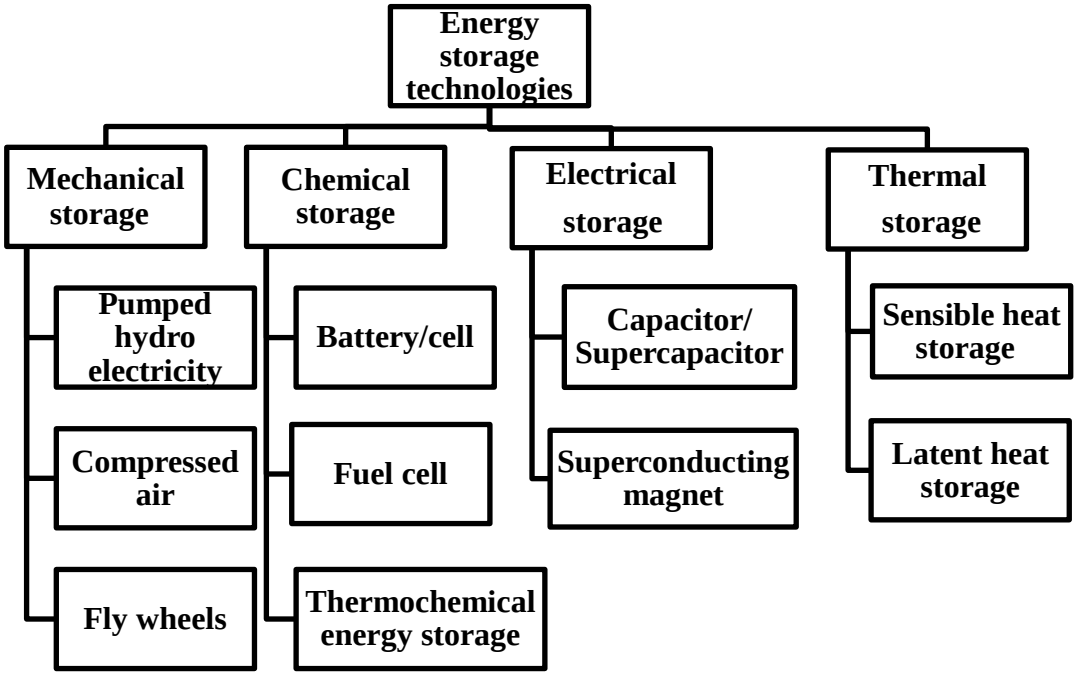

Figure 2.1 Different types of energy storage technologies [82]

2.1.1 Mechanical energy storage

In mechanical energy storage systems, energy is stored in the form of potential energy and mainly consists of pumped hydro energy storage (PHES) and compressed air energy storage (CAES). In PHES water is pumped from a low level reservoir to a high

level reservoir during off peak period utilizing surplus energy which converts electrical energy into potential energy. During peak energy demands, this potential energy is converted back into electricity by using dynamo. PHES is pollution free and having better conversion efficiency (65-80%) depends on the type of instrument used in the process [82].However, the main limitation of this technology is the requirement of geographical site with height difference in the level of two water reservoir and a large volume of water. Depending on the size, the capacity of PHES can be in between 1000-3000 MW with 70-80% efficiency [83] . It is estimated that about7 GW of pumped hydro heat storage (PHES) system is under deployment in European network while various other project are under planning stage in U.S.A. and Japan [17]. PHES can be integrated with other renewable energy generating sources like on Gran Canarias Island a PHES system is connected to the wind farm with output of 20.40 MW to convert extra electricity produced from wind turbine into the potential energy of water for future use [84]. Various other such systems where PHES is integrated with renewable energy sources are available in the literature [85–87].

Another form of mechanical energy storage is compressed air energy storage (CAES), where ambient air is compressed using excess electric power in underground cavern. During peak demand period this compressed air is heated and expanded in an expansion turbine attached to a generator for power production [88] and reported efficiency of CAES is found to be 70-80% [89]. Different applications of CAES systems for storage of surplus energy are studied by different researchers [90–93].

2.1.2 Chemical energy storage

In chemical energy storage, energy is stored in the form of some chemical species like electrochemical storage, thermochemical storage and conventional fuels. Electrochemical storage involves conversion of electrical energy to chemical energy and vice versa, in the case of conventional batteries such as lead acid batteries [94], lithium ion batteries [95] and flow batteries [96]. Electrochemical energy storage systems are compact in size and efficient in nature. However, their major drawback is the environmental pollution which occurred due to the presence of heavy metals and concentrated acids in their contents and therefore, required safe disposal [96,97].

In thermochemical energy storage systems heat is absorbed and released with chemical reactions [99] in the form of hydration-dehydration reactions and oxidation-

reduction reactions . In a study Neises et al. 2012 [100] studied a solar rotatory kiln with cobalt oxide which reduced with the absorption of solar thermal energy during day time and again re-oxidized during off sun period with liberation of heat for kiln operation. Other thermochemical energy storage systems are studied using chemical species such as ammonia [100,101], BaO_2/BaO [103], calcium oxide-calcium hydroxide [104], etc.

Conventional fuel is also one of the forms of chemical energy where energy is stored in the bonds of chemical species. The stored chemical energy is released when chemical species undergo transformations during combustion. Other forms of chemical energy storage are hydrogen storage [104,105], methane storage [106,107], biofuels [108,109] and petroleum gases [110, 111] etc.

2.1.3 Thermal energy storage

Sensible heat storage system and Latent heat storage systems are the two forms of thermal energy storage system.

Heat stored in a sensible heat storage system depends on the temperature and quantity of heat storage material and therefore, these systems are bulkier in size [113]. Latent heat storage systems, stores energy in the form of latent heat of material followed by phase change [114]. The amount of the latent heat stored is greater as compared to the sensible heat as the latent heat is usually more than the specific heat. The materials used in latent heat storage systems are commonly known as Phase Change Materials (PCMs) [26].

2.2 Studies on sensible heat storage

Sensible heat storage systems are being investigated by the different researchers in various parts of the world from the last few decades in order to enhance their efficiency [31,114] and identify new sensible heat storage materials.

2.2.1 Sensible heat storage materials

A variety of materials have been used in the past for sensible heat storage which is classified as liquid and solid heat storage materials. A list of different sensible heat storage materials used along with their properties is presented in Table 2.1.These materials include metals like aluminum, copper, lead etc. [115,116] which are having

high thermal conductivity with less charging and discharging time. However, metals have low heat capacity, high mass density and high cost which restrict their use for wider applications. It is observed from Table 2.1 that water is a good sensible heat storage media due to its high thermal capacity and high energy density [117,118]. However, due to its high vapor pressure, it requires insulation as well as pressure withstanding container for high temperature operation. Some building materials are also studied as sensible heat storage materials to construct thermal controlled buildings or energy efficient buildings [120–122]. However, due to low thermal conductivity these materials require further investigations for different applications.

Table 2.1 Sensible heat storage materials and their thermal properties at 20 °C

Material	Thermal capacity (kJ/kg.K)	Thermal conductivity (W/m.K)	Density (kg/m^3)	Energy density (kJ/m^3)	Ref.
Aluminum	0.945	238.4	2700	2551.50	[116]
Copper	0.419	372	8300	3477.70	[115]
Iron	0.465	59.3	7850	3650.25	[117]
Lead	0.131	35.25	11340	1485.54	[117]
Brick	0.840	0.5	1800	1512	[120]
Concrete	0.879	1.279	2200	1933.80	[123]
Granite	0.892	2.9	2750	2453	[121]
Graphite	0.609	155	2200	13339.80	[122]
Limestone	0.741	2.2	2500	1852.50	[124]
Sandstone	0.710	1.8	2200	1562	[124]
Slag	0.836	0.57	2700	2257.20	[124]
Soil (Clay)	0.880	1.28	1450	1276	[124]
Soil (Gravelly)	1.840	0.59	2040	3753.60	[124]
Water	4.183	0.609	998.3	4175.88	[124]

2.2.2 Sensible heat storage systems

Different sensible heat storage systems are also investigated for obtaining efficient heat storage system. A very good example of a large size sensible heat storage system is solar pond. A natural solar pond was spotted at Medve lake located in Transylvania, Hungary and water temperature upto 70 °C was observed at a depth of

1.32 m at the end of summer season due to the presence of salt (NaCl) at the bottom of the lake with salt concentration of 26% [125]. This type of natural lake having salt gradient formed the basis for the research and development in the area of artificial solar ponds.

Velmurugun et al. 2009 [126] examined in different set of experiments the productivity of solar pond connected with stepped solar still , single basin solar still and wicked type solar still one by one respectively. To enhance the solar pond productivity pebbles, baffle plates, fins and sponges were added to the solar stills during experiments and results showed 80% productivity in first experiment when both fin and sponges were used in the both the solar stills and 78% productivity in second experiment when fins and sponges were used in stepped solar stills. In an another study by Karakilcik et al. 2006 [127] on a solar pond (surface area 4 m^2 and depth 1.5 m) built at Cukurova University in Adana and different temperatures were measured in the months of January, May and August. Results of the study showed that temperature difference was the main factor for heat transfer and maximum thermal efficiency of 4.50% was achieved in August for upper convective zone, 13.80% for non-convective zone and 28.10% for heat storage zone. These three zones of the solar pond also played important role in other applications rather than maintaining thermal gradient of the solar pond. Singh et al. 2011 [128] combined the thermosiphon and thermoelectric module for generation of electricity from solar pond. Results showed that proposed gravity assisted thermosiphon-thermoelectric module (TTM module) provided maximum power of 3.2 W obtained at 13.4 V and 0.24 A when the temperature difference of 27 °C was maintained across 16 thermoelectric cells.

In a salt gradient solar pond, different salts showed different effect on thermal gradient. In a study, Berkani et al. 2015 [129] compared three solar ponds with three different salts i.e. NaCl, Na_2CO_3 and $CaCl_2$ based solar pond performed better in terms of thermal storage and stability as compared to the other two salts. In another similar work, Bozkurt et al. 2015[130] analyzed the potential of sodium and magnesium chloride for their application in solar pond and found the storage efficiency of 27.40% and 25.41% for respective ponds.

Solar ponds also showed their potential when applied with heat exchangers, flat plate collectors and other sensible heat based structures for thermal storage. Tundee et al.

2010 [131] studied the removal of heat from lower convective zone by a pipe heat exchanger using R134 as heat transfer fluid and found 43% increase in effectiveness when air velocity was decreased from from 5 m/s to 1 m/s. In a similar study, Bozkurt et al. 2012 [132] investigated the performance of solar pond integrated with a collector system. They built a cylindrical solar pond (radius 0.80 m and depth 2.0 m) with four flat plate collectors (1.90 m x 0.90 m) to trap solar thermal energy. The system was found to be more productive as compared to stand alone solar pond and the experimental efficiency of four collectors (1, 2, 3, 4) were found to be 21.30%, 23.60%, 24.28% and 26.52% respectively.

A low temperature direct contact type membrane distillation driven by solar pond was studied by Suarez et al. 2015 [133]. The study showed that about 70% of thermal energy from solar pond was utilized to drive the desalination process in which half of the heat was utilized to transfer water to the other side of the membrane, while the remaining heat was lost by conduction through the membrane. Solar pond has many applications, however, the major drawbacks of solar pond are large space requirement and low efficiency which limits their commercial use.

Some other sensible heat storage systems are investigated on fixed bed of thermal storage materials. Prasad et al. 2013 [113] designed and tested a cylindrical thermal storage unit with embedded tubes within the bed of three different kinds of materials i.e. concrete, cast steel and cast iron. Parametric study was carried out by making variations in number of fins on charging tubes and flow rate of HTF. Results of the study showed 35.48% reduction in charging time with four fins and 41.41% of charging time with six fins configuration. It was also found that with increase in the flow rate of heat transfer fluid charging time of cast steel and cast iron was reduced while there is less effect of flow rate was observed on the charging time of concrete. In an another study Zagnesh et al. 2012 [134] investigated charging and discharging of packed bed of rocks which was buried in the ground by passing air as heat transfer fluid from a concentrated solar plant (CSP). Results of the study showed 95% efficiency of fixed bed with repeated charging and discharging cycles and offered the temperature above 590 °C in discharging phase. The same work was repeated with same bed of rocks with exhaust gas as HTF from industrial process [135]. In this study the maximum efficiency of thermal storage system was found to be 95% and it was observed that the efficiency of the bed could increase with decrease in tank

diameter to height ratio as well as the diameter of rock. However, with increase in bed height a pressure drop was also observed across the bed which enhanced the requirement of pumping power for HTF flow.

Yuan et al. 2012 [136] studied the effect of water/cement (w/c) ratio and graphite content on mechanical and thermal properties of composite aluminate cement to optimize its use for solar parabolic trough power plant as thermal storage material and found that both thermal conductivity and volume heat capacity of aluminate cement increased with decrease in w/c ratio and increase in graphite content. In another study, Kuravi et. al. 2013 [137] studied sensible energy storage system made up of high density storage bricks for its use as central receiver of CSP. Parametric studies at different inlet temperatures (300 ℃-600 ℃) and flow rates (50-90 ft^3/min) were performed using air as heat transfer fluid and results showed reduced charging time of the bed with increase in mass flow rate and observed 90% charging efficiency and 80% stratification efficiency of the bed.

Sensible heat storage systems studied by different researchers for wide range of applications [138–140]. However, their deployment to achieve present energy target require more investment, larger space and regular maintenance. Looking to these drawbacks of conventional sensible heat storage system researchers have diverted their attention to identify thermal storage system which is portable, compact, cheaper, efficient and longer life with less maintenance. A latent heat storage system can meet these requirements and which is studied to make them commercially viable.

2.3 Studies on latent heat storage

Latent heat storage systems are considered as a promising option for thermal energy storage as compared to the sensible heat storage systems due to their compactness and high energy density [46]. Figure 2.2 depicts the application of a simple latent heat storage system and its integration with process industries where it can also store waste heat and redistribute it for pre- heating applications. Performance of a latent heat storage system depends on the type of storage material and geometry of heat storage system. Investigations carried out in different studies to improve the thermal performance of latent heat storage systems are presented here.

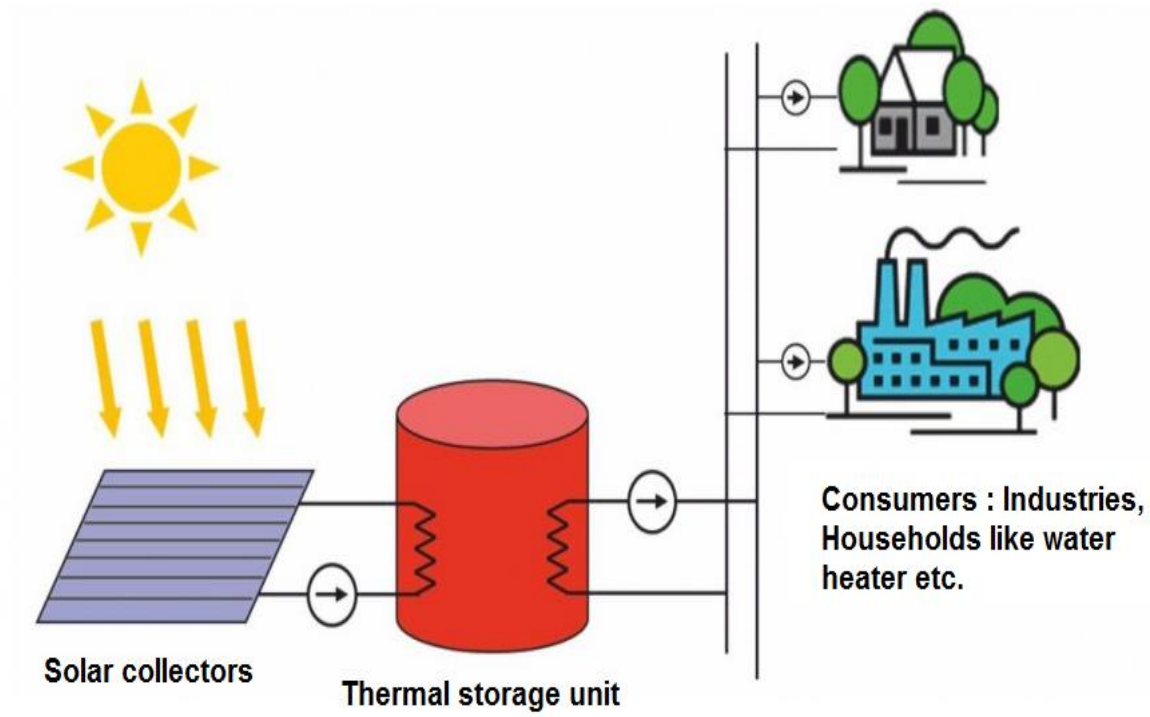

Figure 2.2 Solar thermal storage and distribution system

2.3.1 Phase change materials

Energy storage materials used in latent heat storage systems are also known as phase change materials (PCMs) as they store and liberate heat with change in phase of material [20,140]. A phase change material should have a desired phase change temperature, high latent heat of fusion, good thermal conductivity, high energy density, small volume change, long term chemical stability, non-toxicity, low vapor pressure and cheaper in cost. It is reported that PCMs can store 5 to 14 times more heat energy as compared to sensible heat storage materials at constant temperature [27,141,142] .

On the basis of their chemical composition PCMs are of two types- Organic phase change materials and Inorganic phase change materials as shown in Figure 2.3.

i) Organic phase change materials

Organic phase change materials are composed of hydrocarbons and their derivatives. The melting points of organic PCMs are generally lower and these materials can undergo various cycles of melting and freezing without phase segregation. Organic

phase change materials are further divided into paraffin, non-paraffin and eutectic mixture [27,46].

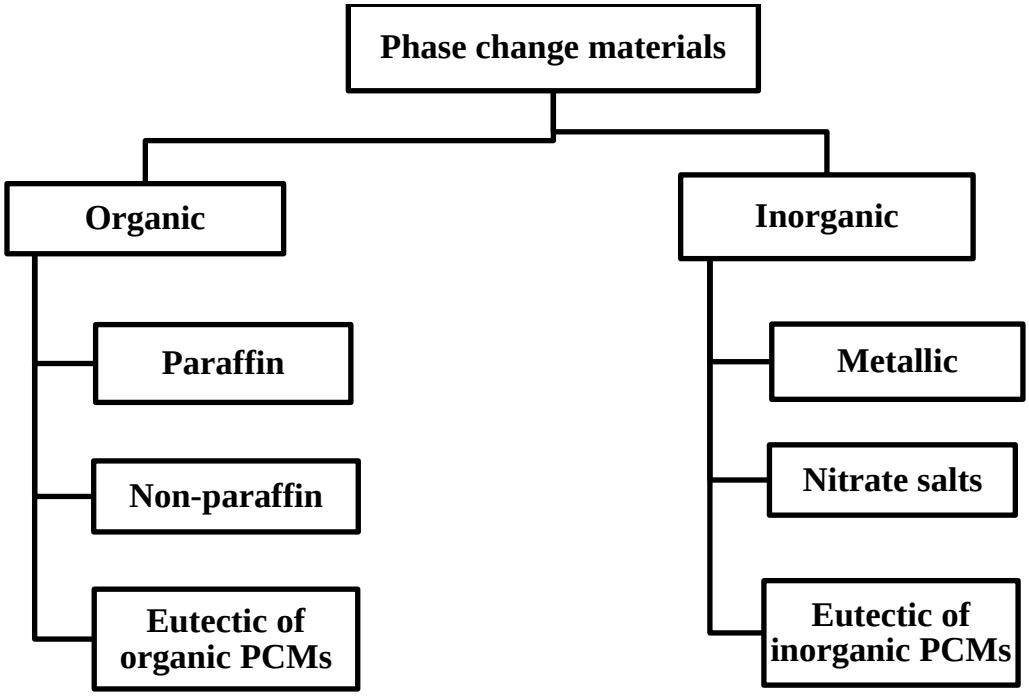

Figure 2.3 Classification of phase change materials

a) Paraffin and their composites

Paraffin is the petroleum derivative that consists of mixture of straight chain hydrocarbons. The melting point and latent heat of paraffin increases with increase in carbon chain and reaches a asymptotic value (generally after C_{100}) [144–147].

In past few decades paraffin have been used in many commercial applications such as manufacture of candles [148], clinical purpose [149],in paint and dye industry [150] etc. In recent years paraffin is identified as an appropriate PCM for different thermal storage applications. Kaygusuz et al. 2005 [151] studied the thermal performance of paraffin wax in a concentric pipe latent heat storage system and observed that the melting and solidification of paraffin take place at 38 °C-43 °C and 36 °C-42 °C respectively rather than at a constant temperature. He et al. 2002 [152] investigated the technical grade paraffin rubitherm RT5 (melting point = 7 °C and heat of fusion = 158.3 kJ/kg) and found it suitable for cold storage applications. In an another study by Kaouskaou et al. 2010 [76], binary mixture of hexadecane-tetradecane was investigated in a differential scanning calorimetry (DSC) cell and noticed dependency

of phase change temperature on the heating rate and mixture composition. Goia et al. 2016 [153] studied the effect of solar radiation on aging process of paraffin in a glazing system and found 5% decrease in the latent heat of paraffin with 1.5 °C reduction in cooling point and 2°C reduction in melting point after the time span of one year.

In a study, Akagun et al. 2008 [154] investigated the melting and solidification characteristics of paraffin wax in a concentric shell and tube type thermal storage unit at four different inlet fluid temperatures (60 °C, 65 °C, 70 °C, 75 °C) and three flow rates (4 kg/min, 6 kg/min and 8 kg/min) and found that charging time of paraffin decreased with increase in inlet fluid temperature and mass flow rate. It was also observed that with 5° inclination of shell surface melting time of paraffin reduced by 30%. Sharma et al. 2002 [155] studied the effect of thermal cycle on stability of paraffin wax over acetamide and stearic acid and observed that after 1500 accelerated thermal cycles, paraffin and acetamide showed good thermal stability in terms of melting point and less variation in latent heat of fusion as compared to stearic acid.

In some of the investigations paraffin wax was encapsulated to improve the heat transfer and in a study by Nemeth et al. 2015 [156] alginated shell was used to prepare the double layered capsules of paraffin. This encapsulated paraffin wax showed good thermal stability with melting and freezing latent heat values of 95 J/kg and 91.7 J/kg respectively. In another work, Karkri et al. 2015 [157] prepared and studied the capsules of paraffin wax (M.P. 42 °C) within the shell of melamine formaldehyde resin and found that the thermal conductivity and diffusivity of PCM decreased with increase in resin content of the capsule while latent heat, sensible heat and total heat of the microcapsules increased with the increase of paraffin wax content in the capsule. Memon et al. 2015 [158] prepared a light weight aggregate to encapsulate paraffin for temperature control of buildings. Results showed that the strength of microcapsules incorporated concrete had better comprehensive strength and volume stability.

As PCM, pure paraffin proved to be a good thermal energy storage material. However, the major disadvantage associated with the use of paraffin wax is its lower thermal conductivity which increases the charging/discharging time and reduces the efficiency of latent heat storage system. To enhance the thermal conductivity of

paraffin wax high thermal conductivity materials like expanded graphite, metallic nanoparticles, carbon nanotubes etc. were added and their thermal performance were studied by different researchers. Table 2.2 shows composites of paraffin wax with the addition of high thermal conductivity materials as used in different studies.

Table 2.2 Composites of paraffin wax used in various studies as PCM

Composite	Thermal conductivity (W/m.K)	Observation	Ref.
Paraffin wax (80 wt. %) with nano magnetite (20 wt. %)	0.40	Addition of 20% nano-magnetite enhanced the thermal conductivity of paraffin by 67%. Use of 10% nano-magnetite increased the composite cost by 20%.	[159]
Liquid paraffin/aluminium foam Solid paraffin/aluminium foam	46.04 46.12	Thermal conductivity of composite increased up to 218 times as compared to the pure paraffin with 26% drop in heat fluxes.	[160]
Liquid paraffin/copper foam	3.11	Copper form reduced the charging time of composite by 40%.	[161]
Paraffin (80 wt. %)/ graphite (20 wt. %) in form of foam, fibers and fins)	0.97	Faster heat transfer was observed in case of graphite fins as compared to its fibers and foam	[162]
Paraffin (80 wt. %)/ waste graphite (20 wt. %) Paraffin (80 wt. %)/ SFG75 (Timrex powder) (20 wt. %)	a) 0.42 b) 0.90	Thermal conductivity enhancement of paraffin with fresh graphite and waste graphite was found to be 300% and 91% respectively.	[163]
a) Paraffin (90 wt. %)/expanded graphite (10 wt. %) b) Paraffin (90 wt. %)/graphite (10 wt. %)	a) 0.93 b) 0.56	Expanded graphite and natural graphite enhanced the thermal conductivity of paraffin by 300% and 150% respectively as compared to pure paraffin.	[164]
Paraffin with expanded graphite (2 wt. %, 4 wt. %, 7 wt. % and 10 wt. %)	0.29, 0.51, 0.68, 0.81 respectively	Thermal conductivity of paraffin increased with graphite content and no leakage of paraffin was observed up to 10% wt. of graphite.	[165]
Paraffin with TiO_2 (1-4 wt. %)	0.7	With increase in TiO_2 loading phase change temperature increases with decrease in latent heat capacity.	[166]
Paraffin with exfoliated graphite nanoplatelets	0.34, 0.43, 0.51, 0.68,	Addition of XGnP enhanced the thermal conductivity of PCM while	[167]

(XGnP) (1 wt. %, 2 wt. %, 3 wt. %, 5 wt. % and 7 wt. %)	0.80 respectively	does not affect its latent heat.	
Paraffin (40%) with light low density polyethylene (60%) and expanded graphite (15wt. %)	1.32	Thermal conductivity of composite increased while latent heat decreased with increase in expanded graphite content in composite.	[168]
Paraffin with kaoline (60%)	0.41	The latent heat of composite was 119.49 J/g while the phase change temperature was 62.4 °C	[169]
Paraffin with multiwalled carbon nanotubes	0.33	Addition of 2% wt. of multiwalled carbon nanotubes enhanced the thermal conductivity of paraffin by 35%.	[170]

It is observed from Table 2.2 that thermal conductivity of paraffin wax changed with the addition of high thermal conductivity materials. However, each additive has its significant role to enhance the thermal property of paraffin wax. In a work Sahan et al. 2015 [159] added nano-magnetite (nanoparticles of magnetite, k=9.7 W/m.K) to enhance the thermal conductivity of paraffin by providing metallic surface for faster heat transfer. In a study by Wang et al. 2014 [166] a composite of paraffin wax with TiO_2 nanoparticles (2 nm diameter) was prepared and its thermal performance was studied and results showed that up to 1% loading of nanoparticles the phase change temperature of PCM decreased with increase in latent heat and with particle loading more than 2% melting point of PCM increased with decreased latent heat. Similarly Nourani et al. 2016 [171] prepared the nano composite of paraffin and aluminium oxide nanoparticles (2.5, 5, 7.5 and 10% wt.) using sodium stearoyl lactyrate as surfactant and found that with the addition of 10% Al_2O_3 nanoparticles, thermal conductivity and melting rate of composite enhanced by 31% and 27% respectively.

Metals foams were also tried with paraffin wax to enhance its thermal properties for efficient thermal storage. In a study, Aluminium foam (k = 218 W/m.K) was added to the paraffin to enhance its thermal conductivity [160] and results showed that in the prepared composite, heat conduction through aluminium foam was more dominant as compared to the natural convection in molten composite which actually enhanced the thermal conductivity of the composite. In another study, Wang et al. 2016 [161] prepared a composite of paraffin with copper foam with pore size of 2-3 nm and porosity of 97.3% and observed that the addition of copper foam reduced the melting

time of composite (M.P. = 42.24 °C, L = 170.4 kJ/kg) by 40% as compared to pure paraffin wax. Studies shows that metallic nanoparticles and metal foams proved to be good enhancer of thermal conductivity of organic PCMs [172–174]. However, due to high cost of these additive materials composite material is not commercially viable for thermal storage systems and their high mass density adds weight to the system.

In addition to the nanoparticles and metal foams there are some other additives such as carbon nanotubes, expanded graphite and exfoliated graphite nano-platelets, which are lighter in weight, having high thermal conductivity and cheaper in cost, and these materials were also tried with paraffin wax to enhance its thermal properties. In a study Fethi et al. 2015 [162] prepared the composite of paraffin wax with different forms of graphite (foams, fibers and fins) and investigated its thermal properties and results showed that with the addition of graphite content (15 wt. %) in the composite its thermal conductivity increased and latent heat decreased. In another study Lacheb et al. 2014 [157] prepared the composites of paraffin wax with waste graphite (obtained from industry) and fresh graphite with 20 wt. % of graphite in each case. Results showed 300% and 91% enhancement in thermal conductivity of paraffin wax with fresh graphite and waste graphite respectively. Raza et al. 2016 [175] prepared the composite of paraffin wax at different weight percent of expanded graphite i.e. 5 wt. %, 10 wt. %, and 15 wt. % and tested them for its thermal conductivity and thermal performance. It was found that for 5 wt. %, 10 wt. %, 15wt. % of expanded graphite, thermal conductivity of composite enhanced by 4 times, 6 times and 6.5 times respectively as compared to pure paraffin.

Wang et al. 2009 [170] prepared the composite of paraffin wax at different weight percentage of multi-walled carbon nanotubes and found that with 2% mass fraction of carbon nanotubes the thermal conductivity of paraffin wax enhanced by 35% in solid phase and 40% in liquid phase. In a similar kind of work Cui et al. 2011[176] prepared the composites of paraffin wax with carbon nanofibers and carbon nanotubes each with mass fraction of 1 wt. %, 2 wt. %, 5 wt. %, and 10 wt. % Results showed that thermal conductivity of composite material increased with the amount of carbon nanotubes and carbon nanofibers. It was also found that composites with carbon nanofibers had more thermal conductivity than the composites with carbon nanotubes. Various other similar studies with graphite, expanded graphite and carbon nanotubes are carried out [173,177–179] which proved that these materials are the promising

option to enhance the thermal conductivity of PCMs. However, due to high production cost of carbon nanotubes their applications are limited while the low cost of expanded graphite dominates its applications for wide range of thermal storage materials.

b) Non-paraffin and their composites

Non paraffin materials consist of various other organic materials like fatty acids, fatty alcohols, amines, glycolic acids etc. These materials have good latent heat and low melting point. However, similar to paraffin wax these materials also have poor thermal conductivity and to improve their thermal performance, materials with high thermal conductivity such as metallic nanoparticles, metal foams, expanded graphite, carbon nanotubes etc. were added. Various non-paraffinic materials and their composites investigated in different studies are shown in Table 2.3.

Table 2.3 Non-paraffin and their composite for thermal storage

Non-Paraffin and composite	Melting point (°C)	Latent heat (kJ/kg)	Thermal conductivity (W/m.K)	Ref.
Polyglycol E600	22	127.20	0.21	[180]
Polyethylene glycol 6000	64.20	231	0.30	[181]
Vinyl stearate	29	122	0.25	[21]
Butyl Stearate	19	140	0.21	[182]
1-Dodecanol	26	200	0.16	[183]
n-Octadecane	28	243.50	0.14	[184]
Palmitic acid	57.80	185.40	0.16	[185]
Palmitic acid (41.1%) with SiO_2	59.76	85.11	n.a.*	[186]
Palmitic acid (50.11%) with graphene oxide	60.05	101.40	1.02	[187]
Palmitic acid (91.94%) with graphene nanoplatelets (GNPs)	61.16	188.90	2.11	[187]
Palmitic acid (80%) with expanded graphite (20%)	60.88	148.36	0.42	[188]
Capric acid	32	152.70	0.15	[189]
Caprylic acid	16	148	0.14	[190]
a) Stearic acid with expanded graphite (2%, 4%, 7% and 10%) b) Stearic acid with carbon nanofibers (2%, 4%, 7% and 10%)	68.80	a) 183.10 b) 184.60	a) 0.79 b) 0.61	[191]
Stearic acid (83%) with expanded graphite	53.12	155.70	n.a.*	[192]

a) Stearic acid /polymethylmethacrylate(PMMA) b) Palmitic acid/PMMA c) Myristic acid/PMMA d) Lauric acid/PMMA	67.31 59.98 51.00 40.96	187.72 173.89 166.56 149.55	n.a.	[193]
Stearic acid with modified expanded vermiculite	65.90	146.80	0.58	[194]
Myristic acid	51.50	204.50	n.a.	[195]
Lauric acid (70%)/vermiculite with 10% expanded graphite	41.88	126.80	0.81	[196]
Polyethylene glycol with expanded graphite (4, 6, 8, 10 wt. %)	50.40, 46.90, 42.90, 41.80 respectively	165.10, 153.20, 116.20, 108.10 respectively	2.10, 2.91, 4.53, 6.11 respectively	[169]
Polyethylene glycol with expanded graphite (10 %)	61.46	161.20	1.32	[197]
Stearic acid (51.80) with polymethylmethacrylate	60.40	92.10	n.a.	[198]

* not available

Sharma et al. 2016 [181] studied the change in thermal properties of polyethylene glycol 6000 for 1500 thermal cycles of charging and discharging and found 6.5% reduction in melting point. It was also observed that after 500 cycles, 1000 cycles and 1500 cycles latent heat of PCM reduced by 19%, 22% and 25% respectively while no change in chemical structure was observed in Fourier transform infra-red (FTIR) analysis. In another study Lv et al. 2016 [169] prepared the composites of polyethylene glycol (PEG) with expanded graphite to enhance its thermal conductivity and found that the melting time of composites with 4 wt. %, 6 wt. %, 8 wt. % and 10 wt. % of expanded graphite was reduced by 46.32%, 30.89%, 15.49% and 4.82% respectively. In a similar study [197] composite of PEG and expanded graphite (10%) was prepared and investigated for its thermal properties. Result showed that thermal conductivity, melting point and latent heat of composite was found to be 1.32 W/m.K, 61.46 °C and 161.2 J/g respectively. All these studies showed that PEG and its composite with expanded graphite can be used as possible thermal storage material and require detail investigation before use.

In some other investigations fatty acids have been used as phase change material for latent heat storage. Sari et. al. 2002 [185] studied the thermal performance of Palmitic acid within a concentric tube type thermal storage unit and found significant reduction in its melting and solidification behavior when PCM tube was aligned in horizontal position as compared to vertical position with 53.3% heat storage efficiency. Sharma

et al. 2016 [199] investigated the Palmitic acid for 1500 thermal cycles and observed the change in melting temperature by 3.27% and latent heat of fusion by 17.80%. Fang et al. 2011[186] prepared the composite of Palmitic acid (41.1 %wt.) with silicon dioxide and studied its thermal and chemical properties. Scanning electron micrographs (SEM) of composite showed that palmitic acid was well dispersed within the porous structure of SiO_2. DSC analysis of composite revealed the melting point and latent heat of composite as 59.76 °C and 60.55 kJ/kg respectively. Mehrali et al. 2013 [187] prepared the composite of Palmitic acid with graphene oxide to enhance its thermal conductivity by 1.02 W/m.K which is three time more as compared to that of pure Palmitic acid (0.21/m.K). From DSC analysis the melting point and latent heat of composite was found to be 60.05 °C and 101.49 kJ/kg respectively. Similar composites of Palmitic acid was prepared by addition of materials with high thermal conductivity such as graphene nanoplates, expanded graphite etc. and investigated for their thermal properties [200–202].

Konukulu et al. 2014 [190] prepared the microcapsules of caprylic acid with different types of shell materials such as urea-formaldehyde (UF) resin, urea-melamine (UM) resin and urea-melamine-formaldehyde (UMF) acid and found that the microcapsules with UF shell were more stable for thermal storage applications. Similarly, Alkan et al. 2008 [193] encapsulated different fatty acids such as Stearic acid (SA), Palmitic acid (PA), Myristic acid (MA) and Lauric acid (LA) with poly-methyl methacrylate (PMMA) and studied them as thermal storage material. The share of fatty acid in a micro-capsule was maintained at 80% and it was found that at the temperatures above the melting point of PCM, these microcapsules did not change their shape and remain stable.

Lauric acid was also used with vermiculite in form of composite [196]. The melting point and latent heat of composite was found to be 41.88 °C and 87.21 kJ/kg respectively. 10% of expanded graphite was further added to this composite to increase its thermal conductivity from 0.49 W/m.K to 0.81 W/m.K. In another work, Karaipekli et al. 2007 [191] prepared the composite of stearic acid with expanded graphite and carbon fibers with 2%, 4%, 7% and 10% wt. of each carbon material. Result of the study showed that with addition of 10 wt. % expanded graphite and carbon fiber the thermal conductivity of composite enhanced by 266% and 206% respectively. It was also found that with the addition of expanded graphite and carbon

fibers the latent heat of stearic acid (198.8 J/g) decreased to 183.1 J/g and 184.6 J/g respectively. In other work composite of stearic acid and expanded graphite (25 wt. %) was prepared and tested by Wu et al. 2016 [203] . In this study it was found that addition of expanded graphite can enhance the thermal conductivity of composite up to 23.27 W/m.K. Similarly various other fatty acids such as Myristic acid, Lauric acid etc. were also studied as potential phase change materials [200, 201].However, it was found that fatty acids are very costlier and having low thermal conductivity which limits their wider range of applications. Findings from the studies showed that eutectic mixture of fatty acids is more efficient in terms of melting point and latent heat as compared to individual fatty acids. Some eutectic mixtures of fatty acids and their composites are presented in Table 2.4 as phase change materials.

Table 2.4: Eutectic mixtures of fatty acids and their composite for thermal storage

Eutectic Mixture of fatty acids	Melting point (°C)	Latent heat (kJ/kg)	Observations	Ref.
Capric acid (65.12 wt. %) and Lauric acid (34.88 wt. %)	19.10	35.24	Variation in melting point and latent heat was observed after 360 thermal cycles.	[206]
a) Lauric acid: stearic acid (75.50:24.50 wt. %), b) Myristic acid and palmitic acid (58:42 wt. %), c) Palmitic acid and stearic acid (64.20:35.80 wt. %)	a) 37.00 b) 42.60 c) 52.37	a) 182.70 b) 169.70 c) 181.70	The melting point and latent heat of each eutectic mixture is less than the melting point and latent heat of individual fatty acid.	[207]
a) Lauric acid-Myristic acid (LA, 66 wt. %-MA, 34 wt. %) b) Lauric acid-Palmitic acid (LA, 69 wt. %-PA, wt. %) c) Myristic acid-Stearic acid (MA, 64 wt. %-SA, 36 wt. %)	a) 34.20°C b) 35.20°C c) 44.10°C	166.80 166.30 182.40	Prepared mixtures were found to be suitable for low temperature solar thermal application.	[208]
Myristic acid (64% wt.) - Stearic acid (36% wt.)	44.13	182.40	The melting point of eutectic mixture is less than the individual fatty acids i.e 67.83 °C for myristic acid and 52.32 °C for stearic acid.	[209]
Palmitic acid (64.2 wt. %)- Stearic acid (35.8 wt. %)	52.30	181.70	Prepared eutectic mixture was found to be suitable for passive space heating and domestic water	[210]

			heating application.	
Eutectic mixture of myristic acid (58.40 wt. %) and palmitic acid (41.60 wt. %)	42.60	169.70	This eutectic mixture has potential for low temperature thermal storage.	[211]
Eutectic mixture of capric acid, 76.50 wt. % and palmitic acid, 23.50 wt. %	21.85	171.22	Prepared composite had long term thermal stability which may be due to chemical impurities or chemical degradation of PCM	[212]
Lauric acid– Palmitic acid	35.20	166.30	Prepared mixture of Lauric acid-palmitic acid can be a potential material for thermal energy storage in terms of its thermal properties.	[213]
Myristic acid (70 wt.%)-Palmitic acid (30 wt. %) with 5 wt. % of sodium myristate.	n.a*	n.a.	Addition of surfactant enhanced thermal conductivity as well as latent heat of PCM	[214]
a) Myristic acid Palmitic acid with sodium myristate b) Myristic acid Palmitic acid with Sodium palmitate	41.36	179.12	Both eutectic mixtures showed little degradation in thermal properties after 3600 thermal cycles. Both mixtures were found to be useful in terms of thermal stability and economy.	[215]
Capric-Myristic acid (50 wt. %) / Expanded perlite composite (40 wt. %)/ Expanded graphite (10 wt. %)	n.a.	n.a.	Addition of expanded perlite and expanded graphite increased the thermal conductivity of eutectic mixture by 60%.	[216]

* not available

Shilei et al. 2006 [206] studied the eutectic mixture of Capric acid (64.12% wt.) and Lauric acid (34.88% wt.) in wall boards of heating, ventilation and air conditioning (HVAC) systems. Characterization of these materials showed melting point and latent heat as 19.108 °C and 35.23 J/g respectively. It was found that after 360 thermal cycles the melting point and latent heat of eutectic mixture reduced to 18.35 °C and 35.06 J/g respectively which proved that the mixture had good thermal stability as PCM for its application in HVAC system. In the series of binary mixtures, Sari et al. 2004 [207] prepared and tested the binary mixtures of different fatty acids such as Lauric acid (LA) and Stearic acid (SA), Myristic acid(MA) and Palmitic acid (PA), Palmitic acid (PA) and Stearic acid (SA). DSC analysis showed that the melting point and latent heat of LA-SA (75.50:24.50 wt. %) MA-PA(58:42 wt. %) and PA-SA

(64.20 :35.80 wt. %) were found to be 37.00 °C, 42.60 °C, 52.30 °C and 182.70 J/g, 169.70 J/g, 181.70 J/g respectively.

In another study, Sari et al. 2005 [208] prepared and characterized the eutectic mixture of Lauric acid (66 wt. %)- Myristic acid (34 wt. %), Lauric acid (69 wt. %)- Palmitic acid (31 wt. %), Myristic acid (64 wt. %)- Stearic acid (36 wt. %) using DSC. The melting point and latent heat of LA-MA, LA-PA and MA-SA mixtures were found to be 34.2 °C, 35.2 °C and 44.10 °C and 166.80 J/g, 166.30 J/g, 182.40 J/g respectively. Results showed that after 146 thermal cycles the change in the melting points and latent heat were found in the range of -0.31-14 °C and 0.9-2.4% for LA-MA mixture, -0.40-0.23 °C and 1.5-3% for LA-PA mixture, 1.11 °C-0.26 °C and -1.10 -2.20% for MA-SA mixture.

Baran et al 2003 studied a eutectic mixture of Palmitic acid (PA, 64.2 wt. %) and Stearic acid (SA, 35.8 wt. %) for low temperature thermal storage application and found it to be stable after various thermal cycles. Fauzi et al. 2015 [215] prepared and studied the eutectic mixture of Myristic acid/Palmitic acid with Sodium myristate (MA/PA/SM) and Myristic acid/Palmitic acid with Sodium palmitate (MA/PA/SP). Thermal properties of both the eutectics were analyzed after 3600 thermal cycles and it was found that the melting point of MA/PA/SM and MA/PA/SP increased by 1.54 °C and 1.39 °C respectively while 2.84% and 6.70% reduction in the latent heat of fusion was observed for MA/PA/SM and MA/PA/SP respectively after 3600 cycles. Various other studies on eutectic mixtures of fatty acids with improved thermal properties have been found in literature which proved their potential as thermal storage material for wider range of applications [189,210,213].

Available studies showed the potential of eutectic mixture as phase change materials. However, their lower thermal conductivity required the addition of material with high thermal conductivity. Table 2.5 listed the outcomes by different researchers on composites of eutectic mixture for thermal storage application.

Wang et. al. 2010 [217] prepared the composites of eutectic mixtures such as Capric acid-Lauric acid, Capric acid-Myristic acid and Lauric acid-Myristic acid with poly methyl methacrylate (PMMA) and tested them for their comprehensive strength and thermal stability. The ratio of each eutectic mixture with PMMA in case of each composite was maintained as 50:50. This study showed maximum strength with latent

heat of 113.2 kJ/kg for the prepared composite material. Thermo gravimetric analysis (TGA) results of all these composites at high temperature revealed their better thermal resistance as compared to pure fatty acids and were found to be the suitable building materials. In another work composite of Capric acid-Myristic acid (CA-MA) eutectic mixture with vermiculite was prepared by vaccum impregnation method [218] and characterized for its surface properties which showed that up to 20% of CA-MA could be retained within the pores of vermiculite without any leakage. To enhance the thermal conductivity of CA/MA/vermiculite composite 2% of expanded graphite was added to it. Measured thermal conductivity of CA-MA, CA-MA/vermiculite and CA-MA/vermiculite/expanded graphite was found to be 0.15, 0.12 and 0.22 W/m.K respectively and it was observed that melting point of composite was reduced by -1.75 °C after 3000 thermal cycles.

Table 2.5 Composite of eutectic mixture of fatty acids for thermal storage application

Composites	Melting point (°C)	Latent heat (kJ/kg)	Observation	Ref.
a) Capric acid-Lauric acid/Polymethylmethacrylate (PMMA) b) Capric acid-Myristic acid/PMMA c) Capric acid-Stearic acid/PMMA, d) Lauric acid-Myristic acid/PMMA	a) 21.11 b) 25.16 c) 26.38 d) 34.81	a) 76.30 b) 69.32 c) 59.29 d) 80.75	All the composite in were found to be suitable for building applications in terms of thermal stability and comprehensive strength	[217]
Capric acid-Myristic acid/vermiculite composite with 2% expanded graphite	23.35	27.46	After 3000 thermal cycles little variation in thermal properties of composite was observed	[218]
Lauric-Myristic-Palmitic acid with expanded graphite	31.41	145.80	The composite was having low melting point and suitable for low temperature thermal storage	[219]
Lauric acid-Stearic acid (43.5 wt. %) with expanded perlite	33.00	131.30	Euctectic mixture of Lauric acid and stearic acid (7:3) was suitable for temperature control in buildings	[220]
Capric-Palmitic-Stearic acid with expanded graphite	21.33	131.70	Thermal properties of the proposed eutectic showed little variation after 500 cycles and found to be suitable for thermal energy storage.	[221]
Myristic (54%)-Stearic	42.70	148.12	Carbon nanotubes (15%)	[222]

acid with carbon nanotubes (15%)			increased the thermal conductivity of eutectic from 0.173 W/m.K to 0.283 W/m.K.	
Capric-Lauric acid with diatomite	16.74	66.81	Latent heat of composite depends on the PCM content of eutectic mixture.	[223]
Capric-Palmitic acid with attapulgite composite	21.71	48.20	Optimum amount of eutectic that can be absorbed onto the surface of attapulgaite was found to be 35%.	[224]
a) Malic-Palmitic-Sodium palmitate/Shorea javanica (3%) b) Myristic-palmitic-sodium stearate/ Shorea javanica (3%)	a) 41.92 b) 41.91	a) 176.23 b) 176.19	In case of both the composites, 3% addition of shorea javanica found to be suitable in terms of both latent heat and thermal conductivity.	[225]
Palmitic-Capric acid (12:88) with diatomite (33%, 50% and 66%) and expanded graphite (3%, 5%)	28.90-29.60	90-149	With addition of 5% of expanded graphite thermal conductivity of composite was enhanced by 25.2% as compared to the pure eutectic.	[226]
Myristic-Palmitic-Stearic acid (52.2:29.4:4.18) with expanded graphite (13:1)	41.64	153.50	After multiple thermal cycles melting point and latent heat of composite was reduced by 0.28°C and -1.63% respectively.	[227]
Capric acid-Lauric acid with expanded graphite	11.13	115.91	Thermal conductivity of eutectic mixture with 5% of expanded graphite was enhanced by 22 times that of the pure acids and found to be more stable.	[226]

In a similar study Zhang et al. 2013 [219] prepared the composite with the eutectic mixture of Lauric (LA,55.24%) -Myristic (MA,29.74%)-Palmitic acid (PA,15.02%) and expanded graphite (EG) for thermal storage application. The mass ratio of eutectic mixture to EG was maintained as 18:1 with 94.7% absorption of eutectic mixture. Thermal characterization of this composite revealed its melting point and latent heat as 31.41 °C and 145.8 J/g respectively.

Carbon nanotubes were also used to prepare the composite of eutectic mixtures of fatty acids for low temperature thermal energy storage. Tang et al. 2016 [222] prepared the composite with binary eutectic mixture of Myristic acid (54 wt. %) Stearic acid (46 wt. %) and carbon nanotubes. Carbon nanotubes at different mass percentage i.e. 3%, 6%, 9%, 12% and 15% were tried with this eutectic mixture and it

was found that the minimum 9% mass fraction of carbon nanotubes could be added eutectics without stratification. Thermal conductivity analysis of composites with 9%, 12% and 15% mass fraction of carbon nanotubes showed 23.2%, 49.4% and 63.7% increase in thermal conductivity in solid state and 15.6%, 32.0% and 39.7% in the liquid state respectively.

Some other composites of eutectic acids are also available in literatures where non-carbon materials were added to fatty acids as support material for faster conduction of heat. Zhang et al. 2016 [221] prepared a composite of ternary mixture of Capric acid (CA, 79.3% wt.)-Palmitic acid (PA, 14.7 wt. %)-Stearic acid (SA, 6.0 wt.%) with attapulgite and characterized it for its thermal and chemical properties. The melting point and latent heat of composite was found to be 21.33 °C and 131.7 kJ/kg respectively suitable for low temperature application. In similar kind of work [226] composite of Palmitic-Capric acid eutectic mixture was prepared with diatomite at ratio of 2:1 which was found to be thermally stable after various thermal cycles.

In one other investigation, Fauzi et. al. 2016 [225] prepared the composite of Myristic acid-Palmitic acid-Sodium palmitate with Shorea javanica (MA/PA/SP/SJ) and Myristic acid-Stearic acid-Sodium palmitate with Shorea javanica (MA/SA/SP/SJ). Shorea javanica also known as damar gum harvested from tropical forest of Indonesia, and used as porous material and thermal conductivity enhancer in this study. Composites of both the eutectic with 1%, 2%, 3%, 4% and 5% mass percentage of shorea javanica was prepared and tested for its thermal properties. Results showed that in both the composites melting point and latent heat of fusion of eutectic was reduced while thermal conductivity increased with increase in mass percentage of shorea javanica up to 3% wt. after which no significant increase in thermal conductivity was observed. Thermal conductivity values for MA/PA/SP/SJ and MA/SA/SP/SJ with 3% wt. of shorea javanica was found to be 0.52 W/m K and 0.56 W/m K respectively.

The available studies show that the organic PCMs including individual fatty acids or their eutectics could be a good option for low temperature thermal storage application. However, due to their high cost of production, application of these organic materials for wide range of applications are limited and there is a need to identify some new phase change material which is locally and naturally available and cheaper in cost.

In this work natural beeswax is introduced as a new phase change material for latent heat storage and to enhance its thermal conductivity expanded graphite was added. Beeswax is obtained from honey bees consisting of fatty acids (mainly palmitic acid, tetracosanoic acid and oleic acid), long chain of alkanes, monoesters (C_{24} to C_{34}), diesters, and hydroxyl-monoesters [228] and mainly used for making sculptures, candles and also in food and medical industries for surface coatings. Beeswax also finds potential application in the field of drug delivery and proved more efficient as compared to other waxes in faster release of drugs [225, 226]. Despite of its wide applications in the food, medical and other sectors the application of beeswax as thermal storage material is not studied much.

Natural beeswax is non-toxic, non-corrosive, having low melting point (60 ºC-68 ºC), high latent heat of transition (145-178 kJ/kg), small volume change, low vapor pressure and long term chemical stability almost similar to conventional paraffin [20, 227]. Being a natural product its cost is quite less as compared to other organic materials and its production and degradation does not involve any toxic byproduct which makes it a sustainable product [232] and could be a potential substitute in place of paraffin and other organic PCMs as latent heat storage material.

ii) Inorganic phase change materials

Inorganic phase change materials include various salt hydrates and metallics. The melting point of inorganic PCM's is generally higher as compared to organic PCM and therefore useful for high temperature thermal storage applications. They also have high latent heat of fusion which does not undergo degradation with repeated cycles of charging and discharging as observed in the case of organic PCMs. A list of different inorganic PCMs which is used as potential phase change material is included in Table 2.6.

Due to high energy density, salt hydrates such as $CaCl_2.6H_2O$, $MgCl_2.6H_2O$, $Na_2S.5\ H_2O$, $Na_2S.9\ H_2O$ etc. are some of the potential inorganic PCMs for high temperature thermal storage uses. There are various investigations performed on these hydrates to study their thermal storage performance. Tyagi et al. 2014 [233] studied the thermal stability of $CaCl_2.6H_2O$ after 1000 thermal cycles and found very little variation in its melting point (24 °C) and latent heat (140 kJ/kg) which was reduced to 23.26 °C and 125.4 kJ/kg respectively.

Table 2.6 List of inorganic materials used for thermal storage application

Inorganic PCM's	Melting point (°C)	Latent heat kJ/kg	Observation	Ref.
$CaCl_2.6H_2O$	24	140	After repeating thermal cycles small variation was observed in the thermal properties of salt.	[233]
$MgCl_2.6H_2O$	110.80	137.96	Little variation in thermal properties was observed after 1000 thermal cycles and solidification occurred without super cooling.	[234]
$Zn(NO_3)_2.6H_2O$	36.10	146.95	Salt with moderate thermal performance.	[235]
$Na_2HPO_4.12H_2O$	38	278.84	Salt of high thermal performance.	[235]
$Na_2SO_4.10H_2O$	32.40	254	Salt of high thermal performance with low cost.	[235]
KNO_3 -$NaNO_3$	260	118	Salt with 3 times more sensible heat and a uniform latent heat over the melting range (220 °C-262 °C).	[236]
$LiNO_3$ or $CaNO_3$ with $KNO_3/NaNO_3$	130	130.61	Addition of calcium nitrate and lithium nitrate reduce the melting point of mixture to 130 °C. Combined viscosity of $LiNO_3$ and $CaNO_3$ is less than the viscosity of individual salts.	[237]
$LiNO_3$-$NaNO_3$-KNO_3	121	140.50	Oxygen environment had favorable effect on nitrate/nitrite environment and thermal stability of mixture was limited up to 500 °C.	[238]
$NaNO_3$-KNO_3	220	122.89	Natural convections were strong in pure salts while weakened for its composite form. Heat retrieval time was reduced by 28.8% and 19.3% for composite with copper foam and nickel foam respectively.	[239]
Na_2CO_3-NaCl	637	283.30	After 50-100 thermal cycles significant weight loss of PCM was observed with marginal variation in its thermos-physical properties.	[240]
NaCl–$CaCl_2$–$MgCl_2$	424	190	The proposed mixture with good latent heat and low viscosity was used as phase change material	[241]
NaCl–KCl–$ZnCl_2$ Eutectic mixture	250	70	Eutectic mixture at different ratios of salts The working temperature range for mixture lies in between 250 °C to 800 °C.	[242]
LiF–Na_2CO_3–K_2CO_3, eutectic ternary system	421.25	222.84	The low melting point and relatively high heat capacity of the mixture (1.90 J/K) makes it a suitable PCM. The experimental enthalpy was found to be 38.7% lower than the calculated indicates the formation of cluster during phase transformation.	[243]

Sebaii et al. 2011 [234] tested the thermal stability of $MgCl_2.6H_2O$ for indoor solar cooking and found that after 1000 thermal cycles of melting and solidification, the melting point of $MgCl_2.6H_2O$ slightly raised from 110.80 °C to 115.39 °C and its latent heat of fusion decreased from 137.96 kJ/kg to 130.28 kJ/kg.

Canbazoglu et al. 2005 [235] studied the heat storage performance of a solar water heater consist of salt hydrates such as zinc nitrate hexahydrate ($Zn(NO_3)_2.6H_2O$), disodium hydrogen phosphate dodecahydrate ($Na_2HPO_4.12H_2O$), calcium chloride hexahydrate ($MgCl_2.6H_2O$) and sodium sulfate decahydrate ($Na_2SO_4.10H_2O$) and observed that the amount of accumulated heat by solar heater with PCM was 2.59-3.45 times greater than the conventional solar energy storage system without PCM. It was also observed that disodium hydrogen phosphate dodecahydrate and sodium sulphate decahydrate were the salts with high thermal energy storage performance which required lower tank volume and less insulation material during application.

In another study, Martin et al. 2013 [236] prepared the non-eutectic mixture of KNO_3 (30%)-$NaNO_3$ (70%) and studied its thermos-physical properties. Results of the study showed the melting point range and sensible heat of the mixture was 220 °C-260 °C and 1.55 kJ/kg.K respectively and no segregation in the melting range was observed even after 90 thermal cycles. However, sensible heat of the proposed mixture was raised by 3 times in this melting range and it can be used as replacement of sensible heat storage material for high temperature thermal storage.

Findings from various studies revealed that the properties of nitrate salt mixture depends on its composition and can be altered by subsequent addition or removal of one or more salt. Fernandez et al. 2015 [237] studied the effect of addition of $LiNO_3$ and $CaNO_3$ on the thermal storage performance of sodium nitrate and potassium nitrate. During the study 20% $LiNO_3$ + 52% KNO_3 + 28% $NaNO_3$ and 30% $LiNO_3$ + 10% $Ca(NO_3)_2$ + 60% KNO_3 salt mixtures were prepared and tested for their thermal and physical properties . Results showed that the melting point of these mixtures were in the range of 130.15 °C-586.32 °C and 132 °C-571 °C respectively and their specific heat were 1.091 J/g °C and 1.395 J/g°C respectively. In a similar study by Olivaris et al. 2013 [238] thermal properties of $LiNO_3$-$NaNO_3$-KNO_3 were studied by DSC analysis, mass spectrometry and thermogravimetric. The nitrite/nitrate equilibrium under different environmental conditions such as argon environment,

oxygen environment and air environment were also studied and results showed that the evolution of NO occurred at 325 °C in argon environment, at 425 °C in nitrogen environment and at 540 °C in oxygen environment and therefore, presence of oxygen environment is good for nitrite/nitrate equilibrium. The salt mixture was found to be less stable at 500 °C in air environment.

Chloride salts were also studied for various thermal storage applications and in one study Wei et al. 2015 [241] prepared a ternary mixture of NaCl, $CaCl_2$ and $MgCl_2$ for high temperature (above 550 °C) thermal storage applications. The density of proposed mixture (M.P. 424 °C) was decreased linearly with increase in temperature from 500°C-750°C and it was thermally stable after various thermal cycles. In another study, [240] a binary eutectic mixture of Na_2CO_3 (59.45 wt. %)-NaCl (50.55 wt. %) was prepared and studied by simultaneous thermal analyzer (STA) which gave melting point and latent heat of mixture as 637 °C and 283.3 J/g respectively. The thermal stability of this mixture was found to be more in CO_2 environment as compared to N_2 environment up to 700 °C temperature.

Another category of inorganic phase change materials are metallic which are metals with low melting point. The properties of metallic are low heat of fusion, low specific heat. Although metallic having high thermal conductivity are not considered for thermal storage applications due to their high mass density [61,199].

Results of the studies carried out by the different researchers on inorganic materials like salts and their mixtures showed that these inorganic materials are suitable for high temperature thermal storage. However, there are certain drawbacks of using inorganic materials for thermal energy storage such as low thermal conductivity, corrosion of container wall, and high cost. Various materials with high thermal conductivity were tried with inorganic PCM to enhance its thermal conductivity such as nanoparticles [172], expanded graphite [177], multiwall carbon nanotubes [170] etc. Out of these additives, graphite and expanded graphite are preferable due to their light weight and high thermal conductivity. A list of composites of inorganic phase change materials investigated by different researchers is compiled and presented in Table 2.7.

Table 2.7 Composites of inorganic phase change materials

Inorganic composite	Thermal conductivity (W/m.K)	Observation	Ref.
$KNO_3/NaNO_3$-graphite composite (80 wt. %/20 wt. %)	20	Thermal conductivity of mixture was raised with the addition of expanded graphite	[244]
Non-eutectic mixture KNO_3 (30 wt. %)/$NaNO_3$ (70 wt. %)	0.50	Salt mixture had wide temperature range between 220-260 °C for melting and freezing cycle	[236]
Na_2CO_3/MgO with multiwall carbon nanotubes (0.5 wt. %)	1.13	Addition of carbon nanotubes improved the thermal conductivity of mixture but reduced its thermal stability.	[245]
Attapulgite granulate impregnate with the mixture of $MgSO_4$ (20 wt. %) and $MgCl_2$ (80 wt. %)	n.a.*	Heat of absorption increased with the amount of $MgCl_2$.	[246]
$LiNO_3$/KCl (70 wt. %)-expanded graphite	15	Expanded graphite increased the thermal conductivity of composite with decreased latent heat	[247]
a) $LiNO_3$–KCl/EG b) $LiNO_3$–$NaNO_3$/EG c) $LiNO_3$–NaCl/EG	a) 5.59 b) 6.61 c) 4.71	Addition of expanded graphite enhanced thermal conductivity of binary salts by 4.9-6.9 times as compared to the pure salts	[248]
NaCl–$CaCl_2$/Expanded graphite (20 wt. %)	4.93	The proposed composite showed promising results 701% increase in thermal conductivity as compared to the pure chloride bi-eutectics.	[249]
$NaNO_3$/Expanded Perlite	1.14	Increase in expanded perlite content from 10 to 60% decreased the thermal conductivity of the composite.	[250]

*n.a.

Acem et al. 2010 [244] tried various percentages of expanded graphite (15%-20%) with the eutectic mixture of $KNO_3/NaNO_3$ and found that the cold compression technique for composite preparation was more efficient to improve the thermal conductivity of the salts. It was also observed that for graphite percentage of 15 wt. % to 20 wt. %, thermal conductivity of composite salt enhanced by 20 times as compared to pure salts. In a similar kind of work, Huang et al. 2014 [247] prepared a composite of $LiNO_3$/KCl and expanded graphite having melting point equal to 200 °C and observed that addition of expanded graphite did not has significant effect on the melting point of the salt, however, its latent heat value was reduced from 178.10 to 142.14 J/g. and thermal conductivity of composite was increased by 15 W/m.K.

Zhong et al. 2014 [248] also prepared the composites of $LiNO_3$–KCl (58.1-48.9%), $LiNO_3$–$NaNO_3$ (49-51%) and $LiNO_3$–NaCl (87-13%) with expanded graphite and notice that at different mass percentages of expanded graphite thermal conductivity of composites raised by 4.6-6.9 times as compared to the pure salts. Due to low cost, lithium salts were also considered as potential salt for thermal storage applications and preferred by most of the researchers.

Some researchers also tried metallic nanoparticles with molten salts to enhance their thermal conductivity. Myres et al. 2016 [251] doped the nitrate salts with cupric oxide nanoparticles and studied its thermal properties. In this study it was found that thermal diffusivity of potassium nitrate and sodium nitrate increased up to 300 °C and 150 °C respectively and there is not much observed variation in the stability of these salts with the addition of CuO nanoparticles. In a similar kind of work [252] composite of NaCl and alumina nanoparticles were prepared and tested for its thermal properties and found that alumina nanoparticles prevented the leakage of NaCl from the composite. The enthalpy of prepared composite was measured as 362 kJ/kg. Similar other works are available with the addition of metallic nanoparticles to enhance the thermal properties of salts [253,254]. Findings of the studies showed that composites of inorganic materials could be promising options for high temperature thermal energy storage. However, due to high cost and corrosive nature their applications for wider applications are still restricted and need to be re-evaluated on large scale before commercial use.

2.3.2 Latent heat storage system

Performance of latent heat storage system significantly depends upon the heat storage material used in the application and the system geometry. Selection of heat storage material is based on the temperature range of application. For low temperature thermal storage applications, organic PCMs and their mixtures are preferable while for high temperature thermal storage inorganic PCMs can be used. Geometry of a heat storage unit should provide maximum surface area for the heat transfer between source and PCM. Different geometrical designs of thermal storage unit studied by the researchers are presented in Table 2.8. These designs include cylindrical or rectangular heat storage unit consisting of single tube, multiple tubes and triplex tube for the flow of HTF. In some geometrical arrangements fins were added with the

tubes to increase the surface area for heat transfer. However, addition of fins increase weight of the system and reduced the amount of PCM used in the storage unit which decreased overall heat storage capacity of the system. Material used for PCM container should be well insulated from outside and it should not react with the phase change material.

Table 2.8 Different geometrical designs used for thermal storage unit

Geometry and container material	PCM used	Parameters studied	Observations	Ref.
Horizontal cylinder of acrylic plastic with copper pipe containing longitudinal and angular fins	Dodecanoic acid	Effect of inlet temperature, flow rate of HTF and configuration of fins	In both fin arrangement conduction is dominant followed by convection, high inlet temperature reduces melting time, flow rate did not have considerable effect on melting profile of PCM.	[255]
Vertical cylindrical of acrylic plastic with two copper pipe connected to longitudinal fins	Dodecanoic acid	Simultaneous charging and discharging rates	Simultaneous heat transfer limited by solid PCM between two pipes, high flow rate of cold HTF allows better heat recovery. Uncertainty in input energy and energy recovery is large.	[256]
Double tube heat storage container with outer tube made of steel for PCM storage while inner tube of brass for flow of HTF	Paraffin wax	Effect of increasing inlet temperature and mass flow rate on charging and discharging process of PCM	Heat flow rate increase by 25% and 11% during melting and solidification on increase and decrease of HTF temperature by 2ºC. Increase in 4ºC of temperature of inlet water reduce the melting time by 31%.	[257]
Vertically arranged cylindrical enclosure with vertical pipe along its axis	Paraffin wax	Analysis of PCM melting process with natural convection, duration of melting followed by time dependent numerical simulations.	Numerical simulation validated the features predicted by theory.	[258]
Cylindrical shell	Paraffin wax	Melting profile of	Melting process	[77]

and tube type with inner copper tube for HTF flow and outer shell part made of polypropylene		paraffin wax were studied at different values of eccentricity i.e. e = 10mm, 20mm and 30mm.	dominated by conduction followed by convection and more enhanced in upper part of shell. 67% decrease in melting time was observed in case of eccentric geometry = 30mm than concentric geometry.	
Triplex tube heat exchanger with outer, inner and middle tubes made of copper with PCM filled between the inner tube and middle tube while HTF flows between the middle tube and outer tube.	RT82	Heat enhancement techniques were studied using inside outside tube, effect of fin length on enhancement technique was studied.	No considerable effect on melting rate of PCM in both the three enhancement techniques. Complete melting was reduced to 43.3% as compare to TTHX without fin.	[259]
Fin and Tube Heat exchanger with space between the rectangular shell and between the fins filled with PCM	R35	Flow rate, Inlet temperature of HTF and effect of fin pitch on charging and discharging process.	Increasing flow rate from 0.2 L/min to 0.4 L/min at temperature 60 ºC showed significant change in PCM melting time while further increase in flow rate reduces it. Melting time also reduces on increasing fin pitch.	[260]
Studied two systems a) Shell and tube type with copper tube embedded along with aluminium fins (PCM-HX). b) Embedded copper tube in the highly conductiv e graphite-wax	PT43 wax	Comparison of technology to enhance the thermal conductivity of wax was studied, economics of system, charging discharging time, inlet and outlet temperature of HTF were also studied.	PCM HX and Copper tube in composite both performed well in their operations. PCM-HX only occupies 38% of water storage volume as compare to the copper tube based unit. The PCM unit can store 5 times more energy than water in useful range 40ºC-52ºC.	[261]

composite				
Flat plate latent heat storage. HTF flow in the chamber between the flat carbon steel.	Mobiltherm 603 Thermal conductivity(0.122 W/K)	Temperature gradients, flow rates and insertion of heat transfer structures	Insertion of various heat transfer structures provide phase change discharge time between 2 to 8 hours. Flat plate's collector offers wide range of flexibility with HTF, insertion of heat transfer enhancement structure.	[262]
Flat plate latent heat storage unit with flat slabs of phase change material.	Carbonate salts(solar salts), liquid sodium, air, CO_2 and steam	Comparison between liquid and gaseous HTF, heat transfer characteristics between the slabs, heat transfer rates and liquid fraction profiles were studied	Liquid sodium delivers maximum 99.4% electrical energy to grid relative to the ideal cases. Solar salts achieved 93.6% of electricity delivered while air, CO_2 and steam delivers 87.9% and 91.3% of electricity delivered.	[263]
Vertical stacks of rectangular cavities filled with PCM	Rubitherm RT28HC Micronal DS5001X (Microencapsulated) PCM	Time required for melting and solidification was studied, control temperature value on hot surface of test sample and period of thermal regulation was studied.	Microencapsulated PCM (Micronal DS5001X) accelerated the charging process with no thermal stratification. Control temperature regulation and thermal regulation period both reduced in microencapsulated form. Sub cooling effect cannot be neglected in case of free PCM	[264]
Rectangular container with one wall made up of aluminium alloy. Holes were dig from the aluminium plate side to allow water to pass through the wall as HTF.	Lauric acid	Melt fraction, temporal heat storage, heat transfer characteristics.	Melting initiated by conduction followed by convection. In liquid state of PCM stratification of temperature occurs led to depression of convection.	[265]

Liu et al. 2014 [263] studied the heat transfer effect in a horizontal acrylic cylindrical container with single copper tube having longitudinal and axial fins and observed that with increase in inlet fluid temperature the melting time of PCM reduced and no

effect was observed with the variation in flow rate. Same effect on melting time of PCM was also observed on vertical heat storage unit with cylindrical geometry.

In another study by Mat et al. 2013 [259], heat transfer fluid was passed through the center and outer part of phase change material (known as triplex tube heat exchanger unit) to reduce charging time of heat storage. However, in such assembly heat loss was observed from the outer surface of the unit when it was not properly insulated and therefore, such geometry was not a attractive option for heat storage application.

Cano et al. 2016 [266] designed and studied a tube in tube type of heat exchanger with outer iron tube (diameter 82 mm) and inner steel tube (diameter 17 mm) and found that PCM Rubitherm RT42 was a good material in terms of storing highest amount of energy transferred from heat transfer fluid i.e. water and the microcapsules of PCM 35 slurry was found to be suitable for counter flow heat storage system. Khan et al. 2016 [267] tested the thermal storage performance of a shell and tube type thermal storage unit with paraffin wax. Parametric investigation analyzed effect on performance due to number of tubes, length and thickness of longitudinal fins, material of shell and inner temperature of heat transfer fluid. Results of the study showed that with increase in the number of tubes from 9 to 21 thermal performance of latent heat system enhanced with 48.5% reduction in melting time. It was also observed that the Fin length of the system has more dominant effect on the thermal performance of the system and with increase in fin thickness from 1mm to 5 mm the thermal storage capacity of the system reduced by 5.7%. Regarding the material of the shell and tube system, fins and tubes made up of copper, aluminium and aluminiun 6063 showed better performance for heat storage as compared to steel AISI 4340. Hence results of this study provide us with variety of data regarding the materials and parameters for an efficient thermal storage.

In another study by Murray et al. 2014 [256], on vertical shell and tube type thermal storage unit with finned tubes, it was observed that flow rates of the HTF affected the charging time of phase change material. Similarly Jesumathy et al. 2014 [257] studied the thermal performance of paraffin wax in horizontal double pipe heat storage unit. The outer tube of heat storage unit was made up of steel with inner diameter of 98 mm and wall thickness of 7 mm. while the inner tube carrying HTF was made up of brass with inner diameter of 43 mm. It was observed from the study that the heat

transfer coefficient between HTF and PCM was affected by Reynolds number more frequently during charging process than the solidification process. and heat flow process during melting and solidification was increased by 25% and 11% respectively. The heat storage system studied was efficient in terms of the melting and solidification of PCM with reasonable charging time.

Rectangular shell and tube assembly unit was studied by Rahimi et al. 2014 [260] to consider the effect of fins, fluid flow rate and inlet temperature. Fins were employed to enhance the heat transfer and to reduce the charging time. Results of the study showed that increase in flow rate reduced the melting time of PCM as well as the thermal efficiency of TSU.

Different geometries of thermal storage units are studied by various researchers using different phase change materials and results are available in literature [268–270]. The efficiency of thermal storage systems also depends on the geometry of thermal storage unit. It was found that for cylindrical thermal storage units with straight tube the efficiency was found in the range of 68-74% [257,258], while for geometries with fin assembly and Flat plate based thermal storage systems efficiency were determined as 80-88% and 85-91% respectively [260,263,264].This variations were due to enhanced surface area for heat transfer. However, thermal storage unit with rectangular shell and tube geometry using embedded helical coil is not much used in the studies.

2.4 Numerical and Simulation studies

Various works have also been reported on the analytical solutions of latent heat storage unit. Becheri et al. 2015 [271] performed analytical study on shell and tube type latent heat storage unit considering the effect of various parameters like flow rate, outer tube diameter and tube length on the charging time of the paraffin wax and obtained analytical solution by exponential integral function and variable separation method. Results of the study showed that as compared to the numerical solutions, analytical solutions showed reduced charging time of PCM and geometrical parameters such as tube diameter and tube length played important role in optimization of thermal storage performance. Lorente et al. 2015 [272] performed numerical and analytical study on phase change material filled inside a vertical cylindrical enclosure integrated with concentric heater and observed that performance

of thermal storage unit was dependent on geometrical parameters like spiral pitch, diameter of the spiral coil and number of spiral turns.

A study was carried out by Pirasaci et. al. 2016 [273] to observe the effect of heat storage unit design on its performance and they used a novel model in which both latent heat as well as sensible heat of phase change material was considered and it was found that the length of the storage unit, diameter of the tubes and flow rate of heat transfer fluid had significant effect on the effectiveness of the tube while distance between the tubes did not have much effect on the performance of thermal storage unit. Niyas et al. 2017 [274] prepared a mathematical model to study the performance characteristics of a shell and tube type latent heat storage system using effective heat capacity method in which latent heat of material and Boussineq approximation was used to add the buoyancy effect in the molten layer of PCM. The governing equations involved in this model were solved by finite element based software COMSOL Multiphysics 4.3a and results showed that the charging of PCM was a convection dominant process and discharging was a conduction dominant process. It was also found that both charging and discharging process were affected by inlet fluid temperature rather than its flow rate.

Aadmi et al. 2014 [275] studied the melting characteristics of PCM based on epoxy resin paraffin wax both experimentally and numerically. COMSOL Multiphysics 4.3 was used to simulate the thermal storage system and it was found that natural convection, contact melting and melting temperature of PCM had evident effect on melting process. Simulation results showed good agreement with the numerical values. In another study Manfrid et al. 2016 conducted a simulation study of solar power plant associated with a latent heat storage and a ORC (Organic Rankine Cycle) unit using TRANSYS and found that the present system was able to provide power for 78.5% of time with weekly average efficiency of 13.4% for ORC unit and 3.4% for whole plant.

Mousa et al. 2016 [276] developed a mathematical model for desalination of water using PCM and effect of various parameters like melting point, flow rate and solar intensity on the productivity of unit was expressed in terms of fresh water produced per day. From this study it was observed that with decrease in flow rates and increase in solar intensity, the productivity of system increased. Other many similar studies

were carried out on latent heat storage systems using various simulators like COMSOL, TRANSYS, FLUENT, CFD, MATLAB etc. and in most of the cases simulated results were in good agreement with the experimental results [277–279].

2.5 Summary of literature review and research gap identified

Based on the literature survey following research gaps have been identified:

a) Investigations of heat storage system have been performed using organic phase change materials such as paraffin, fatty acid and fatty alcohols. These phase change materials are synthetic, harmful, costlier and therefore find limited applications. As such no detail study has been carried out on beeswax as heat storage material, which is naturally available.

b) Composites of synthetic organic phase change materials using additives with high thermal conductivity are reported in many studies. However, natural composite of beeswax is not studied properly and need to be investigated.

c) Different geometries of thermal storage unit such as cylindrical shell with straight single tube, cylindrical shell with straight multiple tubes, rectangular shell with straight single tube etc. (with and without fins) have been mainly used in the studies. Studies on rectangular shell with embedded helical tube are not available and need to be investigated.

d) In most of the studies on heat storage unit water, oil, nanofluids etc. have been commonly used as heat transfer fluid and few more heat transfer fluids need to be studied for better performance.

2.6 Objectives of present research

As per literature review gap between energy demand and supply is widening day by day and there is need to develop energy storage systems for meeting uninterrupted power requirement. Conventional energy sources are depleting and renewable energy is non-uniformly distributed so to tackle these issues energy storage systems is required. Many types of energy storage systems have been studied by different researchers and these systems have many limitations. Based on the literature survey

few research gaps have been identified and in the present study an attempt has been made to bridge the identified gaps.

In this study natural beeswax is introduced as a new phase material and its composite with expanded graphite was developed to analyze the chemical, physical and thermal properties and present research work has following objectives:

1. Identification and preparation of composite of beeswax as thermal storage material.

2. Characterization of thermal storage material.

3. Development of experimental set up.

4. Parametric, performance and simulation study on thermal storage unit.

CHAPTER 3

MATERIALS AND METHODOLOGY

Introduction

In this chapter details regarding materials and methodologies adopted for the preparation of additive material expanded graphite, composite of beeswax with expanded graphite as phase change material and heat transfer fluids such as suspension of expanded graphite in water and Al_2O_3/water nanofluids are presented. Details about the design and fabrication of small and large scale experimental setup used in the study are also included in this chapter. Both experimental set ups were developed at the Chemical Engineering Department, Malaviya National Institute of Technology (MNIT), Jaipur. The small scale rectangular setup with single straight tube was designed to test and compare the potential of beeswax as phase change material while large scale rectangular shell and tube type thermal storage unit with helical tube was used to study the heat storage characteristics of beeswax and its composite along with thermal performance. Characterization methods adopted for natural graphite, beeswax and composite materials are discussed with specifications of the instruments used. Characterization studies were carried out at Material Research Center (MRC) in MNIT Jaipur using sophisticated instruments such as SEM, XRD, FTIR, TGA etc.

3.1 Materials used

The variety of materials and chemicals used in the present study such as Natural graphite (Make-Ases Chemicals, India), nitric acid (65% concentration, Make-Qualikems, India), glacial acetic acid (99.5% concentration, Make-Qualikems, India), potassium permanganate (99% concentration, Make-Qualikems, India) and natural beeswax (Beeswax, (Make-Qualikems, India), Glasswares (Make-Borosil) were purchased from local market of Jaipur, Rajasthan (India). In addition to these materials various instruments were also used at lab scale such as weighing machine (Make- Pascoscale, Precision-±0.0001 g), pelletizer, microwave oven (Make-Samsung, CE1031L), digital oven (Make- Shivam Instruments, India, Model-SHI-102) and hot plate magnetic stirrer (Make-Remi, 300 W, Model-Q19-A).

3.2 Preparation of expanded graphite

Natural graphite (NG) with average particle size of 200 μm was used to prepare expanded graphite through chemical oxidation method suggested by Zeng et al. 2014

[280] with some modifications. Preparation method involved mixing of natural graphite with nitric acid (3 ml/g of NG), glacial acetic acid (3 ml/g of NG) and potassium permanganate (0.25g/g of NG) in a 1000 ml beaker. The ratio of nitric acid and glacial acetic acid per gram of graphite was fixed at 1:1 (3ml/g graphite each) to obtained optimum expansion ratio for expanded graphite. This mixture was stirred on hot plate magnetic stirrer at 45 °C for 90 minutes in order to obtain intercalated material (Nitric acid/acetic acid/graphite intercalation compound) also known as expandable graphite. This intercalated compound was washed three times with distilled water and then dried in digital oven at 60°C overnight. Expanded graphite was then obtained from irradiation of the expandable graphite inside microwave oven at 900 W for 60 seconds per 0.20 g sample mass. Due to hygroscopic nature of expanded graphite, it was stored in an air tight container for further use. Figure 3.1 depicts the physical appearance of natural graphite and expanded graphite used in the experiments.

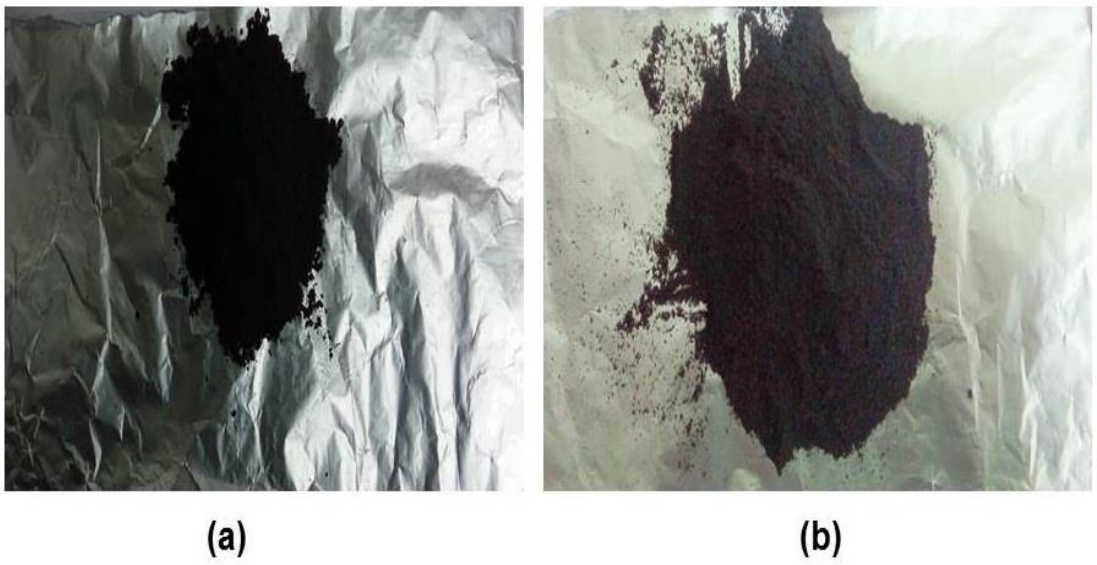

Figure 3.1 Physical appearance of a) Natural graphite b) Expanded graphite

3.3 Preparation of beeswax/expanded graphite composite

Beeswax is a natural product generated by honeybee/Apis and was melted in a 1000 ml beaker using hot plate maintained at 70 °C i.e. above its melting point (60 °C). To improve its thermal conductivity, expanded graphite powder was then added to molten beeswax followed by continuous stirring over magnetic stirrer at low rpm (400-500 rpm) for about one hour to ensure homogeneous dispersion. The reason

behind using low rpm of magnetic stirrer was to prevent the breakage of soft structure of expanded graphite inside molten beeswax due to agitation. Composites of beeswax with different weight percent of expanded graphite (5%, 10%, 15%, 20%) were prepared to analyze the variation in thermal conductivity with the percentage of expanded graphite. The prepared composite with best thermal properties was then filled in the thermal storage unit and allowed to cool down at room temperature. Composites of beeswax with different weight percentages (5%, 10%, 15%, 20%) of natural graphite were also prepared and the variation in thermal conductivity with percentage of natural graphite is studied. Both types of composites of beeswax were tested for their physical and thermal properties. The characteristics of beeswax composite with expanded graphite found to be superior as compared to natural graphite composite and beeswax/expanded graphite composite was selected for further detail experimental studies.

3.4 Preparation of expanded graphite/ water heat transfer fluid

Expanded graphite (EG)/water suspension was prepared by the direct addition of expanded graphite in the distilled water. To prepare 0.05 wt. % suspensions, 1.5 liters of distilled water was taken in a glass beaker of 2 liters capacity and 0.75 grams of expanded graphite was added to it after weighing accurately using electronic balance (Make-Pascoscale, Precision-±0.0001 g). Homogeneous mixture of this solution was obtained through constant stirring over magnetic stirrer at 500 rpm for 30 minutes. Low rpm was used due to soft structure of expanded graphite which might have degraded on vigorous mixing. The homogeneous suspension was then transferred to the hot water tank attached to the experimental set up for pumping to the thermal storage unit. The required volume of (10 Liters) expanded graphite/water suspension was thus prepared for three different concentrations of 0.05 wt. %, 0.5 wt. % and 1 wt. %. Physical appearance of prepared sample of EG/water suspension is shown in Figure 3.2.

Figure 3.2 Sample of homogeneous EG/water suspension just after preparation

3.5 Preparation of Al_2O_3/water nanofluid

Al_2O_3/water nanofluid was prepared from concentrated aluminum oxide dispersion (Make – Nanoshell, India) having 20 wt. % of 30 nm alumina nanoparticles. To prepare aluminium oxide nano-fluid, required volume (V) of aluminium dispersion of alumina nanoparticles as per equation 3.1 was added to fixed volume of distilled water in a 1 liter conical flask and stirred continuously for1 hour on magnetic stirrer. The suspension was then transferred to the ultrasonic vibrator (Labman Scientific Instruments, India) for 1 hour. Using this method alumina nanofluid at different concentrations i.e. 0.2 vol. %, 0.5 vol. %, 1.0 vol. % and 2.0 vol. % were prepared and used for studying the thermal performance of PCM stored in thermal storage unit. Repeating the same procedure 10 L of Al_2O_3 nano-fluid was prepared for its application as HTF. Figure 3.3 shows the sample of homogeneous aluminum nanofluid just after the preparation.

$$V = \frac{100\ ml}{20\ gm}\ X\ wt\%\ X\ 10\ X\ 10\ L \qquad (3.1)$$

where, V = volume of aluminum nanoparticles dispersion required for nanofluid preparation (ml) wt. % = equivalent weight percentage of solution of nanofluid.The prepared HTF was then used for studying thermal performance of phase change material.

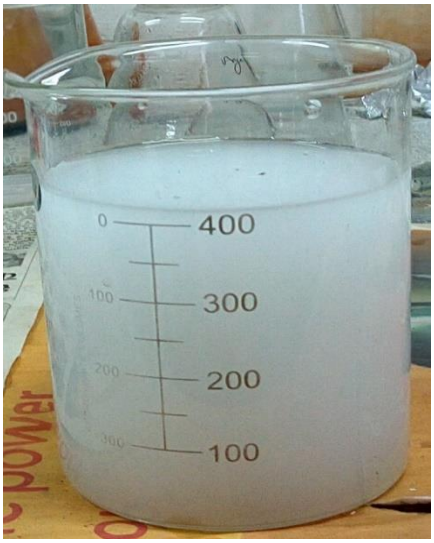

Figure 3.3 Sample of homogeneous Al_2O_3/water nanofluid just after preparation

3.6 Properties of Graphite, PCM and HTF samples

Physical, chemical and thermal properties of prepared samples of graphite, pure beeswax, beeswax/ expanded graphite composite, beeswax/natural graphite composite, EG/water suspension and Al_2O_3 nanofluid were determined using standard methods/correlations.

3.6.1 Thermal Conductivity

Thermal conductivities of natural graphite, beeswax and the prepared composite samples were measured by desktop thermal conductivity meter (Make – Hot Disk, Model –TPS500). To analyze the thermal conductivity, each sample was prepared into disk shape cylindrical pellet (10 mm diameter and 4 mm thick) using pelletizer. These pellets were then tested using Kapton sensor within thermal conductivity meter. For analysis, one face of each pellet was placed on an insulator and the Kapton insulated probe with spiral sensor was placed on the other face and each sample was tested 5 times using same method and then the average of their thermal conductivity values was taken as average thermal conductivity of the sample. The standard deviation of the thermal conductivity meter was provided by manufacturer as ±4%.

Thermal conductivity of expanded graphite/water suspension and Al_2O_3/water nanofluid was calculated [Appendix II] by using Hamilton and Crosser Model as shown in equation 3.2 [275, 276]. This model was developed for calculation of thermal conductivity of heterogeneous phase as function of particle shape,

concentration and thermal conductivities of both continuous and discontinuous phase. The model is valid when the ratio of thermal conductivity of discontinues phase to thermal conductivity of continuous phase is more than 100. In this study the ratio of thermal conductivity of expanded graphite to water obtained was 154 and therefore, the model could be implemented.

$$\frac{K_{eff}}{K_f} = \frac{K_p+(n-1)K_f-(n-1)\emptyset(K_f-K_p)}{K_p+(n-1)K_f+\emptyset(K_f-K_p)} \quad (3.2)$$

Where k_{eff} = effective thermal conductivity of solution (W/m.K), k_p = thermal conductivity of particle (W/m.K), k_f = thermal conductivity of base fluid (W/m.K),. n = 3/ψ, where ψ = sphericity of particle, ø = volume fraction of particle.

Thermal conductivity of molten beeswax and composite was measured at 70 °C i.e. at the temperature above the melting point of beeswax (59.6 °C) and expanded graphite/beeswax composite (57.8 °C). To measure the thermal conductivity both materials were heated above its melting point in a 100 ml beaker and the Kapton sensor with 3 mm of spiral coil was then put in the liquid and reading was then taken on the instrument. During observation data obtained after 1 sec was not considered to avoid convection effect which may takes place in the molten phase change material.

3.6.2 Specific heat capacity

Heat capacity of beeswax and its composite was measured by DSC analysis. Effective heat capacity of expanded graphite and Al_2O_3/water nanofluid was estimated using equation 3.3.

$$\rho_{eff}C_{p_{eff}} = (1-\emptyset)\rho_f C_{p_f} + \emptyset\, C_p\rho_p \quad (3.3)$$

where, $C_{p_{eff}}$ = effective heat capacity of HTF (kJ/kg.K), C_{p_f} = heat capacity of homogeneous phase (kJ/kg.K), C_p = effective heat capacity of heterogeneous phase (J/kg.K).

3.6.3 Density

Density of both the additive materials i.e. natural graphite and expanded graphite was estimated by tapping method in which expanded graphite powder was filled in a 250 ml cylinder and tapping of cylinder was carried out till there is no change in volume was observed. The density (ρ) of expanded graphite was then calculated by the

equation (3.4) where, m = mass of expanded graphite which occupied the 250 ml volume of cylinder (gm), v = volume of cylinder (250 ml).

$$\rho = m/v \quad (3.4)$$

The density of base fluid i.e. water was measured using 100 ml of measuring cylinder. To begin the experiment, mass of empty cylinder was measured and then filled with water up-to the mark of 100 ml and its mass was taken again. To calculate the density of water mass of empty cylinder was subtracted from filled cylinder and the obtained mass was then divided by 100 ml.

Effective density of expanded graphite/water suspension and Al_2O_3 nanofluid was determined by equation (3.5) [282] where, ρ_{eff} = effective density of HTF (kg m^{-3}), $\emptyset$ = volume fraction of solute, ρ_f = density of base fluid (kg m^{-3}), ρ_p = density of solute (kg m^{-3}).

$$\rho_{eff} = (1 - \emptyset)\rho_f + \emptyset\rho_p \quad (3.5)$$

3.6.4 Viscosity of HTF

Viscosity of expanded graphite/water suspension and Al_2O3/water nanofluid was calculated using the equation (3.6) and equation (3.7) [282].

$$\mu_{eff} = \mu_f(1 + 2.5\emptyset + 10.05\emptyset^2) \quad (3.6)$$

$$\mu_{eff} = \mu_f(1 + 2.5\emptyset) \quad (3.7)$$

Where,μ_{eff} = effective viscosity (N.S/m^2) ,μ_f = viscosity of base fluid (N.S/m^2),$\emptyset$ = volume fraction of solute.

3.7 Characterization of samples

Physical, chemical and thermal characterization of samples were carried out using different techniques such as scanning electron microscopy (SEM), fourier transform infra-red (FTIR), X-ray diffraction (XRD), thermogravimetric analysis (TGA) and differential scanning microscopy (DSC).

3.7.1 Physical and chemical characterization of samples

Scanning electron microscopy (SEM) was used to visually inspect the surface of the samples used in this study. SEM analysis of all the samples was done on a scanning electron microscope (Make – FEI, Model- Nova NanoFE-SEM 450). Before starting

the SEM analysis of natural graphite and expanded graphite, the samples of both materials were dried at 80 °C in a digital oven for 24 hours to remove moisture. No coating was required for natural graphite, expanded graphite, beeswax and composite and therefore all the prepared samples were mounted without coating on double coated carbon tape and placed in sample holder one by one for analysis (resolution, 800X-5000X). Figure 3.4 showing the SEM instrument available at MRC and used for the analysis.

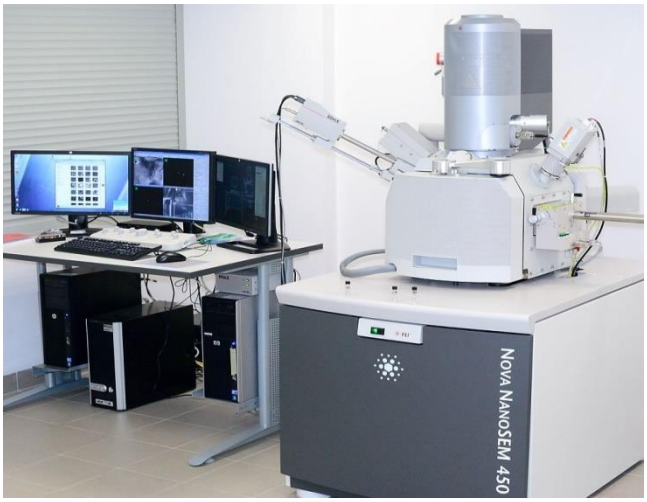

Figure 3.4 Nova NanoFESEM -450 SEM for surface morphology analysis

Fourier Transform Infra-Red (FTIR) spectroscopy was performed to identify the molecular structures present within the samples of beeswax and its composite with expanded graphite. FT-IR analysis of natural and expanded graphite was also done to identify the impurities or any additional chemical species that might be present in these materials. For this study an FTIR spectrometer (Make – Perkin Elmer, Model-FT-IR spectrum 2) as shown in Figure 3.5 was used with scanning measurement range of 4000-400 cm^{-1} for solid samples in the form of KBr (Potassium Bromide) pellet. Samples of natural and expanded graphite were dried at 80°C in a digital oven for 24 hours to remove any traces of moisture while beeswax and its composites samples were tested directly. Before analysis, KBr which shows no absorption of IR and provide uniformity (0.2-1% ratio with sample) was added to all the samples and then cylindrical pellets (7 mm diameter) of mixture were prepared. Pellets of all prepared samples were then tested within the wavelength of 4000-400 cm^{-1}.

Figure 3.5 Perkin Elmer, Model- FT-IR spectrum 2

X-Ray diffraction of samples was carried out to analyze the composition and structure of prepared samples with 2θ value varying from 10° to 90° using X-Ray Diffractometer (Made – Pananalytical, Model- Xpert pro). 10 mm specimen of each sample was prepared and tested on XRD instrument with copper as anode material. The generator settings of XRD instrument was maintained at 40 mA and 40 kV. To perform the XRD analysis, each sample was placed on sample plate in form of thin layer which was then placed on sample stage of XRD instrument. X-ray was allowed to fall on the sample for analysis and plots thus obtained were analyzed. Figure 3.6 shows the Xpert-pro diffractometer used for XRD analysis of prepared samples.

Figure 3.6 Xpert-pro diffractometer

3.7.2 Thermal characterization of samples

Differential scanning calorimetry (DSC) and Thermogravimetric analysis (TGA) of natural graphite, expanded graphite, beeswax and its composite was performed to

study their thermal properties. DSC (Make-Perkin Elmer, Model-Pyris 6 DSC), was carried out by placing 4 mg of beeswax in the alumina sample pan of the instrument. The pan with sample was then placed inside the instrument. Inert environment during the analysis was maintained by passing nitrogen gas at rate of 50 mL/min and melting characteristics were studied by heating the sample at a rate of 5 ºC per minute starting from 10 °C up to 250 ºC. Linear baseline correction for alumina sample pan was performed before calculating latent heat for the samples. After complete melting of the beeswax, the sample was again cooled at the rate of 5 ºC per minute in order to study its solidification/cooling characteristics. Same procedure was performed with composite keeping the sample size of 4 mg. Figure 3.7 showing the Pyris 6 DSC instrument used for this analysis.

Figure 3.7 Pris 6 DSC instrument

Thermal gravimetric analysis of beeswax and its composite with expanded graphite was performed on TGA-DTA instrument (Made – Perkin Elmer, Model – STA 6000). Temperature for analysis was kept in the range of 10 °C-400 °C by maintaining constant heating rate of 10 °C/min. To initiate the analysis about 25.61 mg of beeswax was weighed accurately to fill the sample holder (ceramic crucible) then the crucible with sample was placed within the instrument for TGA analysis. An inert environment was maintained during the study by flowing nitrogen gas at the flow rate of 20 ml/minute. The temperature versus mass loss graph was obtained for further analysis and same procedure was adopted for composite material with sample size of 19.80 mg. The difference in sample size was due to different densities of the samples with fixed volume of crucible. Figure 3.8 showing the TGA instrument used for the study.

Figure 3.8 Perkin Elmer, Model – STA 6000 TGA instrument

3.8 Calibration of thermocouples

K-type thermocouples were used for temperature measurement of material in thermal storage unit. The calibration of thermocouples was done by using DAQ (Data Acquisition system) card, as shown in Figure 3.9, DAQNI 9211 a data acquisition device used for calibration was first connected with four 70 cm long thermocouples to measure the temperature of the reference (Ice). It was assumed that readings of the DAQ card are accurate and therefore, temperature of each thermocouple was recorded using ice as reference (melting point 0°C). Then the thermocouples were attached to the temperature display which was used in the experiments and temperature of the melting ice was recorded. The difference in the temperature recorded by DAQ card and the reading of temperature display was noted as deviation of each thermocouple. The deviation of each thermocouple was found to be in the range of ±0.2 °C to ±0.5 °C.

Figure 3.9 DAQNI 9211 card for thermocouple calibration

3.9 Development of small thermal storage unit

A small scale horizontal rectangular shell and tube type thermal storage unit was designed and fabricated in order to study the thermal storage characteristics of beeswax and beeswax/expanded graphite composite upto 2.5 kg mass. The heat storage unit of dimension 310 mm x 95 mm x 85 mm was fabricated using plywood (2.5 mm thick) and was lined internally with 10 mm thick asbestos sheet to provide heat insulation. This unit was connected to hot water tank made up of stainless steel (Capacity-100 L) with embedded electric heater (2kW, Make–Bajaj, India) through pump (Power-1/2 hp, Make-Crompton, India), brass valves (3 nos.) and rotameter (measurement range – 0-10 LPM, Make-Star flow) as shown in Figure 3.10. Hot water was allowed to pass through a straight copper tube (I.D. = 8 mm, O.D. = 9 mm) located at the center of the unit. Calibrated K- type thermocouples (Material-Ni-Cr, Accuracy ± 0.3 ºC, Range: -200 ºC to 1350 ºC) were used to measure temperatures of storage material at nine location in the thermal storage unit along with inlet and outlet temperature of hot water. The position of different thermocouples used in the thermal storage unit is shown in Figure 3.11. During the experimentation, the inlet temperature and flow rate of hot water was kept constant at 80 ºC and 120 L/hr respectively to record the thermal behavior of material. Figure 3.12 depicts the actual picture of small scale TSU fabricated in the lab.

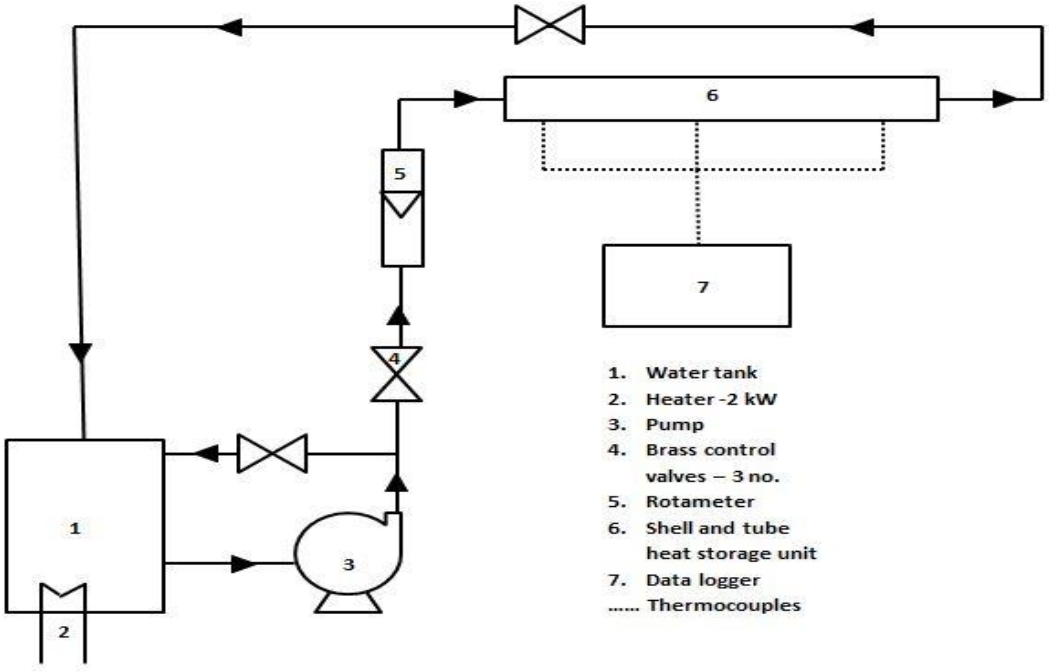

Figure 3.10 Schematic diagram of shell and tube type experimental set up-small TSU

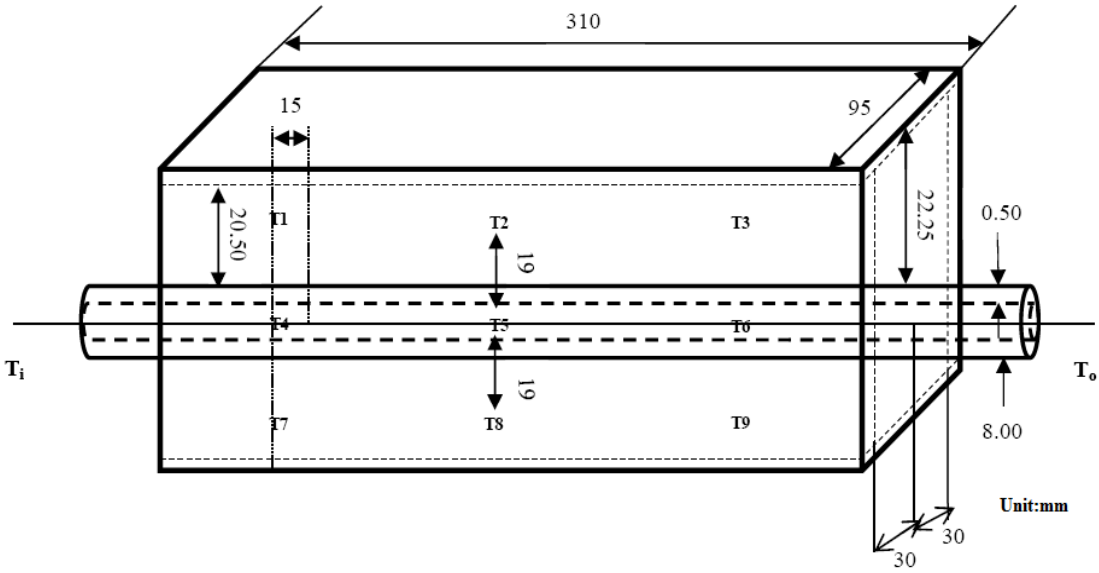

Figure 3.11 Thermocouple position in small TSU

(a)

(b)

Figure 3.12 Photograph of small scale thermal storage unit (a) Interior view (b) exterior view

3.10 Thermal performance evaluation

In the initial set of experiments thermal performance analysis of beeswax and its composite with expanded graphite was performed by using small TSU. To begin the experiment, about 2.5 kg of molten beeswax was filled in small thermal storage unit and allowed to solidify at room temperature. Plain water as heat transfer fluid was then passed through the central tube of TSU using centrifugal pump. The inlet temperature and flow rate of inlet fluid was maintained at 80 °C and 2 LPM with the help of temperature controller attached with hot water tank and rotameter respectively. The heat transfer fluid (water) was allowed to flow through the TSU till the constant temperature is observed in all the thermocouples. The temperatures of nine thermocouples which were placed axially and vertically along the TSU and at inlet and outlet of copper tube were recorded for every 15 minutes from the beginning of experiment and the performance of unit was analyzed in terms of charging time. In the next stage of experiment same procedure is adopted for studying thermal performance of composite of beeswax (2.5 kg).

3.11 Development of large scale thermal storage unit

A large scale rectangular shell with embedded helical tube type thermal storage unit (Figure 3.13) was designed and fabricated to perform experimental study for thermal performance of beeswax, natural graphite and composite beeswax/expanded graphite. The rectangular shell (610 mm x 360 mm x 450 mm) of thermal storage unit was made using teak wood (20mm thick, k = 0.12-0.04 W/m K) to prevent heat loss due to low thermal conductivity of wood [78] and inner side of the shell was well insulated using thermocol (25 mm thick, k = 0.033W/m K) [79] followed by layer of asbestos (10 mm thick, k = 0.08 W/m K) to avoid any heat loss from TSU to the ambient air. A helical coil having 13 turns of copper tube (I.D. = 8 mm, O.D. = 9mm) with pitch of 3 cm and coil diameter of 110.6 mm was placed at the center of the rectangular shell. The unit was connected to (Figure 3.13) a hot water tank made of stainless steel (capacity 100 L) with immerged electric heater (2 kW, Make- Bajaj India), glass rotameter (1 LPM–10 LPM), a centrifugal pump (1/2 hp, Make – Crompton, India) and brass valves. Nine k-type thermocouples (Ni-Cr based) with accuracy of ±0.2 ºC (Figure 3.14) were placed along vertical and axial positions at equal distances within heat storage material inside the thermal storage unit to record

variation in the temperature during charging and discharging cycle. Two more thermocouples were placed at the inlet and outlet of helical copper tube of the TSU in order to measure inlet and outlet temperature of heat transfer fluid. Figure 3.15 represents the picture of actual setup fabricated in the lab and Figure 3.16 showing the inside view of TSU with helical coil before and after filling beeswax. Geometry of helical coil is defined using following parameters:

1. Curvature ratio - a dimensionless parameter of the coil defined as the ratio of inner diameter of the tube to coil diameter, $\delta = \frac{d_i}{2R_c}$ (3.8)

2. Non-dimensional pitch, $\gamma = b/2\pi R_c$ (3.9)

3. Reynolds number, $R_e = \frac{\rho v d_i}{\mu}$ (3.10)

4. Dean number, $D_e = R_e \left(\frac{d_i}{2R_c}\right)^{0.5}$ (3.11)

Where, d_i = inner diameter of copper tube (m), R_c = radius of curvature of the helical coil (m), v = velocity of HTF (m/s), μ = viscosity of HTF (N S/m^2), b = pitch of helical coil (m/s).

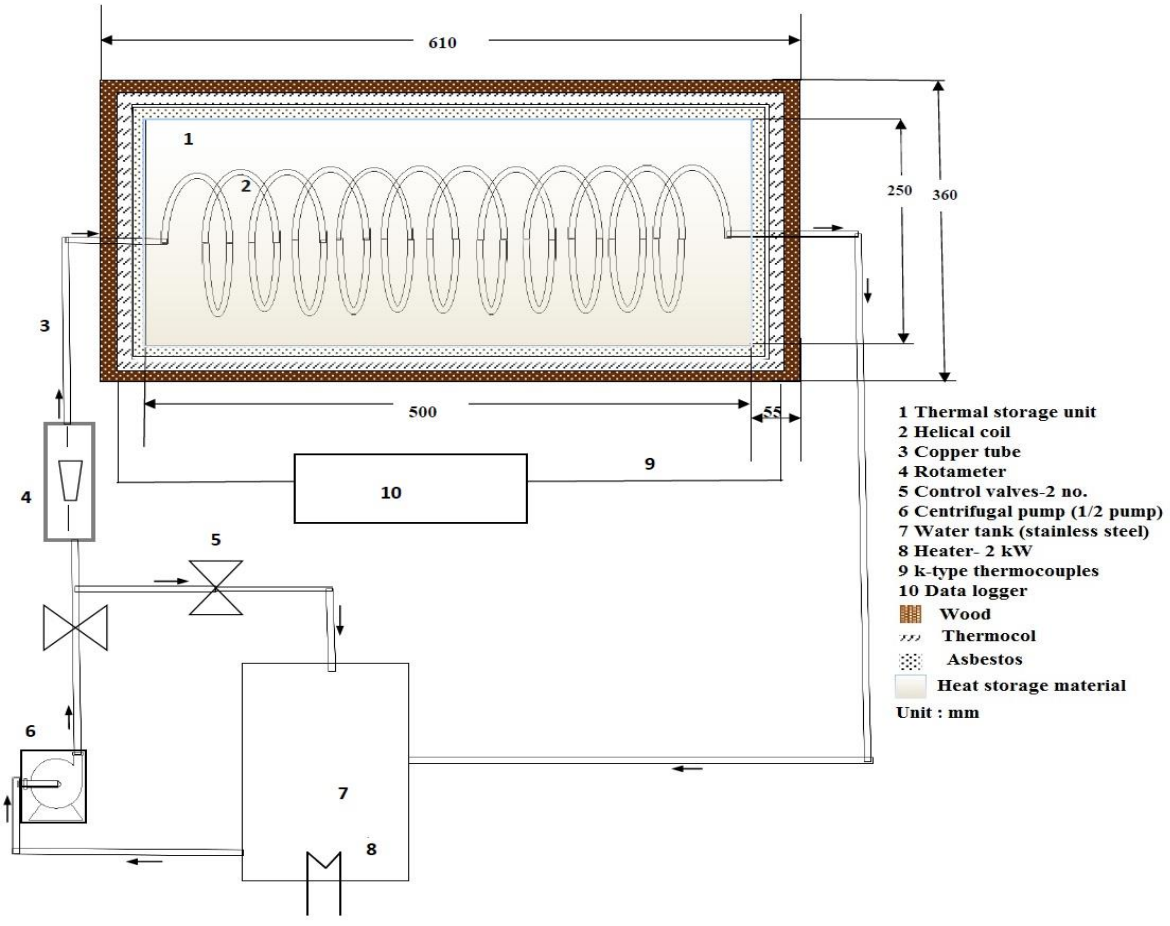

Figure 3.13 Schematic diagram of shell and tube type thermal storage unit-large TSU

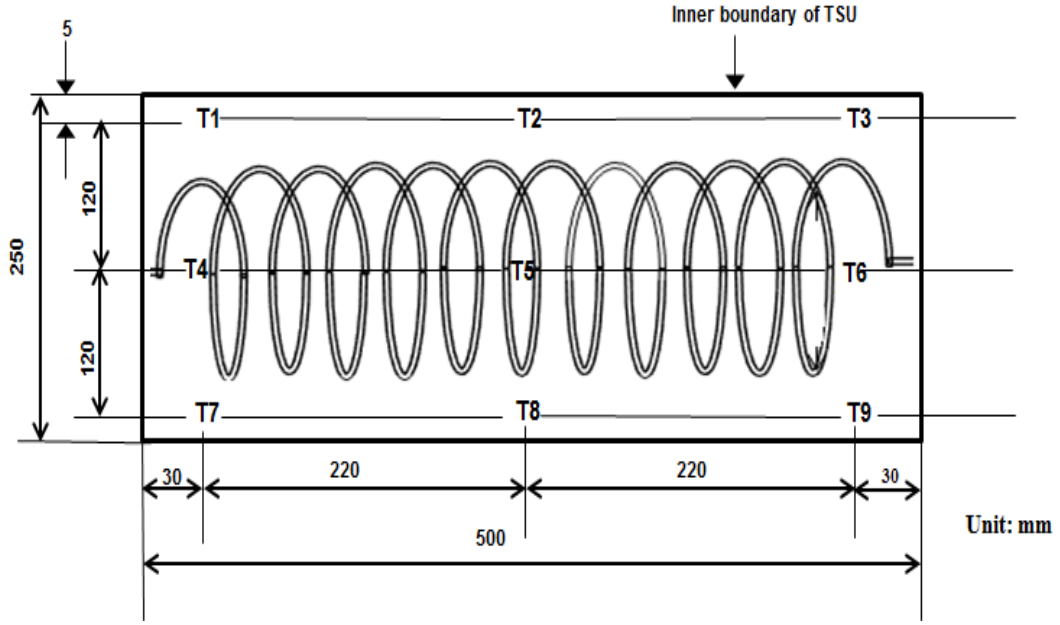

Figure 3.14 Position of nine thermocouples inside PCM in large TSU

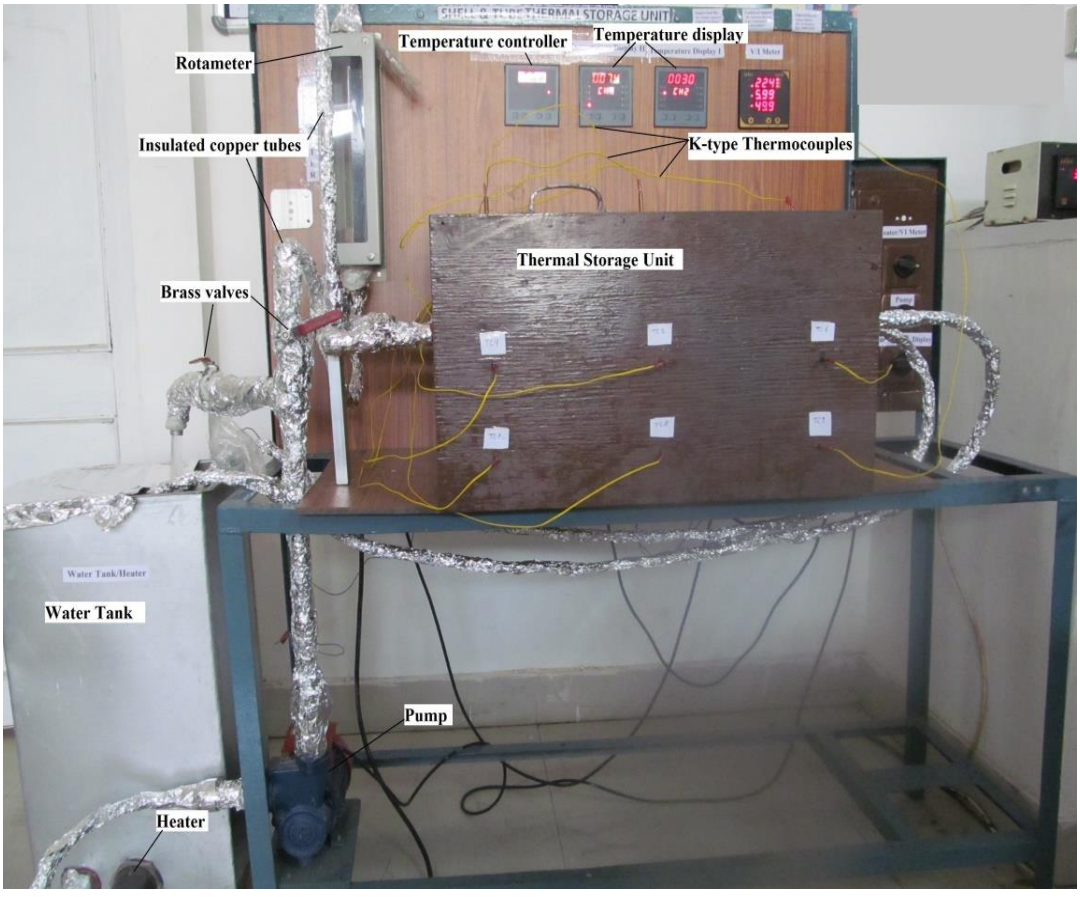

Figure 3.15 Photograph of large scale thermal storage unit

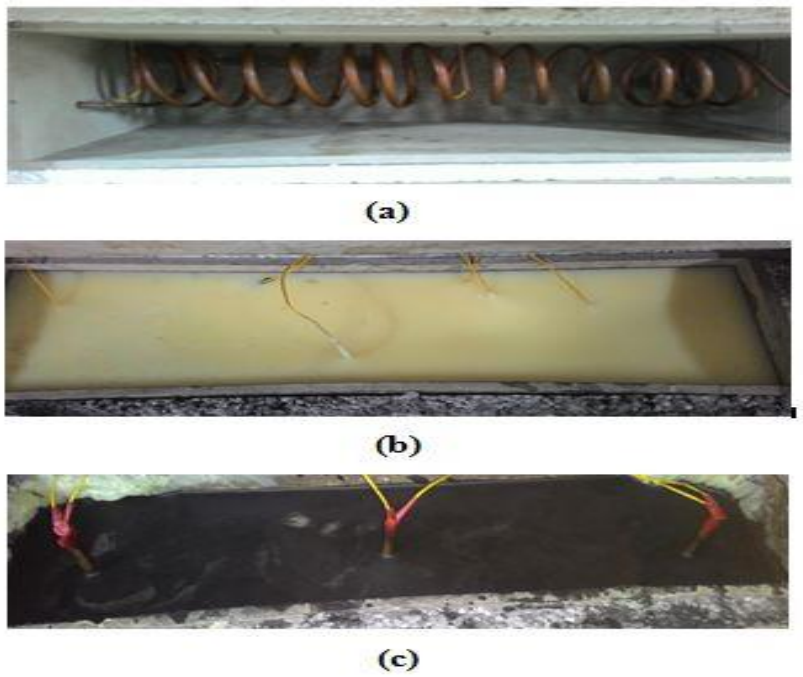

Figure 3.16 Inside view of large TSU (a) empty (b) with beeswax (c) with composite

3.12 Uncertainty analysis

There may be some uncertainties in the experimental results due to uncertainties in measurements of various parameters while conducting experiments. The uncertainty may be in the measurement of temperature by k-type thermocouples, flow rate by rotameter and in thermal conductivity meter reading. Therefore, an uncertainty analysis was performed on various measured data and thermocouples used (Appendix III). Uncertainty for rotameter is provided by manufacturer as 2%. Error bar was calculated using set of data obtained for 0.5 LPM and 80°C to find out the error generated in the readings of the graph.

3.13 Effect of operating parameters

The effect of various operating parameters such as fluid flow rate, inlet fluid temperature, types of HTF and concentration of solids in HTF was studied on thermal performance of TSU containing graphite, beeswax and composite.

3.13.1 Performance evaluation of beeswax in large TSU

To begin the experiment hot molten beeswax of about 18 kg was filled in the shell part of thermal storage unit and allowed to solidify at room temperature. Thermal performance of beeswax in the large TSU using plain water, expanded graphite/water

suspensions, Al_2O_3/water suspensions as HTF was evaluated by varying inlet fluid temperatures and flow rates.

3.13.1.1 Using plain water as HTF

The hot plain water from hot water tank was allowed to pass through the thermal storage unit at various inlet temperatures and flow rates (Table 3.1). For each constant inlet temperature of fluid maintained with the help of temperature controller attached to hot water tank, different flow rates of heat transfer fluid (through rotameter) were allowed through helical coil. The charging time of beeswax at each set of parameter was recorded as time required for reaching constant temperature of all the thermocouples and its thermal profiles were prepared. The amount of heat stored by the unit was also calculated.

Discharging profile was obtained just after completion of charging by passing cold plain water at the flow rate of 0.5 LPM and 20°C. During discharging the temperatures at all the thermocouples were recorded at the time interval of 5 min. as well as inlet and outlet temperature of HTF to calculate the amount of heat recovered from TSU.

Table 3.1 Flow parameters of plain water to evaluate thermal performance of beeswax

Inlet Temperature (°C)	**Flow rates (LPM)**
60	Variable : 0.25, 0.50, 0.75, 1.0
70	Variable: 0.25, 0.50, 0.75, 1.0
80	Variable : 0.25, 0.50, 0.75, 1.0
90	Variable: 0.25, 0.50, 0.75, 1.0

3.13.1.2 Using expanded graphite/water suspension as HTF

In this set of experiments, expanded graphite /water suspensions at different concentrations (0.05% wt., 0.5% wt. and 1.0% wt.) were prepare and used to study the thermal performance of beeswax. Before beginning of experiment both the coil and external tubes of TSU were cleaned by passing distilled water through them at high flow rate of 2-3 LPM to remove any traces of impurities that may settle on the wall of the tube. The EG/water suspension (fixed concentration) was allowed to flow through the helical coil of unit at the flow rate of 0.5 LPM and inlet fluid temperature of

80°C. The temperatures at nine different positions of TSU were recorded at the time interval of every 15 minutes and plotted for analysis.

3.13.1.3 Using Al_2O_3/water suspension as HTF

Al_2O_3/water suspensions at different concentrations (0.2% vol., 0.5% vol., 1.0% vol., 2.0 vol. %) were prepared and used to study the thermal performance of beeswax. Tubes were cleaned by passing distilled water at high flow rate (2-3 LPM). Each concentration of prepared suspension was passed through the helical coil of TSU using centrifugal pump keeping constant flow rate and inlet temperature at 0.5 LPM and 80 °C respectively. Temperature at nine different positions of TSU were recorded at the time interval of every 15 minutes and analyzed.

3.13.2 Performance evaluation of beeswax/expanded graphite composite in large TSU

To begin the experimental study on composite material, previously used hot molten beeswax was removed from the unit and composite of beeswax/expanded graphite was filled (18 kg) in the shell of large size thermal storage unit and allowed to solidify at room temperature. During the study plain water, expanded graphite/water suspensions, Al_2O_3/water suspensions and exhaust gas from engine were used as HTF to evaluate thermal performance by varying inlet fluid temperatures and flow rates.

3.13.2.1 Using plain water as HTF

The hot water was passed through the helical coil of TSU until the temperatures at all the thermocouples become constant. The charging time of composite was noted at all the different combinations of fluid flow parameters such as flow rates and inlet fluid temperatures as mentioned in table 3.1 and respective charging profiles were developed to understand the melting behavior of composite.

After the complete charging of thermal storage unit, discharging of composite material was done by passing cold water (at 20 °C±0.2 °C) through the TSU using centrifugal pump keeping the constant flow rate of 0.5 LPM. Temperatures at all the nine thermocouples were recorded and plotted against time in order to obtain discharging profile of composite.

3.13.2.2 Using expanded graphite/water suspension as HTF

Prepared beeswax/expanded graphite composite was tested using expanded graphite/water suspension of different concentrations (0.05 wt. %, 0.5 wt. % and 1.0 wt. %) in order to study the variation in charging time. The HTF was passed through the helical coil at fixed flow rate of 0.5 LPM and constant inlet temperature of 80°C respectively. The concentration greater than 1.0 wt. % of expanded graphite was not used due to the slurry formation which could block the helical tube and can affect the overall working of TSU. The variations in thermocouple temperatures were recorded till constant temperature is observed. Thermal profile of composite at different concentrations of HTF was studied by plotting graph between the time and temperature at different thermocouples.

3.13.2.3 Using Al_2O_3/water suspension as HTF

Thermal profiles of composite were also plotted by recording temperatures at nine different thermocouples using Al_2O_3/water suspension of different concentration (0.2 vol. %, 0.5 vol. %, 1.0 vol., 2.0 vol. %) of alumina particles at the flow rate of 0.5 LPM and inlet fluid temperature of 80 °C. Higher concentrations of alumina particles results settling and agglomeration that may clog the pipes and hinder the smooth working.

3.13.2.4 Using exhaust gas from petrol engine

Thermal storage performance of composite material was also evaluated using exhaust gas of C.I. engine as heat transfer fluid. The basic aim of this was to store the waste heat from exhaust gases in PCM. The exhaust line of two stroke stationary C.I. engine (Make-Honda, Power – 7.9 HP, Speed – 3600 rpm) was connected to the input of thermal storage unit which allowed the exhaust gases to pass through helical coil of TSU embedded in beeswax/expanded graphite composite. The assembly of TSU with C.I. engine is shown in Figure 3.17. Once the gas started to come out from the outlet of TSU the temperature at nine thermocouples placed in axial and vertical direction of TSU began to increase and was recorded at an interval of 15 minutes. Thermal profile of composite was studied for calculation of heat stored from exhaust gases and efficiency of TSU.

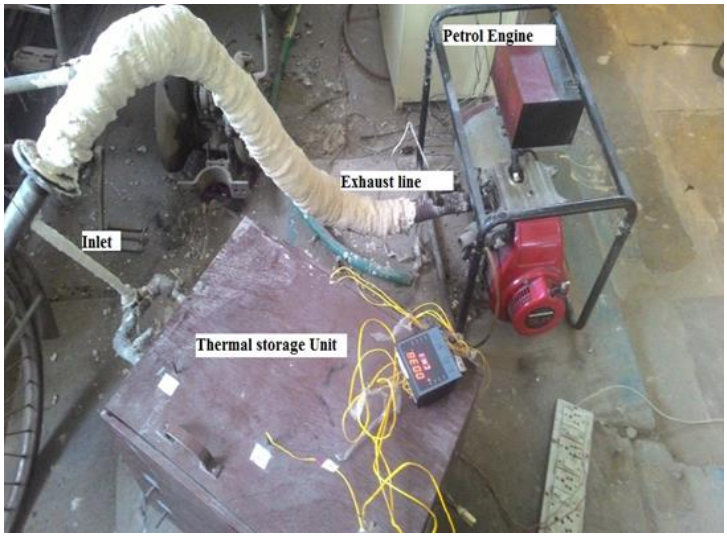

Figure 3.17 Assembly of petrol engine with large TSU

3.13.3 Performance evaluation of natural graphite in large TSU

Natural graphite powder (22 kg) was filled inside the shell part of thermal storage unit for the determination of its heat storage capacity as sensible heat storage material. The heat transfer fluid was passed through the thermal storage unit using a centrifugal pump. All the three types of heat transfer fluids i.e. plain water, EG/water suspension, Al_2O_3/water suspension were used to study the thermal storage behavior of natural graphite.

Plain water was used at different flow rates (0.25 LPM, 0.5 LPM, 0.75 LPM and 1.0 LPM) and different inlet fluid temperatures (60 °C, 70 °C, 80 °C, 90 °C) to study the charging time of natural graphite. Expanded graphite/water suspension at various concentrations (0.05 wt. %, 0.5 wt. % and 1.0 wt. %) were used as HTF to study relationship between the concentration of expanded graphite in water and charging time of natural graphite. Similarly, charging time of natural graphite was obtained at different concentration of alumina nanofluids i.e. 0.2 vol. %, 0.5 vol. %, 1.0 vol. %, 2.0 vol.% In all these cases heat transfer fluid was filled in a hot water tank and passed through the circulation loop of TSU. The variation in temperatures at nine different thermocouples was recorded at the time interval of 5 minutes for all the parameters.

3.14 Efficiency of large TSU

Energy stored in the thermal storage unit with natural graphite, pure beeswax and its composite was calculated as the cumulative of instantaneous heat transfer from HTF

to storage material [43] considering no heat losses from TSU. Inlet and outlet temperatures of HTF were recorded by data logger at an interval of every 15 min and 5 min for PCM and natural graphite respectively. Efficiency calculation was performed using various basic equations of heat transfer as given below: $\dot{Q}$ the instantaneous energy (kJ/s) available for storage in the PCM (beeswax and its composite) from HTF can be calculated using equation 3.12 as :

$$\dot{Q} = \dot{m}\, C_P(T_{in} - T_{out}) \quad (3.12)$$

The total useful energy (Q_a) (kJ) for charging is the cumulative of instantaneous energy and can be calculated using equation 3.13:

$$Q_a = [\dot{m}\, C_p\, \Sigma(T_{in} - T_{out})].\Delta t \quad (3.13)$$

Total energy stored (Q_w) (kJ) by PCM during the charging process can be estimated using equation 3.14 :

$$Q_w = m_w\, [C_{ps}\, (T_m - T_i) + L + C_{pl}(T_f - T_m)\,] \quad (3.14)$$

Thermal storage efficiency (η) of TSU with beeswax and composite was calculated using equation 3.15.

$$\eta = \frac{Q_w}{Q_a} \quad (3.15)$$

Energy stored in the thermal storage unit with natural graphite as sensible heat storage material was calculated using above equations 3.12 and 3.13 with equation 3.16.

Total energy stored (Q_g) (kJ) by graphite during the charging process was calculated using equation 3.16:

$$Q_g = m_w C_{pg}\, (T_f - T_i) \quad (3.16)$$

Thermal storage efficiency of TSU with natural graphite was obtained from equation 3.17:

$$\eta = \frac{Q_w}{Q_a} \quad (3.17)$$

Where, $\dot{m}$ = mass flow rate (kg/s), m_w = mass of heat storage material (kg), C_{ps} = specific heat of solid PCM (kJ/kg.K), C_{pl} = specific heat of liquid PCM (kJ/kg.K), C_{pg} = specific heat of graphite (kJ/kg.K), T_i = initial temperature of natural graphite(K), T_f = final temperature of natural graphite (K).

3.15 Determination heat transfer coefficient of large TSU

Overall heat transfer coefficient (U_o) ($W/m^2.K$) between the coil and beeswax was calculated using equation 3.20:

$$U_o = \frac{Q_a}{A_s \Delta T_{mean}} \quad (3.20).$$

ΔT_{mean}= Log mean temperature difference = $\frac{(T_{in}-T_b)-(T_{out}-T_b)}{\ln\frac{(T_{in}-T_b)}{(T_{out}-T_b)}}$

Where, T_{in} = Inlet fluid temperature (K), T_b = bulk temperature (K), T_{out} = Outlet temperature of HTF (K).

Overall heat transfer coefficient based on outside area of tube and in terms of internal and external heat transfer coefficient can also be represented by equation 3.21:

$$\frac{1}{U_o} = \frac{A_o}{A_i h_i} + \frac{A_o \ln\frac{d_o}{d_i}}{2\pi k L} + \frac{1}{h_o} \quad (3.21)$$

Where, Ao = external surface area of the tube (m^2), A_i = internal surface area of the tube (m^2), h_i = internal heat transfer coefficient ($W/m^2.K$), h_o = external heat transfer coefficient ($W/m^2.K$), d_o = outer diameter of the tube (m), d_i = inner diameter of the tube (m).

Internal heat transfer coefficient from copper helical tube was calculated using Nussle number correlation as given in equation 3.22 [283]

$$Nu_i = 0.152\ D_e^{0.431}\ Pr^{1.06}\ \gamma^{-0.277} \quad (3.22)$$

The above correlation is applicable for tube side heat transfer calculation for constant temperature boundary conditions i.e. constant HTF inlet temperature and low dean number (D_e<3000).

For the determination of external heat transfer coefficient (h_o) between copper tube and beeswax correlation expressed as equation 3.23 [284] was used:

$$Nu_o = 0.381\ (Ra)^{0.293} \quad (3.23)$$

where Ra = Gr.Pr = Rayleigh number.

3.16 Modelling and simulation

Modelling and simulation of small and large thermal storage unit was carried out for predicting thermal performance using COMSOL Multiphysics® software version 5.2a and simulation results were validated with experimental results. The COMSOL software is a simulator and solver package based on finite element method that is used effectively to solve large number of engineering problems.

Input geometrical parameters used for creating model geometry in COMSOL software for TSU were taken from the Table 3.2. In actual experimental set-up PCM was filled

in the shell part of thermal storage unit and a helical tube was passed through the center of the unit. In modelling of TSU the dimension of PCM block was taken for the study rather than the dimension of TSU. Thermo-physical properties of beeswax and composite materials were defined in the blank material section of COMSOL software. 'Heat study in Fluids' physics was selected as study module for PCM materials and 'Heat transfer in solid' physics was selected for natural graphite and during the simulation following assumptions were made:

- The tube surface is maintained at uniform temperature throughout the tube length.
- Pressure drop across tube length is negligible.
- The velocity profile of the fluid is fully developed and remains same for complete tube length.
- Fluid is incompressible and flow in the tube is laminar.

All the simulation studies were carried out at the constant flow rate of 0.5 LPM and fixed inlet fluid temperature of 80°C and simulation results were validated against the 3 experimental data sets for beeswax and composite materials.

Initial temperature of PCM domain and packed bed of natural graphite was taken equal to ambient temperature of 25°C.

Initial boundary condition for the tube was taken as 0.5 LPM flow rate and 80°C as fluid temperature.

Free triangular mesh was selected for all the geometric model consists of 73042 domain elements and 9878 boundary elements. The computation time for PCM simulation and natural graphite simulation was 7 hours and 3.5 hours respectively for an DELL workstation with CORE i5 processor.

Table 3.2 Geometrical properties for thermal storage units

Geometrical property	Small TSU	Large TSU
L XB X H	285 mm x 70 mm x 60 mm (excluding insulation)	500 mm x 340 mm x 250 mm (excluding insulation)
Inner diameter of tube	8 mm	8 mm
Outer diameter of tube	9 mm	9 mm
Number of tubes	1	1

Geometry of tube	Straight	Helical
Mass of PCM	2.5 kg	18 kg

To simulate the heat transfer fluid flowing through the copper tube, inbuilt continuity equation (3.24) and momentum equation (3.25) in COMSOL software were used:

$$\frac{\partial \rho}{\partial t} + \nabla \cdot (\rho u) = 0 \tag{3.24}$$

$$\frac{\partial \rho u}{\partial t} + \rho(u \cdot \nabla)u - \nabla \cdot [\mu(\nabla u) + (\nabla u)^T] + \nabla p = 0 \tag{3.25}$$

Heat transfer from HTF to the inner wall of the tube was through forced convection and energy balance equation for this is given by equation 3.26.

$$\rho C_p \frac{\partial T}{\partial t} + \rho C_p u . \nabla T = \nabla . (k \nabla T) \tag{3.26}$$

After the convective heat transfer from HTF to tube wall, the heat transfer further takes place from tube wall to PCM through conduction as represented by equation 3.27

$$\rho C_p \frac{\partial T}{\partial t} = \nabla . (k \nabla T) \tag{3.27}$$

After heat conduction to PCM, the melting of phase change material occurred,(if φ is the fraction of liquid phase of PCM) then the heat enthalpy equation for the phase change material is expressed by equation 3.28.

$$H = (1 - \varphi) H_{P1} + \varphi H_{P2} \tag{3.28}$$

Where H_{P1} = Enthalpy of phase 1, H_{P2} = Enthalpy of phase 2.

Differentiation of equation 3.28 with respect to temperature will provide the equation for specific heat as :

$$C_{eff} = (1 - \varphi) \frac{dH_{P1}}{dT} + \varphi \frac{dH_{P2}}{dT} + (H_{P2} - H_{p1}) \frac{d\varphi}{dT} \tag{3.29}$$

Equation 3.29 can be represented as :

$$C_{eff} = (1 - \varphi) C_{p1} + \varphi C_{p2} + \left(H_{P2} - H_{p1}\right) \frac{d\varphi}{dT} \tag{3.30}$$

$$C_{eff} = (1-\varphi)C_{p1} + \varphi\, C_{p2} + \left(H_{P2} - H_{p1}\right)\frac{d\alpha}{dT} \quad (3.29)$$

The effective thermal conductivity of PCM during phase change process is given by equation 3.31.

$$k = (1-\varphi)k_1 + \varphi k_2 \quad (3.31)$$

Effective density of PCM during the melting process is given by equation 3.32.

$$\rho = \frac{(1-\alpha)\rho_1 C_{P1} + \alpha\, \rho_2 C_{P2}}{(1-\alpha)C_{P1} + \alpha C_{P2}} \quad (3.32)$$

Where, ρ_1 = density of PCM in solid phase, ρ_2 = density of solid in liquid phase, C_{p1} = specific heat of solid phase, C_{p2} = specific heat of liquid phase.

Using these modeling equations from 3.24-3.31, a mathematical model for the TSU having PCM with embedded tube was developed for both TSU and simulated. The simulation results obtained were validated with experimental results

CHAPTER 4

RESULTS AND DISCUSSION

Introduction

In this chapter results of various physical, chemical and thermal characterization analysis such as scanning electron microscopy (SEM), X-ray diffraction (XRD), Fourier infra-red transform (FTIR), Differential scanning calorimetry (DSC) and Thermal gravimetric analysis(TGA) performed on the samples of pure beeswax, besswax/expanded graphite composite, expanded graphite and natural graphite are presented and discussed. In addition to this thermal storage performance of beeswax, composite of beeswax and natural graphite during charging and discharging in thermal storage unit are presented here. Comparison between the thermal performance of beeswax and composite material has been made and thermos-physical phenomena during charging and discharging of PCMs are presented.

4.1 Sample characterization

Samples of pure beeswax, natural graphite, expanded graphite and composites of beeswax/expanded graphite, beeswax/natural graphite were prepared and characterized for physical, chemical and thermal behavior as per the standard methodology [173, 279, 280]. The results of different characterizations are presented here.

4.1.1 SEM analysis of samples

Scanning electron microscopy of natural graphite, expanded graphite, beeswax and composite materials were carried out to study surface characteristic, surface morphology etc. SEM micrographs of natural graphite and expanded graphite are shown in Figure 4.1. The SEM image in Figure 4.1 (a) reveals that the micro structure of natural graphite is compact due to improper intra layer separation with smaller surface area. Due to this compact structure the density of natural graphite is higher (1289 kg/m^3) and it could not form composite with molten beeswax due to its early settlement in molten composite rather than forming a homogeneous mixture. The SEM image of expanded graphite in Figure 4.1(b) shows clearly visible separation between the layers due to intercalation. These separations between layers of expanded graphite eased the absorption of molten beeswax and hence provided sufficiently large surface area for heat transfer. Density of expanded graphite found to be 46 kg/m^3 which is quite lesser as compared to the natural graphite and therefore formed

a homogeneous composite material with beeswax. Similar layer separations/ microstructures were also observed in expanded graphite by different researchers due to intercalation [173, 279].

SEM micrographs of beeswax and composite material are shown in Figure 4.2 at the resolution of 2000X. The micrograph of beeswax in Figure 4.2(a) is showing superimposed plates of amorphous and heterogeneous polymers containing mainly fatty acids along with esters and hydrocarbons. Figure 4.2(b) is showing the micrograph of composite material in which expanded graphite (10%) has been homogenously distributed within the matrix of beeswax. The molten beeswax is absorbed on the layers of expanded graphite to provide a continuous network for heat transfer. The white scattered pattern observed in the composite image represents the portion of beeswax coming out of the gaps of expanded graphite.

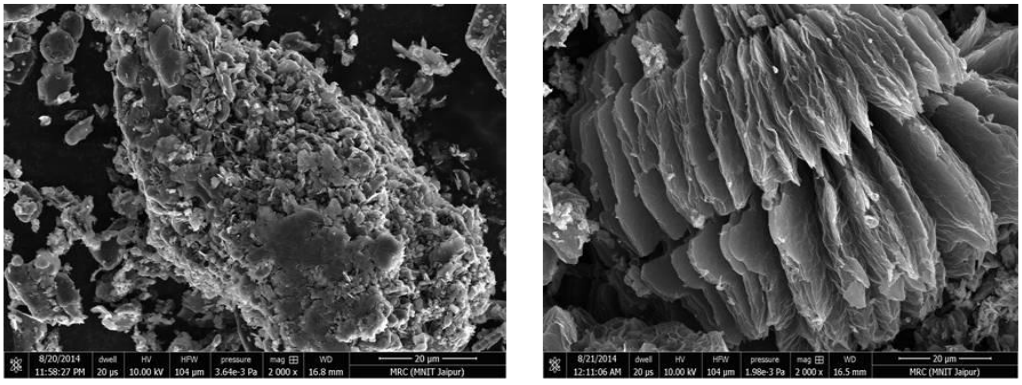

Figure 4.1 SEM micrographs of (a) Natural graphite (b) Expanded graphite

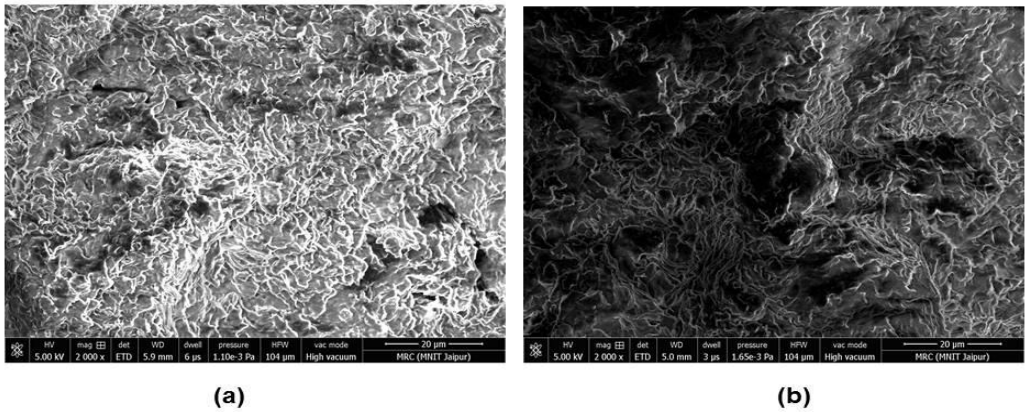

Figure 4.2 SEM micrographs of (a) Beeswax (b) Composite of beeswax and expanded graphite (10 %)

4.1.2 FTIR analysis of samples

FTIR spectra of beeswax, expanded graphite and beeswax/expanded graphite composite (with 10% of EG) are depicted in Figure 4.3. Peak observed at wavelength of 3446 cm^{-1} for expanded graphite represents –O-H stretching mode while peak at 2846 cm^{-1} represents -C-H stretch of the alkane bonds present in the hexagonal structure of the graphite. Peak noticed at 1382 cm^{-1} represents the symmetric N-O stretch which may be due to presence of nitro group, while peak at 1646 cm^{-1} represents -C≡C stretch. Similar peaks were observed and reported by the researchers in their studies for FTIR analysis of expanded graphite [287] .FTIR spectra of beeswax shows peaks at 2922 cm^{-1} and 2852 cm^{-1} representing C-H stretch i.e. presence of alkane/HC chain in the structure of beeswax. Peaks at 1742 cm^{-1} reflect the presence of ester, while peaks at 1104 cm^{-1} and 718cm^{-1} represent alkene and amide groups. Similar FTIR spectra for beeswax were reported in the studies [281, 282]. FTIR spectra of composite material is much similar to FTIR spectra of beeswax due to merging of peaks of expanded graphite (3446 cm^{-1}, 2916 cm^{-1}) within the peaks of composite (3444 cm^{-1}, 2916 cm^{-1}). Absence of any new peak in the FTIR of composite material confirms that composite of beeswax and expanded graphite is just a combination of two materials rather than a chemically new material.

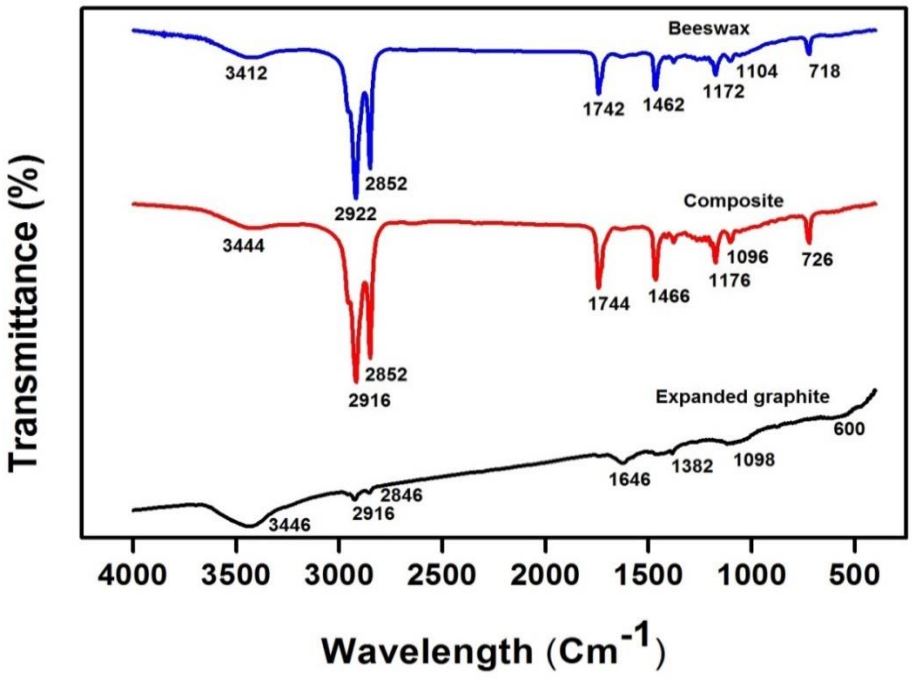

Figure 4.3 FTIR spectrums of beeswax, expanded graphite and composite (10% EG)

4.1.3 XRD analysis of samples

XRD analysis of samples were performed and Figure 4.4 represents the XRD graphs of natural graphite and expanded graphite showing the maximum counts at 2θ = 26.25° for natural graphite with d-spacing value of 3.3639 A° and 2θ = 26.49° for expanded graphite with d-spacing value of 3.3947A°. The values for the characteristic peak of natural graphite and expanded graphite is due to the diffraction of 002 with d-spacing values of 3.38 A° while after intercalation separation of multilayers occurred at the c-axis of the crystal as also suggested by the different researchers [173, 279, 283]. This suggested that chemical oxidation, hot drying and microwave treatment during preparation of expanded graphite process did not alter the order of the multilayer of graphite and thus maintained their proper d-spacing values. Absence of any new peak in the XRD pattern of expanded graphite also proved that no new chemical species was formed during the formation of expanded graphite.

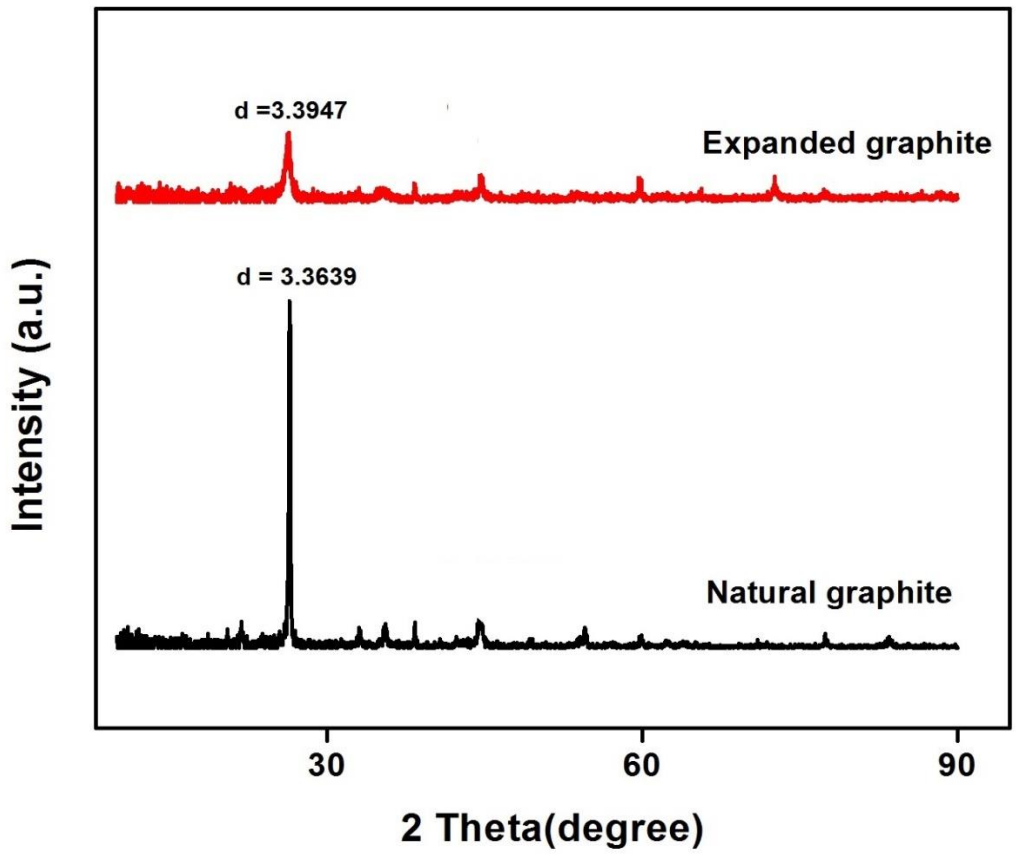

Figure 4.4 XRD graphs of natural graphite and expanded graphite

Figure 4.5 represents the XRD pattern obtained for beeswax, composite and expanded graphite and observed one high intensity peak at 2θ = 21.57° (d spacing = 4.1185), and two low intensity peaks at 2θ = 23.89° (d spacing = 3.6997 A°) and 2θ = 44.64° (d spacing = 2.0298A°) of the composite are corresponding to the peaks found in beeswax at 2θ = 21.16°, 23.53° and 44.64° with d-spacing values 4.1981A°, 3.7805A° and 2.0294A° respectively. Similar peaks were reported in XRD pattern of beeswax in the studies and these peaks represent the orthorhombic crystal structure of beeswax [284, 285].The peak at 2θ = 26.91° with d-spacing value of 3.3127A° in composite representing the corresponding peak of expanded graphite (2θ = 26.49°, d = 3.3947). Thus the XRD results in the present study confirmed that the composite prepared is a homogeneous mixture of beeswax and expanded graphite. No new peaks were observed in the XRD pattern of the composite which showed the formation of no new chemical species.

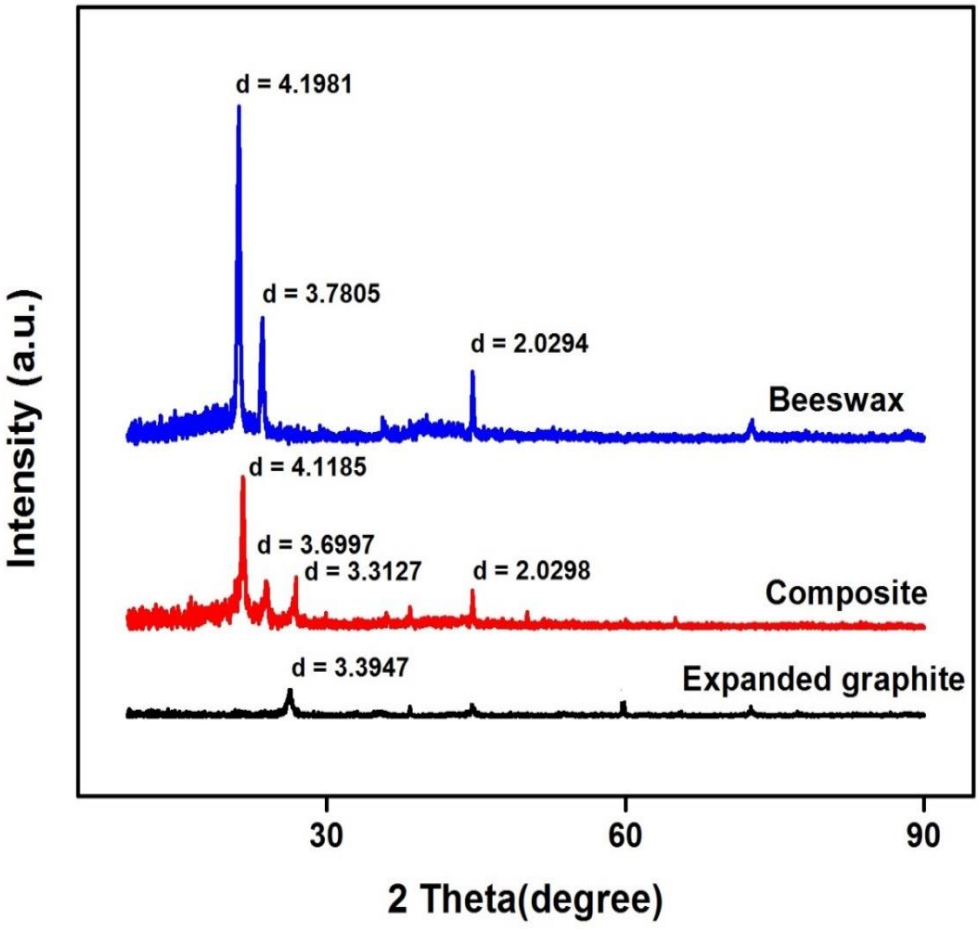

Figure 4.5 XRD pattern for beeswax, composite and expanded graphite

4.2 Thermal characterization of samples

Thermal properties of beeswax and its composite with expanded graphite were studied with the help of thermal conductivity meter, Thermal gravimetric analysis (TGA) and Differential scanning calorimetry (DSC).

4.2.1 Thermal conductivity of samples

Composites of beeswax with different weight percentage of natural graphite and expanded graphite were prepared in order to enhance the thermal conductivity of pure beeswax. The thermal conductivity of these samples were measured and plotted as shown in Figure 4.6. Higher thermal conductivity of beeswax/expanded graphite composite was observed as compared to beeswax/natural graphite composites. It may be due to the presence of continuous matrix of expanded graphite throughout the beeswax which enhanced the heat flow through the composite (beeswax/expanded graphite) while in other case (beeswax/natural graphite composite) discontinuous phase of natural graphite leads to lower heat flow. Composites of beeswax/natural graphite found to be non-homogenous during molten state due to settlement of natural graphite. Optimum weight percentage of expanded graphite was 10 % as further addition of expanded graphite results in cracks in the composite material, which creates air pockets and reduces the thermal conductivity.

The thermal conductivity of composite with 10 wt. % of expanded graphite was found to be 0.63 W/m.K which is 117 % higher as compared to thermal conductivity of pure beeswax (0.29 W/m.K) and similar thermal conductivity enhancement of PCMs were observed in the studies with the addition of expanded graphite [188, 223, 286] . Due to settlement of natural graphite in the molten beeswax, the composite of beeswax/natural graphite was not prepared for experimental studies. The magnitude of errors was found to be 1-3% for thermal conductivity.

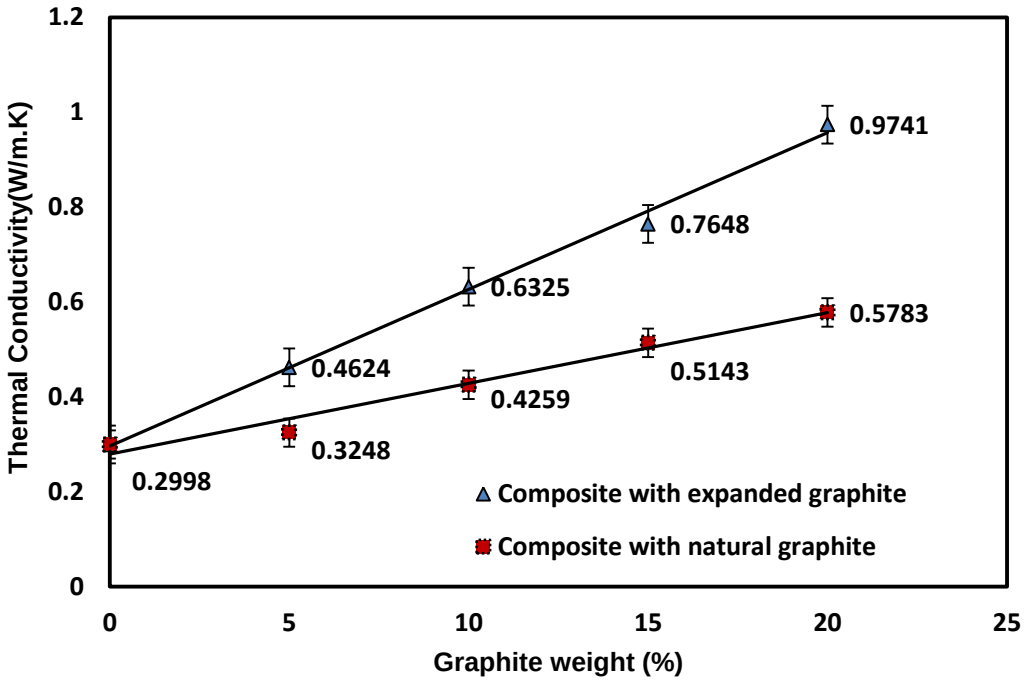

Figure 4.6 Thermal conductivity of composites with different proportion of graphite

4.2.2 DSC results of samples

Differential Scanning calorimetry (DSC) analysis of beeswax and its composite were carried out and Figure 4.7 shows the DSC result for fixed mass of beeswax samples i.e. 4 mg (sample 1 and sample 2). The peak observed at 42.4 ºC represents either some kind of solid-solid phase transition or melting of some other organic component of beeswax. Another peak noticed at 59.6 ºC shows solid-liquid phase transition that might have occurred during melting and hence, represents the melting point of the beeswax. The melting and solidification temperature were found to be same for both the samples (sample 1 and sample 2) with 2% deviation in heat flow. From DSC analysis melting point and freezing point of beeswax were found to be 59.8 ± 0.5 ºC and 56.4 ± 0.5 ºC respectively, while the measured value (Appendix III) of latent heat of melting was 214 kJ/kg in the temperature range of 30.8 °C to 68 °C.

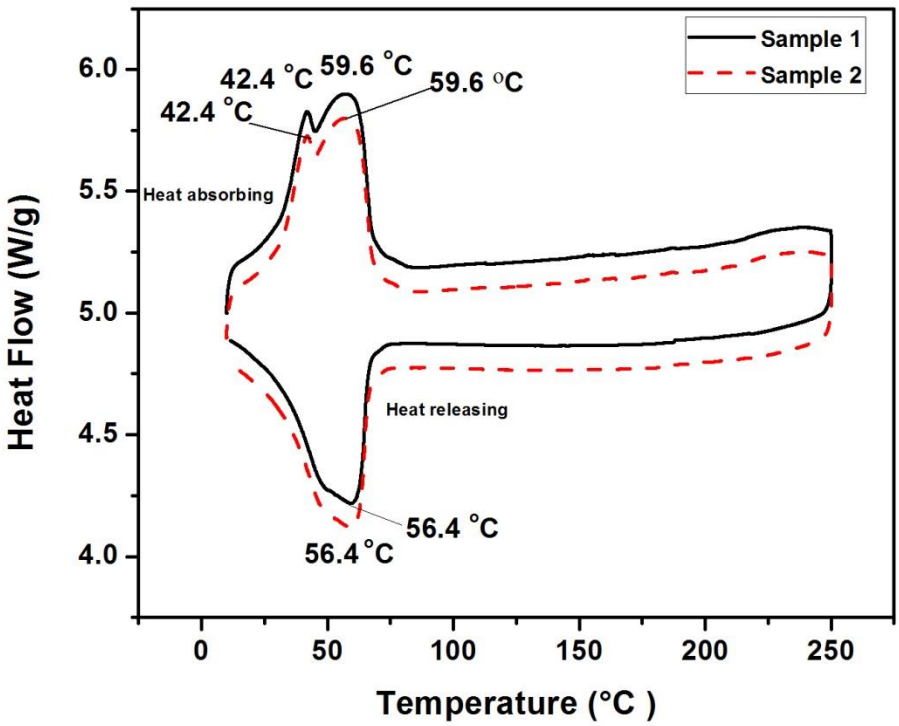

Figure 4.7 DSC curve of beeswax and its melting behavior

Figure 4.8 represents the DSC curve of beeswax/expanded graphite composite. The peak observed at 41.6 °C either represents the solid-solid transition occurred in the composite with temperature rise or may be due to melting of some other organic component present in the beeswax. Broad peak noticed at 57.3 °C represents the melting temperature of composite which is lower than pure beeswax due to presence of expanded graphite in it. The freezing point and latent heat of composite was found to be 57.1 °C and 198 kJ/kg respectively. The lower value of latent heat of composite was due to reduced amount of beeswax due to the addition of expanded graphite in the composite.

DSC curve of the beeswax and beeswax/expanded graphite composite for the melting cycle was compared and shown in Figure 4.9 and it is observed that the addition of expanded graphite results in lower value of melting point of the beeswax/expanded graphite composite. With 10% addition of expanded graphite to the beeswax 8.8% reduction in the latent heat of PCM (beeswax) was observed.

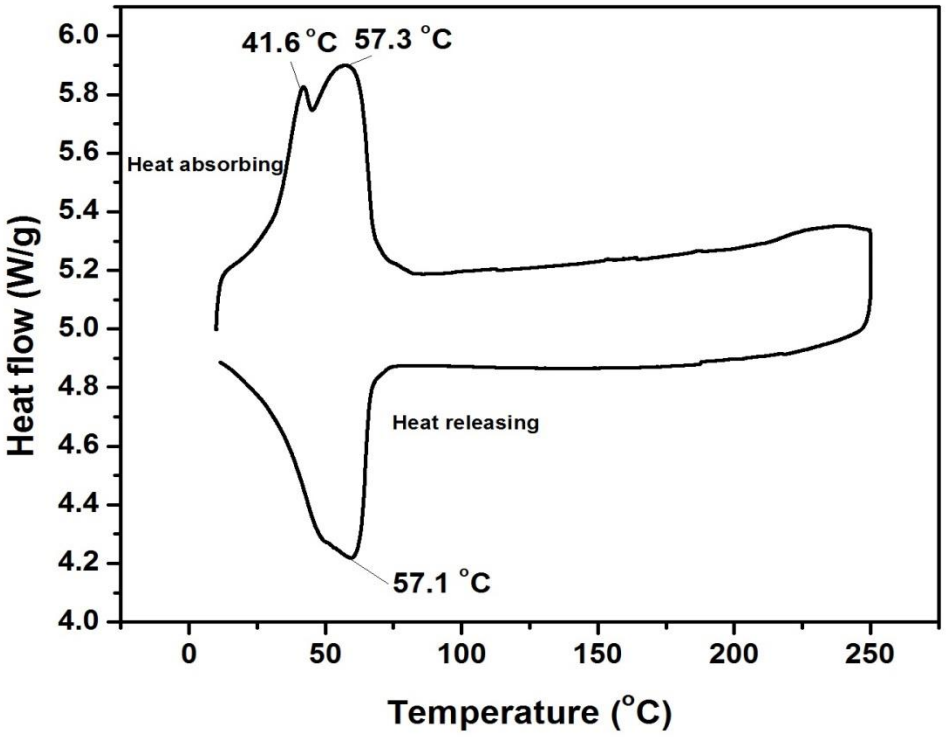

Figure 4.8 DSC curve for beeswax/expanded graphite composite

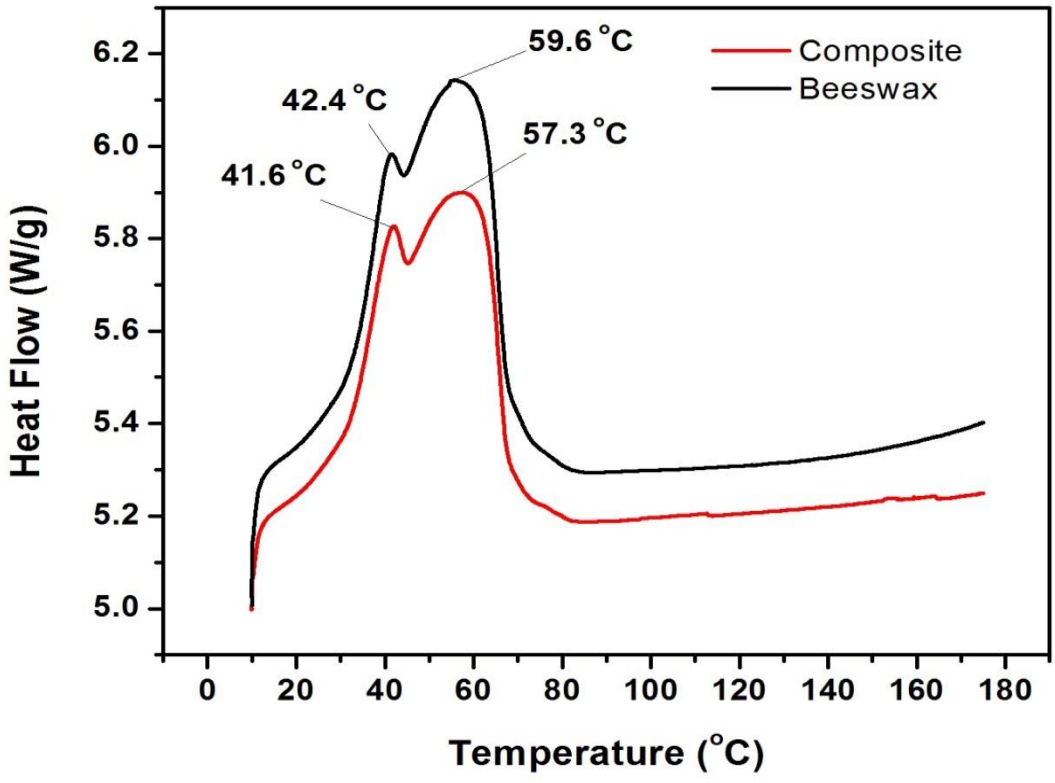

Figure 4.9 DSC comparisons for beeswax and composite material

4.2.3 TGA analysis of samples

TGA analysis of beeswax and composite was carried out and Figure 4.10 represents the graph obtained during TGA analysis of beeswax in which no weight loss was observed with rise in temperature up to 215 ºC (with standard deviation of ±1.8%), confirms its thermal stability up to this temperature. After 215 ºC there is continuous mass reduction of beeswax with further rise in temperature, which could be due to vaporization of beeswax by degradation of hydrocarbons. At 443 °C of temperature complete weight loss of beeswax was observed. Stability of beeswax up to 215 ºC makes it suitable material to be used for domestic and solar applications that works in the low temperature range (60 ºC-90 ºC).

Figure 4.11 represents the TGA analysis of composite material. In case of composite material no weight loss was observed during heating from 10 °C up to 236.8 °C after which its thermal degradation started which may be due to conversion/degradation of higher hydrocarbons to the smaller one. It was also observed that after 412.8 °C only 11.87% mass of composite material remained and no further degradation was observed. This remaining material represents the added graphite and other residuals of beeswax which adhered to graphite after thermal degradation of beeswax. Therefore, TGA analysis also confirmed the better thermal stability of composite compared to natural beeswax and can be used as PCM for low temperature thermal storage applications.

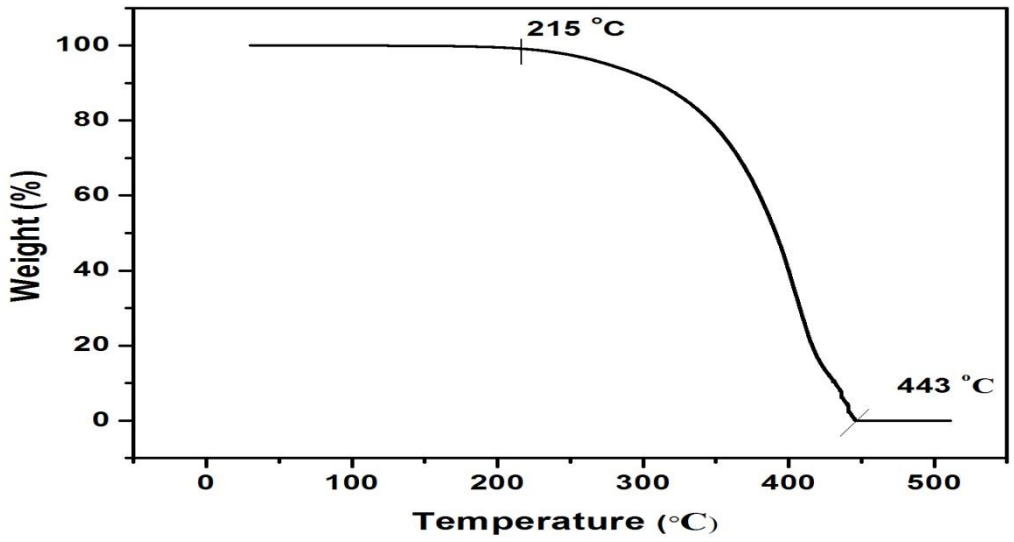

Figure 4.10 TGA curve for beeswax

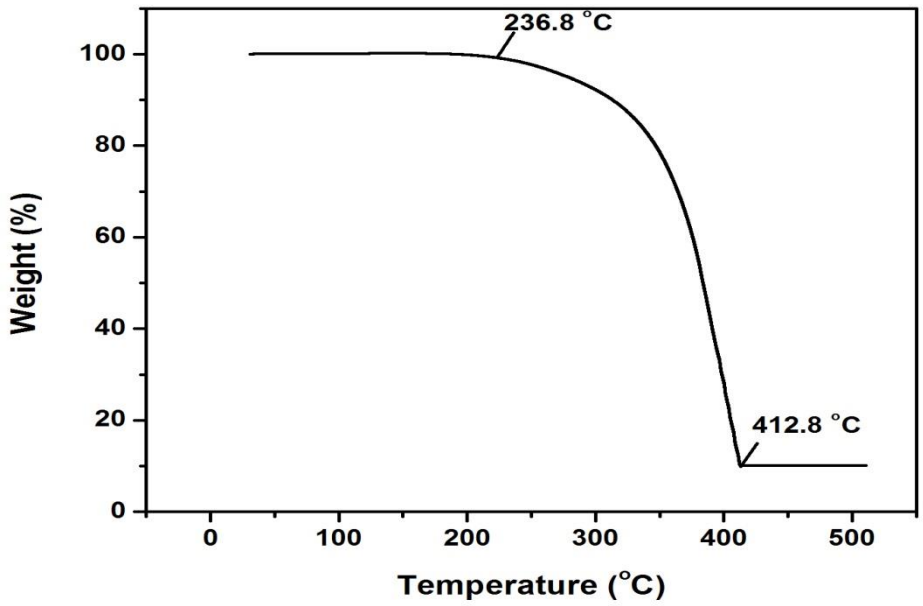

Figure 4.11 TGA curve for beeswax/expanded graphite composite

Physical and thermal properties of beeswax and its composite were measured and presented in Table 4.1. Density of beeswax and its composite are different due to lower density of expanded graphite. Reduction in specific heat was also observed for composite material due to presence of lower specific heat of expanded graphite material. Thermal properties obtained from TGA analysis shows that composite using high thermal conductivity material such as expanded graphite is a better heat transfer material compared to pure beeswax.

Table 4.1 Properties of beeswax and its composite with expanded graphite (10%)

Properties	Beeswax	Composite	Natural Graphite	Expanded Graphite
Density	971.80 kg/m^3	835.20 kg/m^3	1250 kg/m^3	46 kg/m^3
Melting point	59.6 °C	57.3 °C	-	-
Thermal conductivity	0.29 W/m.K	0.63 W/m.K	97 W/m.K	97 W/m.K
Specific heat	2.60 kJ/kg.K	1.70 kJ/kg.K	0.866 kJ/kg.K	0.866 kJ/kg.K
Latent heat	214 kJ/kg	198 kJ/kg	-	-

4.3 Performance evaluation of phase change material in small TSU

Thermal energy storage performance of beeswax and beeswax/expanded graphite composite is performed in a rectangular shell and tube heat storage unit (Capacity PCM 2.5 kg). Shell part of this storage unit contained beeswax and its composite in separate studies as phase change material while hot water passed through the central copper tube and nine temperatures at three axial locations were measured using calibrated k type thermocouples along with hot water inlet and outlet temperature. Figure 4.12 shows the temperature variation at nine locations with time for beeswax and it is observed that the time taken by beeswax to reach the melting point increases from inlet (at T4 point, 360 min), middle point (at T5 point, 540 min) to outlet (at T6 point, 780 min) due to continuous reduction in temperature gradient between the hot water and beeswax. Similar patterns for increase in melting time of the beeswax was observed for the axial points above (T1:810 min, T2:840 min, T3:1140 min) and below the tube (T7:840 min, T8:870 min, T9:11260 min).

However, in case of composite of beeswax and expanded graphite as the melting time was reduced at all the points along the axis (T4:200 min, T5:250 min, T6:330 min) and parallel to the axis at top (T1:540 min, T2:600 min, T3:630 min) and bottom positions (T7:450 min, T8:480 min and T9:720 min) as shown in Figure 4.13. After a certain time the PCM in the shell reaches to the same temperature at almost all the points due to convection effect. All the nine thermocouples reached at constant temperature in 1020 min in case of composite as compared to pure beeswax (1430 min). The reduction in melting time in case of composite was due to enhanced thermal conductivity of beeswax due to the addition of expanded graphite. It is observed from Figure 4.13 that the temperature at the middle location (T4) of heat transfer unit rose most rapidly as compared to other locations i.e. T1 and T7. It was due to the large temperature difference between hot water and phase change material at middle location which caused good heat condction, while in upper and lower location of heat transfer unit heat transferred through conduction followed by convection. It is also observed in thermal profiles of both the PCM that temperature at lower location (T7) initially increased rapidly upto the melting point and then slowed down as compared to the upper location (T1). During this process the phase change

material melted first at middle location and moved down to lower location due to gravitation effect and transfered heat and raised temperature at the lower material.

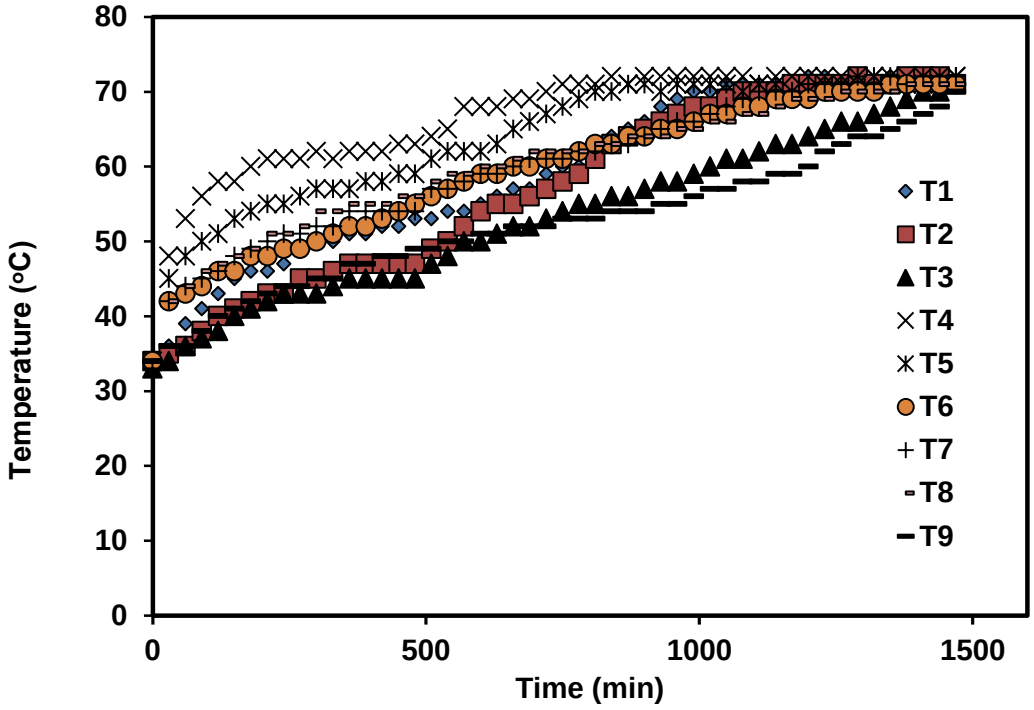

Figure 4.12 Thermal profile of beeswax at nine locations in small TSU

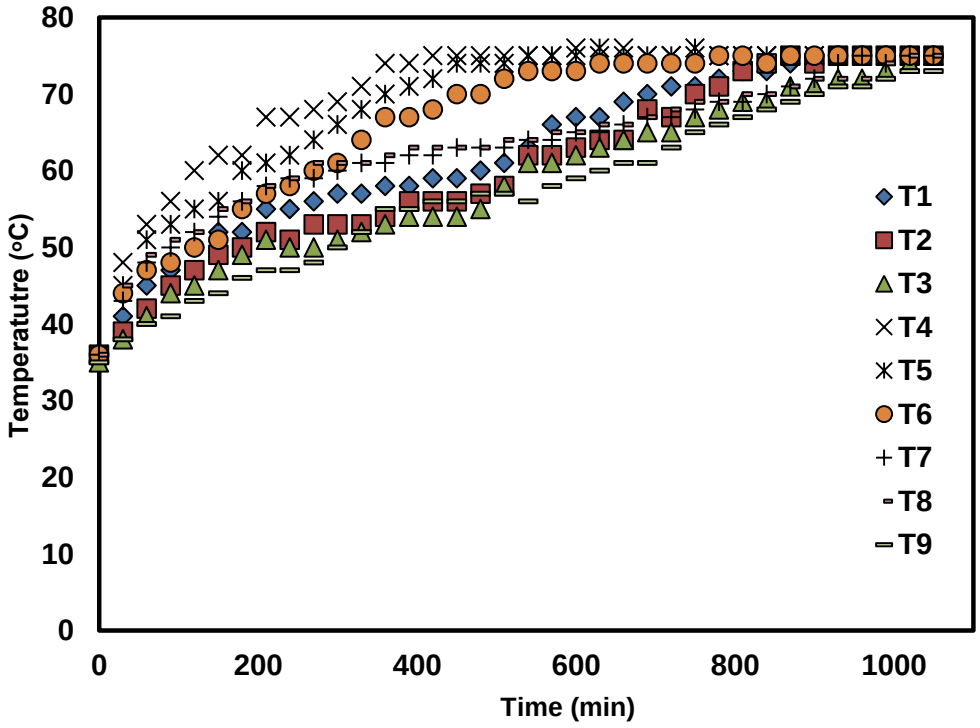

Figure 4.13 Thermal profile of composite at nine locations in small TSU

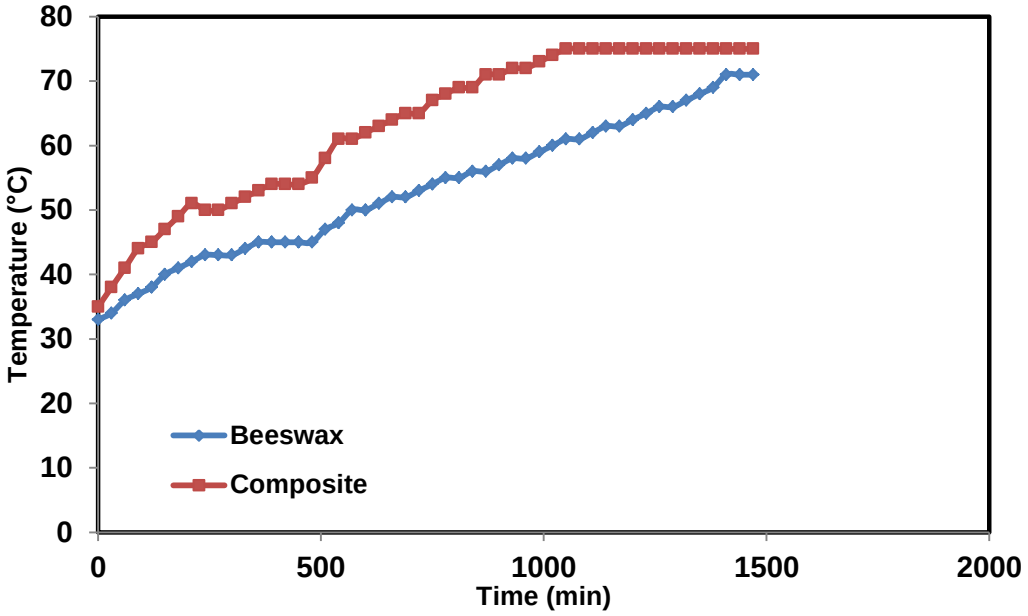

Figure 4.14 Comparison of charging time of beeswax and composite at thermocouple T3

When the temperature of lower material reaches to melting point the convection heat tarnsfer becomes dominant and forces the molten phase change material to move upwards of the unit. Temperature rise of the upper material in the unit is due to combined effect of conduction from middle location followed by convection from the middle and the lower material of the unit.

It is observed from Figure 4.13 that the temperature at the middle location (T4) of heat transfer unit rose most rapidly as compared to other locations i.e. T1 and T7. It was due to the large temperature difference between hot water and phase change material at middle location which caused good heat condction, while in upper and lower location of heat transfer unit heat transferred through conduction followed by convection. It is also observed in thermal profiles of both the PCM that temperature at lower location (T7) initially increased rapidly upto the melting point and then slowed down as compared to the upper location (T1). During this process the phase change material melted first at middle location and moved down to lower location due to gravitation effect and transfered heat and raised temperature at the lower material. When the temperature of lower material reaches to melting point the convection heat tarnsfer becomes dominant and forces the molten phase change material to move

upwards of the unit. Temperature rise of the upper material in the unit is due to combined effect of conduction from middle location followed by convection from the middle and the lower material of the unit. The time taken by beeswax to attain a constant temperature of 72 ºC for complete material was 1430 min, as compared to 1020 min (for constant temperature of 75 ºC) in case of composite material as shown in Figure 4.14. The reduction in charging time to reach constant temperature in whole composite material was due to the presence of interconnected network of expanded graphite which enhanced thermal conductivity.

4.4 Performance evaluation of large scale TSU with beeswax

Experimental study on small TSU using beeswax and its composite showed good results. To conduct detail thermal performance study on graphite, beeswax and composite as heat storage materials using various heat transfer fluids such as water, alumina nanofluid, expanded graphite water solution and engine exhaust gases a large TSU was developed. The large thermal storage unit can store 18 kg of PCM in rectangular shell with helical embedded tube for carrying hot heat transfer fluid.

4.4.1 Repeatability of results

At the beginning of experimental study, in order to ensure repeatability and consistency of data repeated experiments were performed three times at constant flow rate of 0.5 LPM±0.01 LPM and 80 °C of inlet temperature. The temperature variation of beeswax (PCM) with time at three different positions of thermocouples (T3, T6, and T9) along the vertical line in middle of large TSU were obtained and analyzed for variation in reading of thermocouple for same set of data as shown in Figure 4.15. The error was estimated (0.6%-1.2%) and readings (10 min-20 min) were further corrected accordingly.

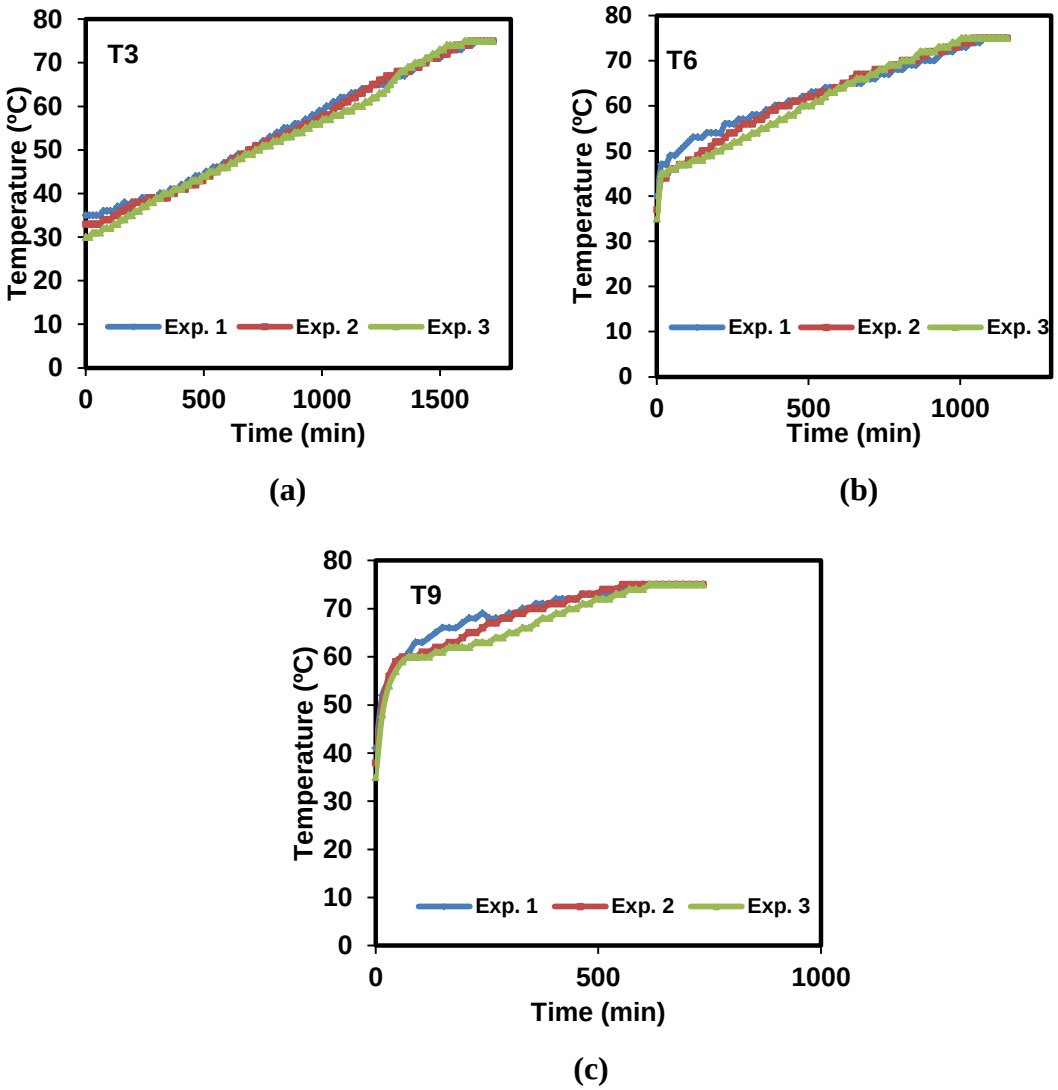

Figure 4.15 Temperature variation measured at three different positions of thermocouples

4.4.2 Using plain water as HTF

Thermal storage performance of beeswax is studied in large TSU by passing hot water through the helical tube of TSU at different flow rates such as 0.25 LPM, 0.5 LPM, 0.75 LPM, 1 LPM and different inlet fluid temperatures i.e. 60 °C, 70 °C, 80 °C, and 90 °C.

i) Effect of flow rate on charging time

Temperature variation at position T3 of TSU at different flow rates and different inlet fluid temperature is shown in Figure 4.16. It is observed that an increase in flow rate of HTF has reduced the charging time of beeswax at constant inlet fluid temperature. From Figure 4.16 (c) the charging time of beeswax obtained is 1830 min, 1650 min,

1590 min, 1530 min at the flow rate of 0.25 LPM, 0.50 LPM, 0.75 LPM and 1.0 LPM respectively for inlet fluid temperature of 80°C. Thus, it is noticed that charging time reduced from 1830 min to 1530 min when flow rate increased from 0.25 LPM to 1.0 LPM. Similar reduction in charging time is observed with increase in fluid velocity for different inlet temperatures of 60 °C, 70 °C, and 90 °C as shown in Figure 4.16 (a), (b), (d).

Decrease in the charging time of beeswax with increase in fluid flow rate is due to increase in Reynolds number which correspondingly enhanced the heat transfer coefficient inside the tube as shown in Table 4.2. The value of Reynold's number for each flow is also lying below the critical Reynold's number of helical coil i.e. 9289 (Appendix III) and therefore the flow pattern is lying in laminar region [293]. The increased heat transfer coefficient at higher fluid flow rates promotes faster heat transfer from fluid inside the tube to the tube surface which in turn increased charging rate of the beeswax. The values of charging times (position T3) obtained at four different flow rates of water and four different inlet fluid temperatures are given in Table 4.3.

Higher fluid flow rates give lower charging time of beeswax, however, at higher flow rates the storage efficiency of thermal storage system decreases and maximum storage efficiency is obtained at 0.5 LPM as shown in Figure 4.17. The efficiency of TSU found to be 83.4%, 84.2%, 72% and 58.3% at flow rates of 0.25 LPM, 0.5 LPM, 0.75 LPM and 1.0 LPM respectively at constant inlet fluid temperature of 80 °C. In the present experimental study flow rate of 0.5 LPM and above are considered while at lower flow rate of 0.25 LPM a large pressure drop is observed that hindered the fluid flow hence not considered in further studies.

Variation of energy available from hot HTF and energy stored by beeswax at different flow rates at constant inlet temperature of 80 °C is shown in Figure 4.18 and it is observed that the amount of available energy has increased with the increase in flow rate due to the enhanced enthalpy content of the fluid (higher mass flow rate) while the energy stored by the beeswax almost remained constant with flow rate. Due to this energy difference the storage efficiency of the system reduced with increase in flow rate.

Various other researchers have also noticed the reduction in charging time of phase change material with increase in the flow rate of HTF. Akagun et al. 2008 [154] studied the melting and solidification profile of paraffin in shell and tube type heat exchanger and observed that the melting time of PCM was reduced by 30% with increase in flow rates (4 kg/min, 6 kg/min and 8 kg/min). In an another study, Sari et al. 2001 [195] also observed the effect of flow rates (1.6, 2, 3, and 6 kg/min) on the thermal performance of energy storage system with myristic acid as phase change material and noticed that with six times increase in flow rate, the melting time of myristic acid reduced by 35%. Similar investigation at different flow rates (1.2-6 kg/min) was performed on stearic acid [211] and found 20% decrease in the melting time with six times increase in the flow rate. However, in all these studies it is also suggested that the lower flow rates are more rational and practical for thermal storage applications due to requirement of less pumping power.

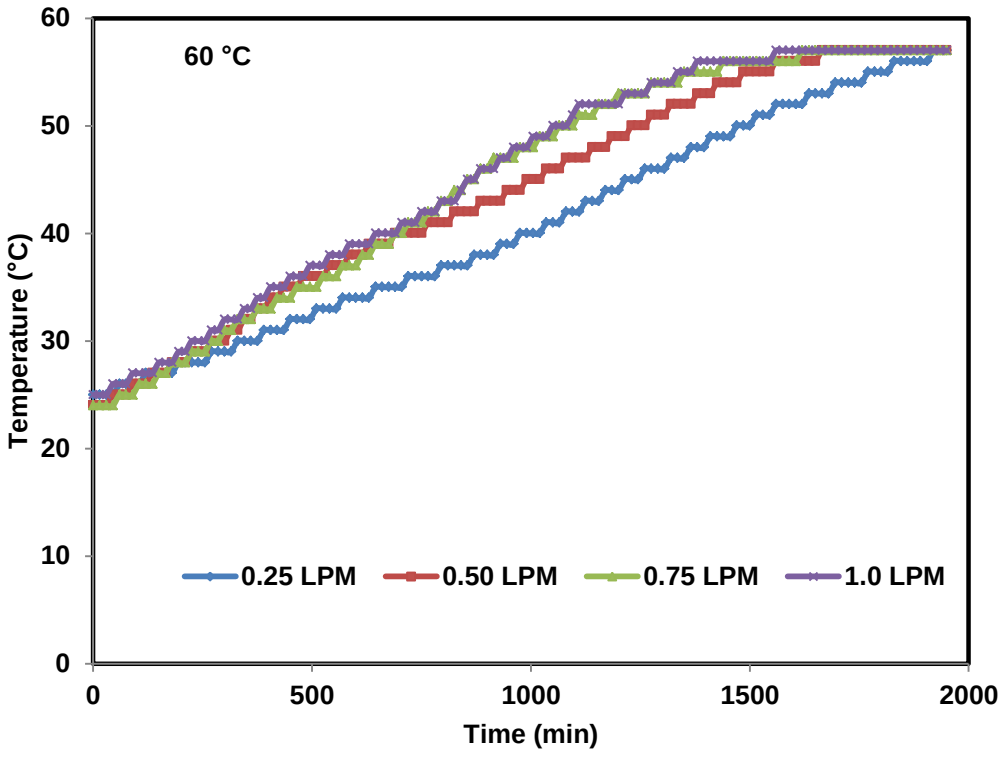

(a)

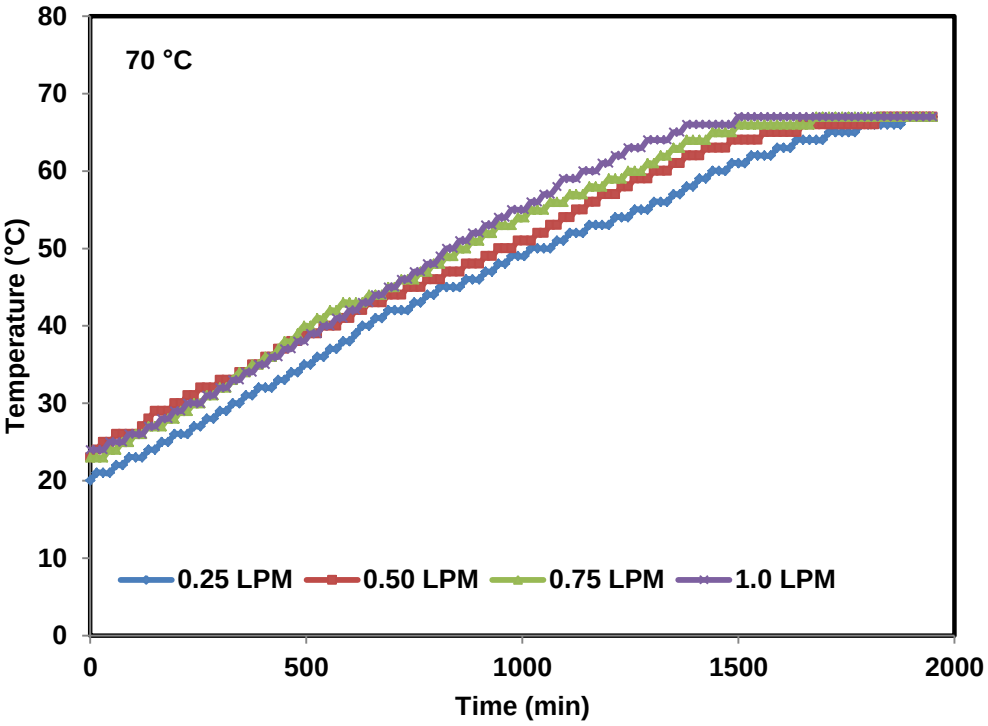
70 °C
Temperature (°C)
Time (min)
0.25 LPM
0.50 LPM
0.75 LPM
1.0 LPM
0
10
20
30
40
50
60
70
80
0
500
1000
1500
2000

(b)

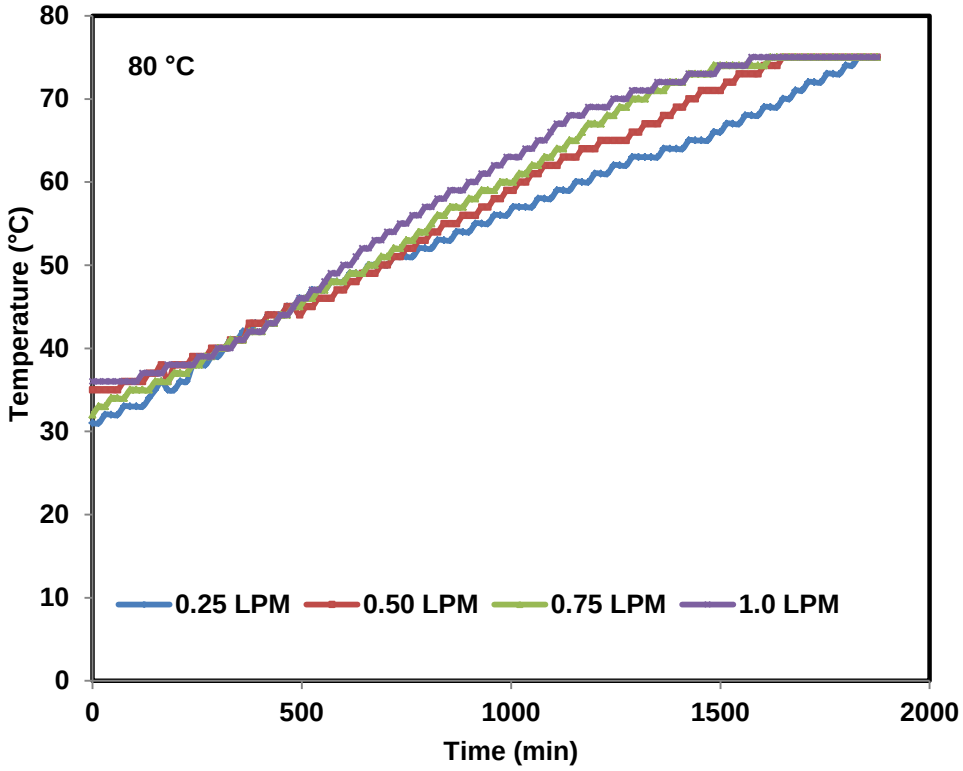
80 °C
Temperature (°C)
Time (min)
0.25 LPM
0.50 LPM
0.75 LPM
1.0 LPM
0
10
20
30
40
50
60
70
80
0
500
1000
1500
2000

(c)

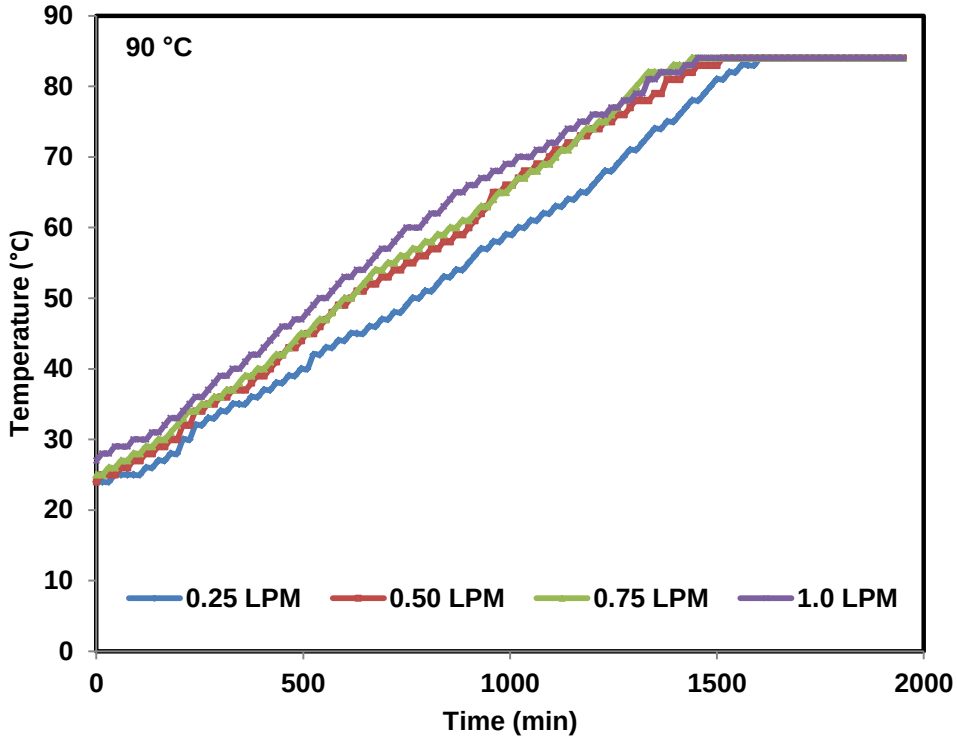

(d)

Figure 4.16 Effect of water flow rate on charging time of beeswax at different inlet temperature

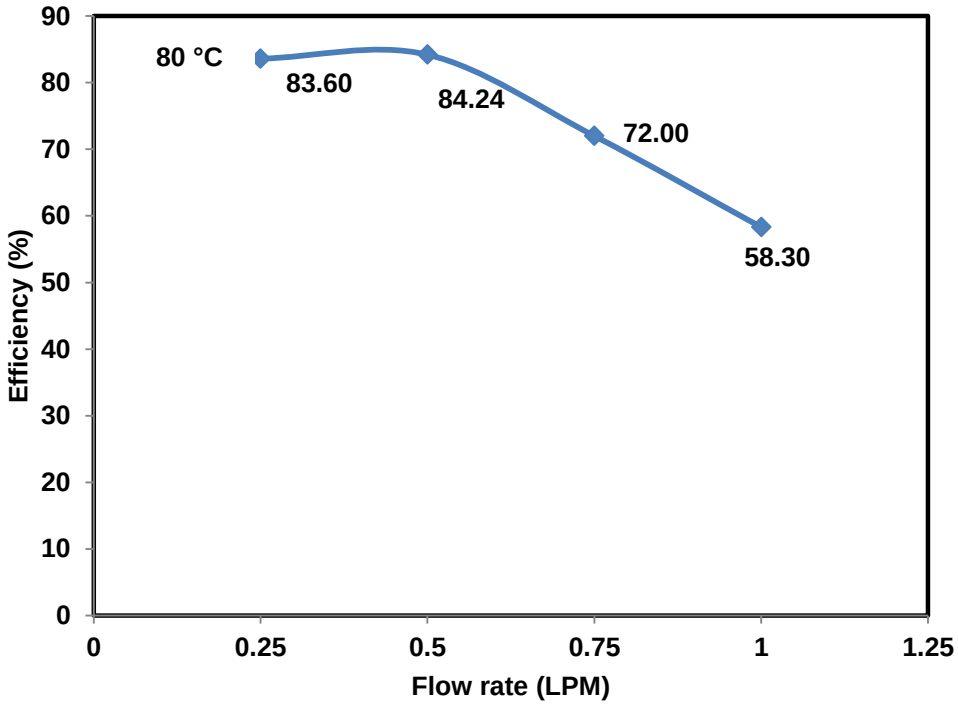

Figure 4.17 Efficiency of large TSU with beeswax at different flow rates of water

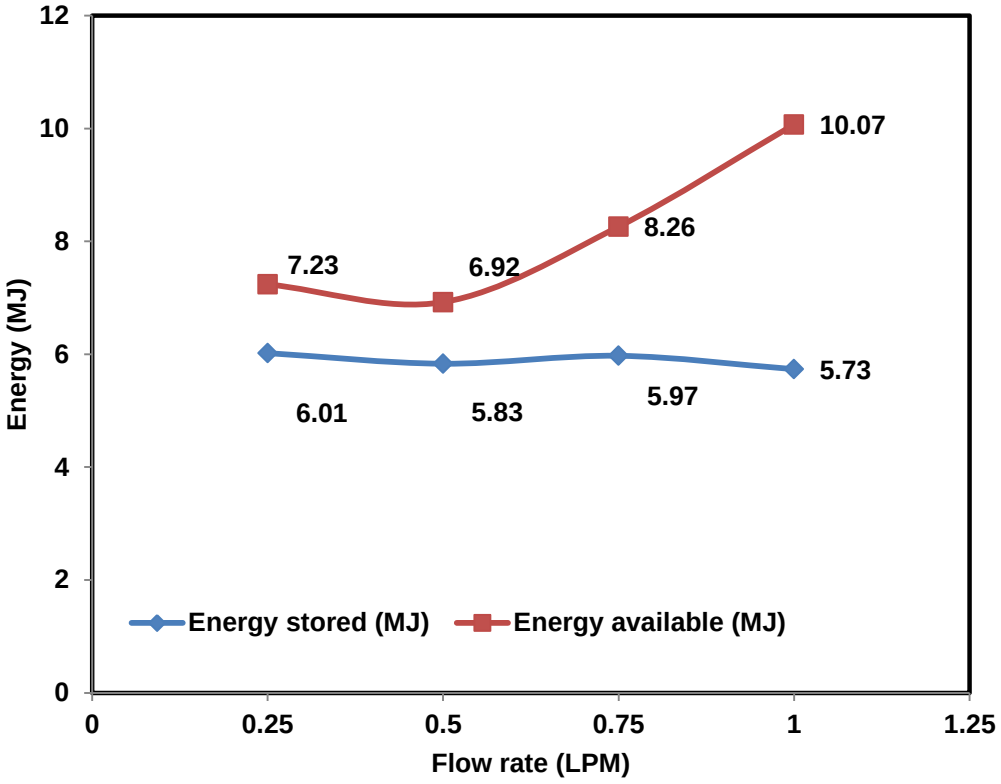

Figure 4.18 Variation of energy available and energy stored at different flow rates of water

Table 4.2 Reynold's number and heat transfer coefficient at different water flow rates at inlet fluid temperature of 80 °C

Flow rate (LPM)	Reynold's No.	Critical Reynold's No.	Internal heat transfer coefficient ($W/m^2.K$)	Overall heat transfer coefficient ($W/m^2.K$)	Flow type
0.25	1818	9289	842.52	225	Laminar
0.50	3613	9289	1134	245	Laminar
0.75	5431	9289	1351	254	Laminar
1.00	7249	9289	2695.91	284	Laminar

ii) Effect of inlet fluid temperature on charging time

Temperature variation of beeswax at position T3 in large thermal storage unit with time at different inlet fluid temperatures (60 °C, 70 °C, 80 °C and 90 °C) are shown in Figure 4.19 keeping fluid flow rate constant. Charging time of beeswax reduced with

increase in the inlet fluid temperature and minimum charging time is obtained at highest inlet fluid temperature of 90 °C. From Figure 4.19 (a) it is observed that the charging time of beeswax is recorded as 1935 min, 1890 min, 1830 min and 1785 min for the inlet fluid temperature of 60 °C, 70 °C, 80 °C and 90 °C respectively at constant flow rate of 0.25 LPM. Similarly the charging time of beeswax obtained is 1755 min, 1695 min, 1650 min and 1575 min for the inlet fluid temperature of 60 °C, 70 °C, 80 °C and 90 °C respectively (Figure 4.19 (b)) at the flow rate of 0.5 LPM.

Decrease in charging time of beeswax with increase in inlet fluid temperature is due to higher temperature difference between the HTF and PCM which causes faster heat transfer. Similar variations in charging time with inlet temperatures were also observed on other two flow rates (0.75 LPM and 1.0 LPM) as shown in Figure 4.19 (c),(d) and Table 4.3.

Table 4.3 Charging time of beeswax at different parametric conditions

Flow rate (LPM)	Inlet temperature (°C)	Charging time (min)
0.25	60 °C	1935
	70 °C	1890
	80 °C	1830
	90 °C	1785
0.50	60 °C	1755
	70 °C	1695
	80 °C	1650
	90 °C	1575
0.75	60 °C	1620
	70 °C	1680
	80 °C	1590
	90 °C	1545
1.00	60 °C	1560
	70 °C	1545
	80 °C	1530
	90 °C	1490

It is also observed from Figure 4.19 that temperature rise pattern at T3 is similar for all the inlet fluid velocities. Due to poor thermal conductivity of beeswax (0.29 W/m.K) heat transfer rate in beeswax through conduction is slower till the complete melting of beeswax. After melting convective heat transfer comes into play and

become dominant contributor for heat transfer leading to upward movement of molten beeswax due to buoyancy forces. At the inlet fluid temperature of 60 °C, the slow rise in temperature of beeswax is observed and the maximum temperature rise of 57 °C is noticed which is lower than melting point (59.8 °C) of beeswax which leads to incomplete melting of beeswax for all the flow rates and therefore it is preferable to use inlet fluid temperature higher than the melting point of PCM.

Decrease in charging time of PCM with increase in inlet fluid temperature is also observed by many researchers [257,294]. Yazici et al. 2014 [77] studied the melting behavior of paraffin wax in a horizontal shell and tube type thermal storage unit at different inlet fluid temperatures (75 °C, 80 °C and 85 °C) at the constant mass flow rate of 850 kg/h and observed 67% decrease in the melting time of PCM. Rathode et al. 2013 [79] also studied the thermal behavior of paraffin wax within a shell and tube type heat exchanger and found that the time required to reach complete melting increased by 22% when inlet fluid temperature decreased from 85 °C to 80 °C. Similarly charging time of paraffin wax increased by 78% when temperature of inlet fluid lowered from 85 °C to 75 °C. In an another work, Avci et al. 2013 [294]on paraffin wax in horizontal shell and tube type thermal storage system also showed that with increase in inlet temperature (75 °C, 80 °C and 85 °C) of HTF the charging time of PCM had decreased. Jesumathy et al. 2014 [257] also studied the effect of inlet temperature on charging time of paraffin wax in double latent heat storage unit and found that the charging time of PCM (Paraffin wax) reduced by 31% with increase in temperature from 70 °C to 74 °C.

Results of the present study show that higher inlet fluid temperatures are suitable for faster charging of beeswax. However, it is difficult to maintain a constant flow rate at the inlet fluid temperature of 90 °C due to the steam formation in helical tube which leads to frequent temperature drop and pressure drop within the helical coil of TSU. Therefore, in order to work efficiently and effectively, further experimental studies were performed at inlet fluid temperature of 80 °C. The efficiency of large TSU at different inlet fluid temperature is shown in Figure 4.20 and it is observed that with increase in the inlet fluid temperature of HTF, efficiency of TSU has increased. However, there is no much variation in the efficiencies at inlet fluid temperature of 80

°C and 90 °C due to formation of steam at high inlet fluid temperature which restrict the flow of HTF at 90 °C which results in reduced efficiency.

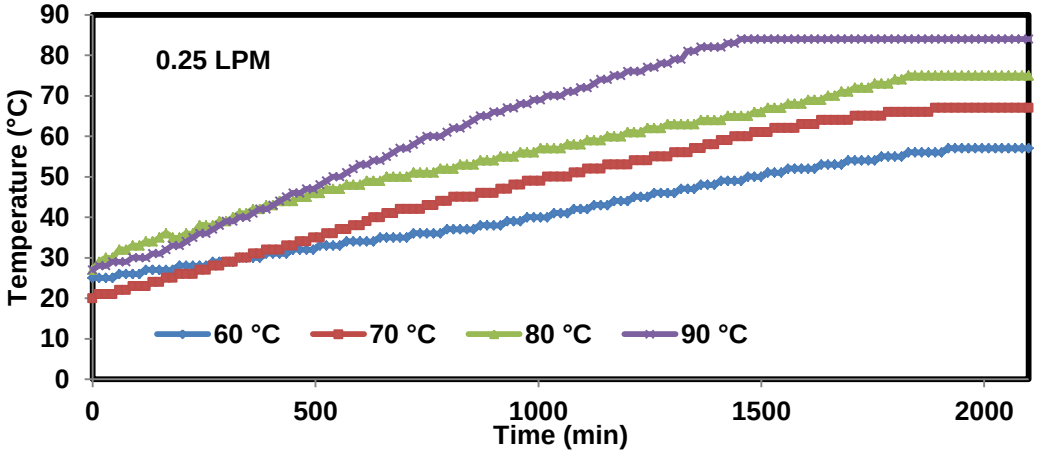

(a)

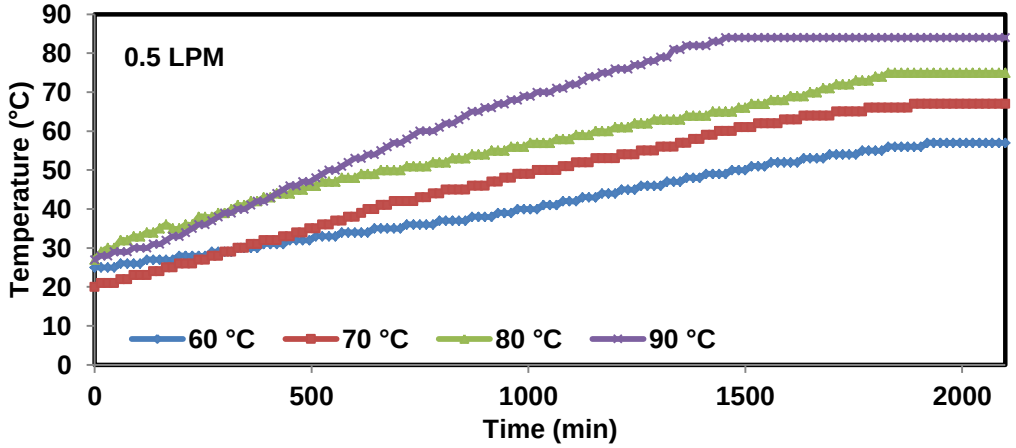

(b)

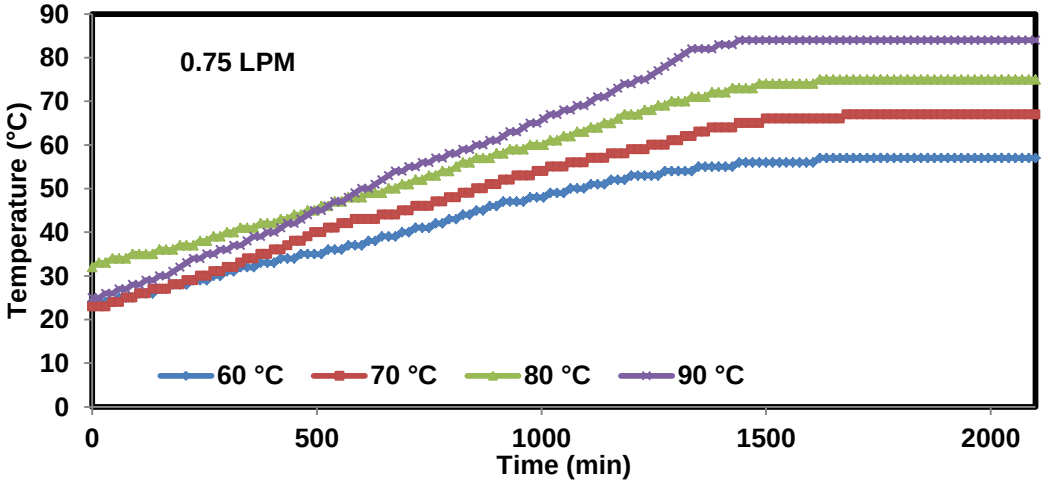

(c)

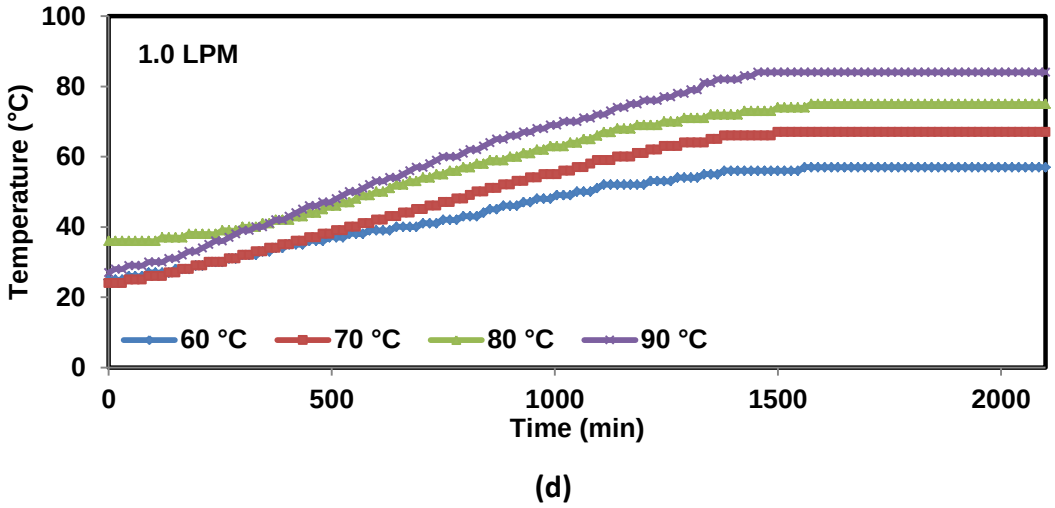

(d)

Figure 4.19 Effect of inlet water temperature on charging time of beeswax at different flow rates

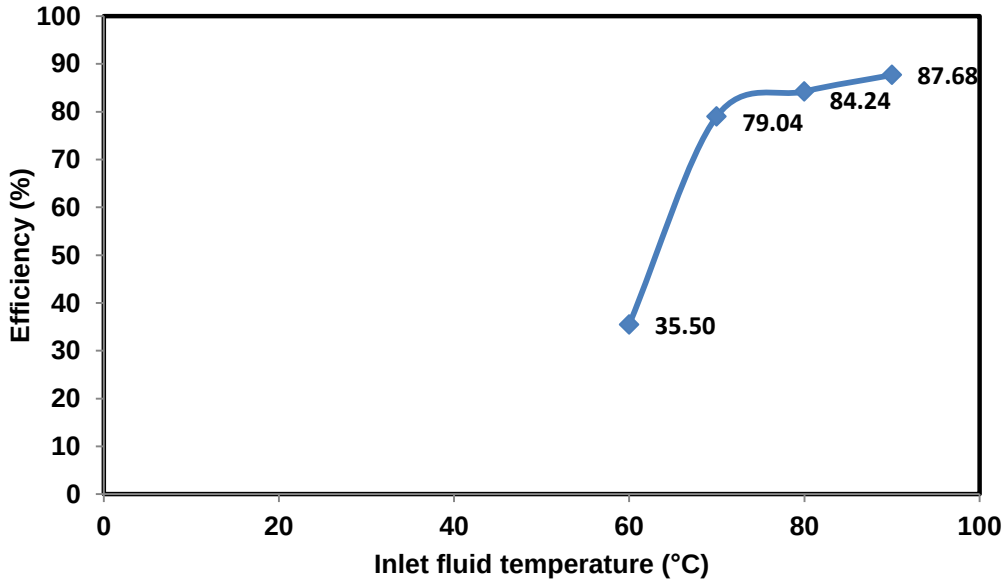

Figure 4.20 Storage efficiency of large TSU at different inlet water temperatures

iii) Thermal profile of beeswax

The thermal profiles of beeswax at different inlet fluid temperatures (60 °C, 70 °C, 80 °C, 90 °C) are presented in Figure 4.21 at fixed fluid flow rate of 0.5 LPM which is showing the temperature variation with time for nine thermocouples of thermal storage unit.

For better understanding, the thermal profile of beeswax at the flow rate of 0.5 LPM and 80°C (Figure 4.21 (c)) is divided into temperature distribution profiles in axial and vertical directions of TSU as shown in Figure 4.22 and Figure 4.23 respectively.

As hot HTF is passing through helical coil from left to right so melting process begins at the left end of TSU i.e. T1, T4, T7 as compared to right end, with smaller melting time on the left side beeswax. The melting pattern was found to be similar for thermocouple positions along the axis at the middle position of coil (T4, T5, T6) and below the coil (T7, T8, T9) as shown in Figure 4.22 b) and Figure 4.22 c) respectively.

It is also observed that time taken by beeswax to reach the melting point at bottom (T7) of the thermal storage unit was the smallest as compared to the middle (T4) and top thermocouples (T1) as shown in Figure 4.23 a) and in the beginning heat transfer between HTF and beeswax is through conduction. Since, beeswax at positon T1 and T7 are in contact with the helical coil and T4 is away from the coil so melting at T1 and T7 begins first as compared to position T4 and the molten beeswax moves downward due to gravitational effect and transfers heat to the bottom part of the thermal storage unit which leads to faster rise in the temperature of the bottom beeswax (T7). Then molten beeswax from bottom part starts moving up due to bouncy effect which causes additional heat transfer to beeswax at position T4 and T1 along with conduction through solid beeswax. The mode of heat transfer and melting pattern are similar for all three vertical planes (T1, T4, T7) as shown in Figure 4.23. Thus there are two dimensional movements in the PCM in rectangular TSU i.e. from left to right and top to bottom.

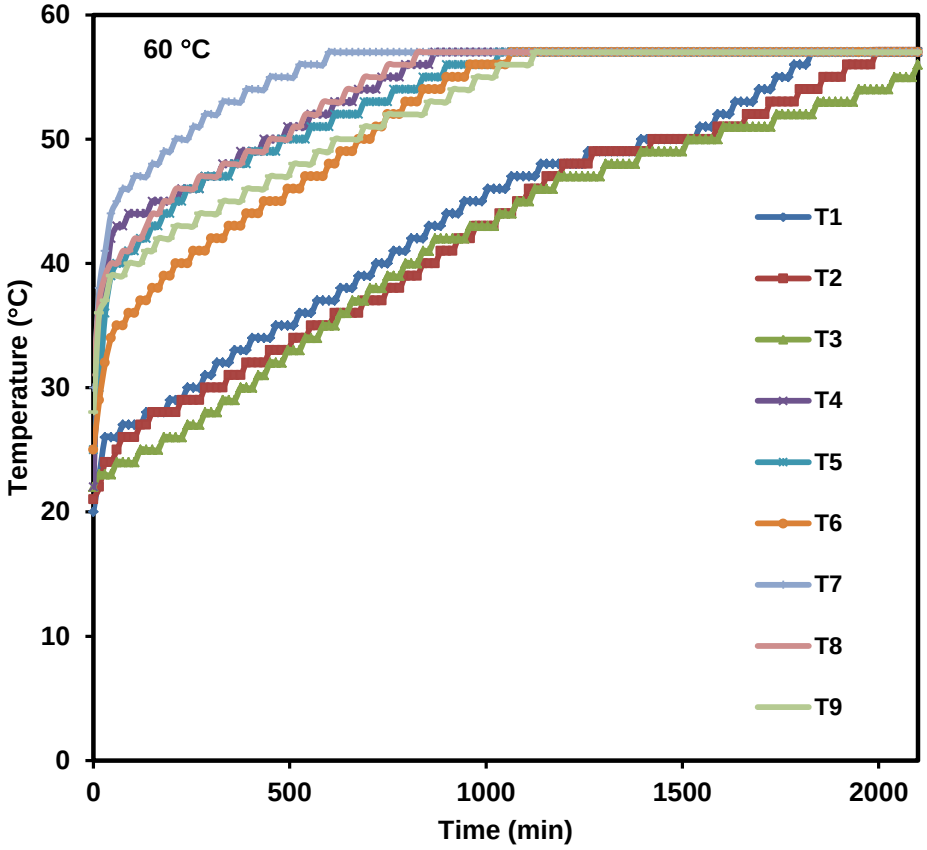
60 °C
Temperature (°C)
Time (min)
0
10
20
30
40
50
60
0
500
1000
1500
2000
T1
T2
T3
T4
T5
T6
T7
T8
T9

(a)

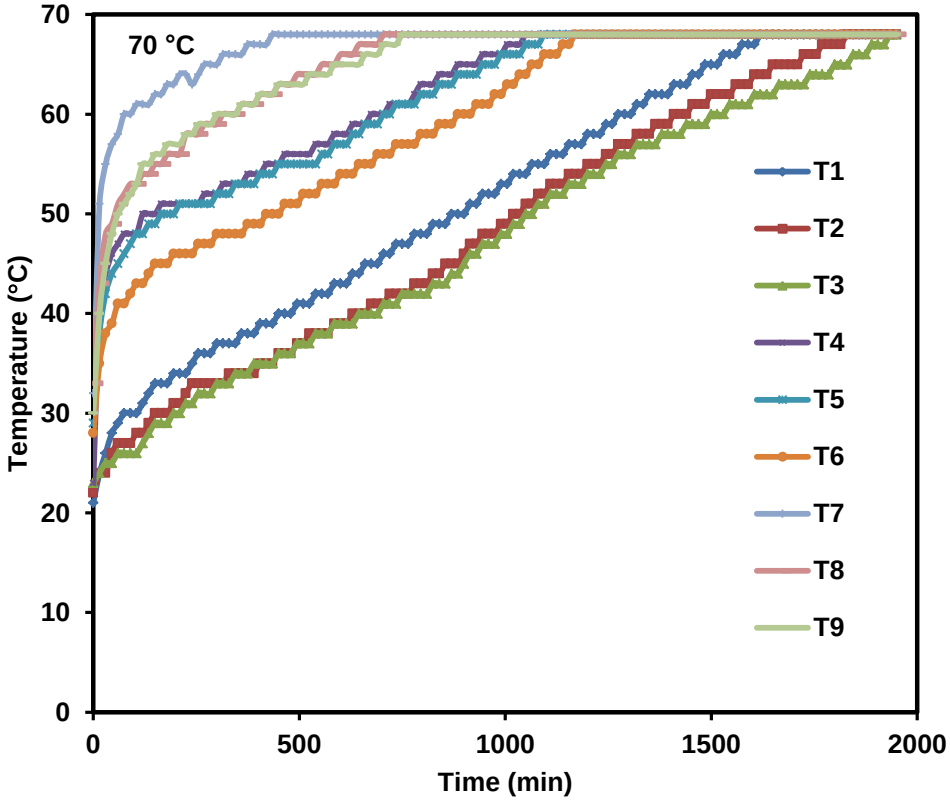
70 °C
Temperature (°C)
Time (min)
0
10
20
30
40
50
60
70
0
500
1000
1500
2000
T1
T2
T3
T4
T5
T6
T7
T8
T9

(b)

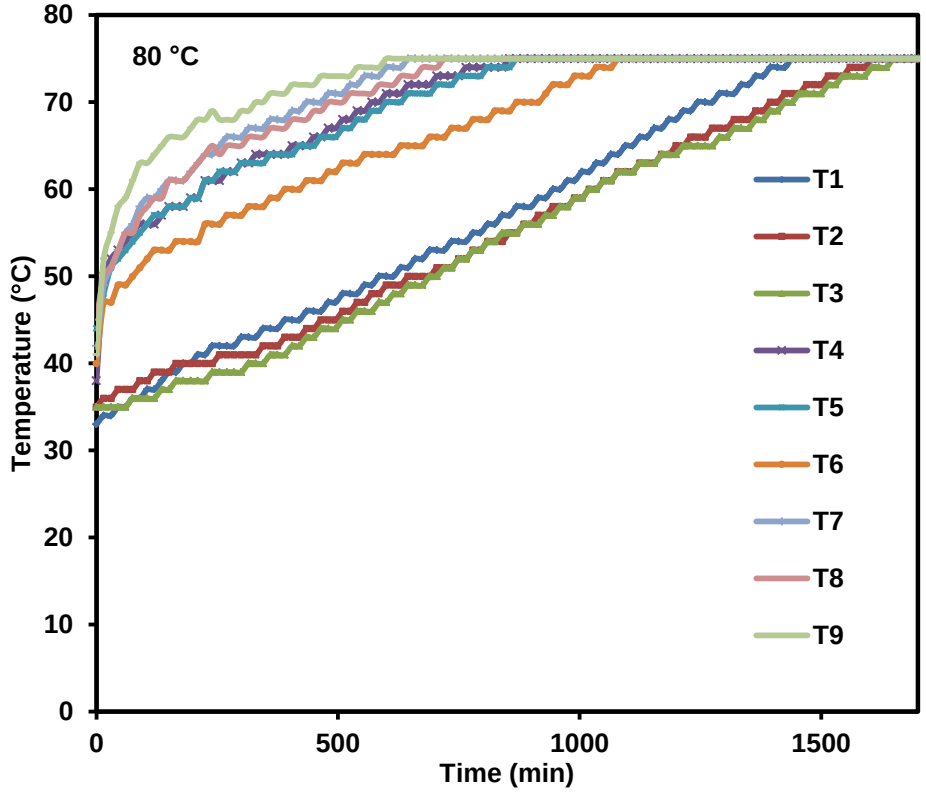

(c)

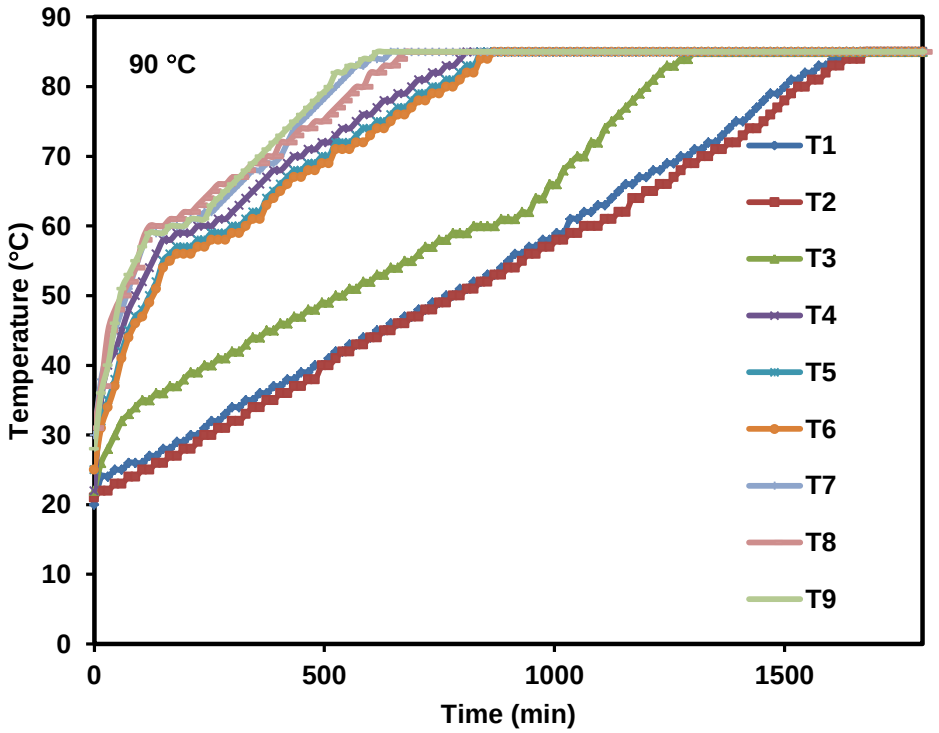

(d)

Figure 4.21 Thermal profile of beeswax at different inlet water temperatures

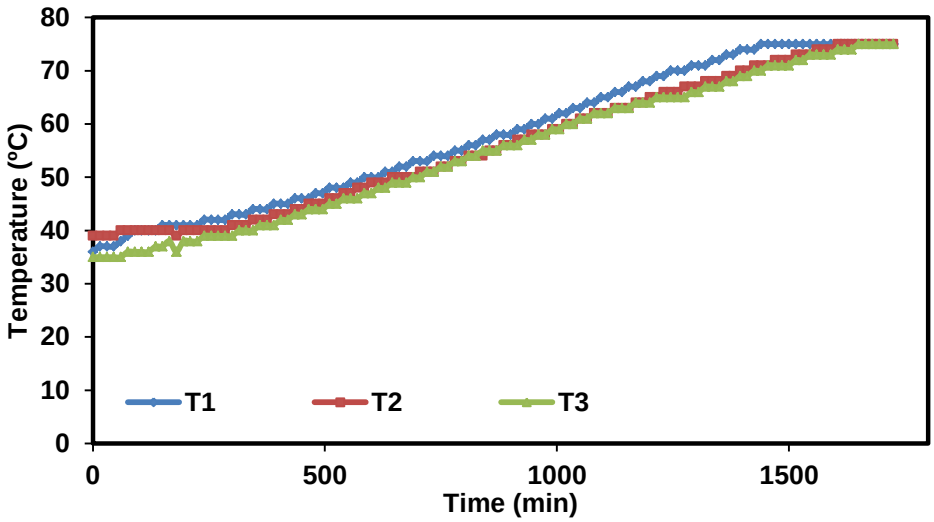

(a)

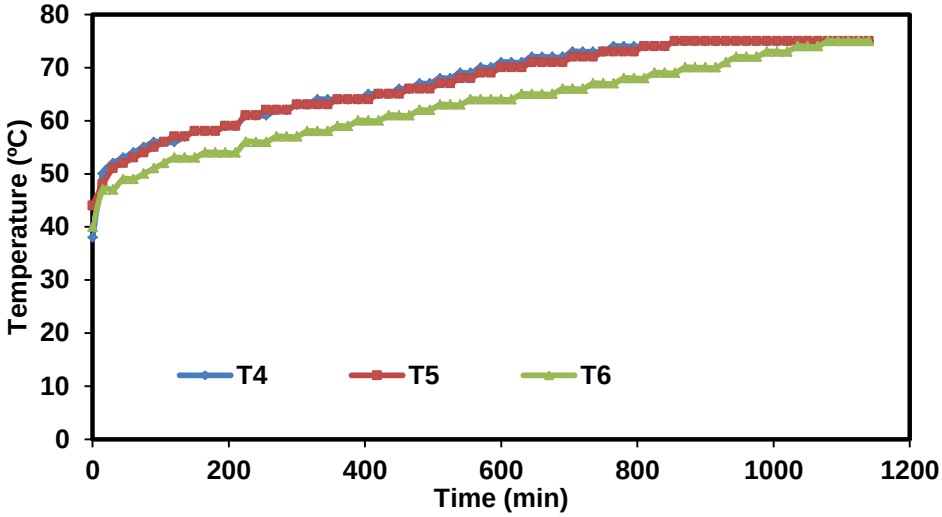

(b)

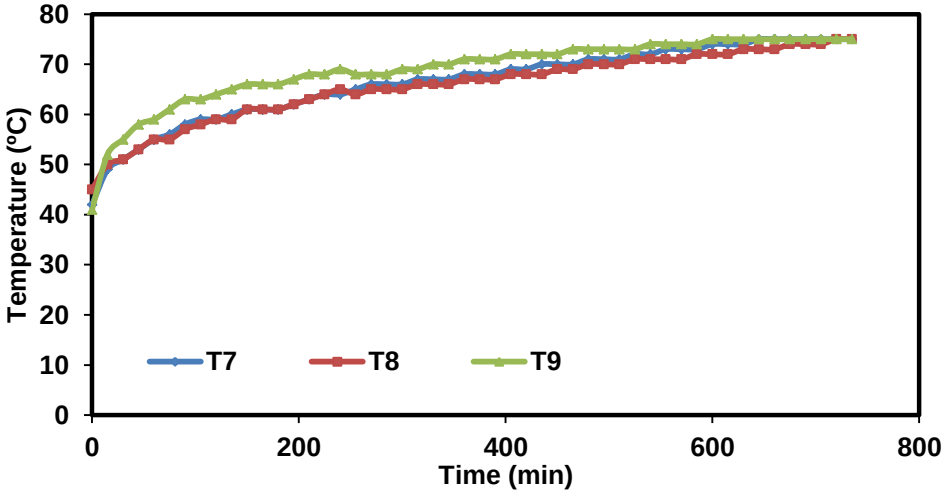

(c)

Figure 4.22 Temperature distributions in large TSU with beewax along horizontal planes

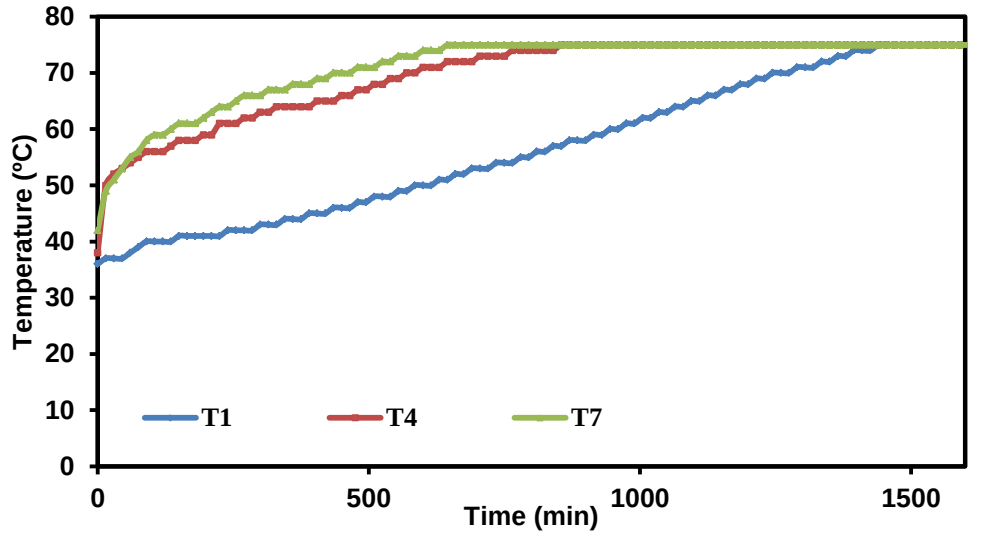

(a)

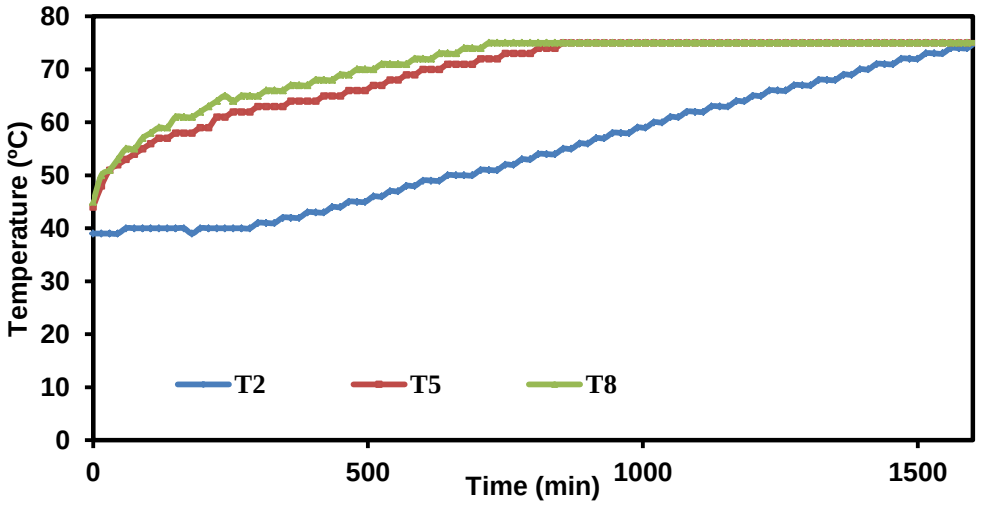

(b)

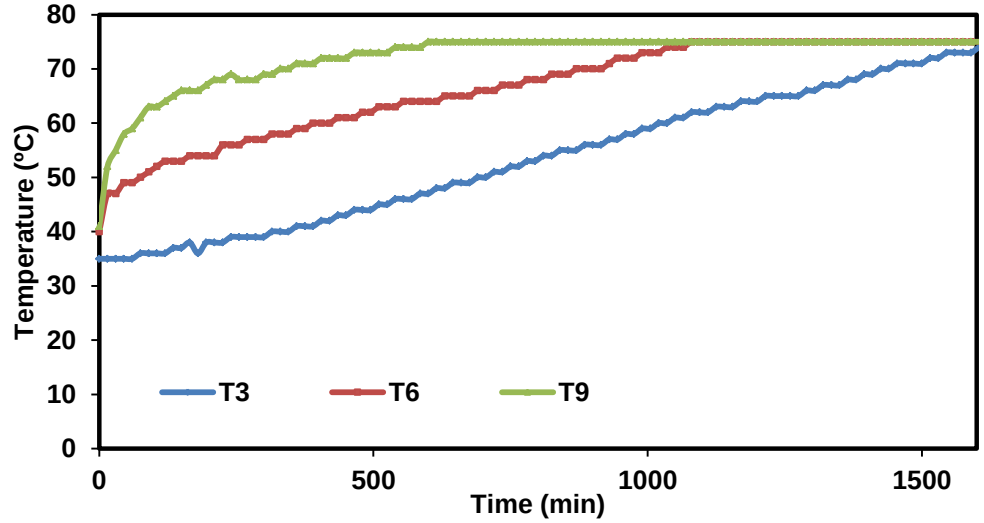

(c)

Figure 4.23 Temperature distributions in large TSU with beeswax along vertical planes

Thermal profile of beeswax at inlet fluid temperature of 60 °C (Figure 4.21 (a)) showed the similar pattern for temperature rise when compared with other temperature profiles. However, during experimentation it was observed that the beeswax did not melt completely when HTF was passed at inlet temperature of 60 °C due to the less temperature difference between HTF and beeswax. It was also observed that the temperature of HTF (60 °C) is not enough to begin the strong convection within the beeswax and conduction part is dominant here throughout the charging process and all thermocouples were reached the constant temperature at 1935 min. In all the thermal profiles of beeswax (Figure 4.21) at different inlet temperatures it was observed that the temperature of lower most part of the system raised first followed by middle and upper part which showed the convection effect on thermal performance of the system. It was also observed form Figure 4.21 that temperature profile of upper most thermocouples are almost linear this is due to slow melting rate of beeswax at the upper part initiated by conduction for most of the time and then followed by convection due to the movement of liquid phase. Thermal profiles of beeswax at all the inlet fluid temperature was almost similar except their charging time which proved that the convection plays dominant role in the charging of beeswax.

iv) Discharging profile of beeswax

Once, all the nine thermocouples reached to saturation temperature in the beeswax then solidification pattern was studied by observing temperature variation in the beeswax. For this solidification study i.e. discharging of thermal storage unit, cold water at 20 °C was passed at the flow rate of 0.5 LPM through helical coil from left to right in exactly same manner immediately after the completion of charging process. During discharging process water coming out of the TSU is collected in a water tank and used again and again in a closed circuit for estimating amount of the heat collected during discharging.

Figure 4.24 and Figure 4.25 shows the temperature profile of beeswax for horizontal and vertical planes of TSU respectively. It is observed from Figure 4.24 that the drop in temperature of PCM reduced from left (inlet) to right (outlet) of thermal storage unit at different axial positions i.e. above the helical coil (T1, T2, T3), middle of the coil (T4, T5, T6) and below the coil (T7, T8, T9). This is due to the fact that

temperature of heat transfer fluid starts increasing while moving from left to right of TSU which leads to decrease in heat transfer gradient i.e. temperature difference between wax and HTF which caused reduction in rate of heat transfer through conduction. The solidification process of beeswax was different from the melting process, as HTF allowed to flow through the helical coil, the molten beeswax around the coil losses heat to the wall of the coil and start accumulating around the coil surface which formed a thin film of beeswax on the coil. The thickness of this film increased further with time due to more heat transfer to the coil through conduction which caused extra resistance for further heat transfer via conduction. It is observed from Figure 4.25 that during solidification, the temperature at the thermocouples along all the vertical planes i.e. near to inlet (T1, T4, T7), at the middle of the coil (T2, T5, T8) and near to the outlet (T3, T6, T9) of TSU dropped simultaneously. This is due to the fact that during solidification of beeswax conduction mode of heat transfer is dominant as compared to the convection mode. The solidification peak for beeswax in TSU was obtained at 58 ºC and for beeswax sample it is 56.4 ºC through DSC analysis and discharging time of beeswax with plain water was found to be 480 min. similar solidification profiles were observed on various other PCM such as paraffin, fatty acids and eutectic by the researchers [148, 292, 293].

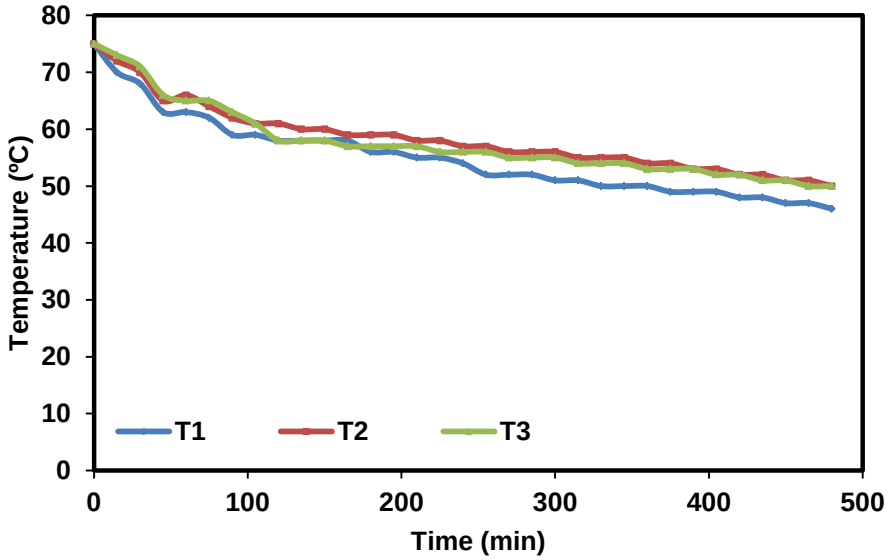

(a)

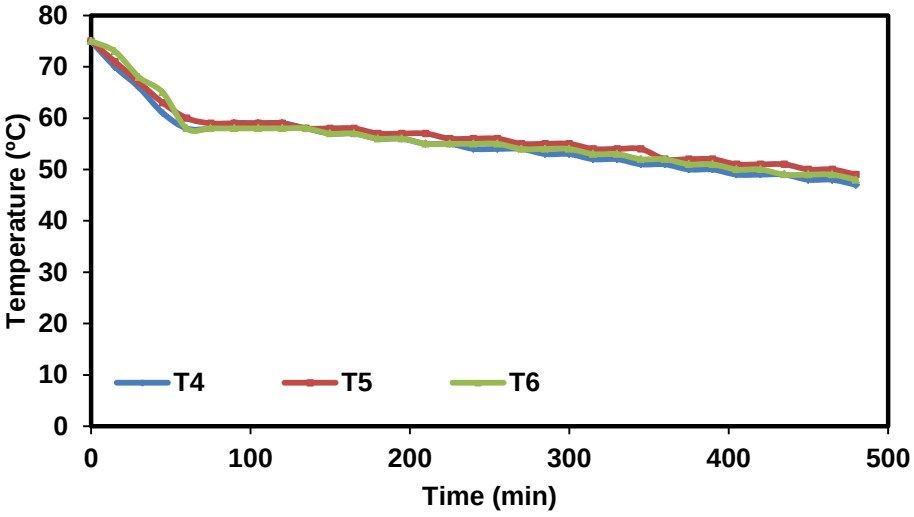

(b)

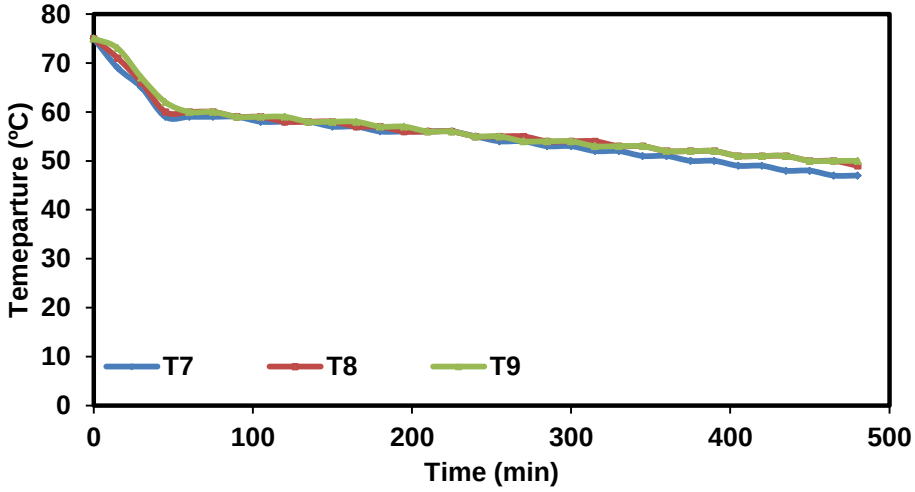

(c)

Figure 4.24 Discharging profile of beeswax along horizontal planes of large TSU

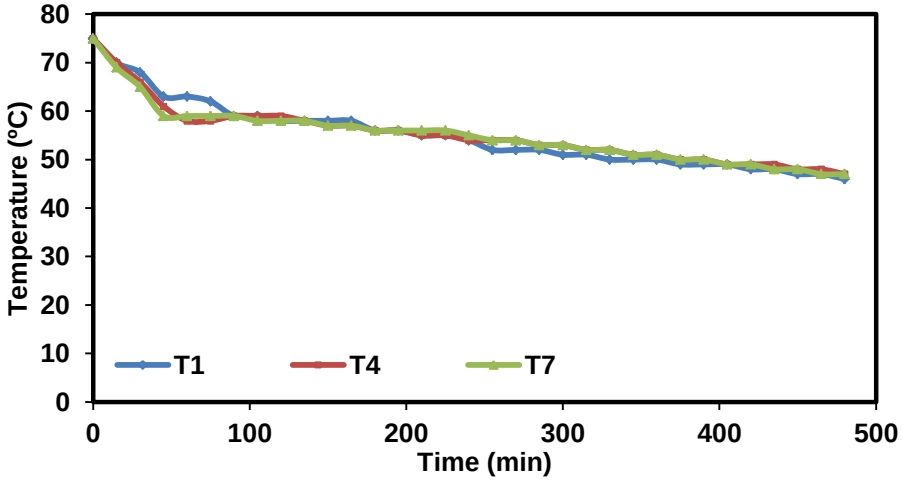

(a)

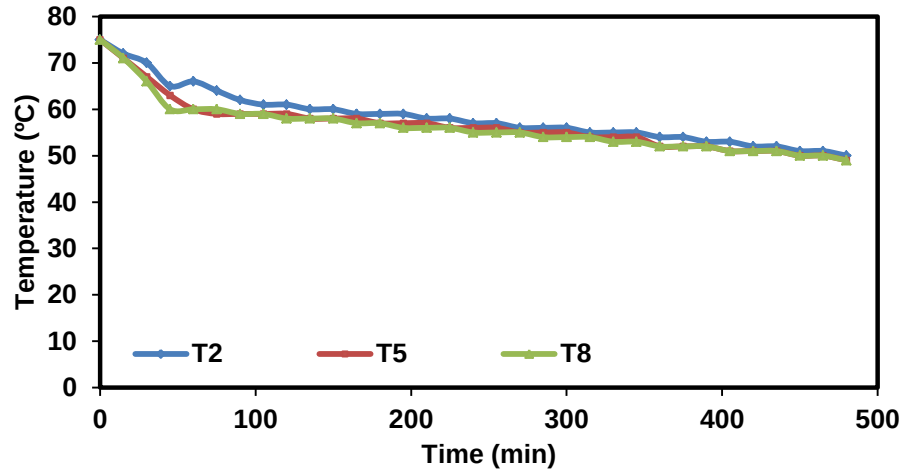

(b)

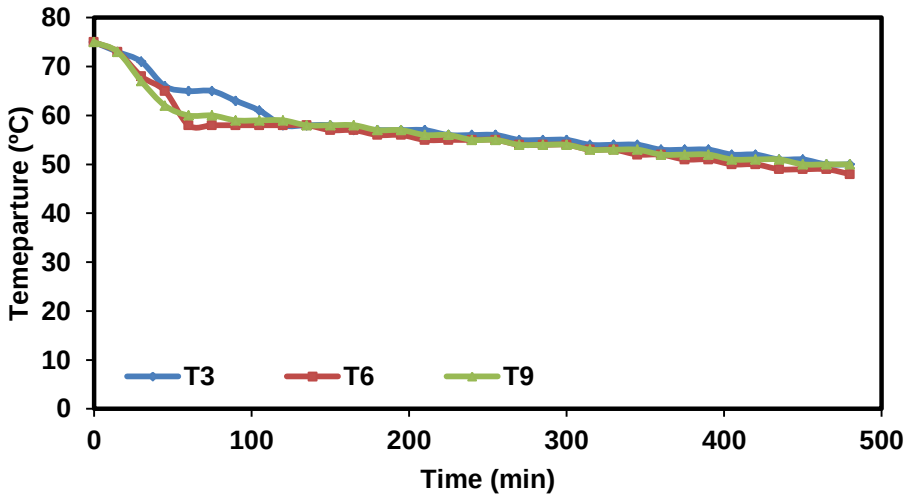

(c)

Figure 4.25 Discharging profile of beeswax along vertical planes of large TSU

4.4.3 Using expanded graphite/water suspension as HTF

Expanded graphite(EG)/water suspension as heat transfer fluid was prepared and allowed to flow through the helical tube of thermal storage unit at different concentrations (0.05 wt. %, 0.5 wt. %, 1.0 wt. %) to study the thermal performance of beeswax results of the study are given below:

i) Effect of fluid concentration on charging time of beeswax

Variation of charging time in large TSU at different concentration of expanded graphite in EG/water suspension is shown in Figure 4.26 and it is observed that with increase in the concentration of expanded graphite in the suspension, the charging time of beeswax reduced. The charging time of beeswax for the expanded

graphite/water suspension of 0.05 wt. %, 0.5 wt. % and 1.0 wt. % concentration is observed as 1605 min, 1440 min and 1395 min respectively. The decrease in charging time with increase in concentration of EG may be due to the enhanced thermal conductivity of heat transfer fluid and improved tube side heat transfer coefficient as shown in Figure 4.27 and Figure 4.28 which promotes faster heat transfer through the tube surface. Table 4.4 shows the reduction in charging time at different concentration of expanded graphite in water as compared to the base fluid. Maximum reduction in charging time i.e. 15.45% was observed for 1.0 wt. % of expanded graphite in water and it was observed that more than 1.0 wt. % of expanded graphite may affect the functioning of centrifugal pump used in the experiment, also the excess expanded graphite in suspension may block the helical tube (ID : 8mm) of thermal storage unit and therefore, the percentage of expanded graphite in the suspension was limited to 1.0 wt. %.

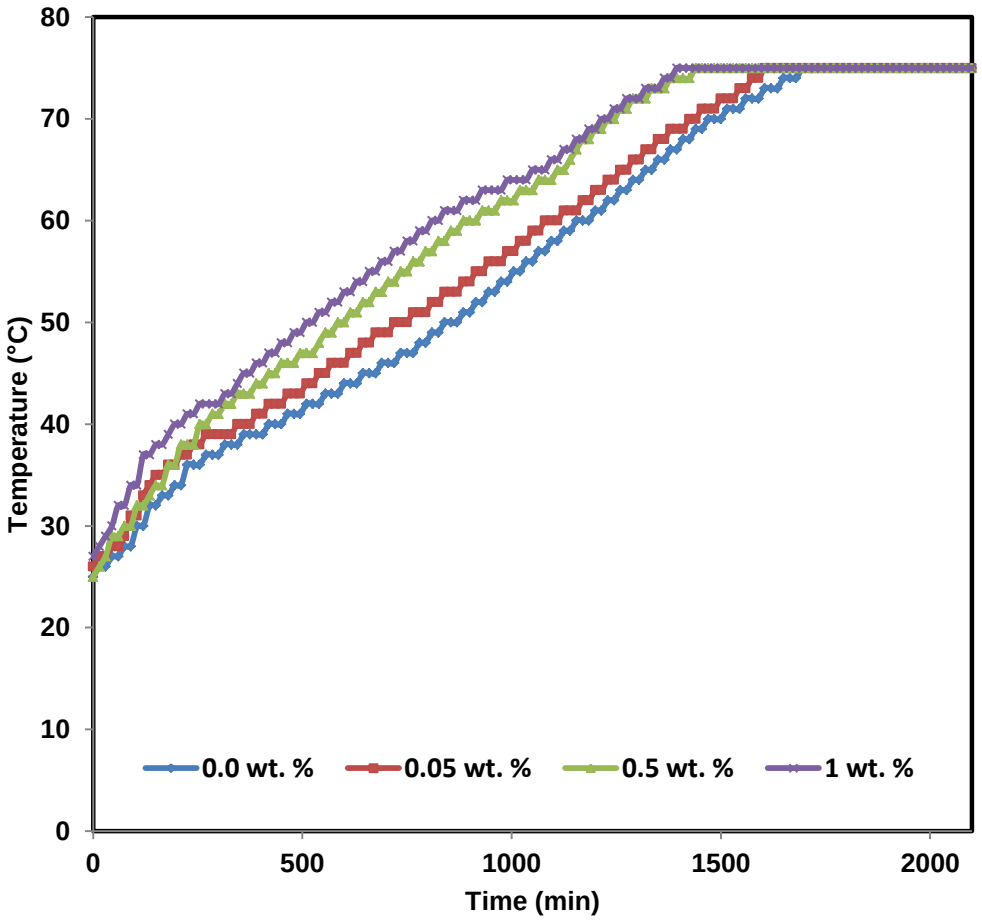

Figure 4.26 Charging time with concentration of expanded graphite in water

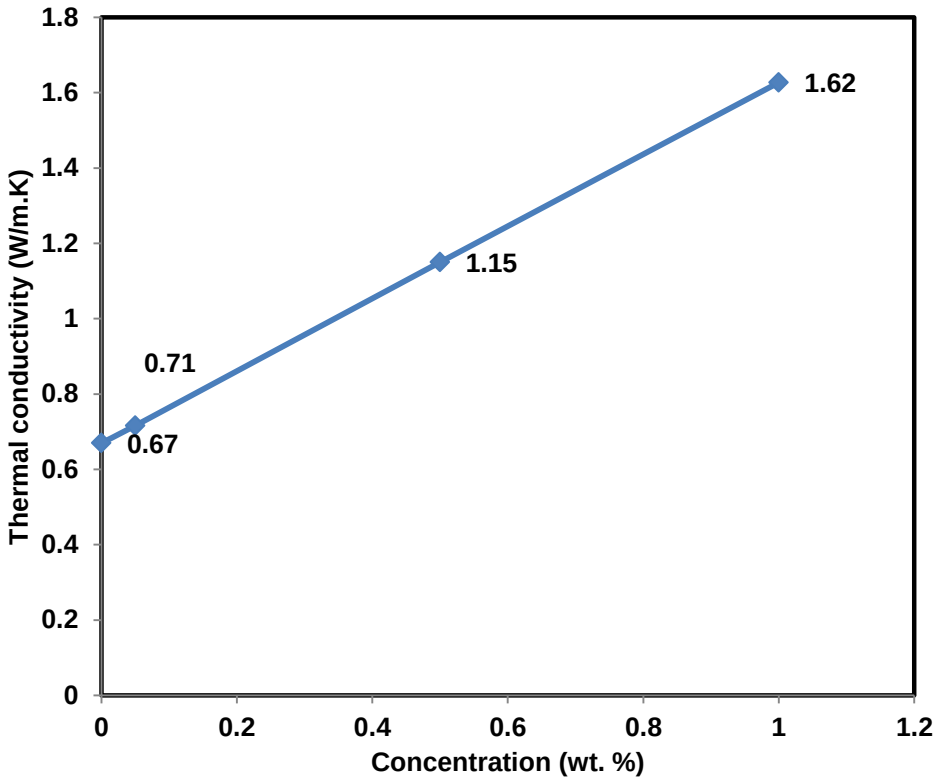

Figure 4.27 Thermal conductivity of EG/water suspension at different concentrations

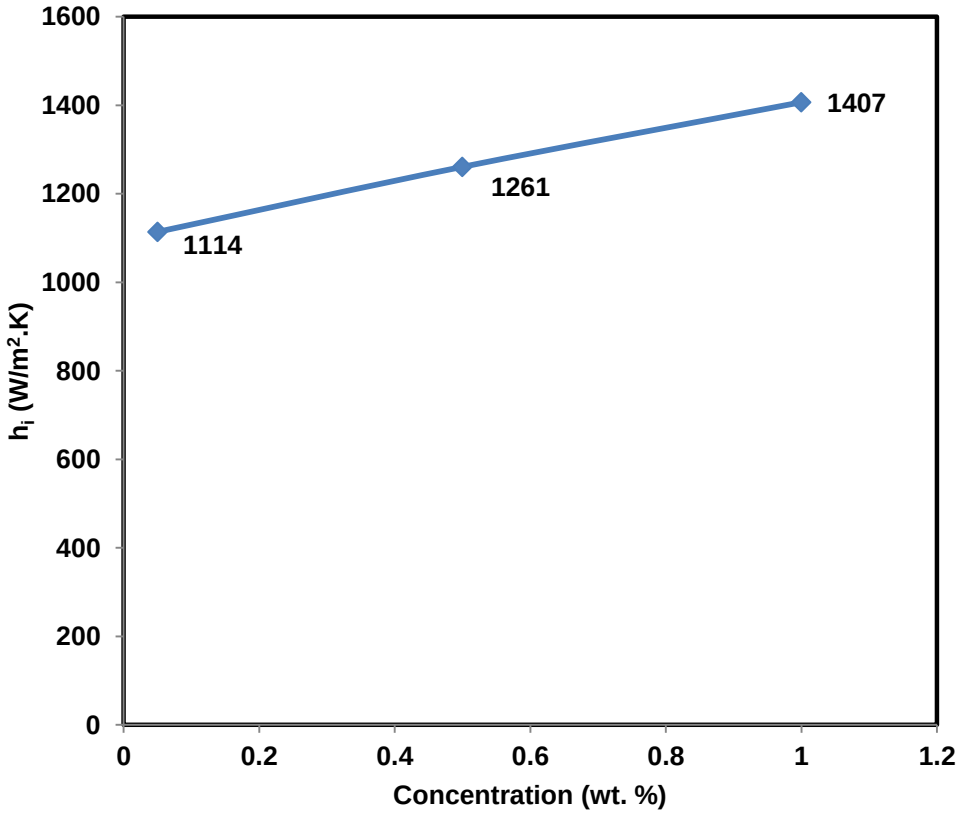

Figure 4.28 Heat transfer coefficient at different concentration of EG/water suspension

Table 4.4 Reduction in charging time at different concentration of EG/water suspension

Concentration of HTF (wt. %)	Thermal conductivity of HTF (W/m.K)	Charging time (min)	% Reduction in charging time
0.00	0.571	1650	--
0.05	0.612	1605	2.72
0.50	0.986	1440	12.70
1.00	1.397	1395	15.40

ii) Thermal profile of beeswax

Thermal profiles of beeswax obtained at different concentration of EG/water suspension are presented in Figure 4.29 and it is observed that temperature of the thermocouples at the position near to inlet in vertical plane (T1, T4, T7) raised earlier as compared to the temperature of thermocouples at planes away from the inlet of TSU. This is due to the fact that as the HTF moves from left to right through the coil in TSU, the temperature difference between the HTF and PCM material reduced. Similarly the temperature of lower part of TSU (T7, T8, T9) raised first followed by temperature of the middle part (T4, T5, T6) and then the top part of TSU (T1, T2, T3). It should be noted that the thermal profiles of beeswax when charged with EG/water suspension at various concentrations (0.05 wt. %, 0.5 wt. %, 1.0 wt. %) are similar to the melting profile of the beeswax when charged with plain water except the variation in charging time. This proves that in the present system movement of melting front was not affected with the type of heat transfer fluid except the variation in charging time which was due to the change in thermal properties of heat transfer fluid.

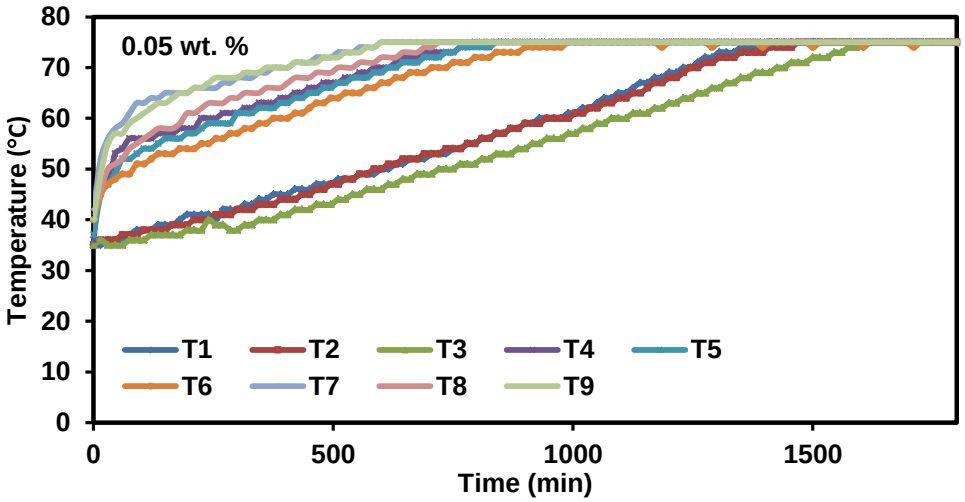

(a)

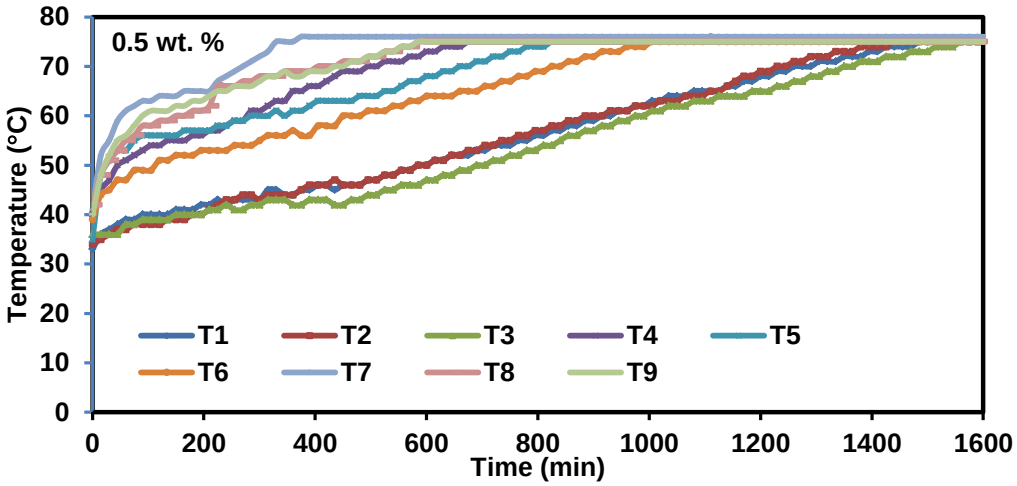

(b)

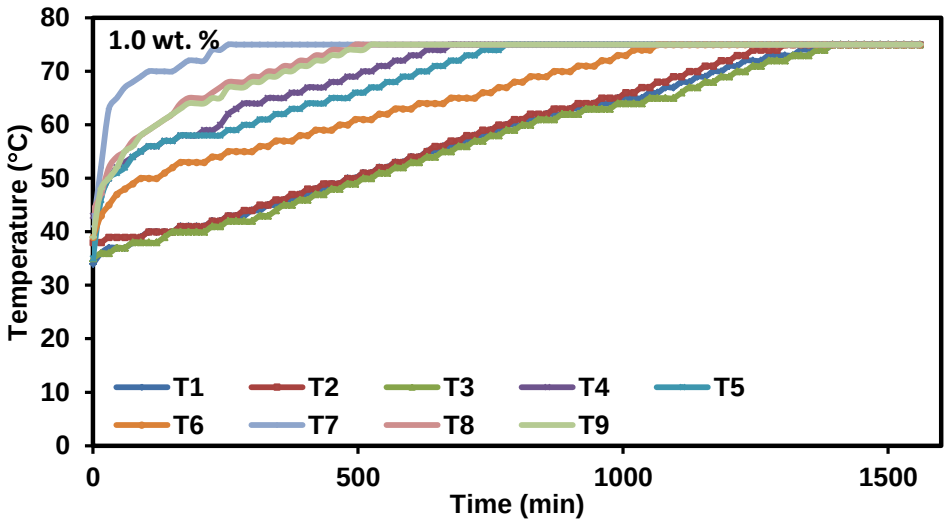

(c)

Figure 4.29 Thermal profiles of beeswax at different concentration of EG/water suspension

4.4.4 Using Al_2O_3 /water suspension as HTF

Al_2O_3 /water suspension as heat transfer fluid was prepared at different concentrations (0.2 vol. %, 0.5 vol. %, 1.0 vol. % and 2.0 vol. %) and allowed to flow through the helical tube of thermal storage unit to study the thermal performance of beeswax results of the study are given below:

i) Effect of fluid concentration on charging time

Charging time of beeswax at different concentration of alumina nano fluid in Al_2O_3/water is shown in Figure 4.30 which depicts that with increase in the concentration of Al_2O_3 nanoparticles in water the charging time of beeswax was

reduced. The charging time of beeswax when charged with nano-fluids having concentration of 0.2 vol. %, 0.5 vol. %, 1.0 vol. % and 2.0 vol. % was found to be 1590 min, 1560 min, 1515 min and 1485 min respectively which is much lesser as compared to the charging time when charged with plain water (1650 min). Percentage reduction of charging time with increasing concentration of heat transfer fluids are given in Table 4.5 which showed that with the addition of aluminium oxide nanoparticles (0.2 vol. %-2 vol. %) in water, the charging time of beeswax was reduced by 3.6-10 %. This reduction in charging time of beeswax was due to enhancement in thermal conductivity of HTF as well as increase in the internal heat transfer coefficient which promotes faster heat transfer with the concentration of alumina nanoparticle as shown in Figure 4.31 and Figure 4.32 respectively.

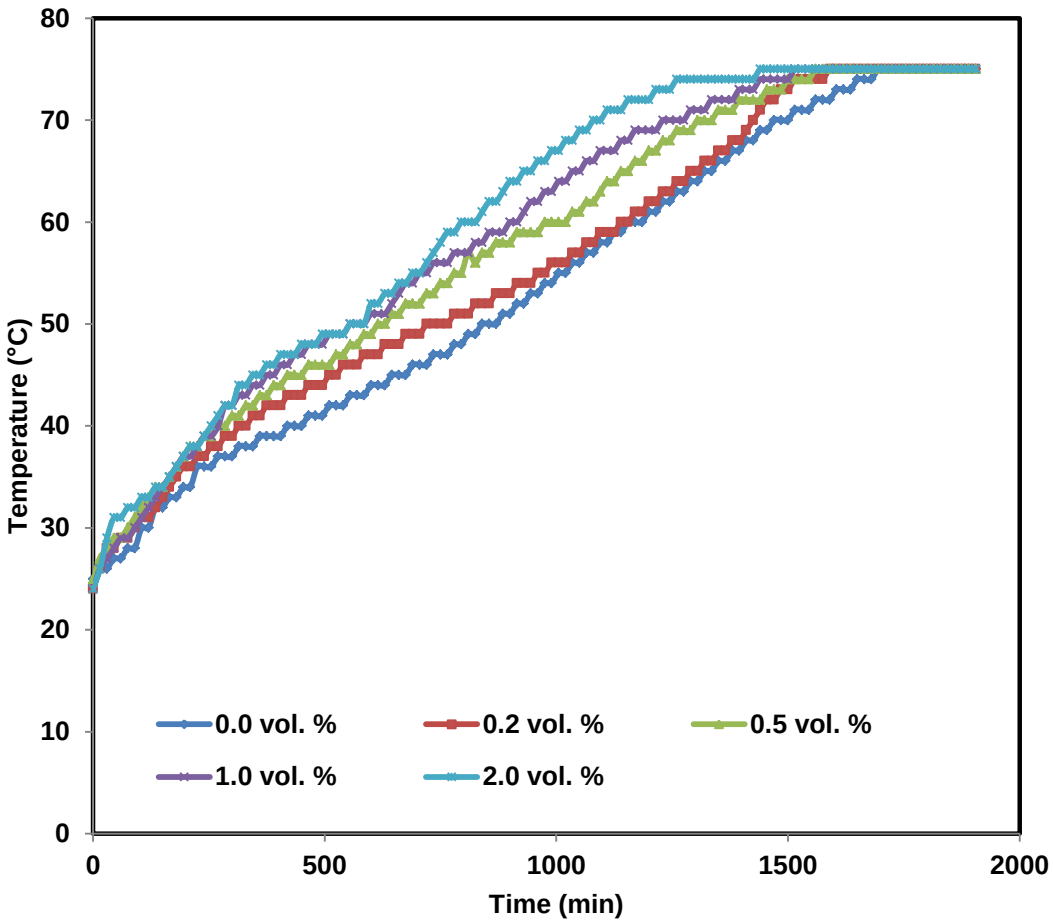

Figure 4.30 Effect of Al_2O_3 nanofluid concentration on charging time of beeswax

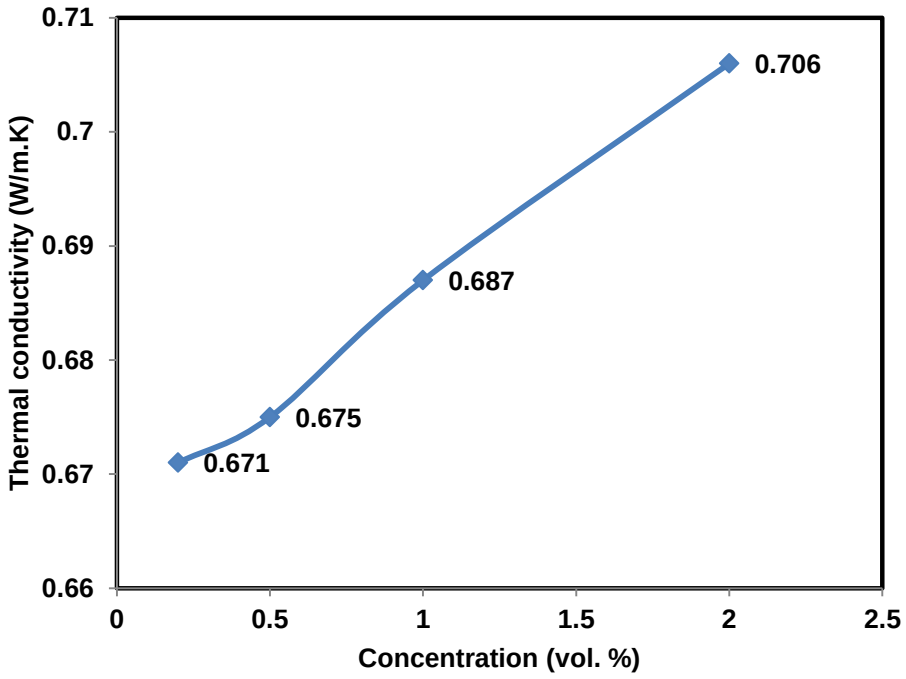

Figure 4.31 Thermal conductivity of Al_2O_3 nanofluids at different concentrations

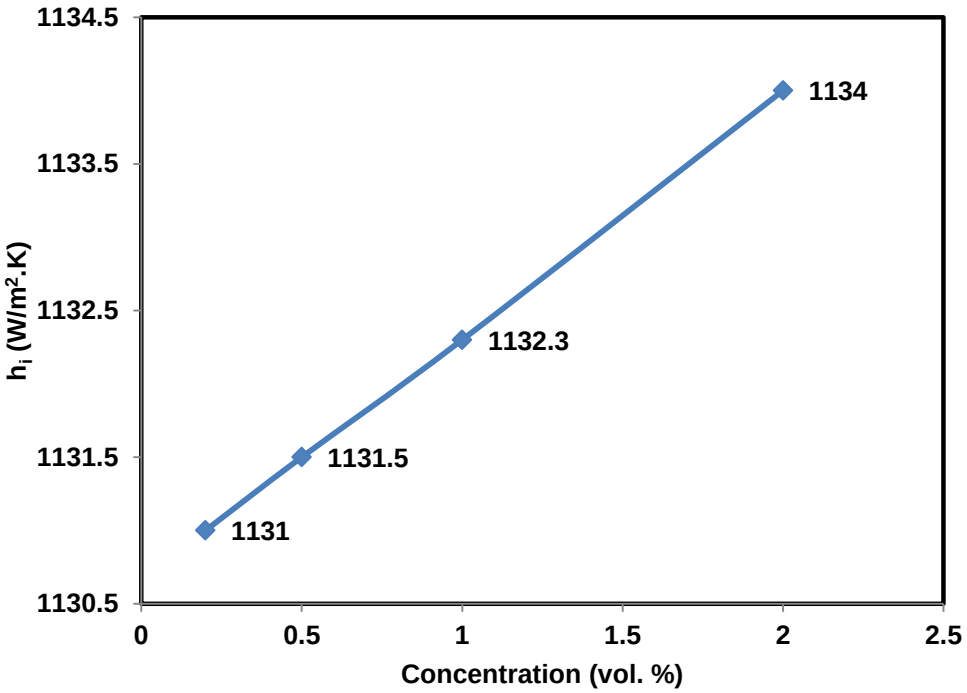

Figure 4.32 Heat transfer coefficient at different concentration of Al_2O_3/water nanofluid

Studies carried out by various researchers in the past also showed similar effect of Al_2O_3/water concentration on the charging time of phase change materials [297–299].

Table 4.5 Charging time of beeswax at various concentration of Al_2O_3 nanofluid

HTF	Concentration (vol. %)	Charging time (min)	% reduction in charging time
Plain water	0.0	1650	--
Al_2O_3nanofluid	0.2	1590	3.6
Al_2O_3nanofluid	0.5	1560	5.4
Al_2O_3nanofluid	1	1515	8.1
Al_2O_3nanofluid	2	1485	10

ii) Thermal profile of beeswax

Thermal profiles of beeswax when charged with different concentrations of Al_2O_3 nanofluids are shown in Figure 4.33 and it is observed that the pattern of temperature rise at all the thermocouples are similar in all the thermal profiles obtained by varying concentration of nanofluid, except the value of charging time. In all the thermal profiles (Figure 4.33 (a), (b), (c), (d)) the solid liquid interface was found to be moving from left (inlet side) to right (outlet side) of the storage unit axially, while in a vertical plane molten beeswax was first moved downward at the bottom of unit due to gravity and then towards the top part of TSU due to buoyancy. It can also be observed in all these profiles that the temperature rise is initially slow due to poor conduction of heat through the matrix of PCM which was then followed by convection once the melting point of PCM was achieved led to faster temperature rise thereafter.

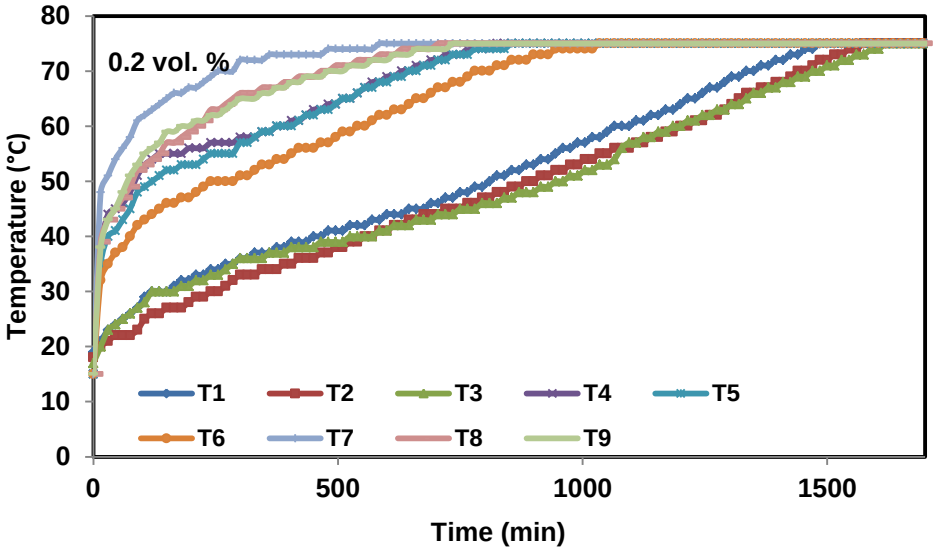

(a)

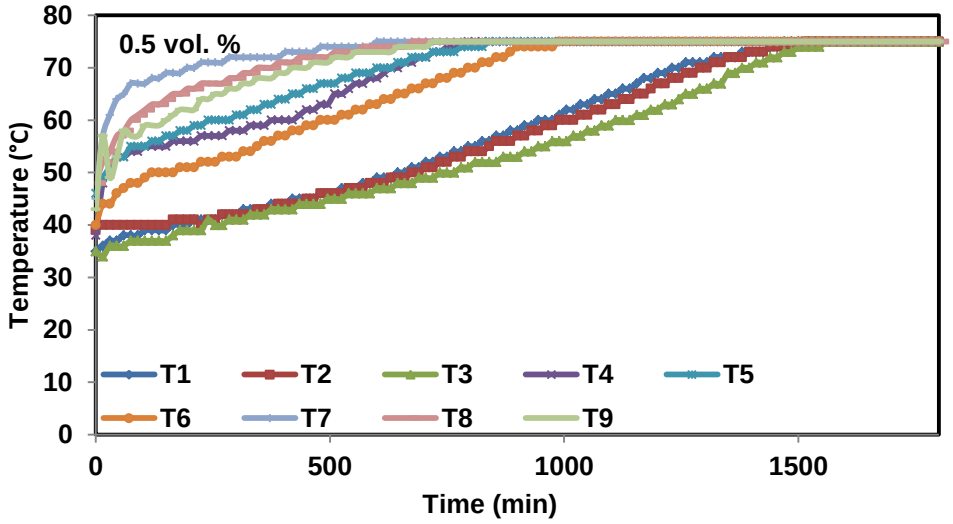

(b)

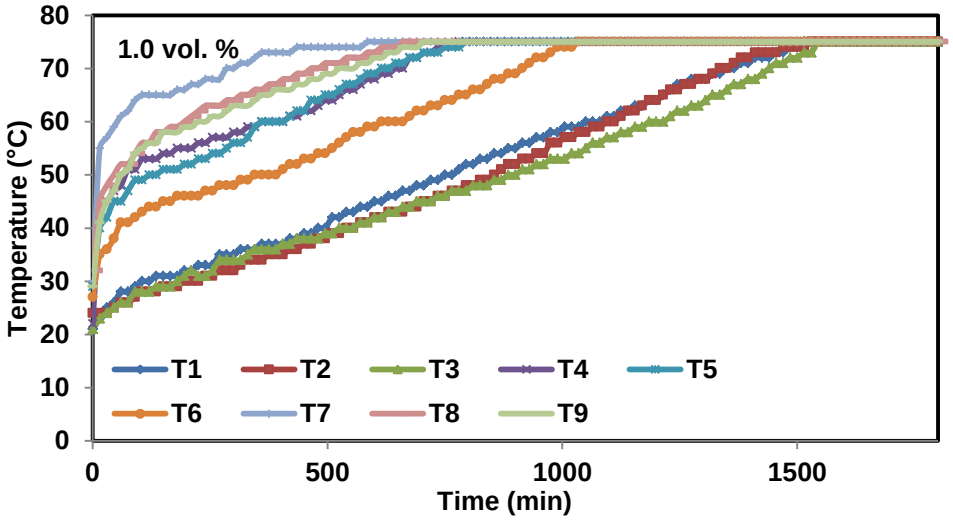

(c)

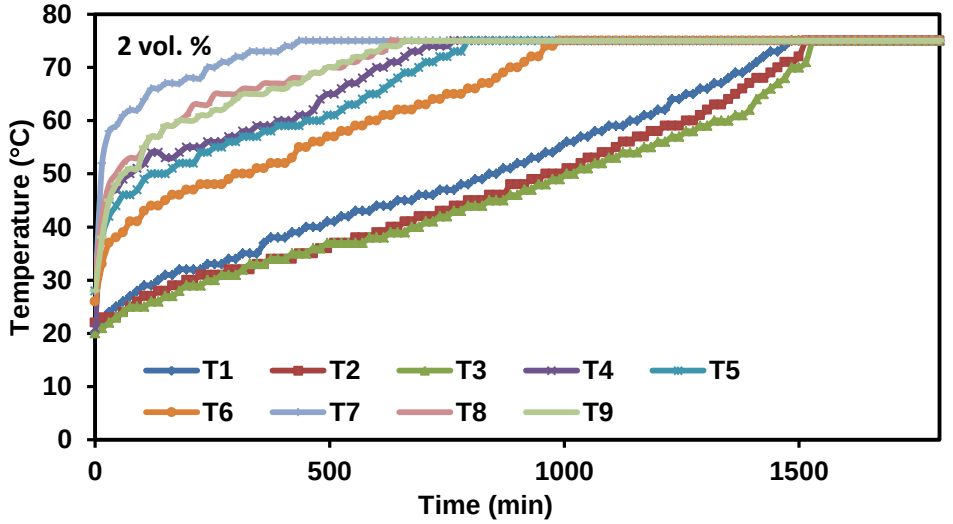

(d)

Figure 4.33 Thermal profile of beeswax at different concentration of Al_2O_3

4.5 Performance evaluation of large TSU using composite material

Composite of beeswax with expanded graphite was prepared and studied for its thermal storage performance in large TSU using four different heat transfer fluids such as plain water, expanded graphite/water suspension, Al_2O_3 nanofluid and exhaust gases at different flow rates and inlet fluid temperatures.

4.5.1 Using plain water as HTF

Thermal storage performance of composite is studied in large TSU by passing hot water through the helical tube at four flow rates such as 0.25 LPM, 0.5 LPM, 0.75 LPM, 1 LPM and four different inlet fluid temperatures i.e. 60 °C, 70 °C, 80 °C, and 90 °C.

i) Effect of water flow rate on charging time

Variation in composite material temperature at position T3 (charging time) for different flow rates are plotted with time as shown in Figure 4.34 keeping constant inlet fluid temperature. It is observed from Figure 4.34 (c) that the charging time of composite material found to be 1185 min, 1125 min, 1080 min and 1020 min for fluid flow rate of 0.25 LPM, 0.5 LPM, 0.75 LPM and 1 LPM respectively at 80°C inlet fluid temperature. The reduction in charging time at higher fluid flow rates may be due to improved heat transfer coefficient inside the tube which promoted faster heat transfer. The enhancement in internal heat transfer coefficient was due to increased Reynold's number as shown in Table 4.2 for same thermal storage unit, temperature and flow rate of fluid. It is also noted that the rate of temperature rise in composite material is more as compared to the rate of temperature rise in beeswax this may be due to enhanced thermal conductivity of composite material which has promoted higher heat transfer inside the PCM matrix.

It is also observed from Figure 4.34 (a) that the temperature of composite material reached above its melting point temperature (i.e. 57 °C) during charging with HTF at 60 °C (same was not observed in case of pure beeswax), therefore, unlike the pure beeswax, composite of beeswax with expanded graphite in storage unit can be charged with water at 60 °C. It is observed that the melting pattern of composite at position T3 found to be similar at other three inlet fluid temperatures. These results

show that the fluid flow rate has similar effect on beeswax and composite material, and heat transfer in both the cases increased due to increase in internal heat transfer coefficient.

Thermal storage efficiency of TSU with composite material decreased with increase in flow rates as shown in Figure 4.35. At the lowest flow rate of 0.25 LPM the efficiency of composite material was 86.19% which is quite close to efficiency at 0.5 LPM i.e. 87.49% however, efficiency at the flow rates of 0.75 LPM and 1.0 LPM has decreased to 68.70% and 59.33% respectively. This is probably due to difficulty in maintaining unrestricted flow in helical tube at such a low flow rate i.e. 0.25 LPM in present thermal storage unit due to high pressure drop with centrifugal pump at high temperature and 0.5 LPM is taken for further study to optimize heat transfer parameters in large TSU. The charging time at different flow rates and at other inlet fluid temperatures are summarized in Table 4.6.

The results obtained in this study are found to be in line with the results reported in literatures that with increase in flow rates of HTF charging time reduced for composite materials and PCM [154, 254, 297].

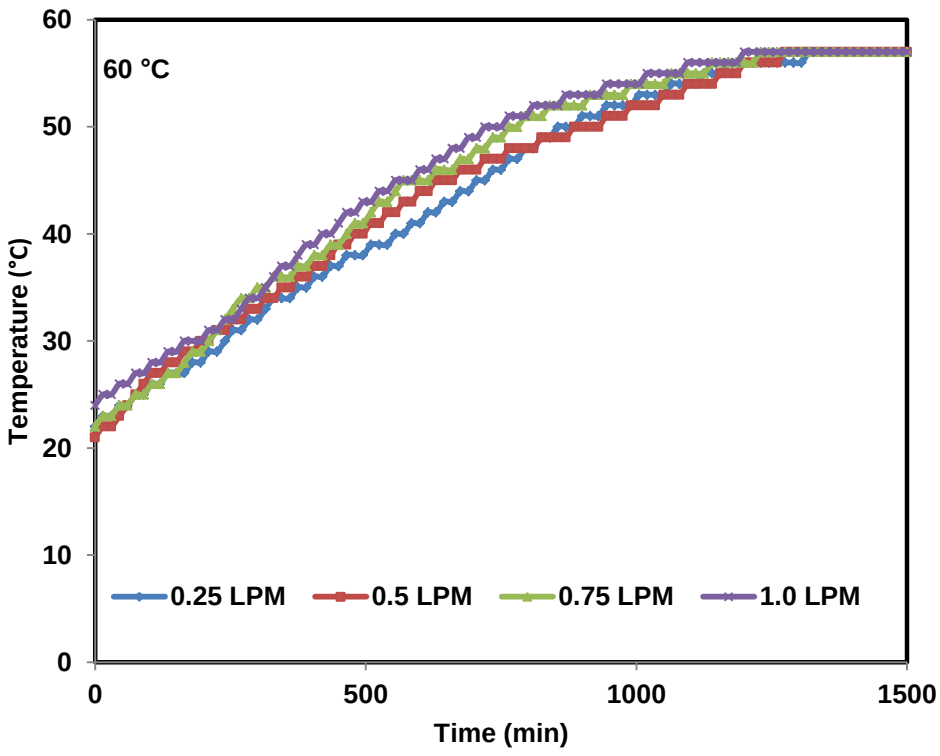

(a)

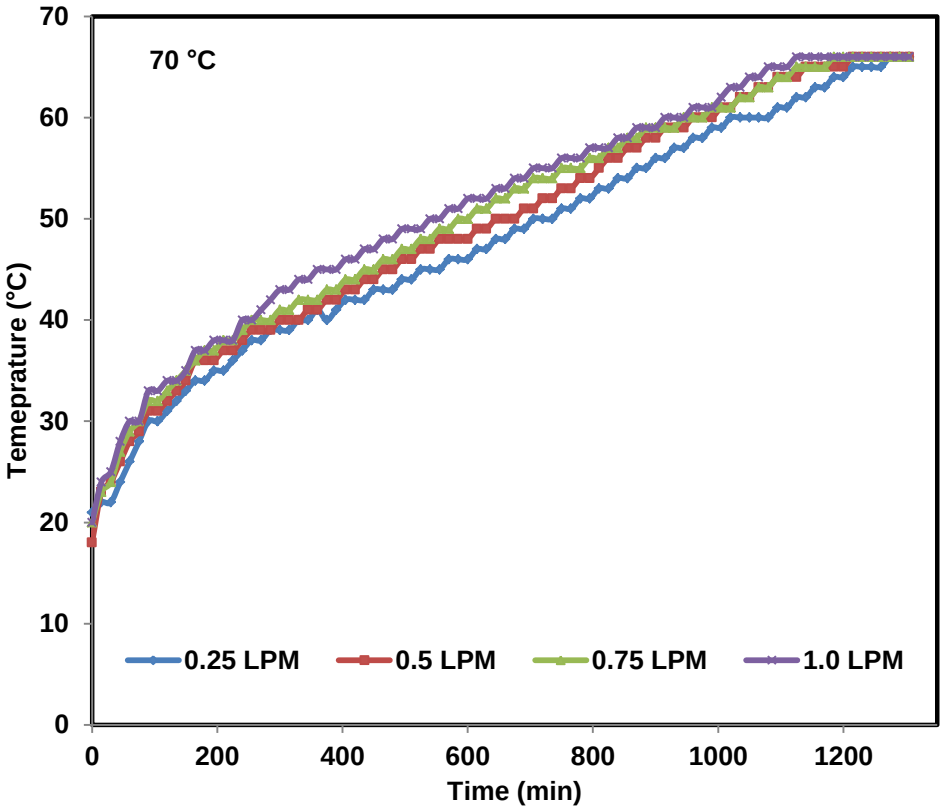
70 °C
Temeprature (°C)
Time (min)
0.25 LPM
0.5 LPM
0.75 LPM
1.0 LPM
0
10
20
30
40
50
60
70
0
200
400
600
800
1000
1200

(b)

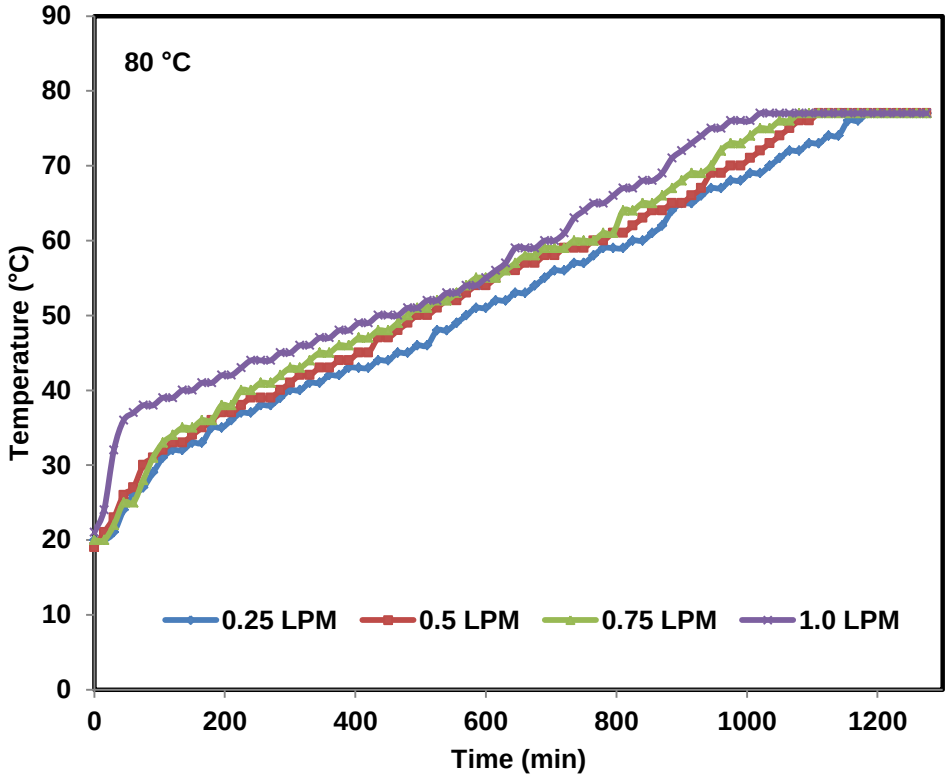
80 °C
Temperature (°C)
Time (min)
0.25 LPM
0.5 LPM
0.75 LPM
1.0 LPM
0
10
20
30
40
50
60
70
80
90
0
200
400
600
800
1000
1200

(c)

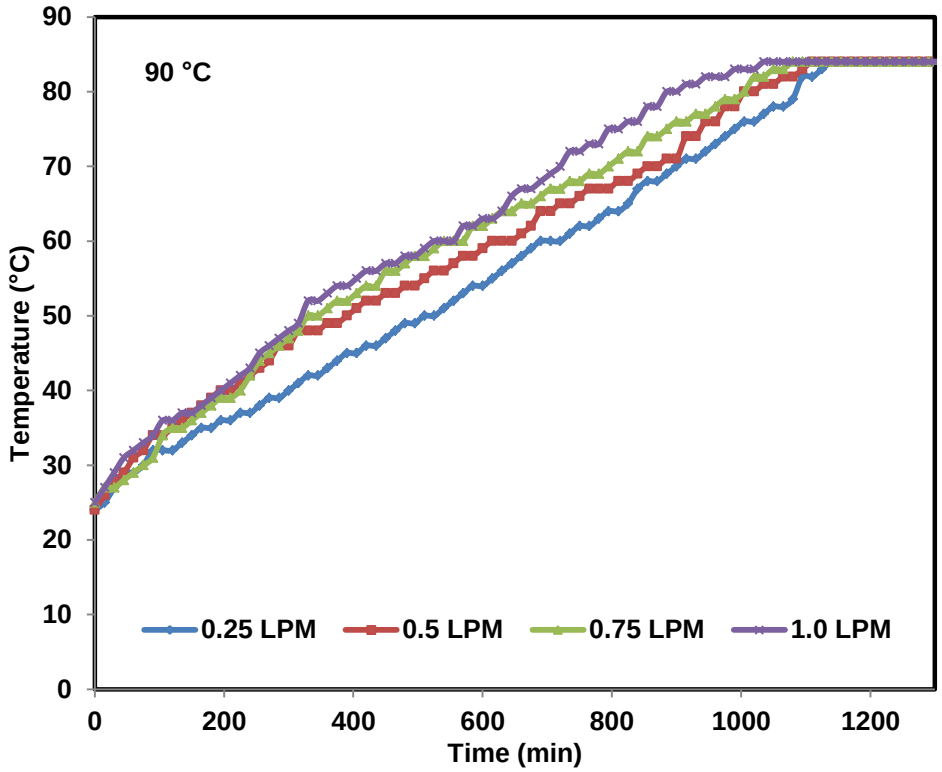

(d)

Figure 4.34 Effect of water flow rate on charging time of composite at different inlet temperature

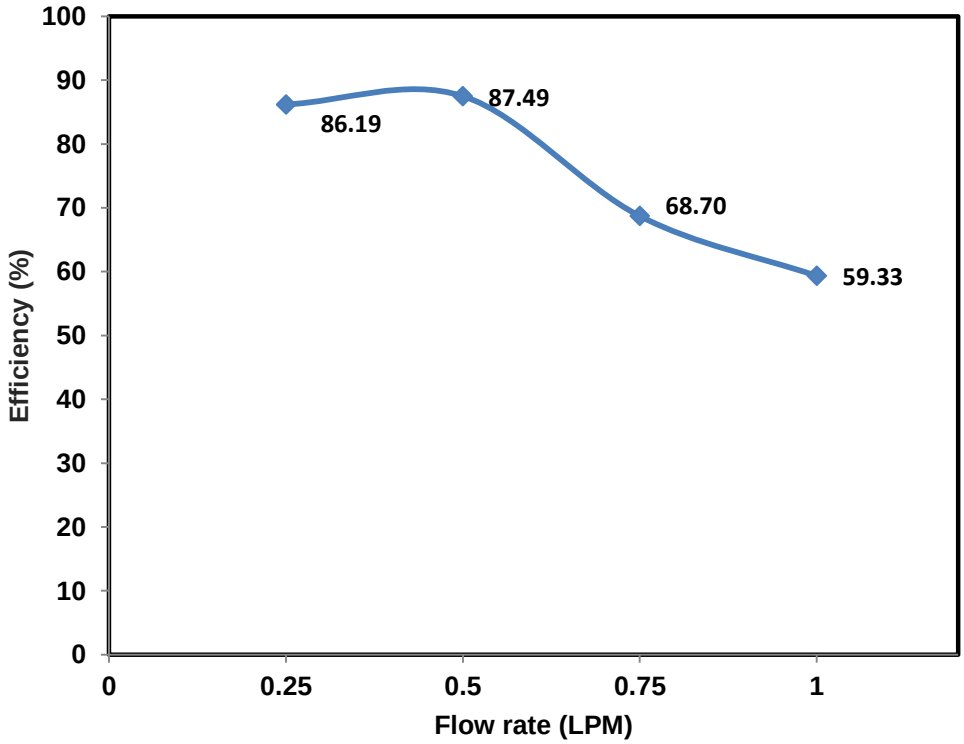

Figure 4.35 Thermal storage efficiency of large TSU with composite at different flow rates of water

ii) Effect of inlet fluid temperature on charging time

Temperature variation of composite material at position T3 in large thermal storage unit with time at different inlet fluid temperatures (60 °C, 70 °C, 80 °C and 90 °C) are shown in Figure 4.36 keeping constant fluid flow rate. Observed charging time of composite material is 1275 min, 1140 min, 1125 min and 1110 min for the inlet fluid temperature of 60 °C, 70 °C, 80 °C and 90 °C respectively at flow rate of 0.5 LPM.

Therefore, the charging time of beeswax/expanded graphite composite reduced with increase in the inlet fluid temperature and minimum charging time is obtained at the highest inlet fluid temperature of 90 °C. Decrease in charging time of composite material with increase in inlet fluid temperature is due to higher temperature difference available between the HTF and PCM which caused faster heat transfer. Similar variations in charging time with inlet fluid temperatures were also observed on other three flow rates (0.25 LPM, 0.75 LPM and 1.0 LPM) as shown in Table 4.6.

Table 4.6 Charging time of composite material at different conditions

Flow rate (LPM)	Inlet temperature (°C)	Charging time (min)
0.25	60 °C	1320
	70 °C	1215
	80 °C	1185
	90 °C	1140
0.50	60 °C	1275
	70 °C	1140
	80 °C	1125
	90 °C	1110
0.75	60 °C	1230
	70 °C	1125
	80 °C	1080
	90 °C	1065
1.00	60 °C	1200
	70 °C	1080
	80 °C	1020
	90 °C	1035

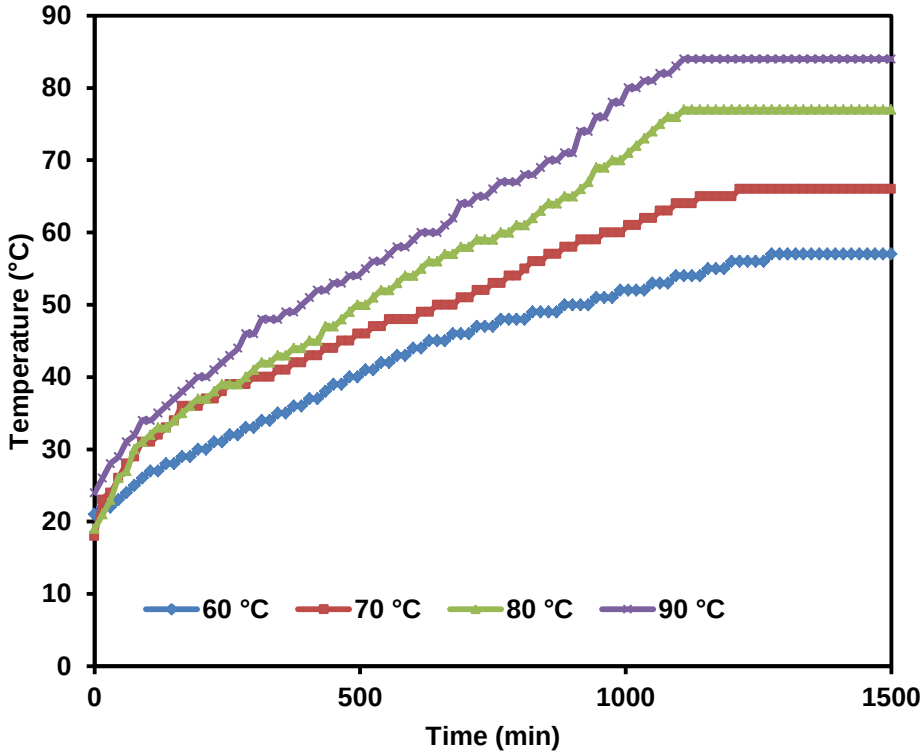

Figure 4.36 Effect of inlet water temperature on charging time of composite at 0.5 LPM

iii) Thermal profile of composite

Thermal profiles of composite material at different inlet fluid temperature and fixed flow rate of 0.5 LPM are shown in Figure 4.37 and it is observed that the temperature rise pattern at all the nine thermocouple positions is similar in all the profiles. For better understanding of thermo-physical phenomena during heat storage, the charging profile of composite at 80 °C and flow rate of 0.5 LPM is divided into temperature distribution profiles in axial direction and vertical direction of TSU as shown in Figure 4.38 and Figure 4.39 respectively. Figure 4.38(a) represents the temperature distribution of composite material in axial direction of the thermal storage unit above the helical coil (T1, T2, T3) and it can be seen that the temperature of thermocouple near to inlet (T1) raised faster as compared to the thermocouple at the middle plane (T2) followed by the thermocouple near to outlet of TSU (T3). This difference has been arrived due to higher temperature difference available between PCM and HTF at inlet position compared to the temperature difference at T2 and T3 that has led to faster heat transfer near the inlet as compared to T2 and T3. Similar pattern of temperature rise has been observed at other two axial positions i.e. middle of the coil

(T4, T5, T6) and below the coil (T7, T8, T9) as shown in Figure 4.38 (b) and Figure 4.38 (c) respectively.

Thermal profile of composite material along the vertical plane of thermal storage unit is shown in Figure 4.39. Variation in temperature at the thermocouples in the vertical plane near the inlet (T1, T4, T7) is shown in Figure 4.39 (a) which depicts that the temperature of thermocouple (T7) at the bottom of the helical coil raised first as compared to thermocouple at middle (T4) of the coil followed by top of the helical coil (T1). As the HTF is allowed to flow through the thermal storage unit it started delivering heat to the composite material, and the melting of composite material began, molten PCM moved toward the bottom of thermal storage unit due to gravity and transferred its heat via conduction and convection both caused fast melting of bottom wax, hence, faster rise in temperature at bottom part took place. With the rise in temperature, the molten PCM at the bottom part moved towards the upper part of thermal storage unit due to buoyancy effect and delivered its heat to the PCM through convection which further increased the temperature of the middle part and then the upper part of thermal storage unit. Similar variations of temperature was also observed for thermocouples at the other two vertical planes i.e. middle of the coil (T2, T5, T8) and at the vertical plane near to outlet of TSU (T3, T6, T9) as shown in Figure 4.39 (b) and (c) respectively.

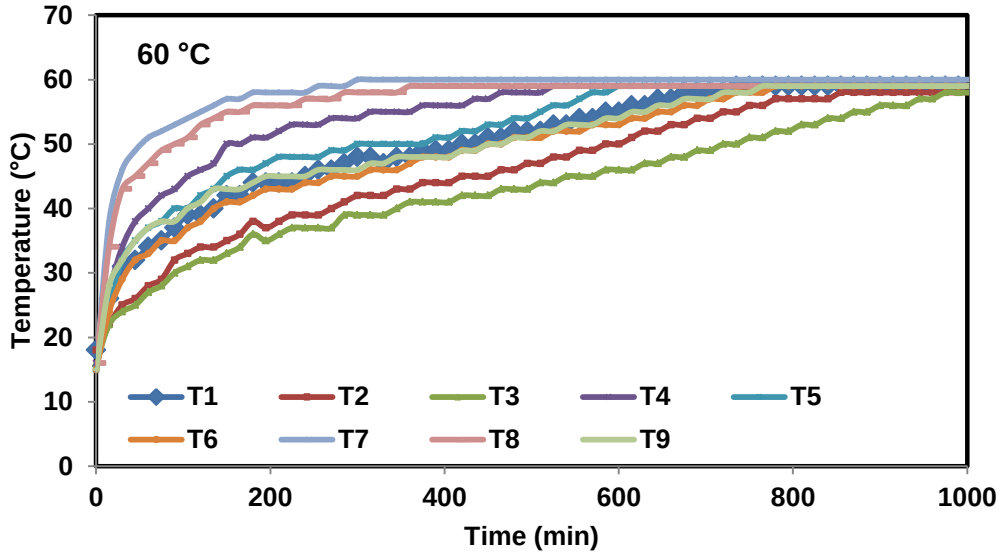

(a)

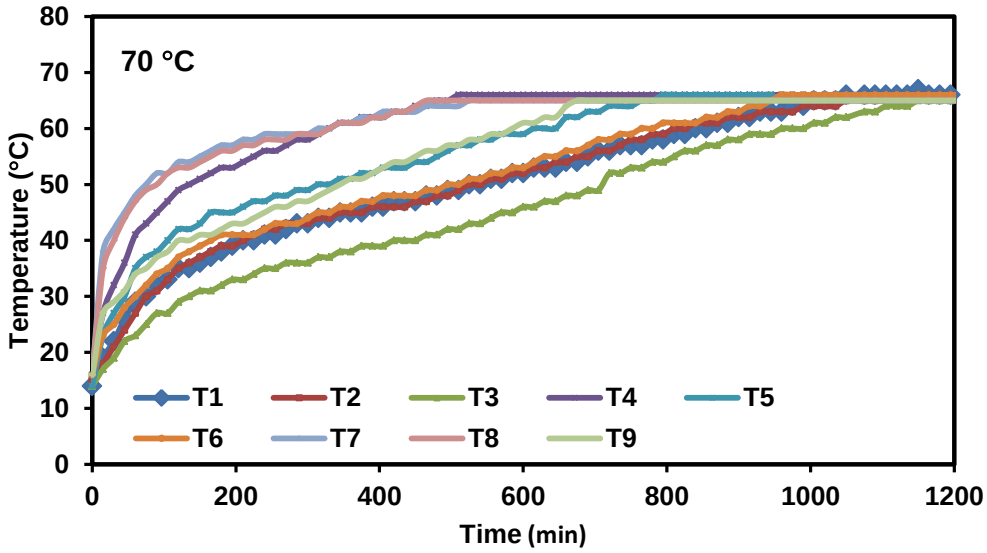

(b)

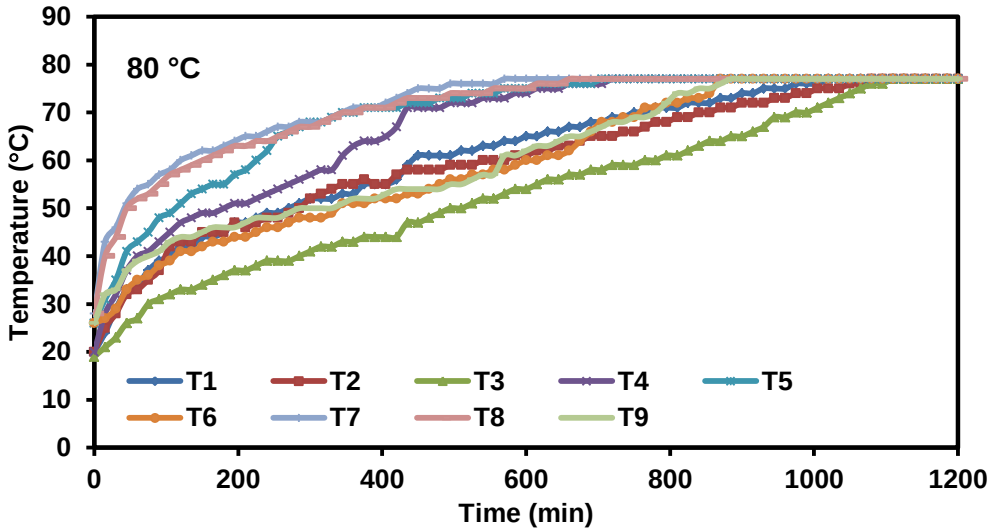

(c)

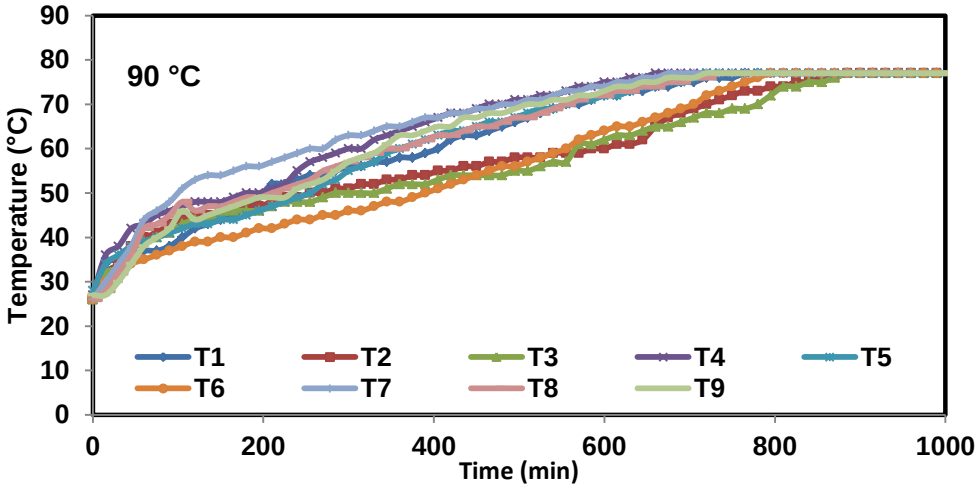

(d)

Figure 4.37 Thermal profiles of composite at different inlet water temperatures

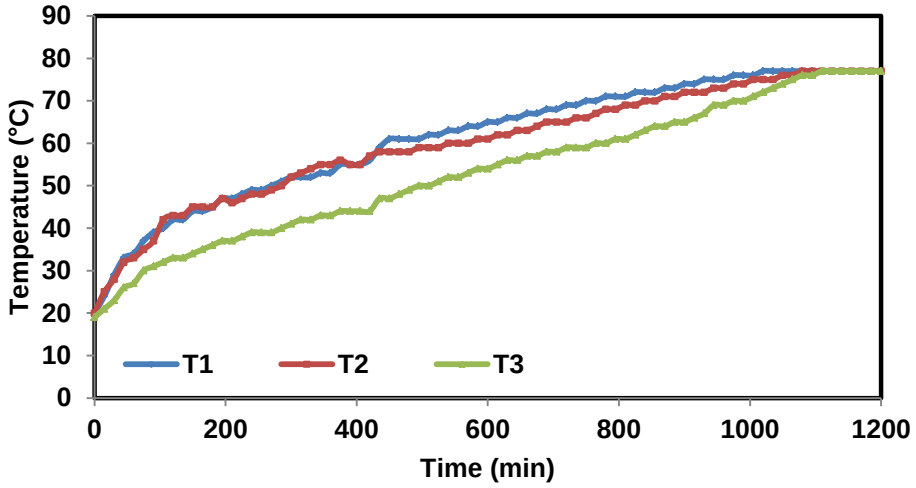

(a)

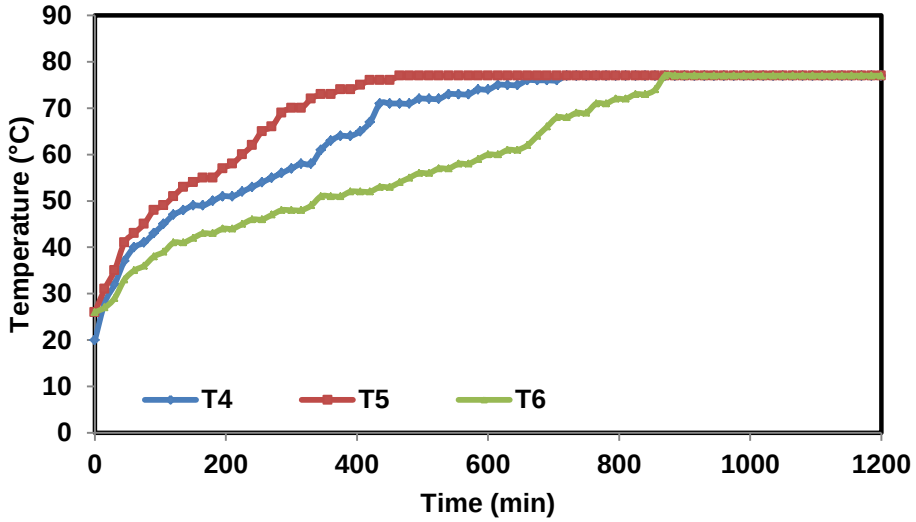

(b)

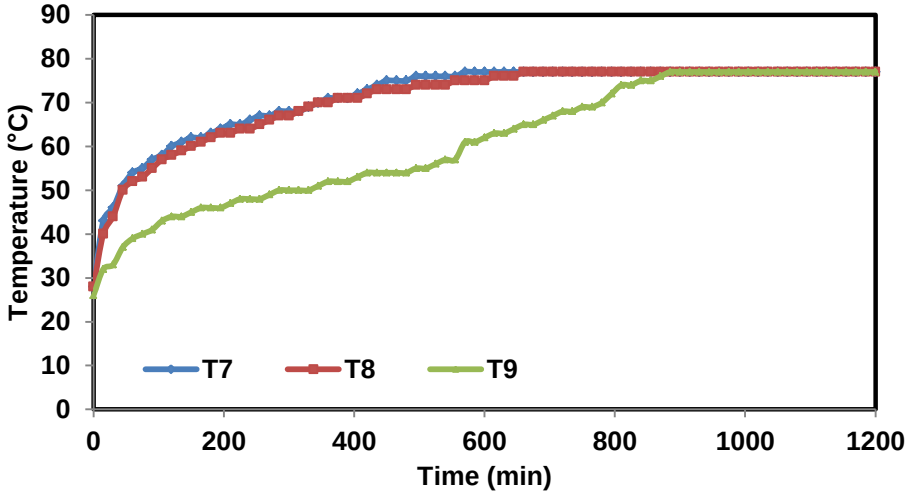

(c)

Figure 4.38 Temperature distributions in large TSU with composite along horizontal planes

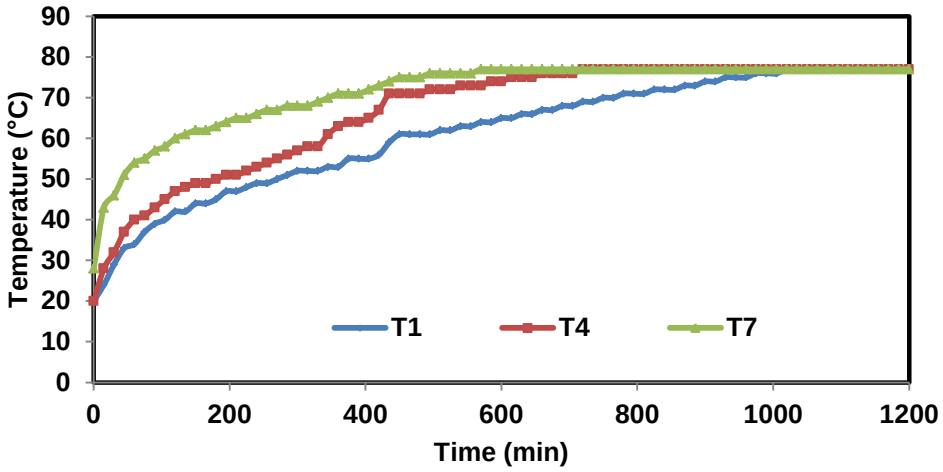

(a)

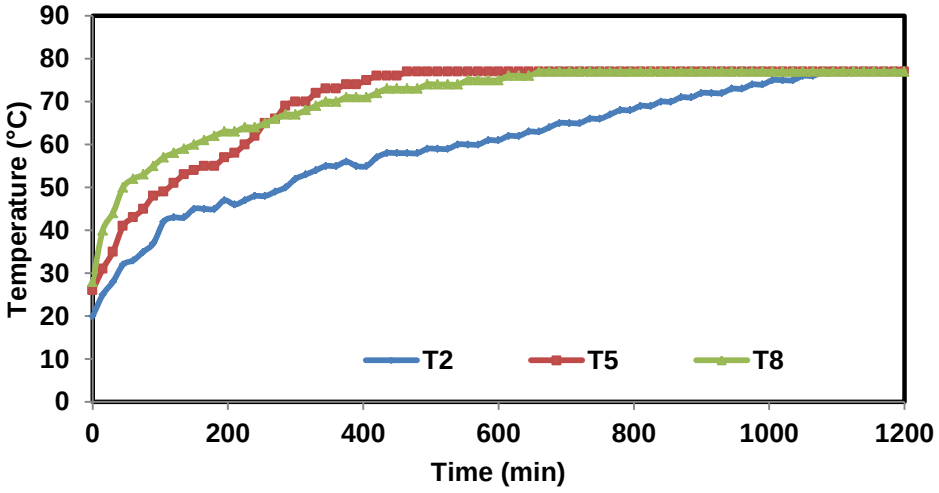

(b)

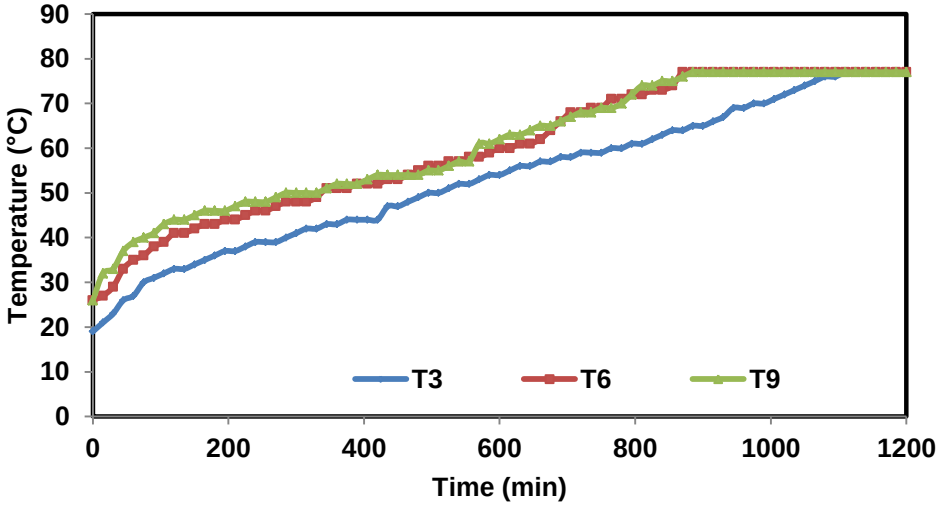

(c)

Figure 4.39 Temperature distributions in large TSU with composite along vertical planes

iv) Discharging profile of composite material

Discharging profile of composite material was studied using plain water of 20 °C and the temperature variations in axial and vertical planes of thermal storage unit are shown in Figure 4.40 and Figure 4.41 respectively. As per Figure 4.40 (b) the temperature at the position T4 near the inlet of TSU is droped at faster rate as compared to the temperature at middle of the coil (T5) followed by temperature at the end of coil (T6) in axial direction. The rate of temperature drop along the axis is reduced due to decrease in temperature difference of HTF and PCM material. Similar pattern of temperature drop is also observed for the other axials positions above the coil (T1, T2, T3) and below the coil (T7, T8, T9). This is due to the fact that temperature of heat transfer fluid increased while moving from left to right of TSU which decreased heat transfer gradient i.e. temperature difference between composite and HTF and reduced heat transfer rate by conduction.

The solidification process of composite was different from the melting process, as HTF allowed to flow through the helical coil, the molten composite around the coil lost heat to the wall of the coil and started accumulating around the coil surface which formed a thin film of composite on the coil. The thickness of this film increased further with time due to more heat transfer to the coil through conduction which caused extra resistance for further heat transfer via conduction. It is observed from Figure 4.41 that during solidification, the temperature at the thermocouples along all the vertical planes i.e. near to inlet (T1, T4, T7), at the middle of the coil (T2, T5, T8) and near to the outlet (T3, T6, T9) of TSU dropped simultaneously. This is due to the fact that during solidification of composite material conduction mode of heat transfer is dominant as compared to the convection mode.

Conduction dominates the heat transfer in discharging process of PCMs is also observed by many researchers in their studies [301–304].

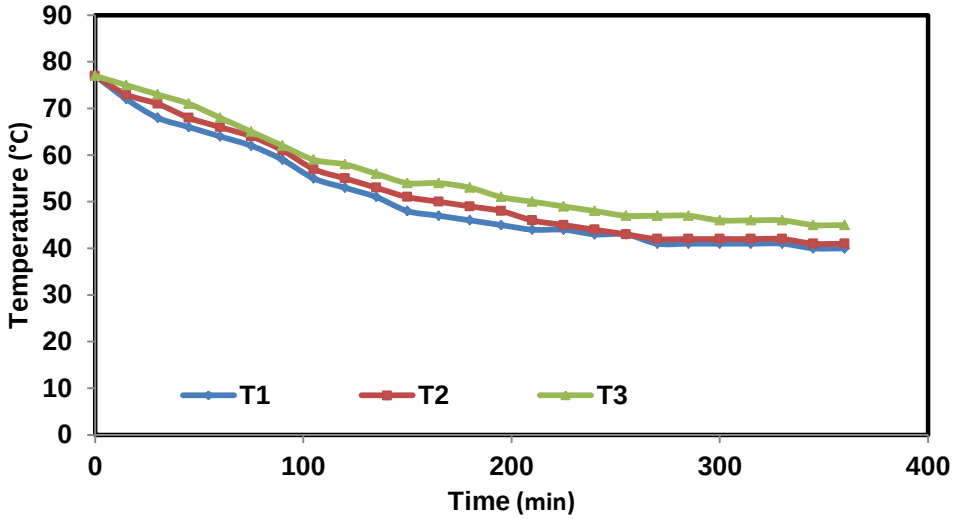

(a)

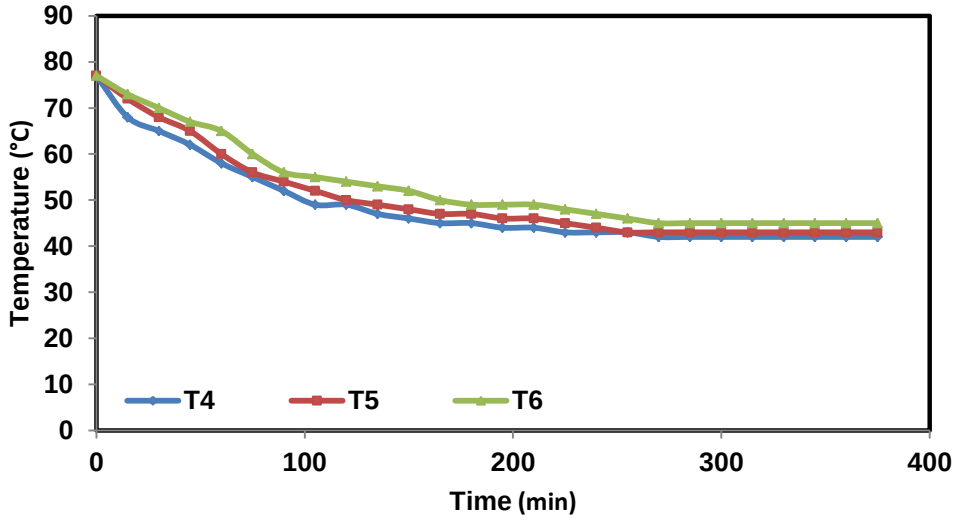

(b)

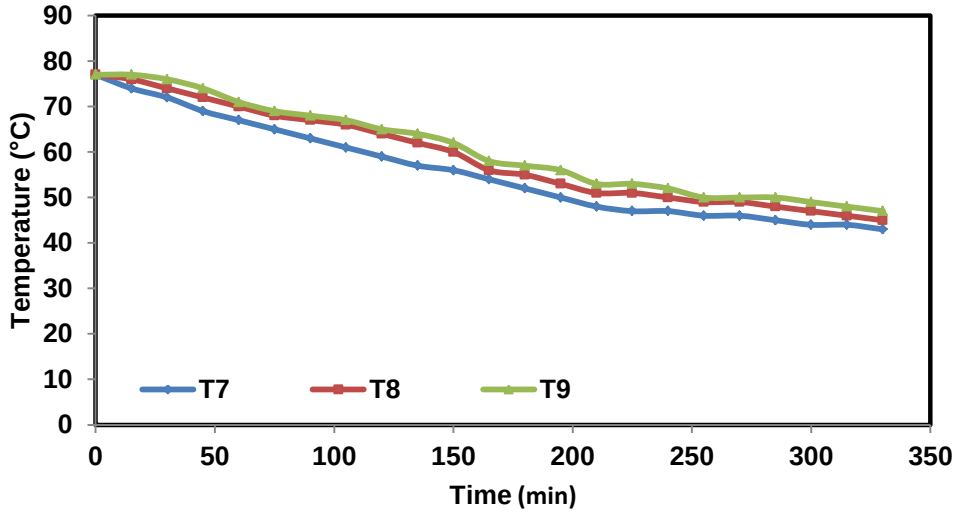

(c)

Figure 4.40 Discharging profile of composite material along axial planes in large TSU

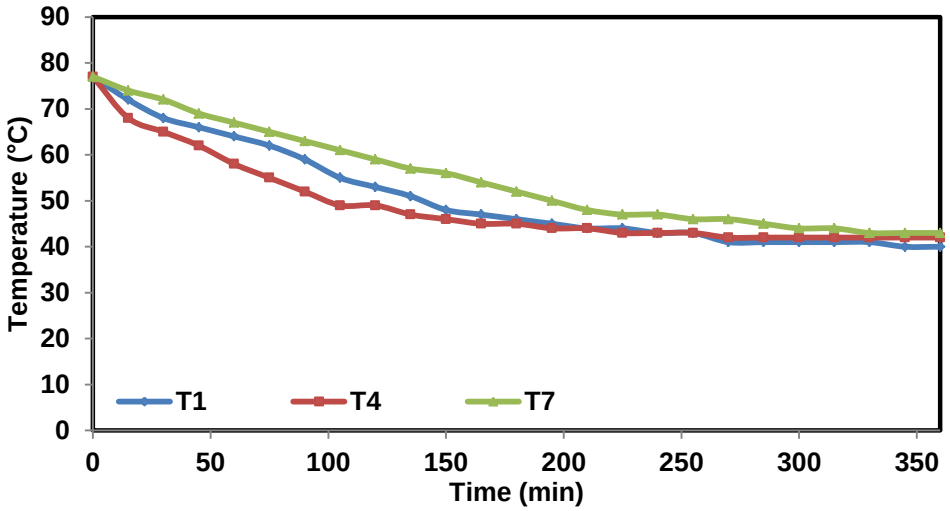

(a)

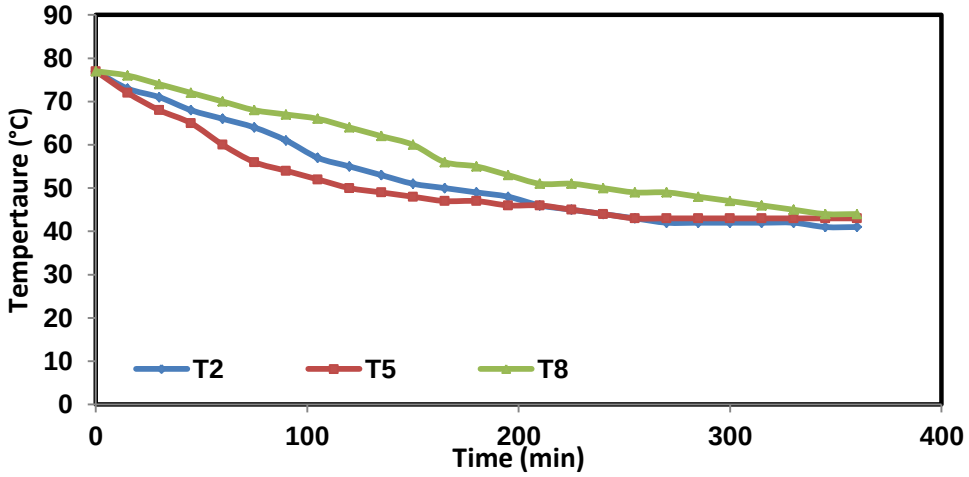

(b)

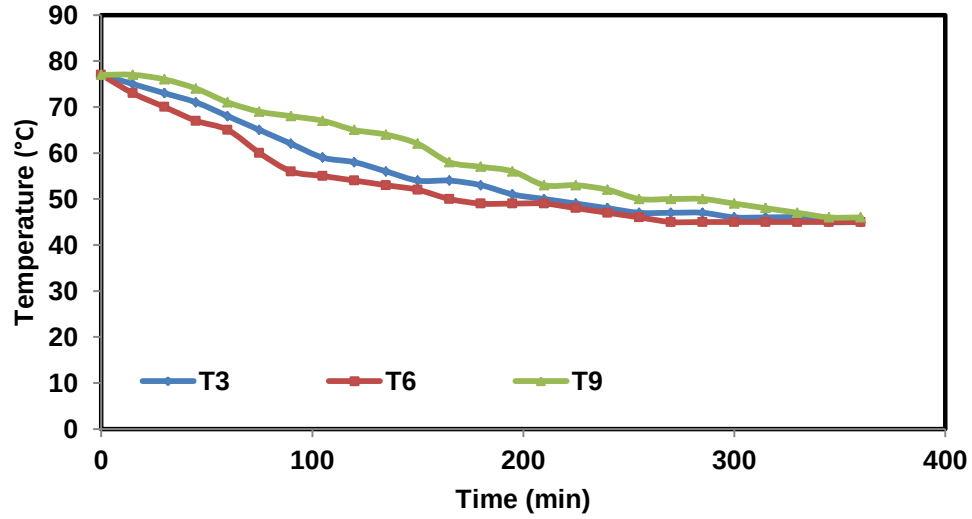

(c)

Figure 4.41 Discharging profile of composite material along vertical planes in large TSU

v) Comparison of charging time of beeswax and composite

With 10% addition of expanded graphite in beeswax, thermal conductivity of beeswax/expanded graphite composite material increased to 0.63 W/m.K which is 117% more than pure beeswax (0.29 W/m.K). Due to this enhancement in thermal conductivity the charging time of composite material reduced as compared to beeswax under similar operating conditions.

Comparison of charging time pattern between beeswax and composite material using plain water is shown in Figure 4.42 at inlet fluid temperature of 80 °C and flow rate of 0.5 LPM. Observed values of charging time for beeswax and composite material are 1650 min and 1125 min respectively, this is due to the presence of continuous matrix of expanded graphite within the continuous phase of beeswax which promoted faster heat conduction with 31.81% reduction in the charging time. Table 4.7 shows the charging time comparison for beeswax and composite material using hot plain water of 80 ^{o}C. Minimum charging time is obtained for the composite material with 10% expanded graphite in beeswax and this newly developed PCM is a promising option as heat storage material in low temperature thermal applications.

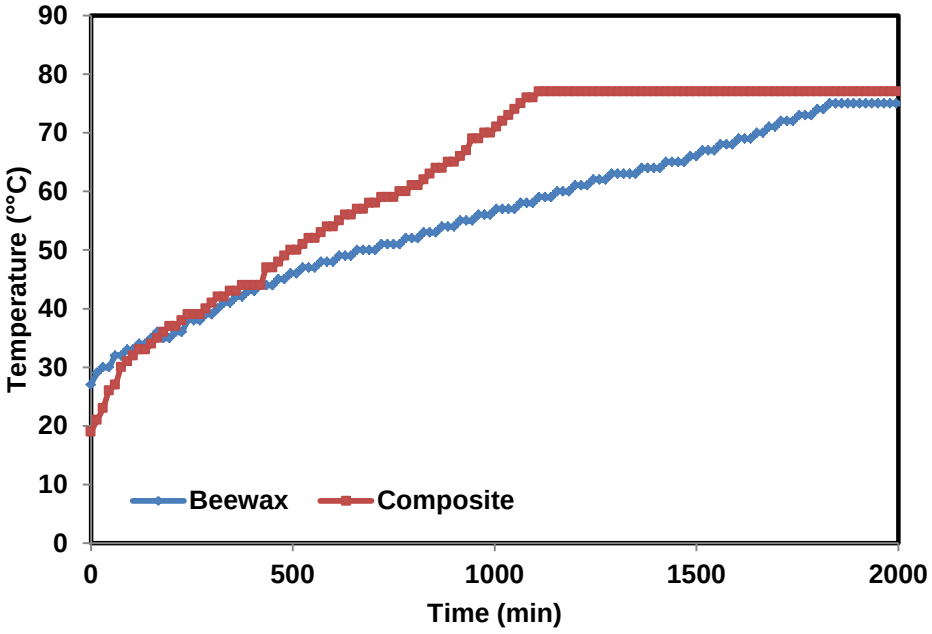

Figure 4.42 Comparison of charging time of beeswax and its composite material

Table 4.7 Charging time comparison for beeswax and composite material with plain water at 0.5 LPM and 80 ^{o}C .

Flow rate of water (LPM)	Charging time of beeswax (min)	Charging time of composite (min)	% reduction in charging time
0.25	1830	1185	35.24
0.50	1650	1125	31.81
0.75	1590	1080	32.00
1.0	1530	1020	33.33

4.5.2 Using expanded graphite/water suspension as HTF

Expanded graphite(EG)/water suspension as heat transfer fluid was prepared and passed through the helical tube of thermal storage unit at three different concentrations (0.05 wt. %, 0.5 wt. %, 1.0 wt. %) to study the thermal performance of beeswax/expanded graphite composite material in large TSU.

i) Effect of fluid concentration on charging time

The variation of charging time with solute concentration in expanded graphite/water suspension is presented in Figure 4.43 at the flow rate of 0.5 LPM and inlet fluid temperature of 80 °C and observed that the charging time of composite material decreased with increase in the expanded graphite concentration in water. For three fluid concentrations of 0.05 wt. %, 0.5 wt. % and 1 wt. %, charging time found to be 1065 min, 1020 min and 960 min respectively. This reduction in charging time with EG concentration is due to increased thermal conductivity of expanded graphite/water suspension. Suspension having more than 1wt. % of EG may choke the helical tube of thermal storage unit and not considered for the present study.

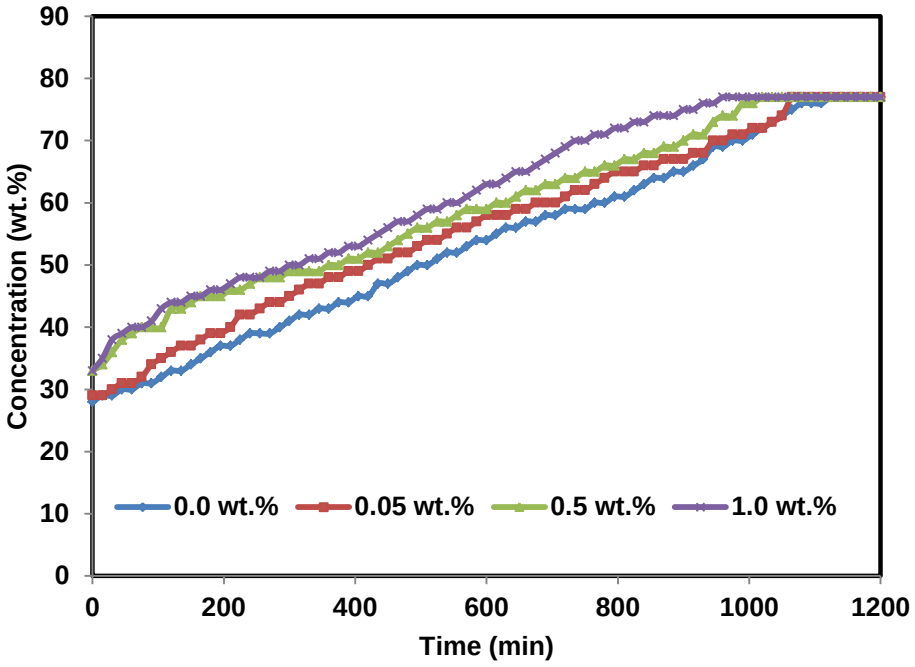

Figure 4.43 Effect of expanded graphite/water concentration on charging time of composite

ii) Thermal profile of composite material

Thermal profiles of composite material using different concentration (0.05 wt. % 0.5 wt. % and 1 wt. %) of expanded graphite/water suspension are shown in Figure 4.44 and it is observed that when the HTF was passed through the helical coil, the heat transfer from HTF to PCM initially occurred through conduction followed by the convection. Similar to beeswax the melting of composite beings at the coil surface from where it moves towards the bottom of thermal storage unit due to gravitational effect which rises the temperature of lower part of the unit. This molten beeswax in the lower part of TSU (T7, T8, T9) then moves towards the middle (T4, T5, T6) and upper part (T1, T2, T3) of the TSU due to buoyancy effect and explains the temperature variation in the vertical planes of thermal storage unit. While in the axial direction temperature raised first at the thermocouples near to inlet (T1, T4, T7) followed by the thermocouples at the middle (T2, T5, T8) and then near to outlet (T3, T6, T9) of TSU. In this way the solid-liquid interface moves from left hand (fluid inlet) side of TSU to right hand side (fluid outlet) of TSU and thermal profiles of composite material when charged with different concentrations of EG/water suspensions are similar except their charging time.

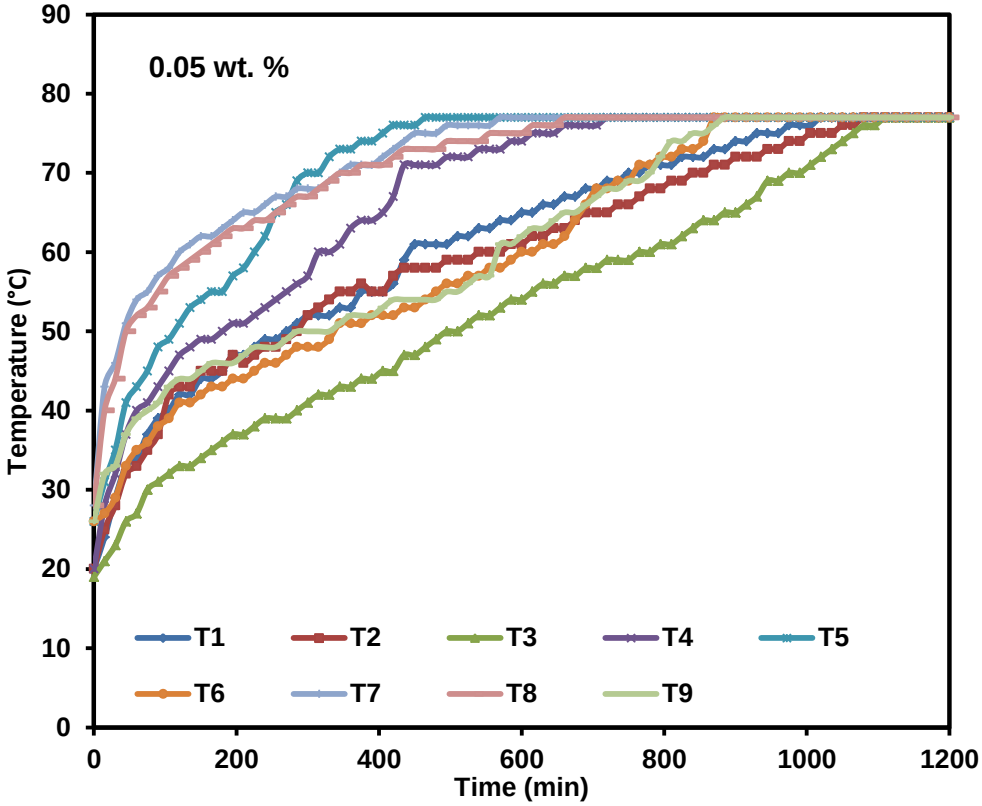
0.05 wt. %
Temperature (°C)
Time (min)
T1
T2
T3
T4
T5
T6
T7
T8
T9
0
10
20
30
40
50
60
70
80
90
0
200
400
600
800
1000
1200

(a)

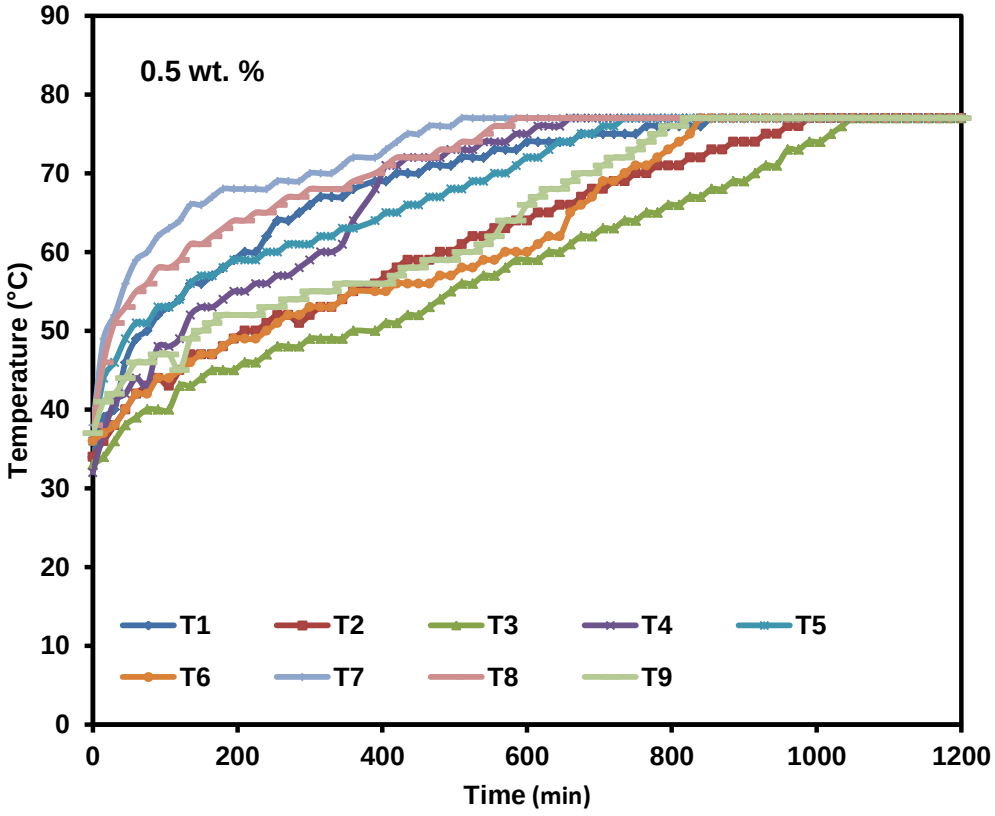
0.5 wt. %
Temperature (°C)
Time (min)
T1
T2
T3
T4
T5
T6
T7
T8
T9
0
10
20
30
40
50
60
70
80
90
0
200
400
600
800
1000
1200

(b)

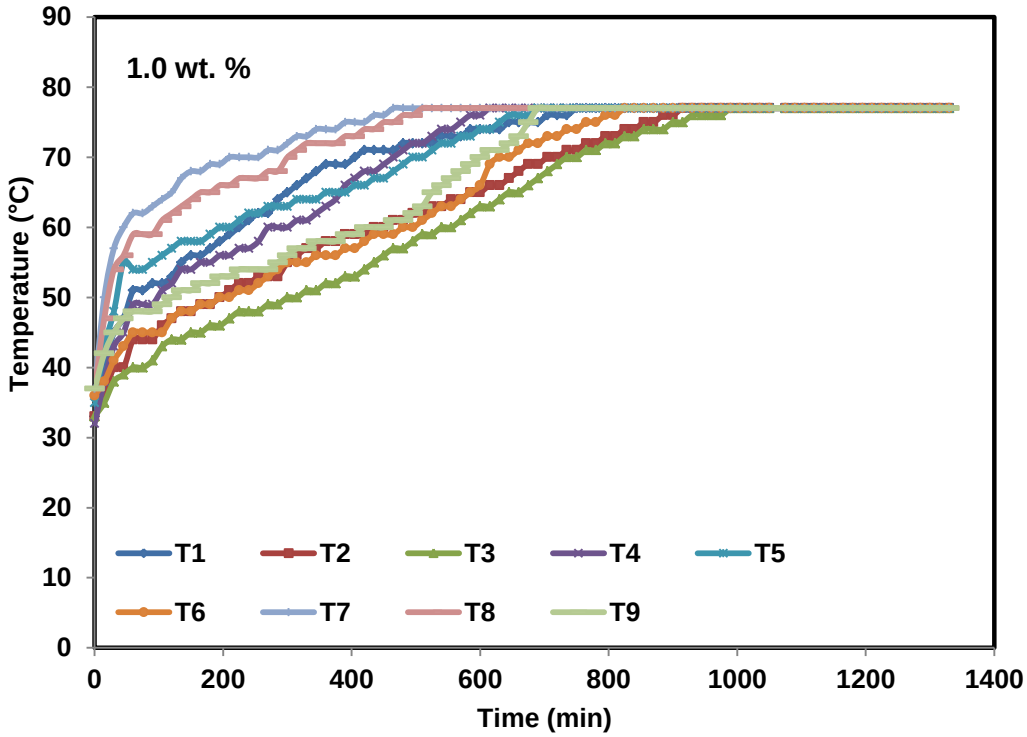

(c)

Figure 4.44 Thermal profiles of composite material at different EG concentrations

iii) Charging time comparison between beeswax and composite material

Results of the present study shows that the melting time and charging time of beeswax and its composite gets reduced with the use of expanded graphite/water suspension of different concentrations.

However, it is found that the composite of beeswax showed greater reduction in charging time as compared to pure beeswax at same concentration of expanded graphite/water suspension and same operating conditions (0.5 LPM, 80 °C) as shown in Figure 4.45. Comparison of charging time of beeswax and composite material are given in Table 4.8 which shows that there is continuous reduction in charging time with increase in concentration of EG in water for both beeswax and composite but it is more in case of beeswax at higher concentration due to higher heat transfer rate (by convection) from HTF. Plain water as HTF is equally good in comparison to 0.5 % or more of EG/water suspension from charging time reduction point of view.

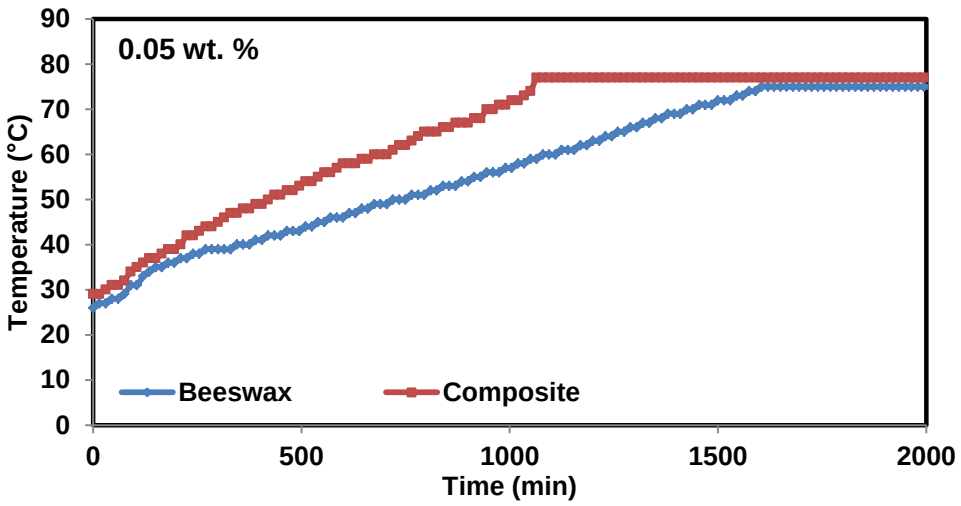

(a)

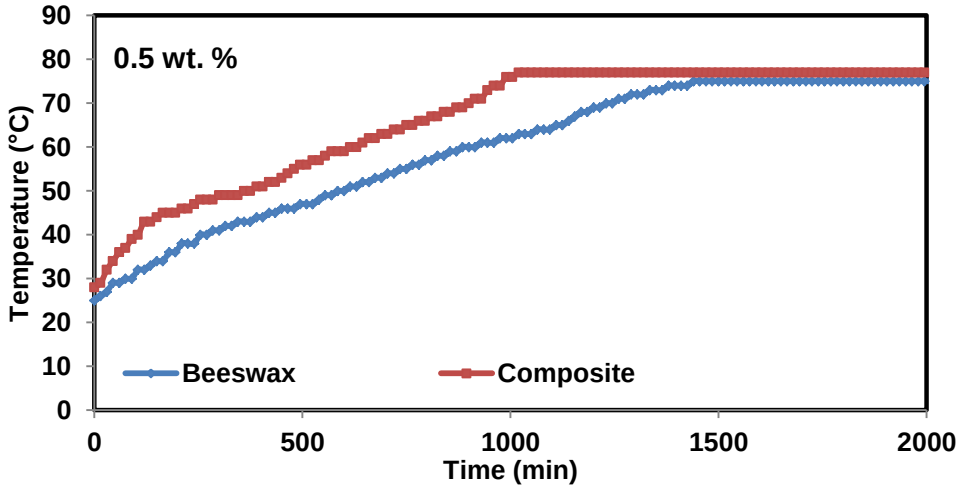

(b)

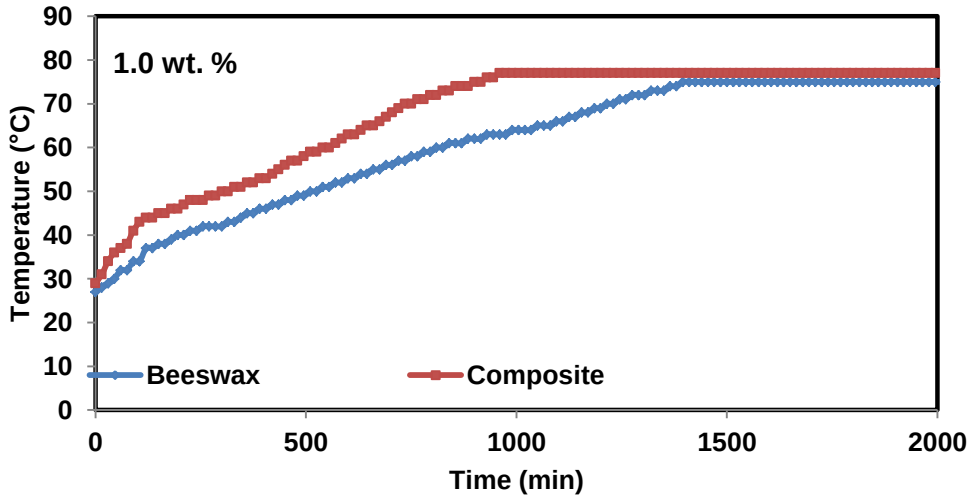

(c)

Figure 4.45 Temperature variation in composite and beeswax at position T3

Table 4.8 Charging time comparison of beeswax and its composite using EG/water suspension at 0.5 LPM and 80 °C

Inlet fluid concentration (wt.%)	Charging time of beeswax (min)	% reduction in charging time	Charging time of composite (min)	% reduction in charging time	Comparative % reduction in charging time of beeswax and composite
0.0	1650	-	1125	-	31.8
0.05	1605	2.72	1065	5.33	33.6
0.50	1440	12.72	1020	9.33	29.1
1.0	1395	15.45	960	14.66	31.1

4.5.3 Using Al_2O_3-water nanofluid as HTF

Al_2O_3/water suspension nanofluid of different concentrations (0.2 vol. %, 0.5 vol. %, 1.0 vol. %, and 2.0 vol. %) was prepared and circulated through the helical coil of thermal storage unit at constant flow rate of 0.5 LPM and inlet fluid temperature of 80 °C to study the thermal storage performance of beeswax/expanded graphite composite material. Experimental results from the present study considering mainly the effect of fluid concentration and thermal profile are discussed here.

i) Effect of fluid concentration

Effect of different concentrations of alumina nanofluid on the charging time of composite is shown in Figure 4.46, which depicts that the charging time of composite material decreased with increase in concentration of nanoparticles in HTF. The charging time of composite material is found to be 1095 min, 1050 min, 1020 min and 1005 min at Al_2O_3/water suspension concentration of 0.2 vol. %, 0.5 vol. %, 1.0 vol. %, and 2.0 vol. % respectively. At maximum concentration of 2.0 vol. % of Al_2O_3/water suspension, the charging time of composite material reduced by16.94% as compared to plain water. The presence of nanoparticles improves the thermal conductivity of the suspension and promotes faster heat transfer which gives reduced charging time of composite material.

Concentration higher than 2 vol. % has not been recommended due to agglomeration which may increase wear and tear, sedimentation etc. in the helical coil and can disturb the normal fluid flow through the system.

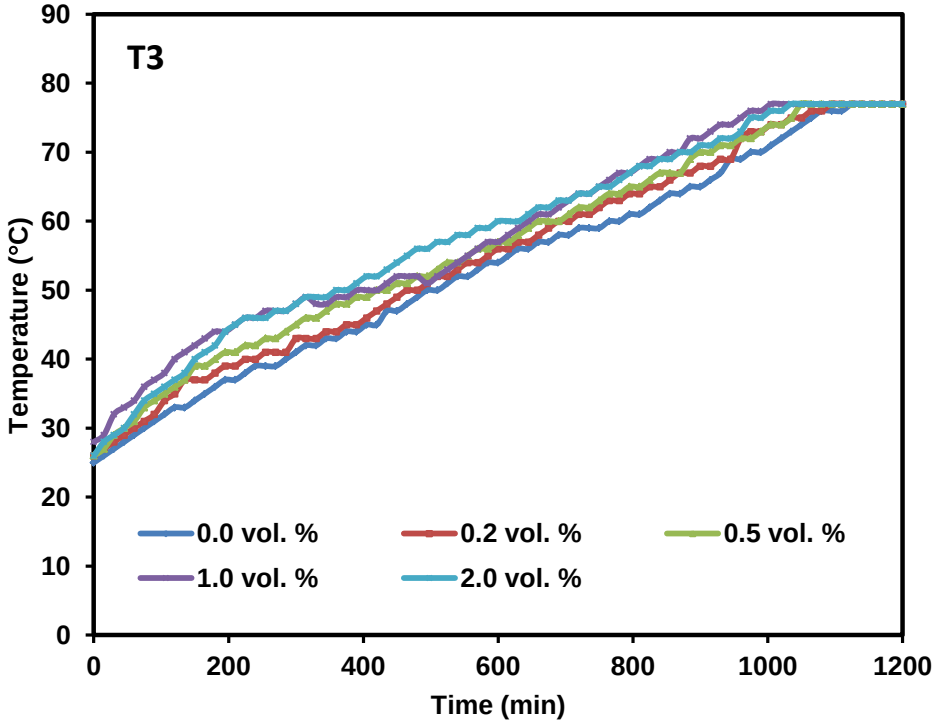

Figure 4.46 Effect of Al_2O_3 nanofluid concentration on charging time of composite

ii) Thermal profile of composite

Thermal profiles of composite with different concentrations (0.2 vol. %, 0.5 vol. %, 1.0 vol. %, and 2.0 vol. %) of Al_2O_3/water suspensions are shown in Figure 4.47. The temperature rise patterns observed with the use of nanofluid is similar to the thermal profiles observed with the use of plain water. However, different charging times are obtained with different heat transfer fluids.

Thermo fludic phenomena observed in these profiles can be understood from the fact that as soon as the melting of composite begins inside the thermal storage unit it first starts moving downwards due to gravity and temperature of thermocouple placed at the lower part of thermal storage unit (T7, T8, T9) increases, which then promotes natural convection and movement of molten composite to the upper part of TSU and hence, the temperature rise at the middle (T4, T5, T6) and upper part (T1, T2, T3) is observed. Table 4.9 is showing the percentage reduction in charging time at different concentrations of alumina nanofluid.

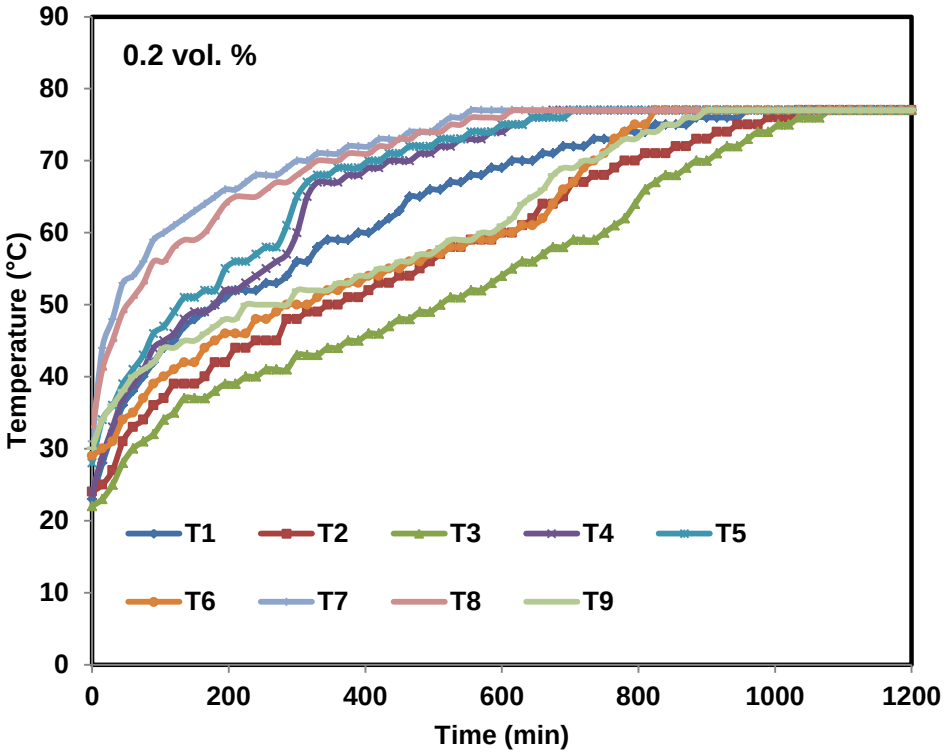
0.2 vol. %
Temperature (°C)
Time (min)
T1
T2
T3
T4
T5
T6
T7
T8
T9

(a)

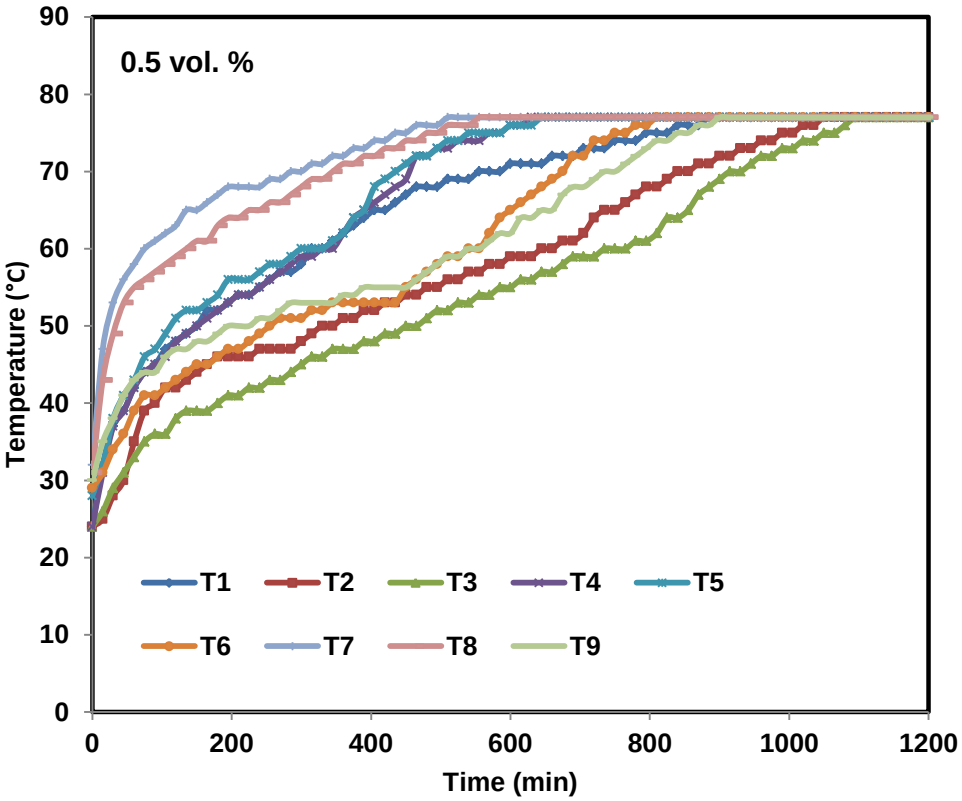
0.5 vol. %
Temperature (°C)
Time (min)
T1
T2
T3
T4
T5
T6
T7
T8
T9

(b)

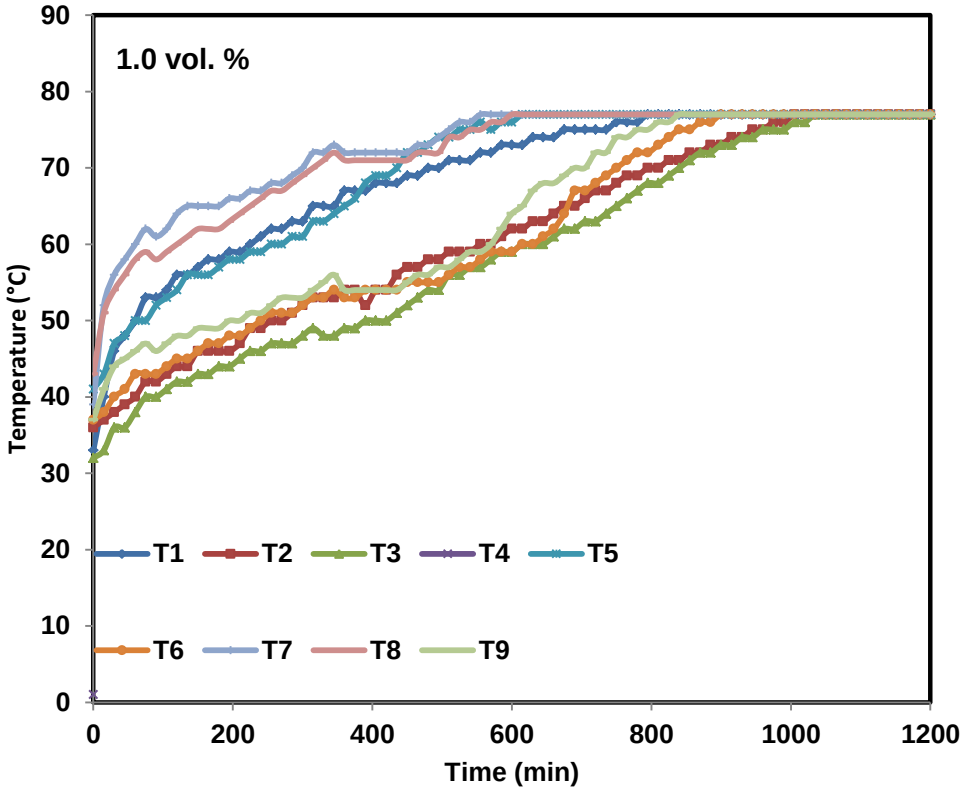

(c)

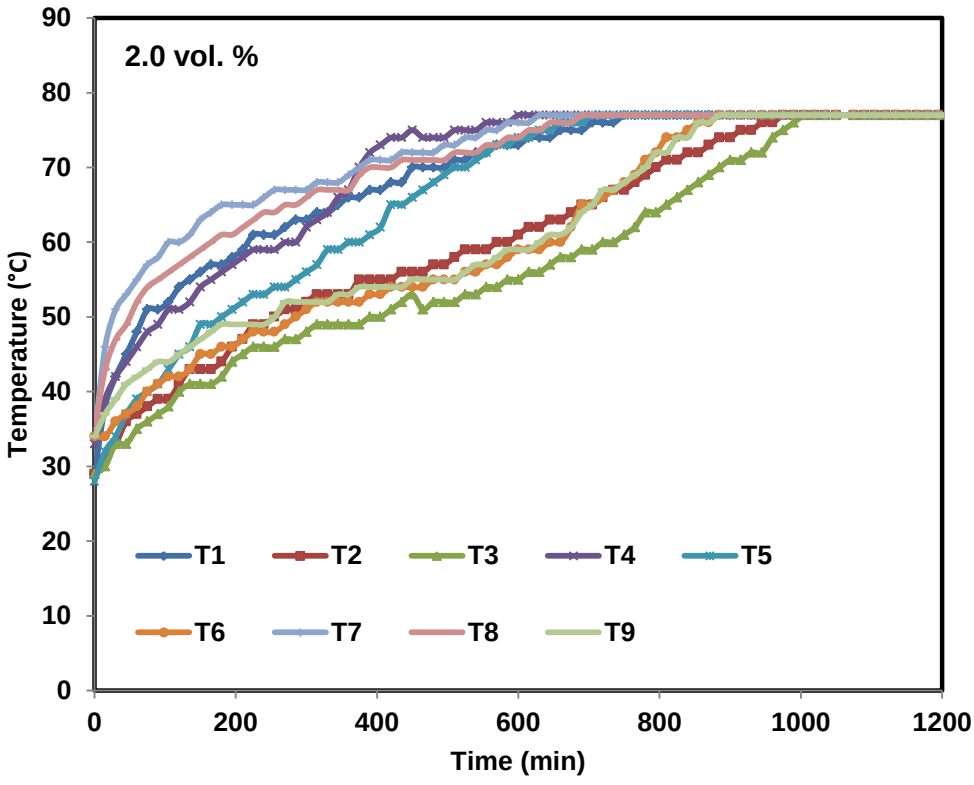

(d)

Figure 4.47 Thermal profiles of compsoite at different concentrations of Al_2O_3

iii) Comparison of charging time of composite material and beeswax

Results of the present study show that the charging time of composite and pure beeswax gets reduced with increase in the concentration of Al_2O_3/water suspension. The charging time of composite material is (32.60 %) lesser as compared to the pure beeswax for 0.5 vol. % concentration of Al_2O_3/water suspension keeping other conditions same.

Comparison of temperature variation with time at four different concentration of Al_2O_3/water suspension for thermocouple position T3 in composite and beeswax is shown in Figure 4.48 and it is found that temperature rise in composite takes place at the faster rate as compared to the beeswax. Table 4.9 represents the comparison of charging time between composite material and beeswax at different concentration of Al_2O_3 nanofluid. Charging time of composite of beeswax/expanded graphite is quiet reasonable and should be preferred over beeswax.

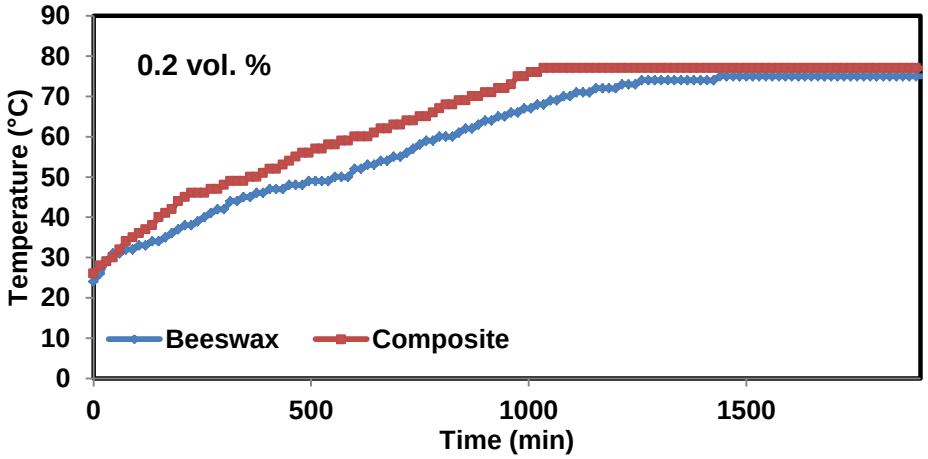

(a)

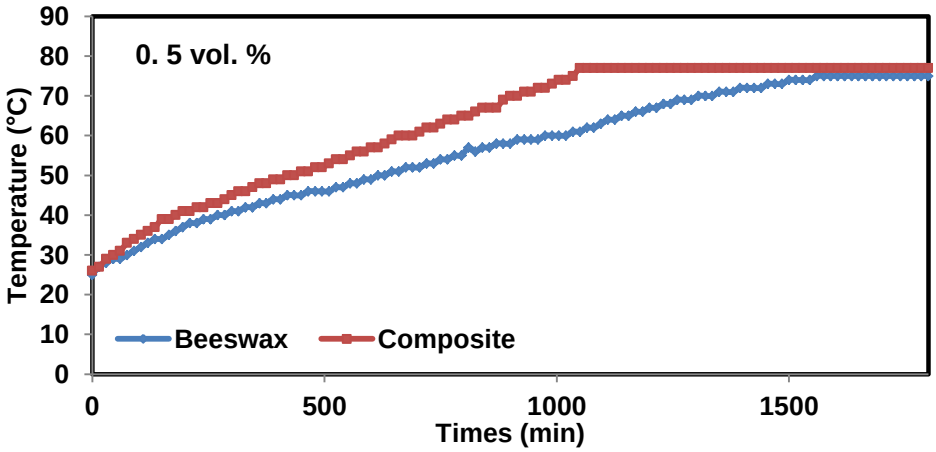

(b)

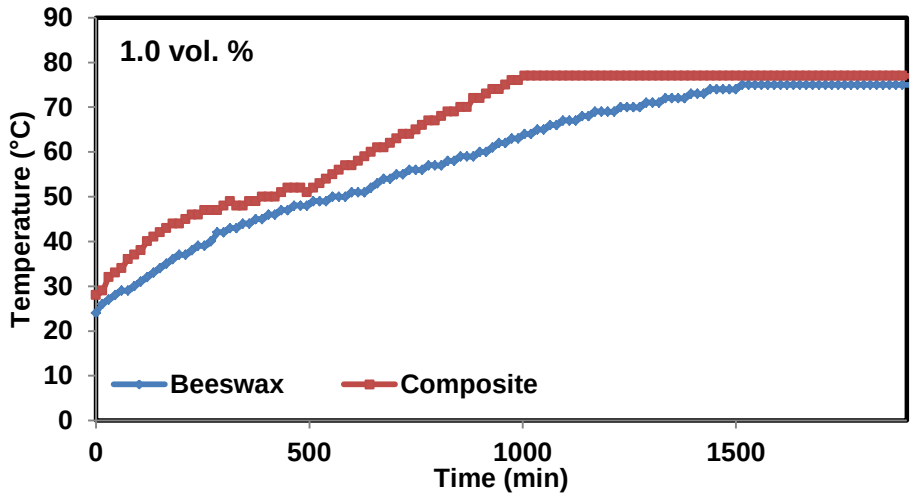

(c)

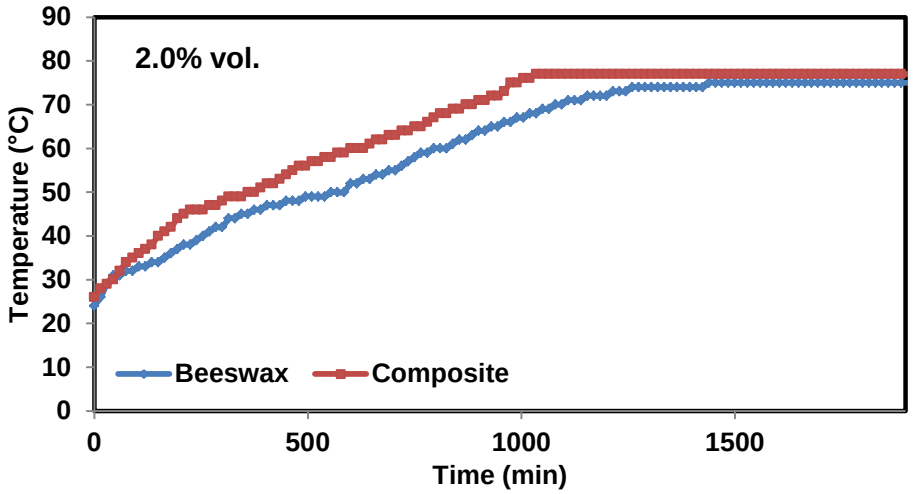

(d)

Figure 4.48 Temperature variation of composite and beeswax at position T3

Table 4.9 Charging time comparison of beeswax and its composite using Al_2O_3/water suspension at 0.5 LPM and 80°C

Inlet fluid conc.	Charging time of beeswax (min)	% reduction in charging time	Charging time of composite (min)	% reduction in charging time	Comparative % reduction in charging time of beeswax and composite
0.0	1650	--	1125	--	31.80
0.2	1590	3.63	1095	2.66	31.30
0.5	1560	5.45	1050	6.66	32.60
1.0	1515	8.18	1020	9.33	32.67
2.0	1485	10.00	1005	10.66	32.32

4.5.4 Using exhaust gas as HTF

Apart from using different liquids as HTF in the study of thermal performance for PCMs, the exhaust gas from petrol engine was also tried as heat transfer fluid with the output temperature of 165 °C. This exhaust gas was passed through the helical coil of TSU and temperatures at various positions of thermocouples were recorded.

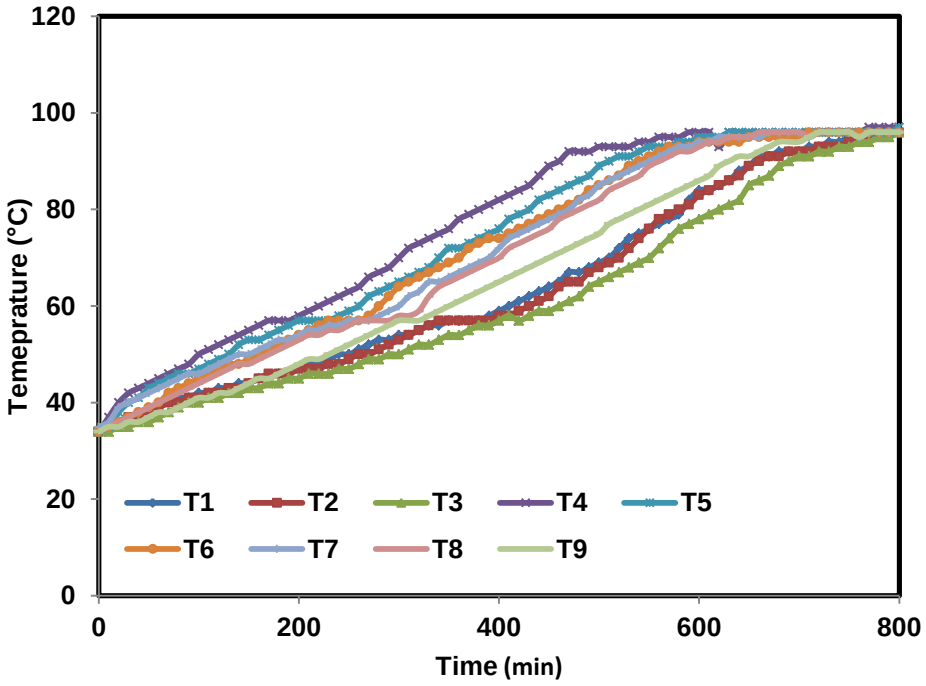

Figure 4.49 Charging profile of composite with exhaust gases

Thermal profile of composite material when charged with exhaust gas is shown in Figure 4.49 and these profiles are similar to the thermal profile of composite when charged with plain water and other liquids as HTF. It is observed during the experimentation study that the temperature of composite material raised quickly in the beginning of charging up to 92 °C and then it was at slow pace. Similar thermo-physical phenomena are present during thermal profiles in which the charging of composite starts by conduction followed by the convection and movement of solid liquid interface takes place from left (inlet) to right (outlet) and from bottom (T7, T8, T9) to top (T1, T2, T3) of the thermal storage unit.

During experimentation with exhaust gases pressure drop was observed across the thermal storage unit which is due to the accumulation of carbon in the helical tube of TSU (having small diameter of 8 mm) and this is also responsible for lower storage efficiency of TSU. The charging time and efficiency of composite material was found

to be 690 min and 46% respectively at the inlet fluid temperature of 165 °C. The waste heat of exhaust gases from internal combustion engines, boilers etc. can be usefully store in different PCMs.

4.6 Performance evaluation of natural graphite

Natural graphite is a sensible heat storage material and in powder form 22 kg of natural graphite was filled inside the rectangular shell of thermal storage unit and after step wise and systematic tapping a packed bed was formed. Then testing of the bed for its thermal storage performance was carried out using three different heat transfer fluids such as plain water, EG/water suspension and Al_2O_3/water suspension at different operating parameters.

4.6.1 Using plain water as HTF

Plain water as heat transfer fluid was used to study effect of flow rates (0.25 LPM-1.0 LPM) and inlet fluid temperatures (60 °C-90 °C) on the charging time of natural graphite.

i) Effect of flow rate on charging time

Variation of temperature with time at different flow rates to obtain charging time of natural graphite at Position T3 and position T4 are shown in Figure 4.50 and it is observed that with increase in the flow rate of HTF charging time of the natural graphite reduced. At higher fluid flow rates more enthalpy is carried with the HTF which provides greater heat for conduction. Charging time of natural graphite for position T3 with plain water found to be 195 min, 180 min, 150 min and 120 min for the flow rates of 0.25 LPM, 0.5 LPM, 0.75 LPM and 1.0 LPM respectively at 80°C inlet fluid temperature.. However, at point T4, such variation of charging time with flow rate is not observed because the position of thermocouple at T4 is near to the entrance of TSU and where more temperature rise was observed as compared to the other locations of thermocouples. Efficiency of TSU with natural graphite as sensible heat storage material is shown in Figure 4.51 and it is found that the efficiency of this sensible heat storage system reduces at higher flow rate of HTF. The thermal storage efficiency of packed bed found to be 59.34 %, 60.21 %, 48.47 %, 26.37 % at the flow rate of 0.25 LPM, 0.50 LPM, 0.75 LPM and 1.0 LPM respectively.

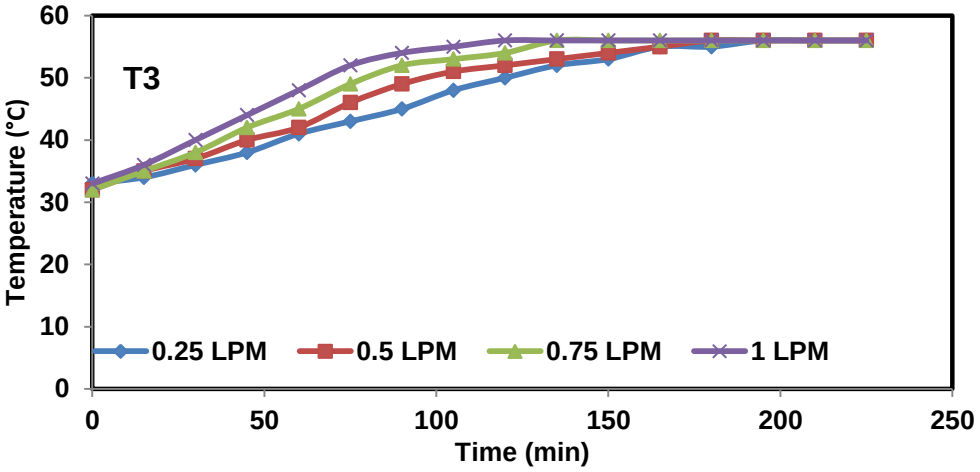

(a)

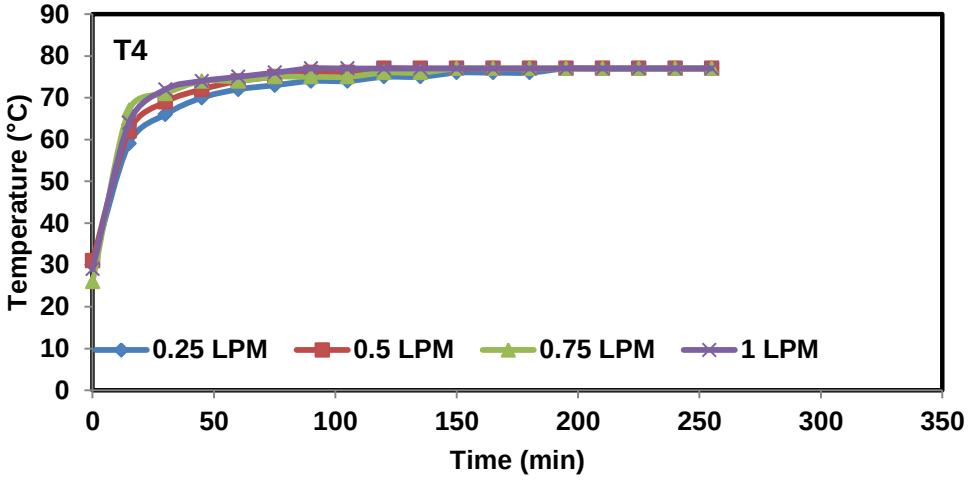

(b)

Figure 4.50 Effect of water flow rate on charging time of natural graphite at position T3 and T4

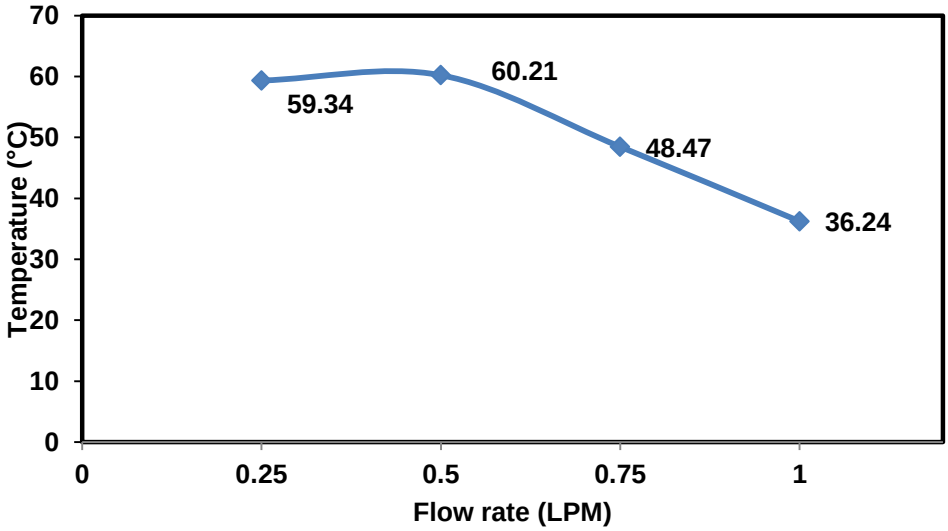

Figure 4.51 Efficiency of large TSU with natural graphite at different water flow rates

ii) Effect of inlet fluid temperature on charging time

Temperature variation of natural graphite with time at four different inlet fluid temperature is shown in the Figure 4.52 which depicts that the temperature of natural graphite is higher at the maximum inlet fluid temperature of 90°C. The charging time of packed bed of natural graphite was found to be 210 min, 195 min, 180 min, 165 min for inlet temperatures of 60 °C, 70 °C, 80 °C and 90 °C. This reduction in charging time at higher inlet fluid temperature may be due to the increase in temperature difference of hot fluid and natural graphite which causes better the heat conduction from HTF to the bed of natural graphite.

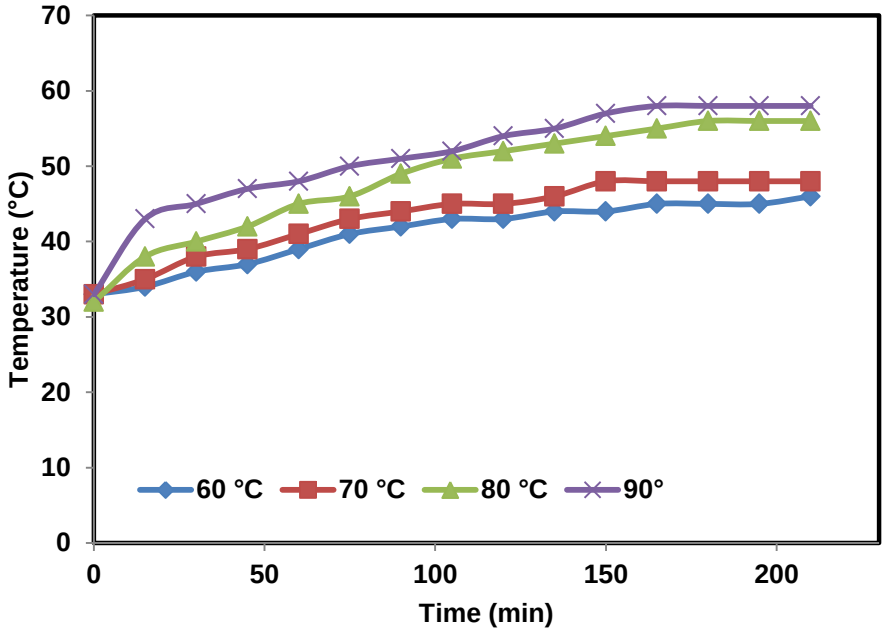

Figure 4.52 Effect of inlet water temperature on charging time of natural graphite at 0.5 LPM

iii) Thermal profile of natural graphite

Thermal profiles of natural graphite at four different inlet fluid temperatures are shown in Figure 4.53 with constant flow rate of 0.5 LPM. It was observed from Figure 4.53 (a) that the temperature of thermocouples at the center of packed bed (T4, T5, T6) raised quickly as compared to the thermocouples located above (T1, T2, T3) and below the coil (T7, T8, T9). Also temperature along the axis of coil reduced as the HTF moves from inlet to outlet of TSU and therefore the temperature at the points T1, T4, T7 are higher as compared to temperature at the middle (T2, T5, T8)

and at the end of TSU (T3, T6, T9). These pattern of temperature variations are due to the quite high value of thermal conductivity of graphite bed (k = 97 W/m.K) which is responsible for faster heat transfer and quick charging. Similar thermal profiles of natural graphite were observed at other inlet temperatures (Figure 4.53 (b), (c), (d)) with different charging times. These thermal performance results suggest natural graphite as a potential material for sensible heat storage but due to its less specific heat (C_p = 0.866 kJ/kg.K), it can store limited amount of heat per unit mass of material.

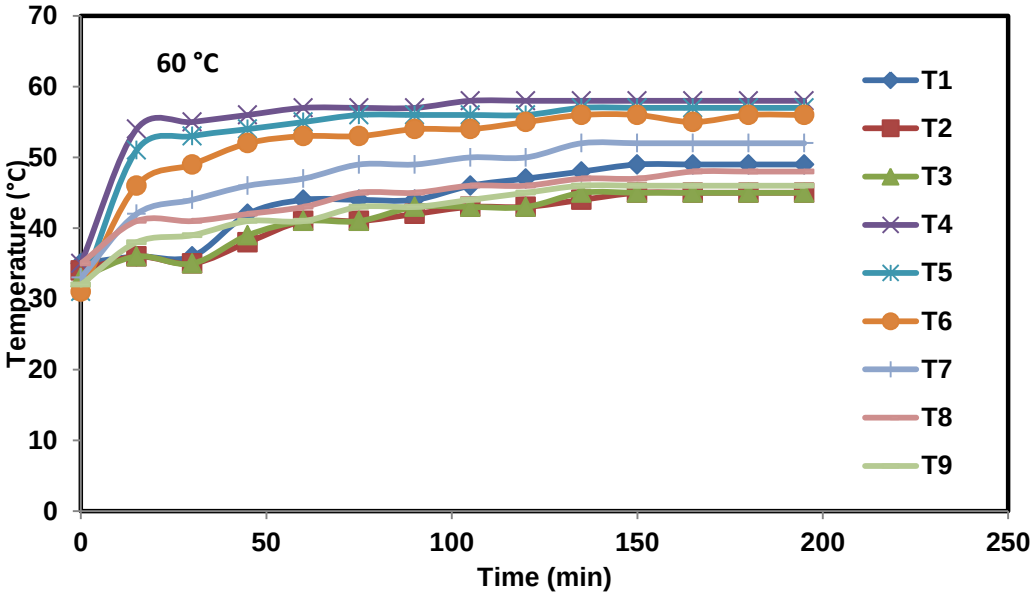

(a)

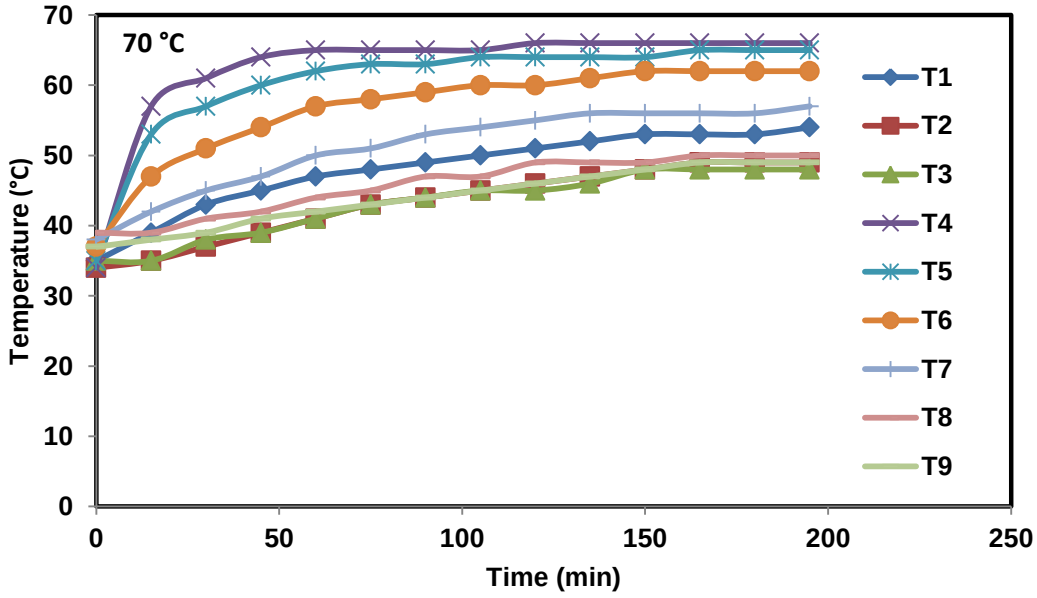

(b)

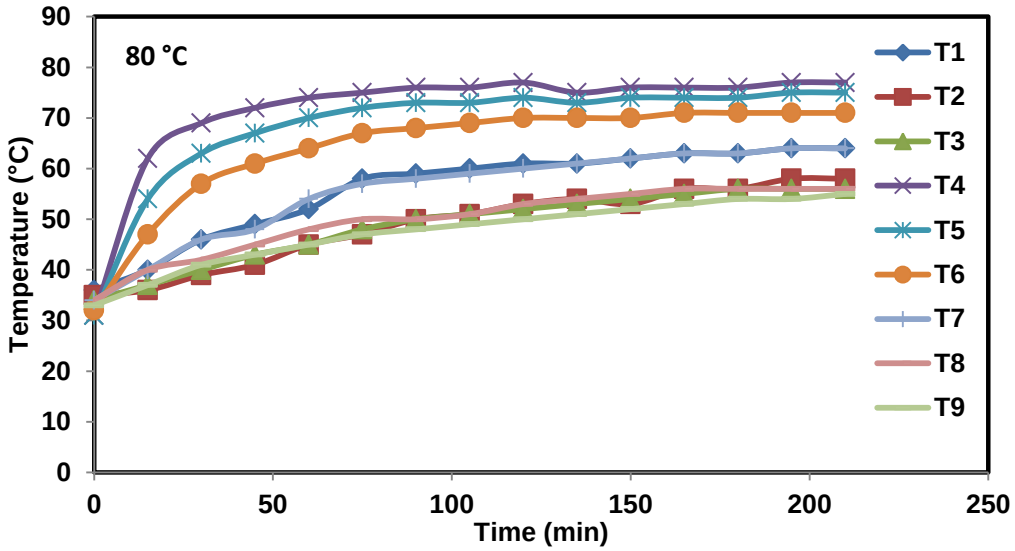

(c)

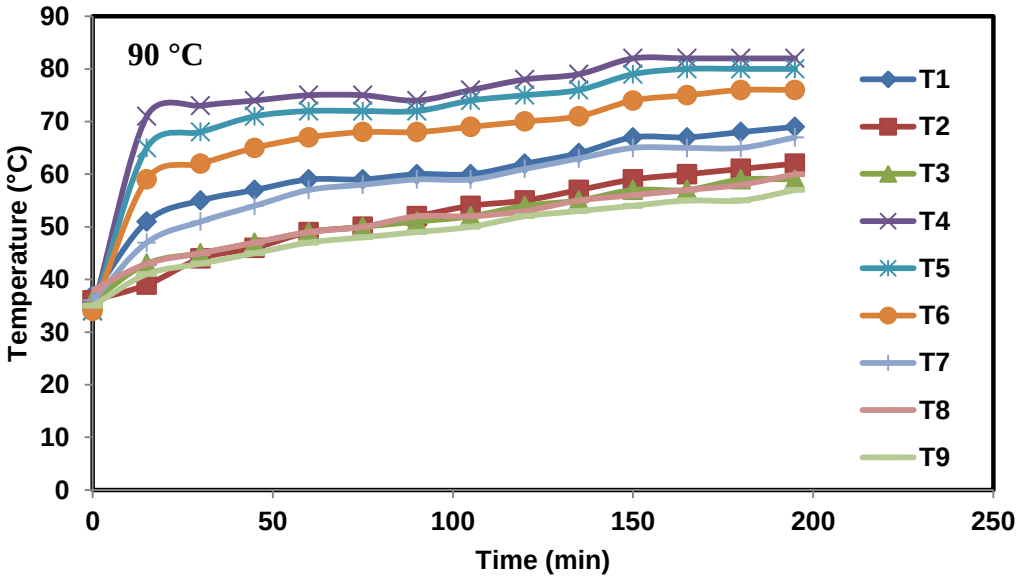

(d)

Figure 4.53 Thermal profile of natural graphite charging at different inlet water temperatures

4.6.2 Using expanded graphite/water suspension as HTF

Temperature variation with time for determining the charging time of natural graphite is shown in Figure 4.54 is obtained by passing expanded graphite/water suspension at different concentrations i.e. 0.05 wt. %, 0.5 wt. % and 1.0 wt. % through the helical coil at 60°C inlet temperature and 0.5 LPM flow rate. Charging time of natural graphite is found to be 195 min., 190 min. and 180 min at EG/water suspension concentration of 0.05 wt. %, 0.5 wt. % and 1.0 wt. % respectively.

Charging time decreases with the increase in the concentration of expanded graphite/water suspension due to increase in thermal conductivity of the suspension. The values of charging time for natural graphite with increasing percentage of EG/water suspension are shown in Table 4.10 and it is observed that at 1.0 wt. % concentration of EG/water suspension, the charging time of natural graphite reduced by 14.28% as compared to the plain water.

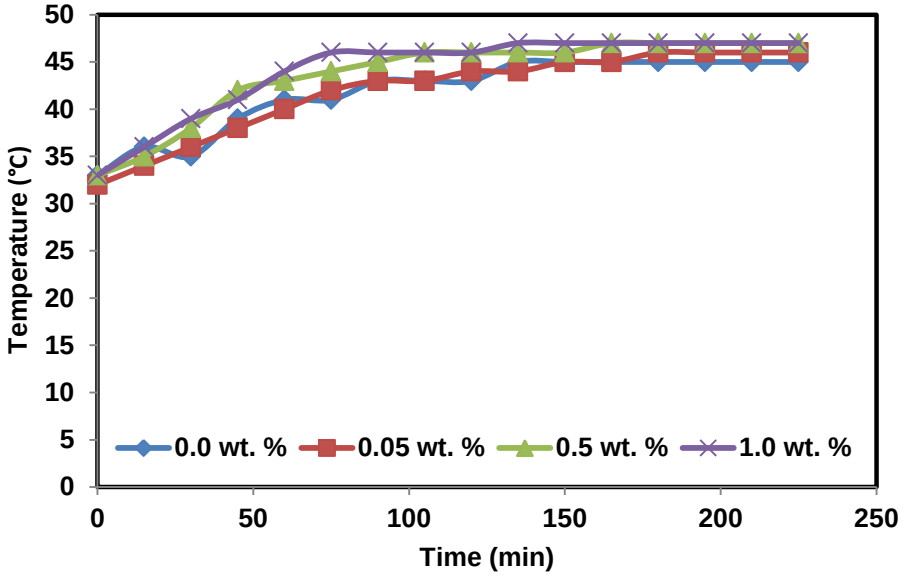

Figure 4.54 Effect of expanded graphite/water concentration on charging time of natural graphite

Table 4.10 Charging time of natural graphite at different concentration of EG/water suspension

Concentration of HTF (wt.%)	Charging time (min.)	Percentage reduction in charging time (%)
0	210	--
0.05	195	7.14
0.5	190	9.52
1.0	180	14.28

Thermal profiles of natural graphite at different concentrations (0.05 wt. %, 0.5 wt. % and 1.0 wt. %.) of expanded graphite/water suspension for flow rate of 0.5 LPM and inlet fluid temperature of 60 °C are presented in Figure 4.55. These profiles are similar to the thermal profile of natural graphite with plain water however, values of charging time are different. In all these profiles the temperature rise at the middle locations (T4, T5, T6) of TSU raised first as compared to the temperature rise at the

top locations (T1, T2, T3) and bottom locations (T7, T8, T9) of helical coil. This was due to the reduction in temperature difference between the heat storage material and heat transfer fluid when moves from inlet to outlet of thermal storage unit.

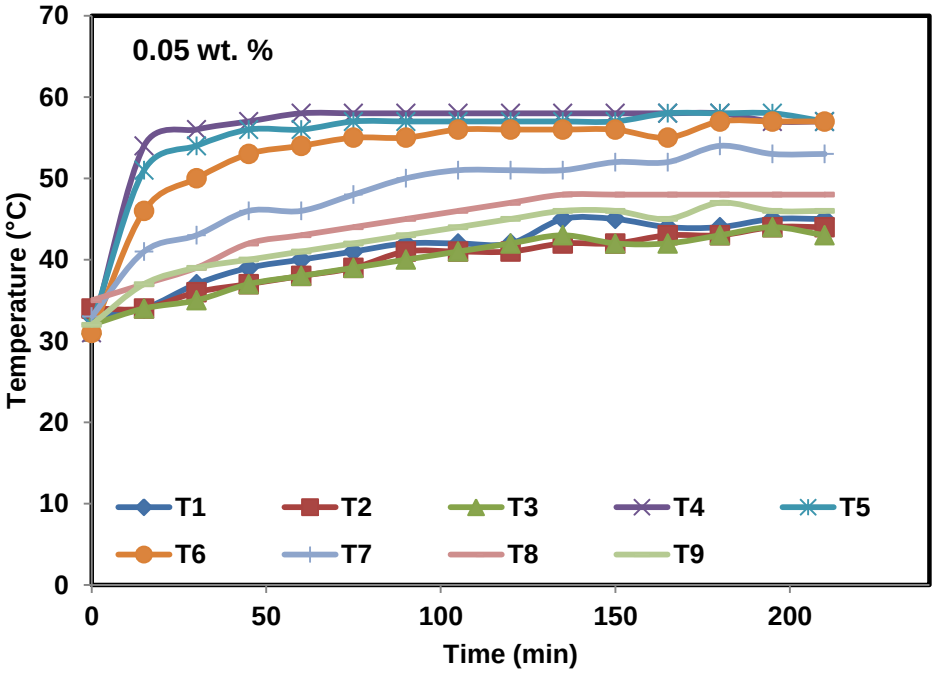

(a)

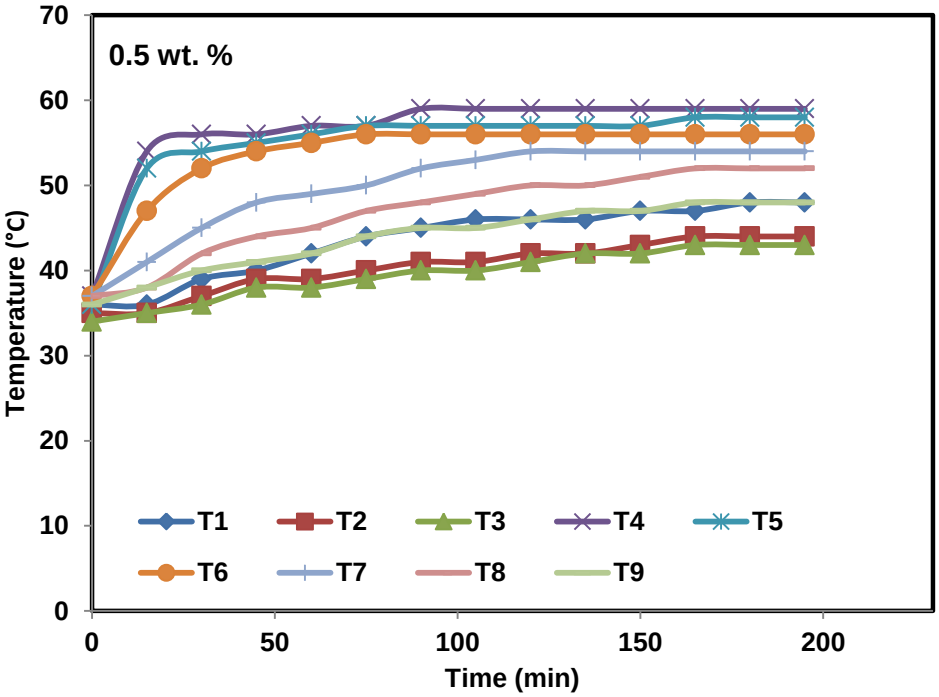

(b)

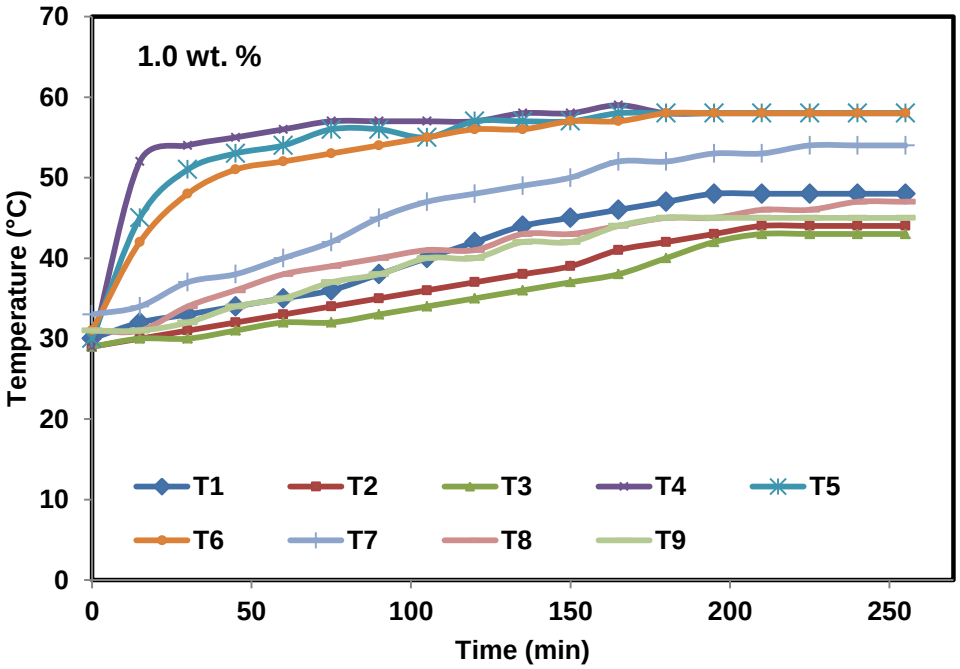

Figure 4.55 Thermal profile of natural graphite at different concentration of EG/water suspension

4.6.3 Using Al_2O_3/water nanofluid as HTF

Al_2O_3/water nanofluid of four different concentrations i.e. 0.2 vol. %, 0.5 vol. %, 1.0 vol. % and 2.0 vol. % was prepared and used as heat transfer fluid to study the charging behavior of natural graphite. The temperature variation of natural graphite with respect to time at different concentration of Al_2O_3/water nanofluid is shown in Figure 4.56 and the charging time of natural graphite was found to be 210 min, 180 min, 170 min ,165 min and 160 min for Al_2O_3/water nanofluid concentration of 0.0 vol. %, 0.2 vol. %, 0.5 vol. %, 1.0 vol. % and 2.0 vol.% respectively at fluid flow rate of 0.5 LPM and 60 °C fluid inlet temperature. This reduction in charging time at higher concentration of alumina nanoparticles is due to increased thermal conductivity of heat transfer fluid (percentage increase in value). Charging time of natural graphite with Al_2O_3/water nanofluid of 2.0 vol. % concentration found to be 23.80% lower as compared to charging time with plain water. Charging time of natural graphite using plain water and Al_2O_3/water suspension of different concentrations is shown in Table 4.11.

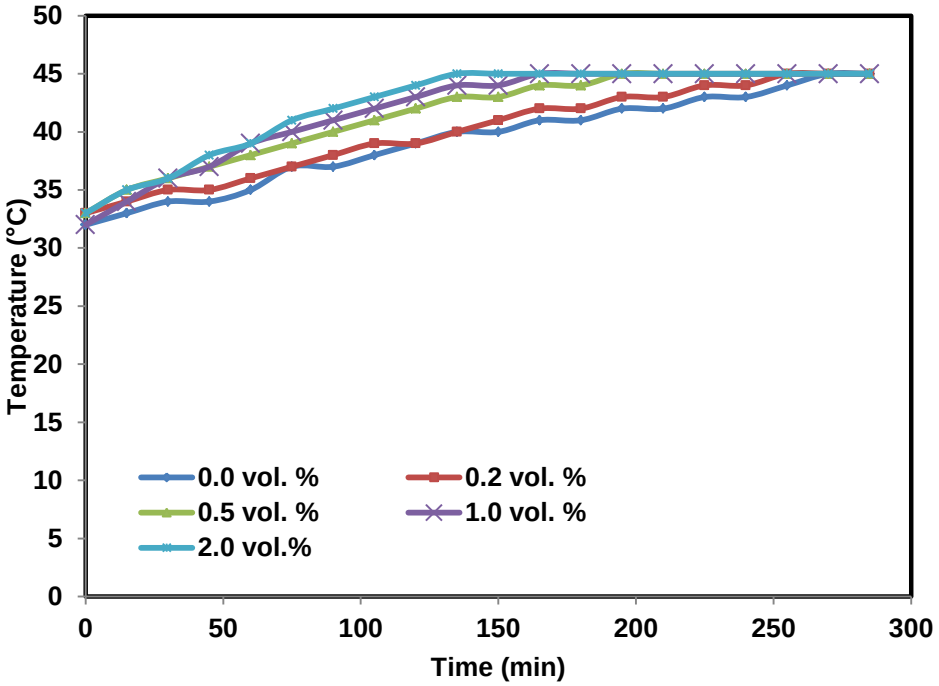

Figure 4.56 Effect of Al_2O_3 nanofluid concentration on charging time of natural graphite

Table 4.11 Charging time of natural graphite at different concentration of Al_2O_3 nanofluids

Concentration of HTF (wt.%)	Charging time (min.)	Percentage reduction in charging time (%)
0	210	--
0.2	180	14.28
0.5	170	19.04
1.0	165	21.42
2.0	160	23.82

Thermal profiles of natural graphite with four different concentrations of aluminum nanofluids are shown in Figure 4.57 which depicts the similar pattern of temperature rise in the packed bed as observed with different fluids. The temperature of thermocouples at the middle of coil (T4, T5, T6) and near to inlet (T1, T4, T7) raised first as the HTF moves from inlet to outlet of thermal storage unit.

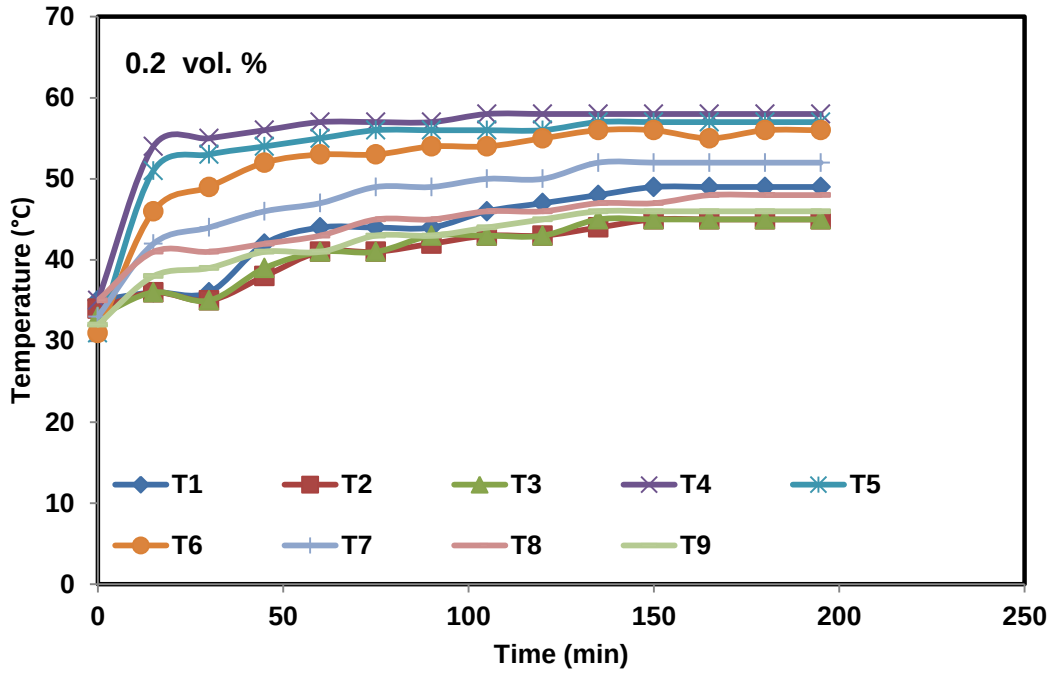
0.2 vol. %
Temperature (°C)
Time (min)
T1
T2
T3
T4
T5
T6
T7
T8
T9

(a)

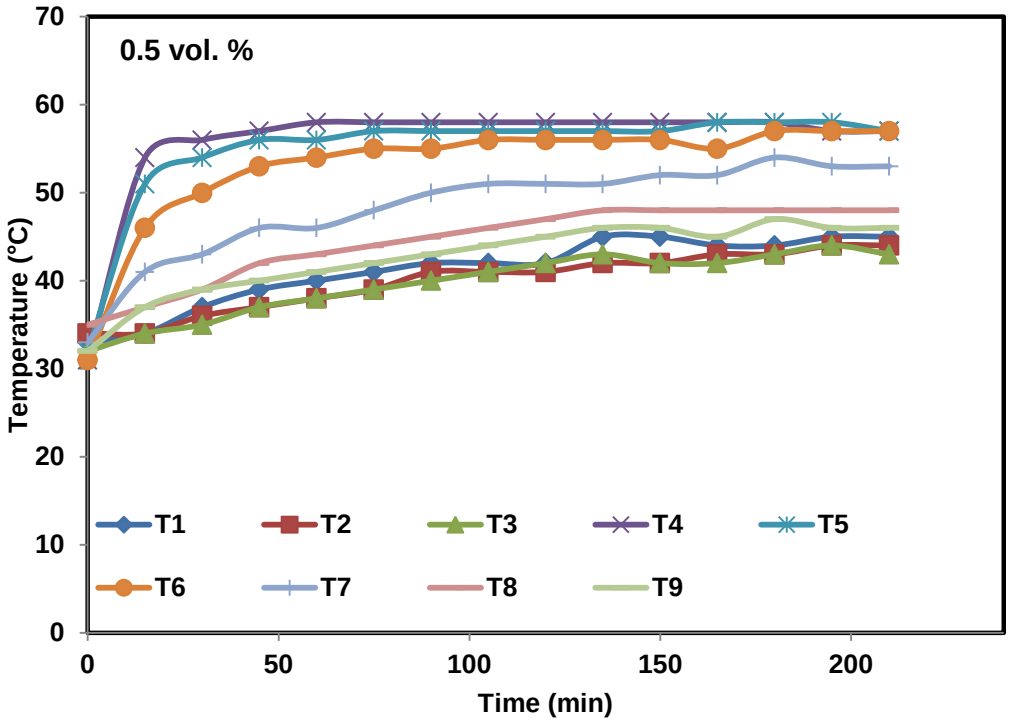
0.5 vol. %
Temperature (°C)
Time (min)
T1
T2
T3
T4
T5
T6
T7
T8
T9

(b)

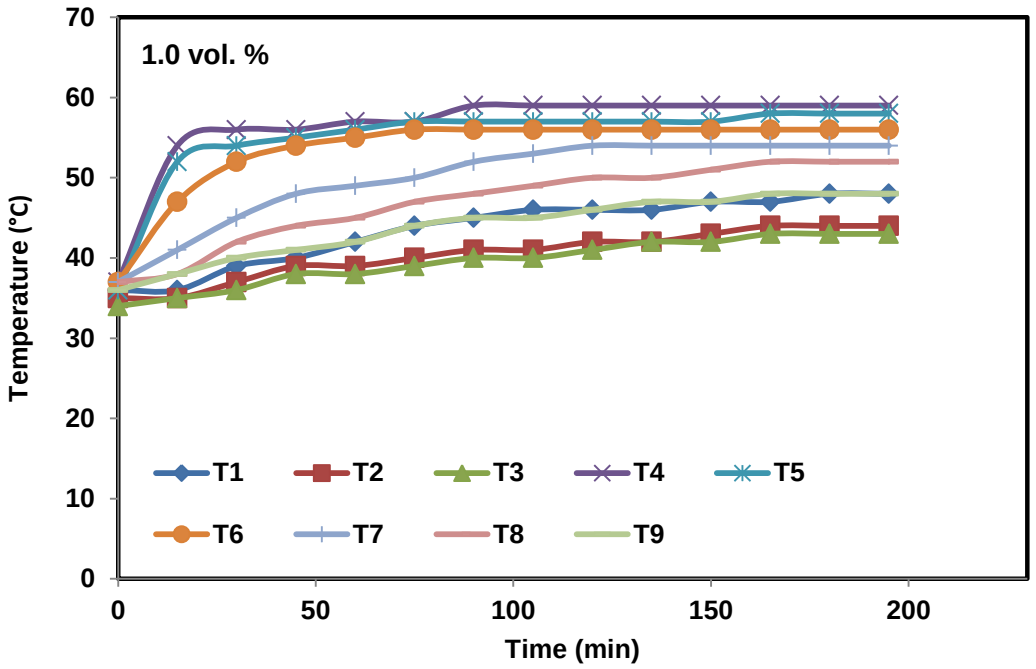

(c)

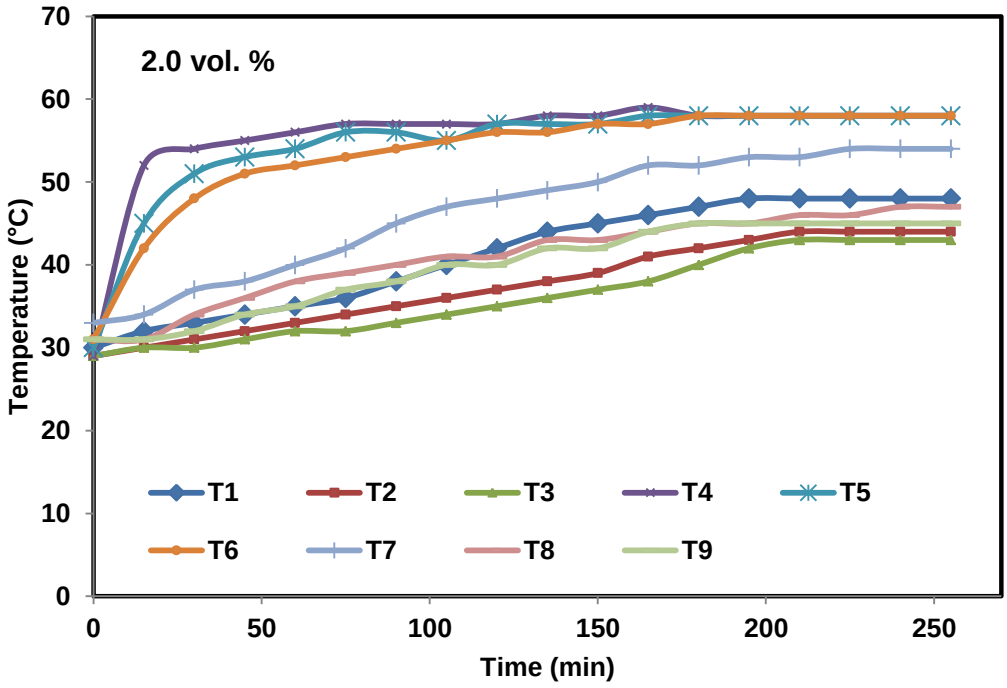

(d)

Figure 4.57 Thermal profiles of natural graphite at different concentrations of nanofluid

4.7 Comparison between sensible and latent heat storage

Experimental results obtained in the present study on two phase change materials such as beeswax and beeswax/expanded graphite composite and on sensible heat storage material natural graphite give good thermal storage efficiency as observed from thermal profiles. Energy density of phase change materials found to be greater in comparison to natural graphite for similar geometry and sample size. Table 4.12 shows the comparison of heat stored and charging time for phase change materials (beeswax and composite) and natural graphite. The amount of energy stored by beeswax and composite material is 5.823 MJ and 5.785 MJ respectively. Little lower value of energy stored in composite material is due to the addition of 10% of expanded graphite in the composite which reduces weight of pure beeswax in the composite material but increases the thermal conductivity. It is also observed that the energy stored by a sensible heat storage system with packed bed of natural graphite powder (22 kg) is 0.956 which is 83.58% and 83.47% lower as compared to the energy stored by beeswax and composite material respectively at constant flow rate of HTF 0.5 LPM and inlet temperature at 80°C. The comparison of energy densities of heat storage materials is shown in Table 4.13.

Table 4.12 Thermal performance comparison of beeswax, composite material and natural graphite

Heat storage material	Heat transfer fluid	Inlet temperature (°C)	Charging time (min)	Energy stored (MJ)
Beeswax	Plain water	80	1650	5.823
Composite	Plain water	80	1125	5.785
Natural graphite	Plain water	80	180	0.956
Beeswax	Plain water	70	1695	5.766
Composite	Plain water	70	1175	5.648
Natural graphite	Plain water	70	195	0.727

Table 4.13 Energy density of different heat storage materials

Heat storage materials	Heat transfer fluid	Inlet temperature (°C)	Flow rate (LPM)	Energy stored per unit mass (kJ/kg)
Beeswax	Plain water	80°C	0.5	324.81
Composite	Plain water	80°C	0.5	302.88
Natural Graphite	Plain water	80°C	0.5	43.45

4.8 Modelling and Simulations

Modelling and simulation of heat storage materials in small scale TSU and large scale TSU was performed using COMSOL Multiphysics and discussed here.

4.8.1 Modelling and simulation of small scale TSU

A 3D model of small scale thermal storage was prepared as shown in Figure 4.58 which consists of two parts i.e. the shell part filled with PCM and the tube part through which HTF is passed and then simulation study is carried out to determine the heat transfer behavior between phase change material and heat transfer fluid.

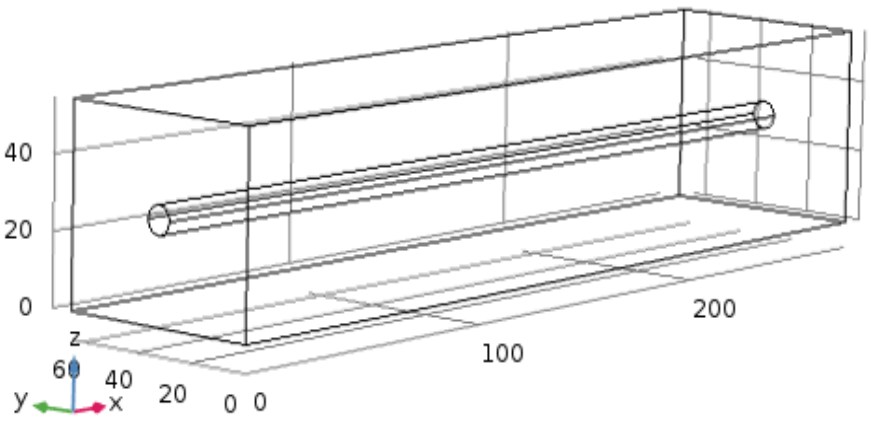

Figure 4.58 Geometrical model of small scale TSU

Temperature variation pattern with time for three vertical planes in the domain of beeswax is presented in Figure 4.59 and it is observed that the temperature of beeswax increased slowly and continuously with the passage of time and the complete charging of beeswax occurred in 1310 min, which is 8.39% lesser as compared to the charging time observed experimentally (1430 min).

The melting profile of beeswax observed in simulation analysis at different time is shown in Figure 4.60 and it is observed that the complete melting of beeswax took place in 550 min (at position T3). It is also observed from Figure 4.60 that the melting of beeswax starts from the surface of the tube and the solid-liquid interface then moves towards the edges of TSU. The pattern of temperature rise at position T3 of

thermal storage unit in simulation and experimental studies are compared in Figure 4.61 and it is noticed that the temperature rise patterns are almost similar in both the cases. However, lower values of temperature during experimental study is observed as compared to the simulation values. This may be due to the presence of heat losses from helical tube surface and radiation losses from TSU in actual conditions. Thus, simulation data are in good agreement with the experimental results.

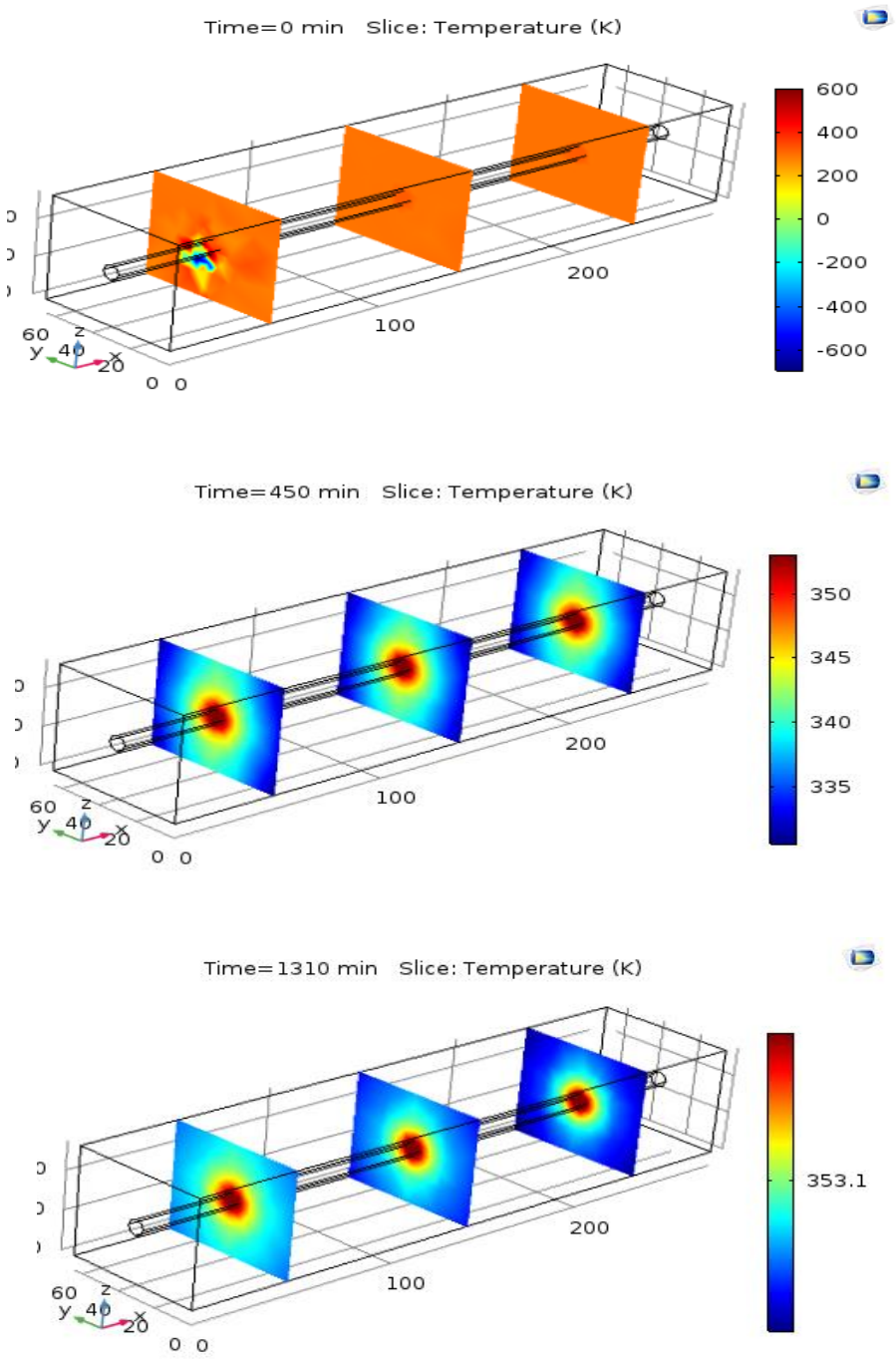

Figure 4.59 Simulated temperature variation during charging of beeswax in small TSU

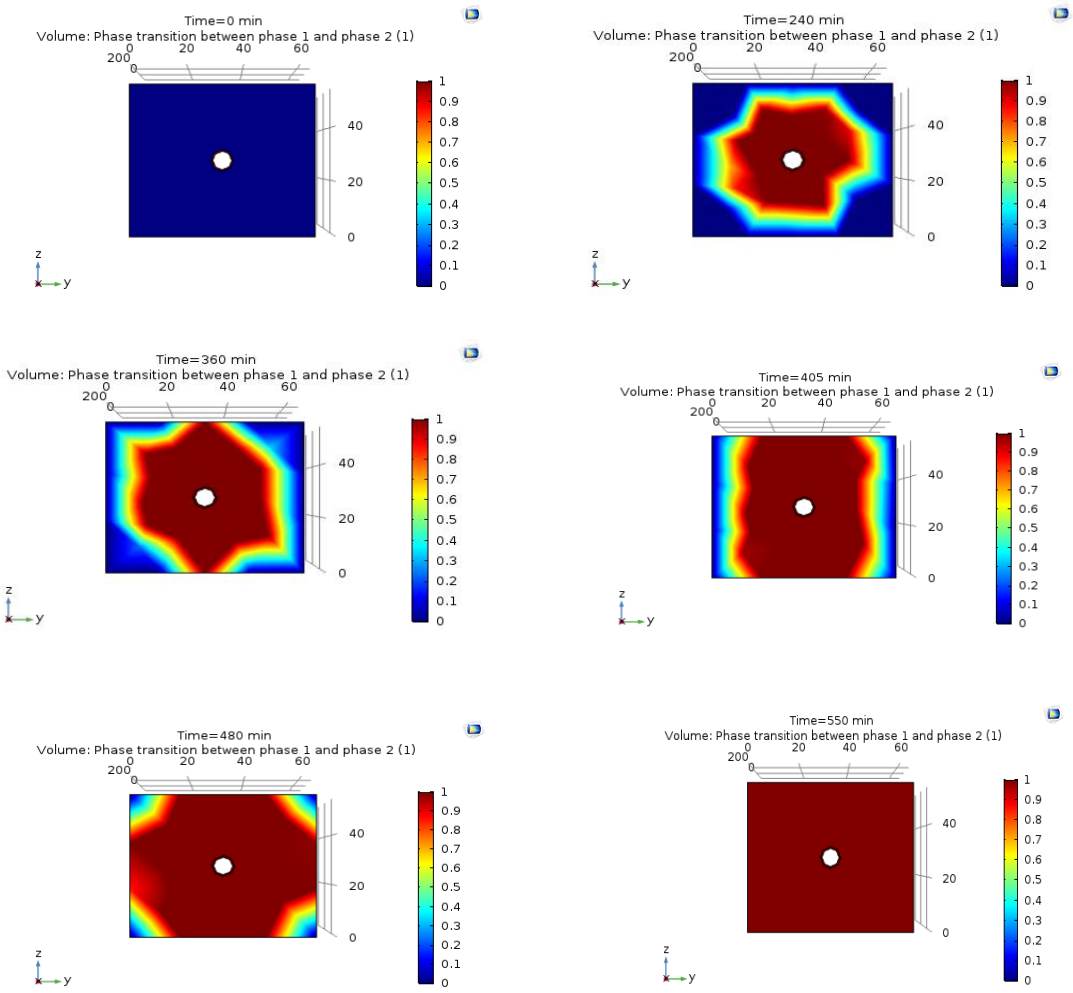

Figure 4.60 Simulated melting profile of beeswax at different time in small TSU

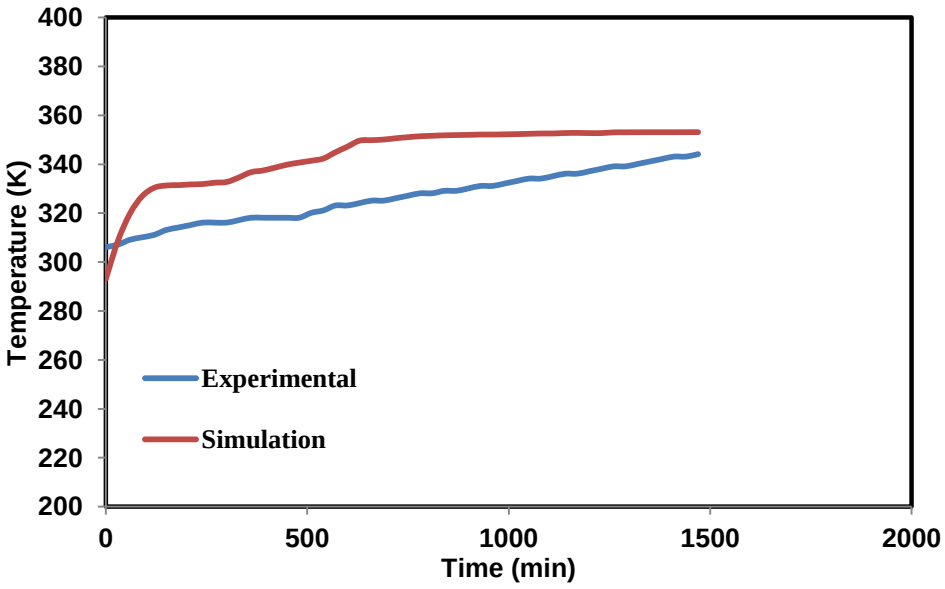

Figure 4.61 Comparison of experimental and simulated temperature variation of beeswax in small TSU

Similar temperature rise and melting pattern were observed for beeswax/expanded graphite composite material in small TSU as shown in Figure 4.62 and Figure 4.63. Simulations results show the charging time and melting time for composite material as 950 min and 340 min (at position T3) which is 6.86% and 38.18% lesser as compared to the pure beeswax. This reduction in charging time and melting time may be due to enhanced thermal properties of composite material with the addition of expanded graphite. The comparison of simulated values and experimental values of temperature variation at position T3 in shown in Figure 4.64. As both the temperature variations are similar and prove good agreement with each other.

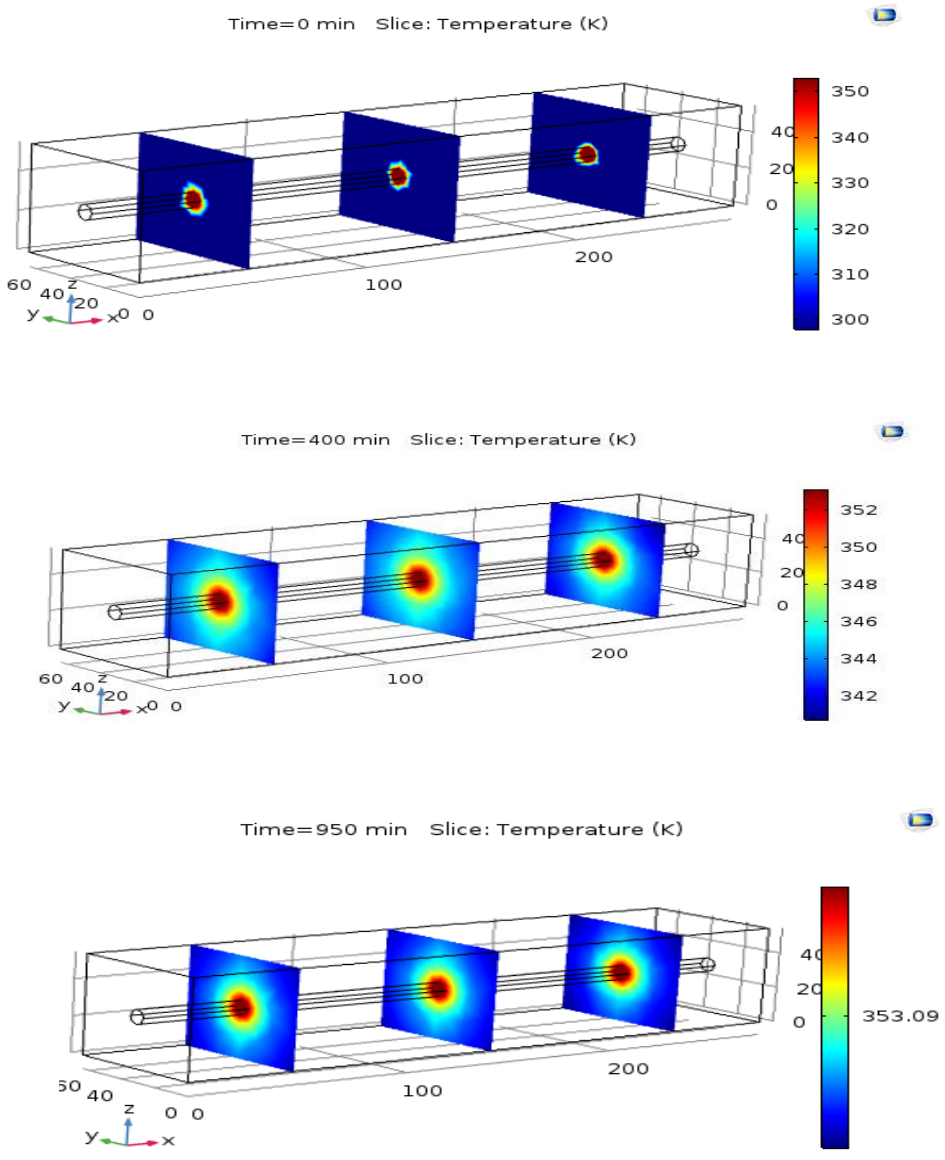

Figure 4.62 Simulated temperature variation during charging of composite in small TSU

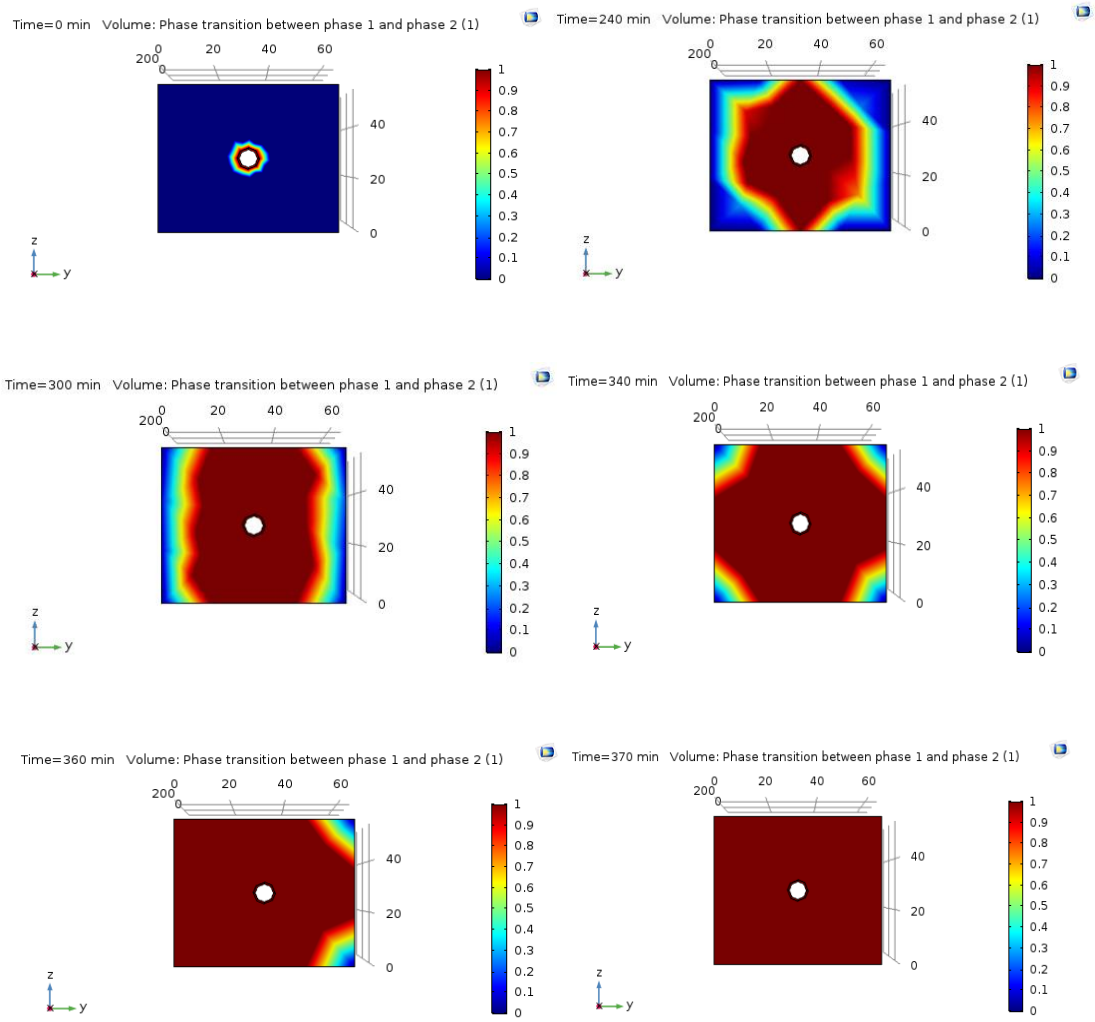

Figure 4.63 Simulated melting profile of composite at different time in small TSU

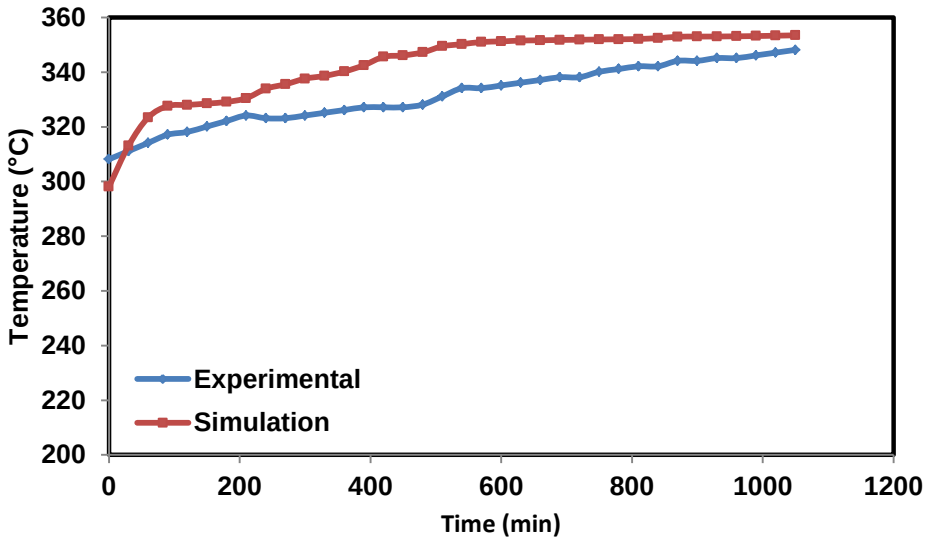

Figure 4.64 Comparison of experimental and simulated temperature variation of composite in small TSU

4.8.2 Simulation of beeswax charging in large TSU

The geometrical model of large TSU developed using COMSOL Multiphysics software is represented in Figure 4.65, in which PCM was filled in the outer rectangular shell while the HTF was passed through the helical coil of the thermal storage unit. Parameters used in the simulation study are taken from the actual experimental setup and simulation study was carried out with fluid flow rate of 0.5 LPM and 80 °C inlet fluid temperature.

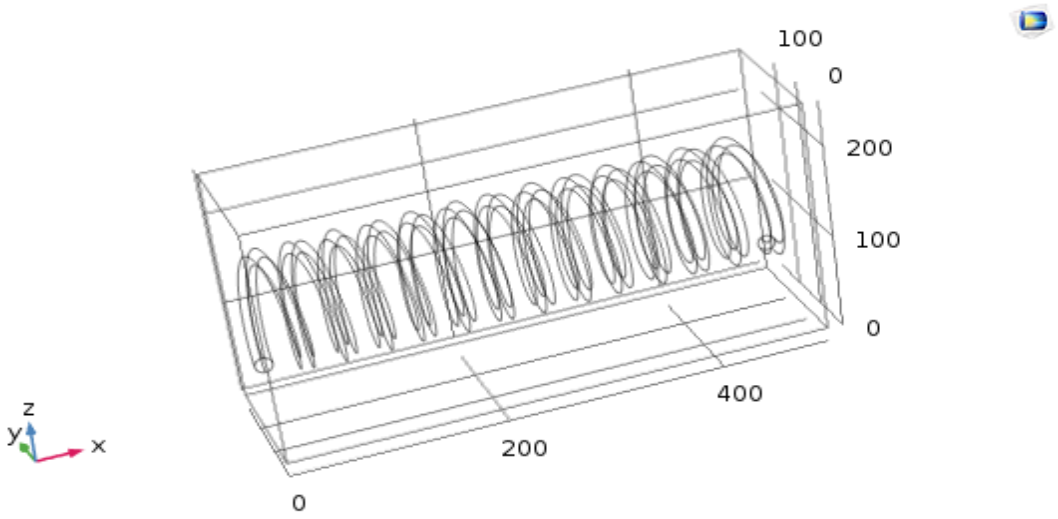

Figure 4.65 Geometric model of large TSU

Temperature variation in the volume of beeswax at four different times is presented in Figure 4.66. The observed charging time of beeswax in large TSU from simulation study is 1515 min. which is 6% smaller as compared to experimental value. Figure 4.67 representing the melting pattern of beeswax in large TSU at different time and it is observed that during charging the solid-liquid interface moves in upward direction due to the dominance of convection heat transfer and the complete melting of beeswax occurred in 660 min. The comparison between experimental results and simulated results for temperature variation at position T3 with respect to time is shown in Figure 4.68 and it is found that simulation results are in line with experimental results . Lower values of temperature in experimental study are due to the heat losses taking place.

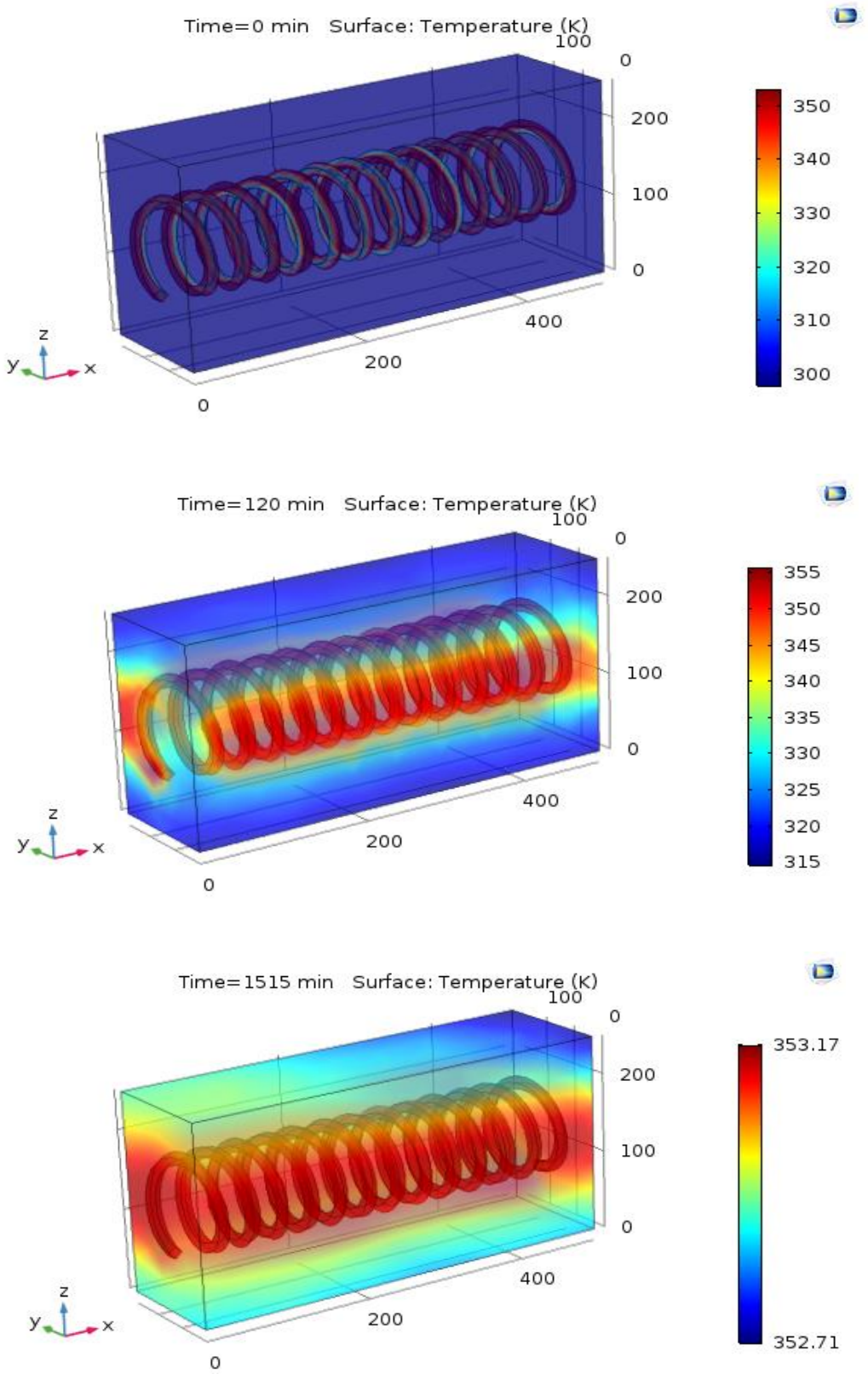

Figure 4.66 Simulated temperature variation during charging of beeswax in large TSU

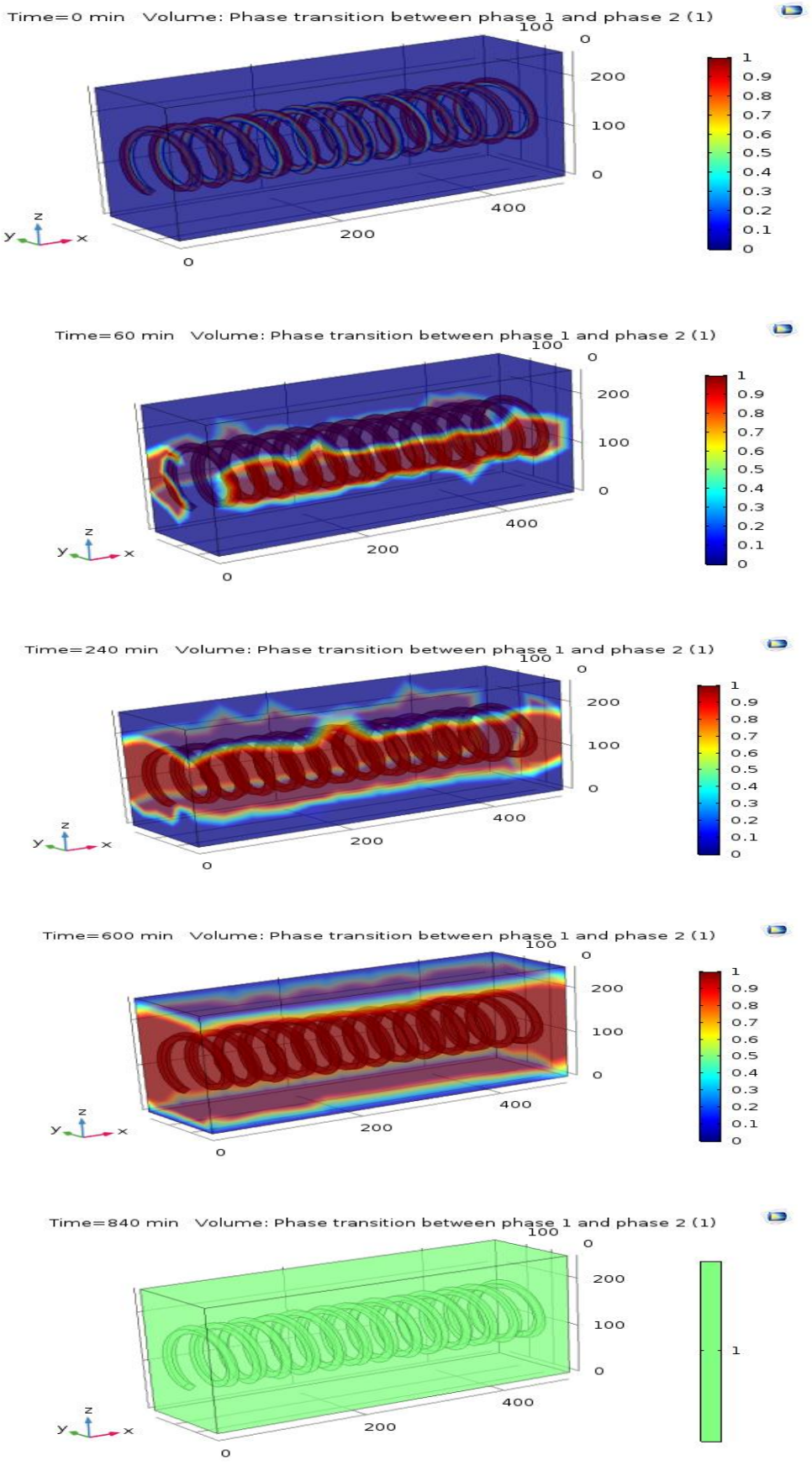

Figure 4.67 Melting profile of beeswax at different time during charging

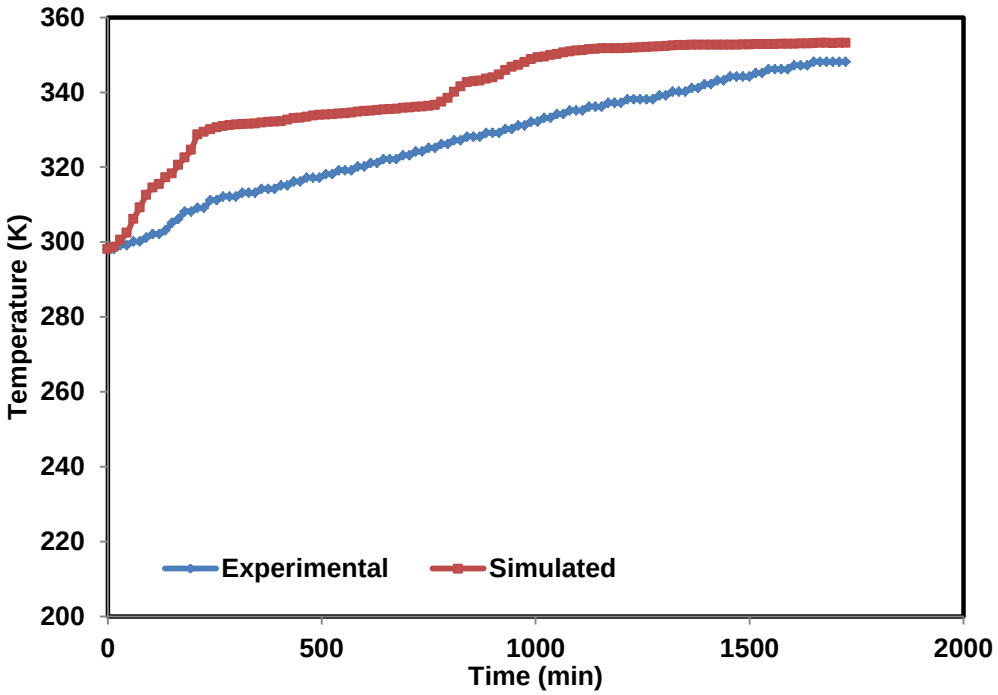

Figure 4.68 Comparison of experimental and simulated temperature variation of beeswax in large TSU

4.8.3 Simulation of composite material in large TSU

Simulation study on beeswax/expanded graphite composite material was also performed on the developed 3D geometric model for large TSU. Charging time of composite material is 1040 min which is found to be lower as compared to pure beeswax i.e. 1515 min and which is also lower as compared to experimental value of 1125 min as shown in Figure 4.69. The melting profile of composite material is presented in Figure 4.70 and complete melting of composite material took place in 700 min. Comparison of temperature variation with time at position T3 of TSU from experimental study and simulation analysis is shown in Figure 4.71. since both the temperature profiles are almost similar prove that the simulation results are in agreement with experimental results. Lower values (7.5%) of temperature in experimental study are due to heat losses taking place from TSU and helical tube.

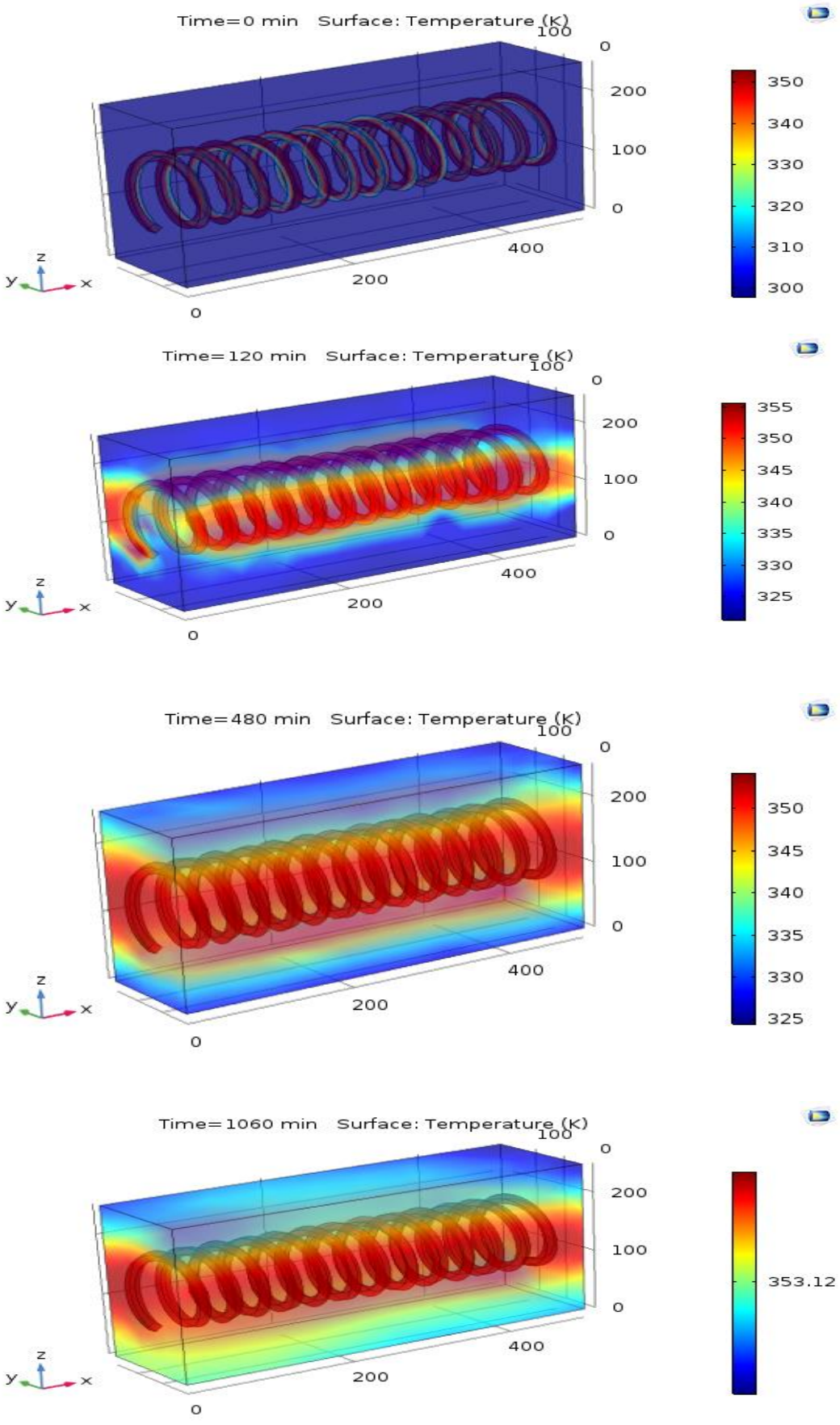

Figure 4.69 Simulated temperature variation during charging of composite in large TSU

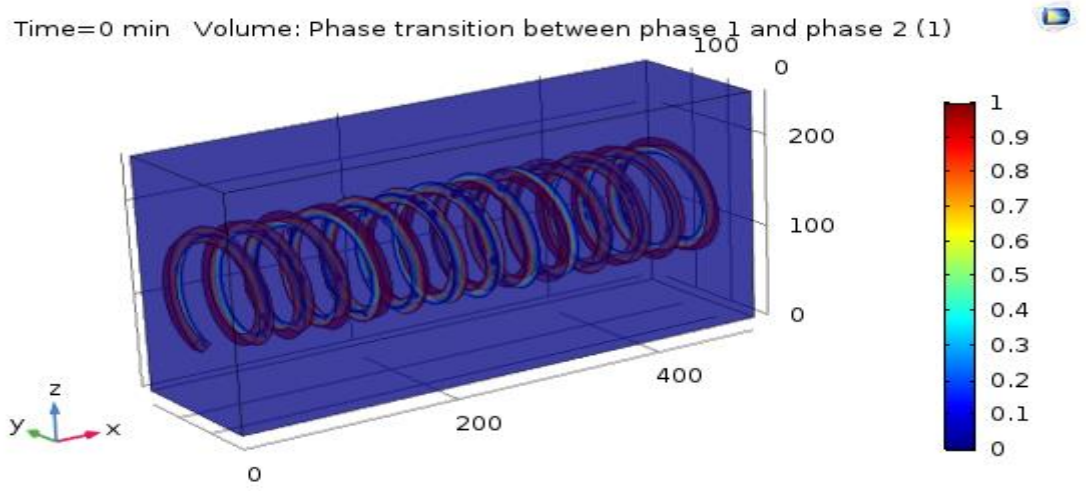
Time=0 min Volume: Phase transition between phase 1 and phase 2 (1)
100
0
200
100
0
400
200
0
z
y
x
1
0.9
0.8
0.7
0.6
0.5
0.4
0.3
0.2
0.1
0

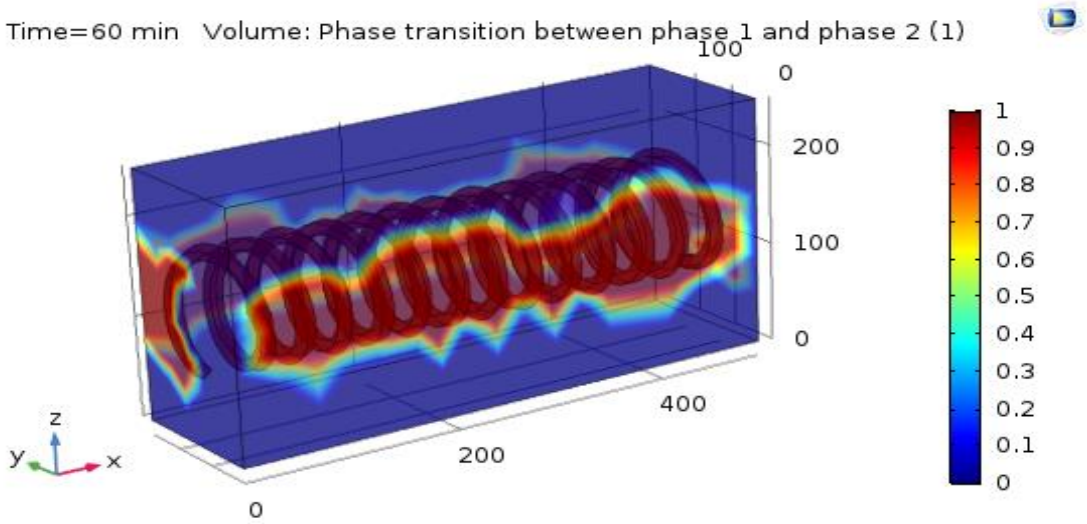
Time=60 min Volume: Phase transition between phase 1 and phase 2 (1)
100
0
200
100
0
400
200
0
z
y
x
1
0.9
0.8
0.7
0.6
0.5
0.4
0.3
0.2
0.1
0

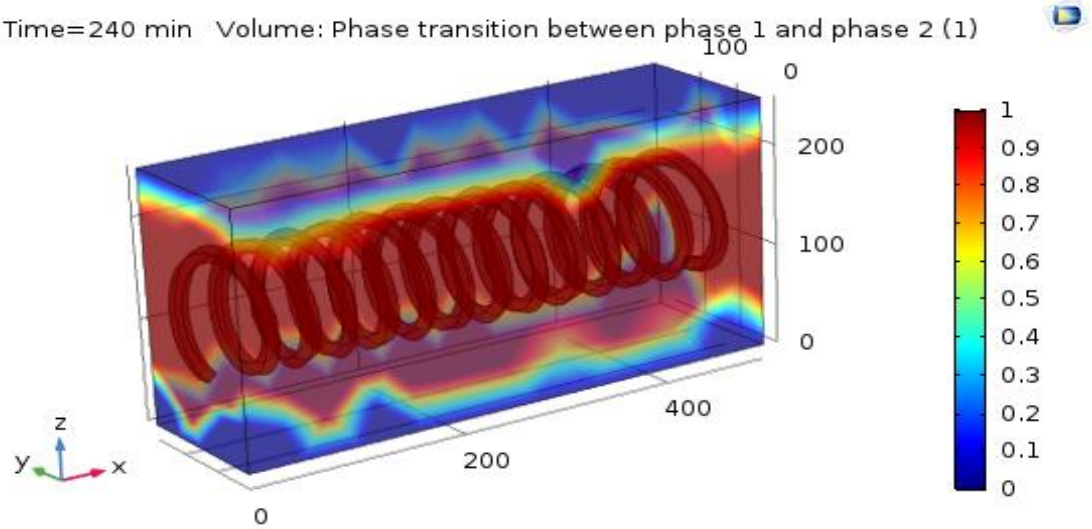
Time=240 min Volume: Phase transition between phase 1 and phase 2 (1)
100
0
200
100
0
400
200
0
z
y
x
1
0.9
0.8
0.7
0.6
0.5
0.4
0.3
0.2
0.1
0

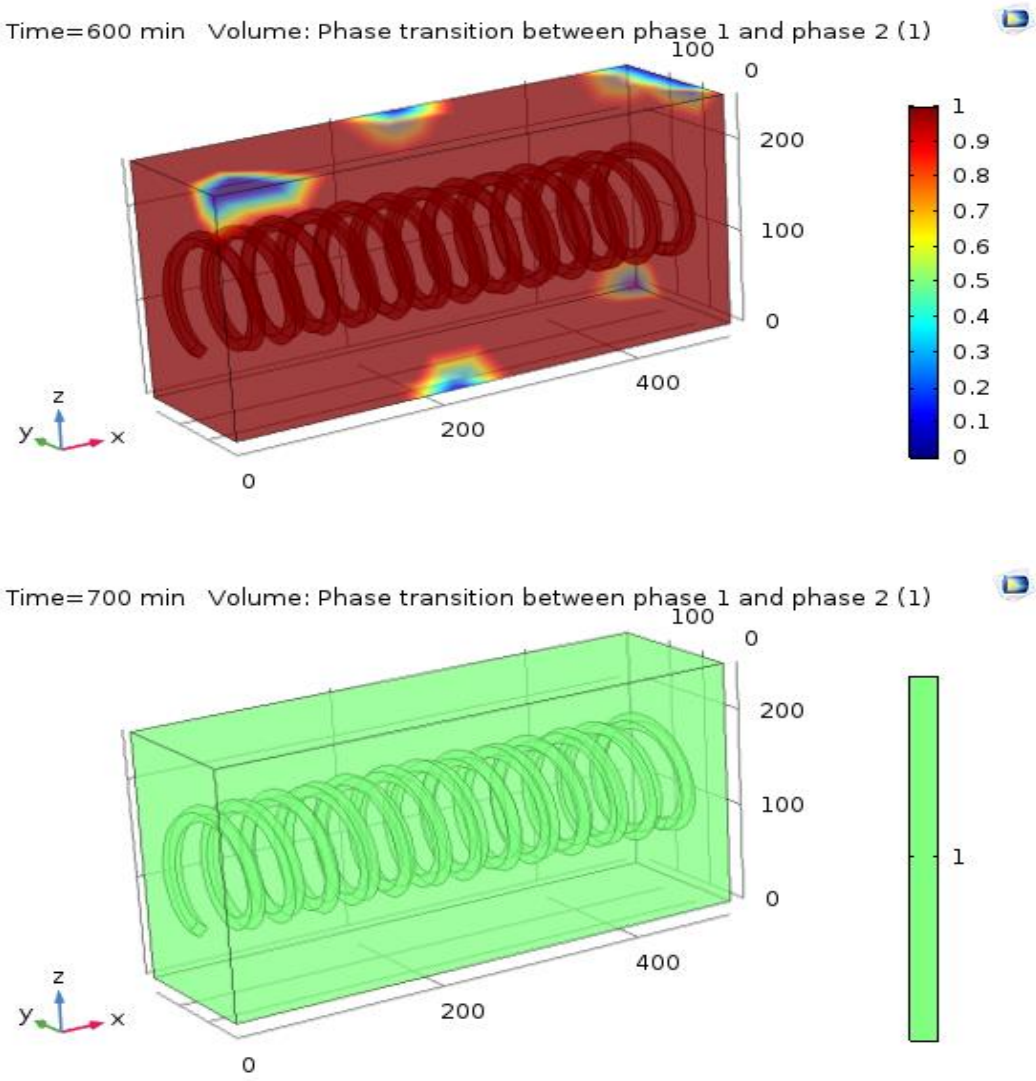

Figure 4.70 Melting profile of composite material from simulation analysis

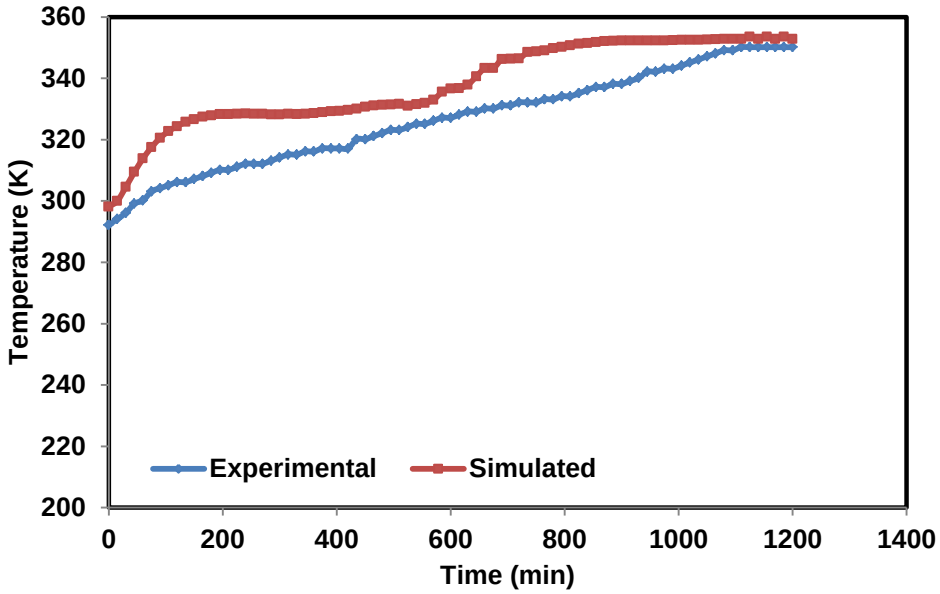

Figure 4.71 Comparison of experimental and simulated temperature variation of composite in large TSU

4.8.4 Simulation of natural graphite in large TSU

Simulation study on natural graphite was also performed on the developed 3D geometric model for large TSU. Charging time of natural graphite was found to be 200 min through simulation as compared to 210 min obtained from experimental study as shown in Figure 4.72. Comparison of temperature variation with time at position T3 of TSU from experimental study and simulation analysis is shown in Figure 4.72 and it was observed that temperature rise in simulations takes place at faster rate as compared to the temperature rise in experiment. It was also observed that charging temperature of graphite in simulation is higher as compared to the experimental at position T3 which may be due to the presence of air pockets and voids in the bed of natural graphite.

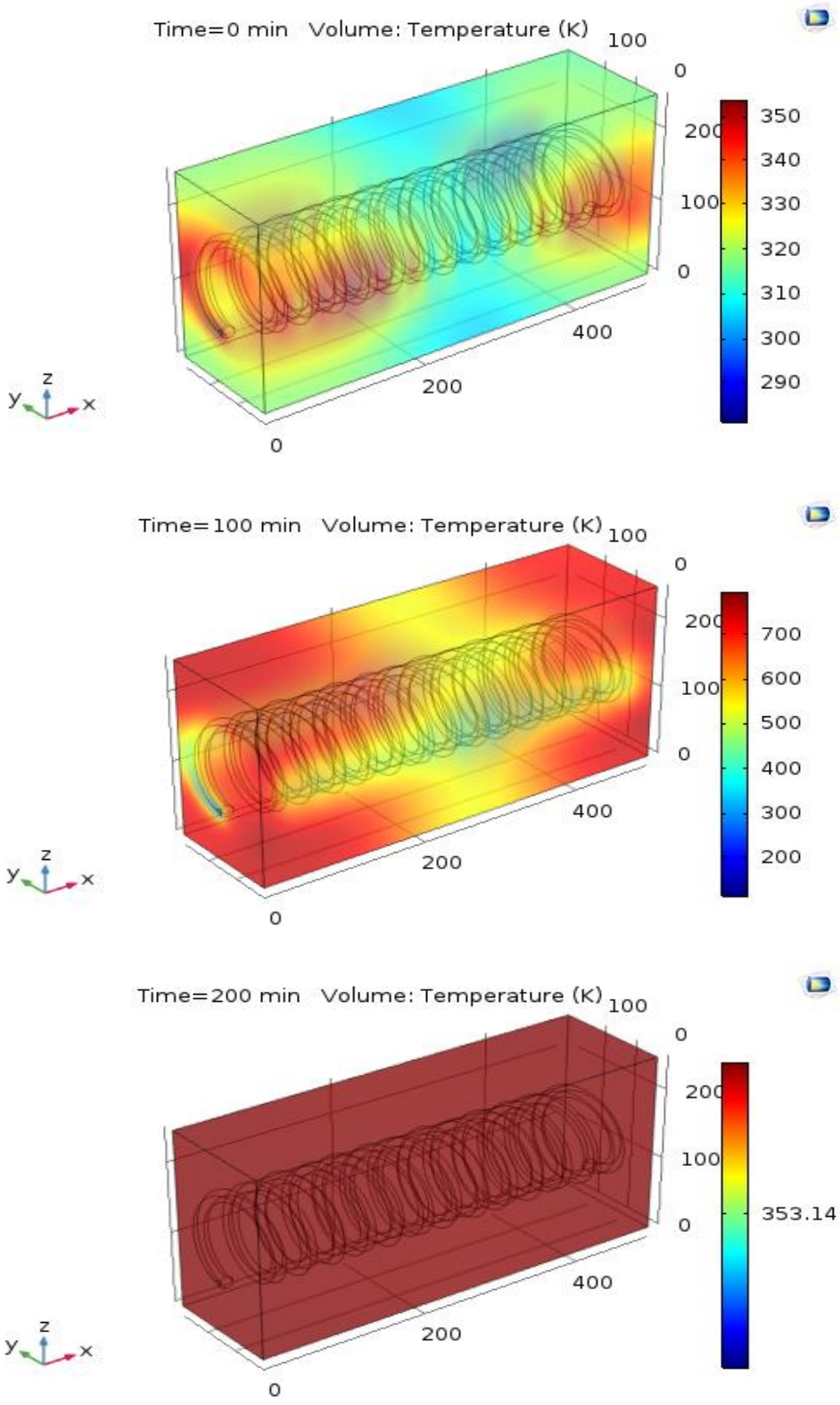

Figure 4.72 Simulated temperature variation during charging of natural graphite

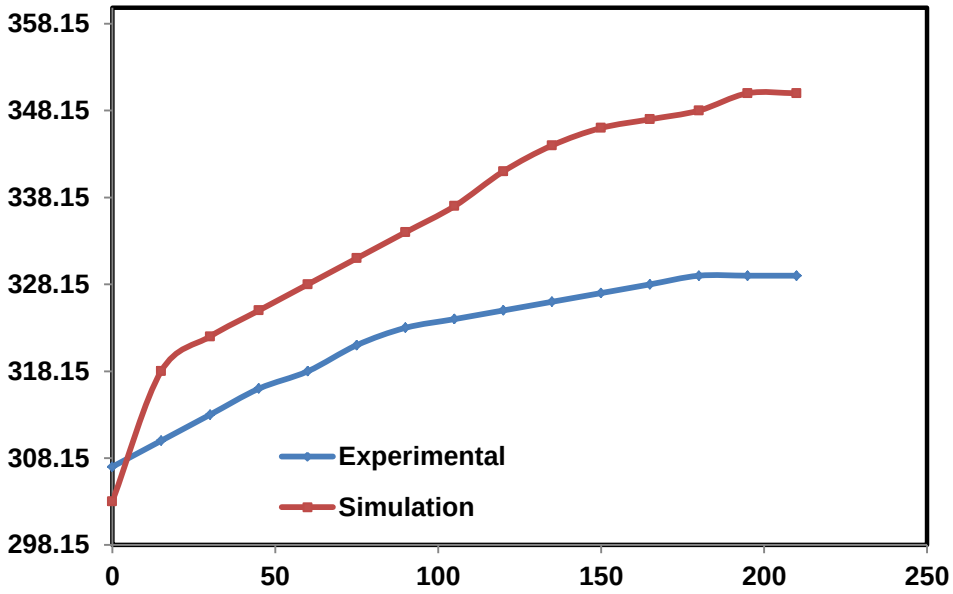

Figure 4.73 Comparison of experimental and simulated temperature variation of natural graphite in large TSU

CHAPTER 5

CONCLUSION

In the present study beeswax was introduced as a new phase change material for low temperature thermal energy storage. In order to improve the thermal properties of beeswax its composite was prepared by adding varying percentage of expanded graphite. Expanded graphite was prepared by chemical oxidation of natural graphite and its surface area increases significantly as compared to natural graphite.

Physical, chemical and thermal properties of beeswax, natural graphite, expanded graphite and composite of beeswax was studied using different characterization techniques such as Fourier transform infra-red (FTIR), X-ray diffraction (XRD), scanning electron microscopy (SEM) analysis , differential scanning calorimetry (DSC) and thermogravimetric analysis (TGA) .

The phase change behavior and thermal performance of beeswax and its composite was studied in a small scale thermal storage unit consisting of a straight tube passing through the center of a rectangular shell. Both beeswax and its composite (2.5 kg) were tested at the fixed flow rate of 2 LPM and 80 °C fluid inlet temperature. The temperature, at nine different thermocouples placed axially and vertically throughout the unit, were recorded and analyzed. Thermal profiles of phase change material were prepared by plotting the graph between temperature and the time variation at different positions of thermocouples. Beeswax and its composite behaved like a good PCM in small size thermal storage unit and to conduct further detail study a large size thermal storage unit was developed.

The bigger thermal storage unit having rectangular shell with helical tube in the center was used to study the thermal performance of beeswax, its composite with expanded graphite and natural graphite. Shell part of TSU was filled with heat storage materials (18-22 kg) and hot HTF was passed through the helical tube. Nine k-type thermocouples were uniformly installed in the unit to record temperatures at an interval of every 15 min to obtained thermal behavior of heat storage materials.

During the experimental study different heat transfer fluids such as plain water, expanded graphite/water suspension (0.05 wt. %-1.0 wt. %) and aluminium nanofluid (0.2 vol. %-2.0 vol. %) were passed. The hot plain water as HTF (60 °C-90 °C) at different flow rates (0.25LPM- 1.0 LPM) were used to study the charging behavior and thermal efficiency. Thermal performance variation was also studied using three

different concentration of expanded graphite/water suspension (0.05 wt. %, 0.5 wt. %, 1.0 wt. %) and four concentrations of aluminium -nanofluid (0.2 vol. %, 0.5 vol. %, 1.0 vol. %, 2.0 vol. %)

Along with the experimental measurements and study, geometric modelling and simulation of phase change materials in small scale and large scale thermal storage units was carried out using COMSOL Multiphysics software package. The generated model results were validated with the experimental results and then compared.

5.1 Conclusions from the present study

Characterization of samples

- SEM analysis of expanded graphite was carried out to determine inter layer separation and these layer separations were used for the impregnation of beeswax which enhanced the thermal properties of beeswax.
- 10% addition of expanded graphite to pure beeswax improved thermal conductivity of the composite (0.63 W/m.K) by 117% as compared to pure beeswax (0.29 W/m.K).
- FTIR and XRD analysis of samples showed that the prepared composite was merely a mixture of two different materials (i.e. beeswax and expanded graphite) rather than a new material.
- The melting point of beeswax and its composite found to be 59.6 ℃ and 57.3 ℃ respectively and latent heat found to be 214 kJ/kg and 198 kJ/kg respectively from DSC analysis.
- TGA analysis showed the thermal stability of beeswax and composite up-to the temperature of 215 ℃ and 236.8 ℃ respectively but above this temperature both materials degraded thermally by losing their mass.

Thermal performance of phase change materials in small TSU

- Charging time of beeswax and composite material found to be 1430 min and 1020 min respectively
- Thermal profiles of pure beeswax and composite material during charging process showed that heat transfer began with conduction followed by convection.

- Charging time of composite material found to be 28.67% lesser as compared to pure beeswax due to the presence of expanded graphite at 2 LPM and 80 °C fluid inlet temperature.
- Reasonable charging time obtained for beeswax and its composite show both of them as potential PCM for low temperature thermal storage applications.

Thermal performance of phase change materials in large TSU

- Charging time of natural beeswax in rectangular shell and helical tube type thermal storage unit is reduced from 1830 min to 1530 min (reduced by 16.39 %) when flow rate of plain water was increased from 0.25 LPM to 1.0 LPM at constant inlet temperature of 80 °C.
- Charging time of composite is reduced from 1185 min. to 1020 min (reduced by 13.92 %) when flow rate of water increased from 0.25 LPM to 1.0 LPM at constant inlet temperature of 80°C.
- Heat transfer coefficient increased with increase in the flow rate of HTF which enhanced the heat transfer from the tube wall to the phase change material.
- Thermal storage efficiency of pure beeswax was reduced from 84.24 % to 58.30% with increase in flow rate from 0.50 LPM to 1.0 LPM.
- Thermal storage efficiency of pure beeswax (at 0.25 LPM) was found to be 83.60% as compared to 84.24% at 0.5 LPM due to the presence of pressure drop at 0.25 LPM.
- Reduction in thermal storage efficiency for composite material was observed from 87.49 % to 59.33% with increase in flow rate from 0.50 LPM to 1.0 LPM.
- Thermal storage efficiency of composite material (at 0.25 LPM) was found to be 86.19% as compared to 87.49% due to pressure drop.
- Optimum flow rate found to be 0.50 LPM from the study for both the PCMs as it gave maximum storage efficiency.
- Charging time of beeswax is reduced from 1755 min to 1575 min (10.25% reduction) when water inlet temperature increased from 60 °C to 90 °C (at constant flow rate of 0.5 LPM) as it increased the temperature difference between HTF and PCM.

- Similarly, charging time of beeswax/expanded graphite composite was reduced from 1275 min to 1110 min (12.94% reduction) when water inlet temperature increased from 60 °C to 90 °C at 0.5 LPM.
- Thermal storage efficiency of beeswax and composite found to be 84.24% and 87.49% respectively at flow rate of 0.5 LPM and water inlet temperature of 80 °C.
- Charging time for composite material is smaller (31.81% reduction) as compared to pure beeswax.
- The energy stored by beeswax was found to be 323.52 kJ/kg as which is 6.51% more as compared to the energy stored by composite material (321.80 kJ/kg).
- 2.72-15.40% reduction in charging time of pure beeswax was observed with the use of EG/water suspension (0.05 wt.%-1.0 wt.%) as HTF as compared to plain water.
- With Al_2O_3 nano-fluid (0.2 vol. %-2.0 vol. %) as HTF charging time of natural beeswax was reduced between 3.63% to 10% as compared to plain water.
- For composite material charging time is reduced by 5.33-14.66% with increase in EG/water concentration from 0.05 wt. % to 1.0 wt. % .
- Increase in concentration of Al_2O_3 nano-fluid from 0.2 vol. %-2.0 vol. %, reduced charging time of composite material by 2.66-13.33% as compared to plain water.
- Both PCMs i.e. beeswax and its composite showed reduction in charging time with increased concentration of EG/water suspension and Al_2O_3 nanofluid.
- Thermal storage efficiency of beeswax/expanded graphite composite found to be 46% with the use of exhaust flue gases from petrol engine.
- These results from experimental study show beeswax and its composite with expanded graphite as a potential phase change material for low temperature thermal storage applications.

Thermal performance of large TSU with natural graphite as heat storage material

- Natural graphite is a potential sensible heat storage material for low temperature thermal energy storage.
- Using plain water as HTF, charging time of natural graphite reduced from 195 min to 120 min (38.46% reduction) with increase in flow rate from 0.25 LPM to 1.0 LPM
- Charging time of natural graphite reduced from 195 min to 160 min (17.94% reduction) with increase in inlet fluid temperature from 60 °C to 90 °C.
- Increase in expanded graphite/water suspension concentration from 0.05 wt. % to 1.0 wt. % reduced charging time of natural graphite by 7.14-14.28%.
- Similarly, increase in concentration of aluminium nanofluid from 0.2 vol. % to 2.0 vol. %. reduced charging time of natural graphite by 14.28-23.82 %.

Modelling and Simulation of small scale and large scale TSU

- Modelling of thermal storage unit showed 8.39 % variation in charging time of beeswax as compared to experimental values.
- Simulation of composite material showed 6.86% deviation in charging time as compared to the experimental data.
- Melting time of beeswax and composite material found to be 1310 min and 950 min respectively from simulation study.
- Simulated charging time of natural graphite was found to be 200 min as compared to the experimental value of 210 min.
- Experimental data was having heat losses from surface of the pipe, convective losses and radiative heat losses which are not present in simulation data and causes little variation in these two results.
- Simulation results of beeswax, composite material and natural graphite are in good agreement with the experimental results.

5.2 Scope of future work

In the present research beeswax, its composite with expanded graphite and natural graphite have been studied in a rectangular shell with embedded helical coil type thermal storage unit as a potential thermal storage materials. The scopes for further studies have been identified as:

i) Various composites of beeswax can be developed using different materials with high thermal conductivity such as carbon nanotubes, metallic nanoparticles etc. and need to be investigated thoroughly for their thermal performance.

ii) Beeswax as PCM need to be studied for different specific low temperature applications such as solar water heater, solar air heater and as a composite material in building.

iii) More new materials which are natural in origin but has potential of phase change materials needs to be identified and study on the present thermal storage unit.

ii) Study should be carried out on different geometries of thermal storage unit such as circular tube, straight tube, with fins etc. and results should be compared with rectangular shell and helical tube type geometry.

iv) The design of present thermal storage unit can be improve by addition of new insulation materials such as brick, concrete, urea foam etc. to reduce thermal losses and to optimize the performance of TSU.

REFERENCES

[1] N. Abas, A. Kalair, N. Khan, Review of fossil fuels and future energy technologies, Futures. (2015). doi:10.1016/j.futures.2015.03.003.

[2] J.C. Zachos, G.R. Dickens, R.E. Zeebe, An early Cenozoic perspective on greenhouse warming and carbon-cycle dynamics., Nature. 451 (2008) 279–283. doi:10.1038/nature06588.

[3] R. Lal, Global Potential of Soil Carbon Sequestration to Mitigate the Greenhouse Effect, CRC. Crit. Rev. Plant Sci. 22 (2003) 151–184. doi:10.1080/713610854.

[4] M. Carlowicz, No Title, World Chang. Glob. Temp. Featur. Artic. (2010).

[5] R. Falkner, Business power and conflict in international environmental politics, 1st ed., 2008.

[6] V. Papadimitriou, Prospective Primary Teachers' Understanding of Climate Change, Greenhouse Effect, and Ozone Layer Depletion, J. Sci. Educ. Technol. 13 (2004) 299–307. doi:10.1023/B:JOST.0000031268.72848.6d.

[7] V. Devabhaktuni, M. Alam, S. Shekara Sreenadh Reddy Depuru, R.C. Green, D. Nims, C. Near, Solar energy: Trends and enabling technologies, Renew. Sustain. Energy Rev. 19 (2013) 555–564. doi:10.1016/j.rser.2012.11.024.

[8] P. Alotto, M. Guarnieri, F. Moro, Redox flow batteries for the storage of renewable energy: A review, Renew. Sustain. Energy Rev. 29 (2014) 325–335. doi:10.1016/j.rser.2013.08.001.

[9] A. Poullikkas, A comparative overview of large-scale battery systems for electricity storage, Renew. Sustain. Energy Rev. 27 (2013) 778–788. doi:10.1016/j.rser.2013.07.017.

[10] S. Vasudevan, M.A. Oturan, Electrochemistry: As cause and cure in water pollution-an overview, Environ. Chem. Lett. 12 (2014) 97–108. doi:10.1007/s10311-013-0434-2.

[11] T. Khatib, A. Mohamed, K. Sopian, A review of photovoltaic systems size optimization techniques, Renew. Sustain. Energy Rev. 22 (2013) 454–465. doi:10.1016/j.rser.2013.02.023.

[12] A.S. Joshi, I. Dincer, B. V. Reddy, Performance analysis of photovoltaic systems: A review, Renew. Sustain. Energy Rev. 13 (2009) 1884–1897. doi:10.1016/j.rser.2009.01.009.

[13] T.T. Chow, A review on photovoltaic/thermal hybrid solar technology, Appl. Energy. 87 (2010) 365–379. doi:10.1016/j.apenergy.2009.06.037.

[14] V.V.N. Obreja, On the performance of supercapacitors with electrodes based on carbon nanotubes and carbon activated material-A review, Phys. E Low-Dimensional Syst. Nanostructures. 40 (2008) 2596–2605. doi:10.1016/j.physe.2007.09.044.

[15] B. Sakintuna, F. Lamari-Darkrim, M. Hirscher, Metal hydride materials for solid hydrogen storage: A review, Int. J. Hydrogen Energy. 32 (2007) 1121–1140. doi:10.1016/j.ijhydene.2006.11.022.

[16] L.H. Rude, T.K. Nielsen, D.B. Ravnsbæk, U. Bösenberg, M.B. Ley, B. Richter, L.M. Arnbjerg, M. Dornheim, Y. Filinchuk, F. Besenbacher, T.R. Jensen, Tailoring properties of borohydrides for hydrogen storage: A review, Phys. Status Solidi Appl. Mater. Sci. 208 (2011) 1754–1773. doi:10.1002/pssa.201001214.

[17] J.P. Deane, B.P. Ó Gallachóir, E.J. McKeogh, Techno-economic review of existing and new pumped hydro energy storage plant, Renew. Sustain. Energy Rev. 14 (2010) 1293–1302. doi:10.1016/j.rser.2009.11.015.

[18] H.S. de Boer, L. Grond, H. Moll, R. Benders, The application of power-to-gas, pumped hydro storage and compressed air energy storage in an electricity system at different wind power penetration levels, Energy. 72 (2014) 360–370. doi:10.1016/j.energy.2014.05.047.

[19] H.H. Harris, Review of *Chemical Energy Storage* Chemical Energy Storage, edited by Robert Schlögl. Walter de Gruyter GmbH: Berlin/Boston, 2013. 479 pp. ISBN 9783110264074 (paper). $112.00., J. Chem. Educ. (2015) 150805071740001. doi:10.1021/acs.jchemed.5b00403.

[20] A. Sharma, V. V. Tyagi, C.R. Chen, D. Buddhi, Review on thermal energy storage with phase change materials and applications, Renew. Sustain. Energy

Rev. 13 (2009) 318–345. doi:10.1016/j.rser.2007.10.005.

[21] D. Zhou, C.Y. Zhao, Y. Tian, Review on thermal energy storage with phase change materials (PCMs) in building applications, Appl. Energy. 92 (2012) 593–605. doi:10.1016/j.apenergy.2011.08.025.

[22] Y. Tripanagnostopoulos, T. Nousia, M. Souliotis, P. Yianoulis, Hybrid photovoltaic/thermal solar systems, Sol. Energy. 72 (2002) 217–234. doi:10.1016/S0038-092X(01)00096-2.

[23] D. Mori, K. Hirose, Recent challenges of hydrogen storage technologies for fuel cell vehicles, Int. J. Hydrogen Energy. 34 (2009) 4569–4574. doi:10.1016/j.ijhydene.2008.07.115.

[24] K. Mazloomi, C. Gomes, Hydrogen as an energy carrier: Prospects and challenges, Renew. Sustain. Energy Rev. 16 (2012) 3024–3033. doi:10.1016/j.rser.2012.02.028.

[25] K. Mukhopadhyay, O. Forssell, An empirical investigation of air pollution from fossil fuel combustion and its impact on health in India during 1973-1974 to 1996-1997, Ecol. Econ. 55 (2005) 235–250. doi:10.1016/j.ecolecon.2004.09.022.

[26] B. Zalba, J.M. Marín, L.F. Cabeza, H. Mehling, Review on thermal energy storage with phase change: Materials, heat transfer analysis and applications, 2003. doi:10.1016/S1359-4311(02)00192-8.

[27] M.M. Farid, A.M. Khudhair, S.A.K. Razack, S. Al-Hallaj, A review on phase change energy storage: Materials and applications, Energy Convers. Manag. 45 (2004) 1597–1615. doi:10.1016/j.enconman.2003.09.015.

[28] I. Llorente García, J.L. Álvarez, D. Blanco, Performance model for parabolic trough solar thermal power plants with thermal storage: Comparison to operating plant data, Sol. Energy. 85 (2011) 2443–2460. doi:10.1016/j.solener.2011.07.002.

[29] S. Kalogirou, The potential of solar industrial process heat applications, Appl. Energy. 76 (2003) 337–361. doi:10.1016/S0306-2619(02)00176-9.

[30] C. Thormark, A low energy building in a life cycle—its embodied energy, energy need for operation and recycling potential, Build. Environ. 37 (2002) 429–435. doi:10.1016/S0360-1323(01)00033-6.

[31] S. Khare, M. Dell'Amico, C. Knight, S. McGarry, Selection of materials for high temperature sensible energy storage, Sol. Energy Mater. Sol. Cells. 115 (2013) 114–122. doi:10.1016/j.solmat.2013.03.009.

[32] S.M. Hasnain, Review on sustainable thermal energy storage technologies, Part II: Cool thermal storage, Energy Convers. Manag. 39 (1998) 1139–1153. doi:10.1016/S0196-8904(98)00024-7.

[33] M.M. I. Fernandez, C.J. Renedo, S. Perez, J. Carcedo, Advances in phase change materials for thermal solar power plants Quality, in: Int. Conf. Renew. Energies Power Qual., European Association for the Development of Renewable Energies, Environment and Power Quality (EA4EPQ), 2010.

[34] A. Mawire, M. Mcpherson, Experimental and simulated temperature distribution of an oil-pebble bed thermal energy storage system with a variable heat source, Appl. Therm. Eng. 29 (2009) 1086–1095. doi:10.1016/j.applthermaleng.2008.05.028.

[35] A. Sakhrieh, A. Al-Salaymeh, Experimental and numerical investigations of salt gradient solar pond under Jordanian climate conditions, Energy Convers. Manag. 65 (2013) 725–728. doi:10.1016/j.enconman.2012.01.046.

[36] R. Shukla, K. Sumathy, P. Erickson, J. Gong, Recent advances in the solar water heating systems: A review, Renew. Sustain. Energy Rev. 19 (2013) 173–190. doi:10.1016/j.rser.2012.10.048.

[37] M. Appadurai, V. Velmurugan, Performance analysis of fin type solar still integrated with fin type mini solar pond, Sustain. Energy Technol. Assessments. 9 (2015) 30–36. doi:10.1016/j.seta.2014.11.001.

[38] S. Sadhishkumar, T. Balusamy, Performance improvement in solar water heating systems - A review, Renew. Sustain. Energy Rev. 37 (2014) 191–198. doi:10.1016/j.rser.2014.04.072.

[39] A. Saxena, Varun, A.A. El-Sebaii, A thermodynamic review of solar air heaters, Renew. Sustain. Energy Rev. 43 (2015) 863–890. doi:10.1016/j.rser.2014.11.059.

[40] V. V. Tyagi, N.L. Panwar, N.A. Rahim, R. Kothari, Review on solar air heating system with and without thermal energy storage system, Renew. Sustain. Energy Rev. 16 (2012) 2289–2303. doi:10.1016/j.rser.2011.12.005.

[41] K.E. N'Tsoukpoe, T. Schmidt, H.U. Rammelberg, B.A. Watts, W.K.L. Ruck, A systematic multi-step screening of numerous salt hydrates for low temperature thermochemical energy storage, Appl. Energy. 124 (2014) 1–16. doi:10.1016/j.apenergy.2014.02.053.

[42] Y.A. Criado, M. Alonso, J.C. Abanades, Kinetics of the CaO/Ca(OH) 2 Hydration/Dehydration Reaction for Thermochemical Energy Storage Applications, Ind. Eng. Chem. Res. 53 (2014) 12594–12601. doi:10.1021/ie404246p.

[43] A.J. Carrillo, J. Moya, A. Bayón, P. Jana, V.A. De La Peña O'Shea, M. Romero, J. Gonzalez-Aguilar, D.P. Serrano, P. Pizarro, J.M. Coronado, Thermochemical energy storage at high temperature via redox cycles of Mn and Co oxides: Pure oxides versus mixed ones, Sol. Energy Mater. Sol. Cells. 123 (2014) 47–57. doi:10.1016/j.solmat.2013.12.018.

[44] E. Alonso, C. Perez-Rabago, J. Licurgo, E. Fuentealba, C.A. Estrada, First experimental studies of solar redox reactions of copper oxides for thermochemical energy storage, Sol. Energy. 115 (2015) 297–305. doi:10.1016/j.solener.2015.03.005.

[45] P. Pardo, A. Deydier, Z. Anxionnaz-Minvielle, S. Roug??, M. Cabassud, P. Cognet, A review on high temperature thermochemical heat energy storage, Renew. Sustain. Energy Rev. 32 (2014) 591–610. doi:10.1016/j.rser.2013.12.014.

[46] Sharma S.D and Sagara K, Latent heat storage materials and systems: A review, Int. J. Green Energy. 2 (2005) 1–56. doi:10.1081/ge-200051299.

[47] J.. Buchanan, The chemistry of olefins production by ZSM-5 addition to

catalytic cracking units, Catal. Today. 55 (2000) 207–212. doi:10.1016/S0920-5861(99)00248-5.

[48] S. Bogdanov, Beeswax: Quality issues today, Bee World. 85 (2004) 46–50. doi:10.1080/0005772X.2004.11099623.

[49] M.A. Rojas-Graü, R. Soliva-Fortuny, O. Martín-Belloso, Edible coatings to incorporate active ingredients to fresh-cut fruits: a review, Trends Food Sci. Technol. 20 (2009) 438–447. doi:10.1016/j.tifs.2009.05.002.

[50] M.L. Navarro-Tarazaga, A. Massa, M.B. Pérez-Gago, Effect of beeswax content on hydroxypropyl methylcellulose-based edible film properties and postharvest quality of coated plums (Cv. Angeleno), LWT - Food Sci. Technol. 44 (2011) 2328–2334. doi:10.1016/j.lwt.2011.03.011.

[51] S. Sen, S. Ganguly, A. Das, J. Sen, S. Dey, Renewable energy scenario in India: Opportunities and challenges, J. African Earth Sci. 122 (2016) 25–31. doi:10.1016/j.jafrearsci.2015.06.002.

[52] A. Sharma, A comprehensive study of solar power in India and World, Renew. Sustain. Energy Rev. 15 (2011) 1767–1776. doi:10.1016/j.rser.2010.12.017.

[53] A. Kumar, K. Kumar, N. Kaushik, S. Sharma, S. Mishra, Renewable energy in India: Current status and future potentials, Renew. Sustain. Energy Rev. 14 (2010) 2434–2442. doi:10.1016/j.rser.2010.04.003.

[54] N.K. Sharma, P.K. Tiwari, Y.R. Sood, Solar energy in India: Strategies, policies, perspectives and future potential, Renew. Sustain. Energy Rev. 16 (2012) 933–941. doi:10.1016/j.rser.2011.09.014.

[55] I.R. Pillai, R. Banerjee, Renewable energy in India: Status and potential, Energy. 34 (2009) 970–980. doi:10.1016/j.energy.2008.10.016.

[56] P.P. Systems, Increased orders from Indian dairies validate commercial necessity for refrigeration purposes, (2015) http://coolectrica.com/2015/07/08/promethean-power.

[57] C. Industries, Thermal energy storage sees ongoing development in India, (2015) http://www.calmac.com/energy-storage-article-therm.

[58] A. Pasupathy, R. Velraj, R. V. Seeniraj, Phase change material-based building architecture for thermal management in residential and commercial establishments, Renew. Sustain. Energy Rev. 12 (2008) 39–64. doi:10.1016/j.rser.2006.05.010.

[59] A. Pasupathy, L. Athanasius, R. Velraj, R. V. Seeniraj, Experimental investigation and numerical simulation analysis on the thermal performance of a building roof incorporating phase change material (PCM) for thermal management, Appl. Therm. Eng. 28 (2008) 556–565. doi:10.1016/j.applthermaleng.2007.04.016.

[60] T. Power, Tata Power launches India's first "thermal energy storage" incentive programme, (2014) http://www.tata.com/media/releasesinside/Tata-Powe.

[61] A.M. Khudhair, M.M. Farid, A review on energy conservation in building applications with thermal storage by latent heat using phase change materials, Energy Convers. Manag. 45 (2004) 263–275. doi:10.1016/S0196-8904(03)00131-6.

[62] P. Schossig, H.M. Henning, S. Gschwander, T. Haussmann, Micro-encapsulated phase-change materials integrated into construction materials, Sol. Energy Mater. Sol. Cells. 89 (2005) 297–306. doi:10.1016/j.solmat.2005.01.017.

[63] R.. Dell, D.A.. Rand, Energy storage — a key technology for global energy sustainability, J. Power Sources. 100 (2001) 2–17. doi:10.1016/S0378-7753(01)00894-1.

[64] X.H. Ruqiang Zou, Mitigating Global Warming by Thermal Energy Storage, in: Energy Solut. to Combat Glob. Warm., 2016: pp. 573–594. doi:10.1007/978-3-319-26950-4.

[65] M. Pérez de Arce, E. Sauma, J. Contreras, Renewable energy policy performance in reducing CO_2 emissions, Energy Econ. 54 (2016) 272–280. doi:10.1016/j.eneco.2015.11.024.

[66] E. Gençer, R. Agrawal, A commentary on the US policies for efficient large scale renewable energy storage systems: Focus on carbon storage cycles,

Energy Policy. 88 (2016) 477–484. doi:10.1016/j.enpol.2015.11.003 0301-4215/.

[67] P. Pinel, C.A. Cruickshank, I. Beausoleil-Morrison, A. Wills, A review of available methods for seasonal storage of solar thermal energy in residential applications, Renew. Sustain. Energy Rev. 15 (2011) 3341–3359. doi:10.1016/j.rser.2011.04.013.

[68] A. Shukla, D. Buddhi, R.L. Sawhney, Solar water heaters with phase change material thermal energy storage medium: A review, Renew. Sustain. Energy Rev. 13 (2009) 2119–2125. doi:10.1016/j.rser.2009.01.024.

[69] A. Arteconi, N.J. Hewitt, F. Polonara, Domestic demand-side management (DSM): Role of heat pumps and thermal energy storage (TES) systems, Appl. Therm. Eng. 51 (2013) 155–165. doi:10.1016/j.applthermaleng.2012.09.023.

[70] J. Yagi, T. Akiyama, Storage Of Thermal-Energy For Effective Use Of Waste Heat From Industries, J. Mater. Process. Technol. 48 (1995) 793–804. doi:10.1016/0924-0136(94)01723-E.

[71] S. Popli, P. Rodgers, V. Eveloy, Gas turbine efficiency enhancement using waste heat powered absorption chillers in the oil and gas industry, Appl. Therm. Eng. 50 (2013) 918–931. doi:10.1016/j.applthermaleng.2012.06.018.

[72] V. Pandiyarajan, M. Chinna Pandian, E. Malan, R. Velraj, R. V. Seeniraj, Experimental investigation on heat recovery from diesel engine exhaust using finned shell and tube heat exchanger and thermal storage system, Appl. Energy. 88 (2011) 77–87. doi:10.1016/j.apenergy.2010.07.023.

[73] N. Sarier, E. Onder, Organic phase change materials and their textile applications: An overview, Thermochim. Acta. 540 (2012) 7–60. doi:10.1016/j.tca.2012.04.013.

[74] L.F. Cabeza, C. Castellón, M. Nogués, M. Medrano, R. Leppers, O. Zubillaga, Use of microencapsulated PCM in concrete walls for energy savings, Energy Build. 39 (2007) 113–119. doi:10.1016/j.enbuild.2006.03.030.

[75] E. Oró, A. de Gracia, A. Castell, M.M. Farid, L.F. Cabeza, Review on phase

change materials (PCMs) for cold thermal energy storage applications, Appl. Energy. 99 (2012) 513–533. doi:10.1016/j.apenergy.2012.03.058.

[76] H.P.N.S. De Alwis, A. a. Mohamad, A.K. Mehrotra, Exergy Analysis of Direct and Indirect Combustion of Methanol by Utilizing Solar Energy or Waste Heat, Energy & Fuels. 23 (2009) 1723–1733. doi:10.1021/ef8007129.

[77] M.Y. Yazıcı, M. Avcı, O. Aydın, M. Akgun, ScienceDirect Effect of eccentricity on melting behavior of paraffin in a horizontal tube-in-shell storage unit : An experimental study, 101 (2014) 291–298. doi:10.1016/j.solener.2014.01.007.

[78] V. Kumar, B. Faizee, M. Mridha, K.D.P. Nigam, Numerical studies of a tube-in-tube helically coiled heat exchanger, 47 (2008) 2287–2295. doi:10.1016/j.cep.2008.01.001.

[79] M.K. Rathod, J. Banerjee, Numerical Investigation on Latent Heat Storage Unit of Different Configurations, 5 (2011) 652–657.

[80] P.L.P. Li, Energy storage is the core of renewable technologies, IEEE Nanotechnol. Mag. (2008) 13–18. doi:10.1109/MNANO.2009.932032.

[81] S. Weitemeyer, D. Kleinhans, T. Vogt, C. Agert, Integration of Renewable Energy Sources in future power systems: The role of storage, Renew. Energy. 75 (2015) 14–20. doi:10.1016/j.renene.2014.09.028.

[82] H. Ibrahim, A. Ilinca, J. Perron, Energy storage systems-Characteristics and comparisons, Renew. Sustain. Energy Rev. 12 (2008) 1221–1250. doi:10.1016/j.rser.2007.01.023.

[83] S. Rehman, L.M. Al-Hadhrami, M.M. Alam, Pumped hydro energy storage system: A technological review, Renew. Sustain. Energy Rev. 44 (2015) 586–598. doi:10.1016/j.rser.2014.12.040.

[84] C. Bueno, J.A. Carta, Wind powered pumped hydro storage systems, a means of increasing the penetration of renewable energy in the Canary Islands, Renew. Sustain. Energy Rev. 10 (2006) 312–340. doi:10.1016/j.rser.2004.09.005.

[85] L. Qiang, Y. Yue, L. Zhen-jie1, W. Wei-sheng, L. Hua-yong, Research on Energy Shifting Benefits of Hybrid Wind Power and Pumped Hydro Storage System Considering Peak-Valley Electricity Price, Power Syst. Technol. 9 (2009).

[86] T. Ma, H. Yang, L. Lu, J. Peng, Technical feasibility study on a standalone hybrid solar-wind system with pumped hydro storage for a remote island in Hong Kong, Renew. Energy. 69 (2014) 7–15. doi:10.1016/j.renene.2014.03.028.

[87] M. Kapsali, J.S. Anagnostopoulos, J.K. Kaldellis, Wind powered pumped-hydro storage systems for remote islands: A complete sensitivity analysis based on economic perspectives, Appl. Energy. 99 (2012) 430–444. doi:10.1016/j.apenergy.2012.05.054.

[88] L.E. N. Hartmann, O. Vohringer, C. Kruck, Simulation and analysis of different adiabatic compressed air energy storage plant configurations, Appl. Energy. 93 (2012) 541–548.

[89] B. Elmegaard, W. Brix, Efficiency of Compressed Air Energy Storage, 24th Int. Conf. Effic. Cost, Optim. Simul. Environ. Impact Energy Syst. (2011) 1–12.http://orbit.dtu.dk/fedora/objects/orbit:72193/datastreams/file_6324034/content.

[90] A.N. Ghalelou, A.P. Fakhri, S. Nojavan, M. Majidi, H. Hatami, A stochastic self-scheduling program for compressed air energy storage (CAES) of renewable energy sources (RESs) based on a demand response mechanism, Energy Convers. Manag. 120 (2016) 388–396.

[91] N.S. Hasan, M.Y. Hassan, H. Abdullah, H.A. Rahman, W.Z.W. Omar, N. Rosmin, Improving power grid performance using parallel connected Compressed Air Energy Storage and wind turbine system, Renew. Energy. 96 (2016) 498–508.

[92] H. Sun, X. Luo, J. Wang, Feasibility study of a hybrid wind turbine system-Integration with compressed air energy storage, Appl. Energy. 137 (2015) 617–628.

[93] M. Saadat, F.A. Shirazi, P.Y. Li, Modeling and control of an open accumulator Compressed Air Energy Storage (CAES) system for wind turbines, Appl. Energy. 137 (2015) 603–616.

[94] R.A. Huggins, Lead-Acid Batteries, in: Energy Storage, Springer, 2016: pp. 309–323.

[95] Y. Wang, B. Liu, Q. Li, S. Cartmell, S. Ferrara, J.X. Z.D. Deng, Lithium and lithium ion batteries for applications in microelectronic devices: A review, J. Power Sources. 286 (2015) 330–345.

[96] Z. Yuan, Y. Duan, H. Zhang, X. Li, H. Zhang, I. Vankelecom, Advanced porous membranes with ultra-high selectivity and stability for vanadium flow batteries, Energy Environ. Sci. 9 (2016) 441–447.

[97] A. Chowdhury, S.K. Maiti, Assessing the ecological health risk in a conserved mangrove ecosystem due to heavy metal pollution: A case study from Sundarbans Biosphere Reserve, India, Hum. Ecol. Risk Assess. An Int. J. (2016).

[98] J. Zheng, P. Yan, J. Xiao, C. Wang, J.G. Zhang, The Effects of Synthesis Conditions on the Performances of Ni-Rich $LiNi_xMn_yCo_zO_2$ Cathode Materials for Lithium-Ion Batteries, in: 18th Int. Meet. Lithium Batter., 2016.

[99] J. Cot-Gores, A. Castell, L.F. Cabeza, Thermochemical energy storage and conversion: A-state-of-the-art review of the experimental research under practical conditions, Renew. Sustain. Energy Rev. 16 (2012) 5207–5224. doi:10.1016/j.rser.2012.04.007.

[100] M. Neises, S. Tescari, L. de Oliveira, M. Roeb, C. Sattler, B. Wong, Solar-heated rotary kiln for thermochemical energy storage, Sol. Energy. 86 (2012) 3040–3048. doi:10.1016/j.solener.2012.07.012.

[101] R. Dunn, K. Lovegrove, G. Burgess, A review of ammonia-based thermochemical energy storage for concentrating solar power BT - SPECIAL ISSUE: The Intermittency Challenge: Massive Energy Storage in a Sustainable Future, Proc. IEEE. 100 (2012) 391–400. doi:10.1109/JPROC.2011.2166529.

[102] C. Chen, H. Aryafar, G. Warrier, K.M. Lovegrove, A.S. Lavine, Ammonia synthesis for producing supercritical steam in the context of solar thermochemical energy storage, AIP Conf. Proc. 1734 (2016). doi:10.1063/1.4949108.

[103] A.J. Carrillo, D. Sastre, D.P. Serrano, P. Pizarro, J.M. Coronado, Revisiting the BaO2/BaO redox cycle for solar thermochemical energy storage, Physicl Chem. Chem. Phys. 18 (2016) 8039–8048.

[104] S. Chattopadhyay, A. Mitchell, Thermochemistry of calcium oxide and calcium hydroxide in fluoride slags, Metall. Trans. B. 21 (1990) 621–627.

[105] Y.Y. Jiang, H.B. Dai, Y.J. Zhong, D.M. Chen, P. Wang, Complete and Rapid Conversion of Hydrazine Monohydrate to Hydrogen over Supported Ni–Pt Nanoparticles on Mesoporous Ceria for Chemical Hydrogen Storage, Chem. A Eur. J. 21 (2015) 15439–15445.

[106] S. Dürr, M. Müller, H. Jorschick, M. Helmin, A. Bösmann, P.R. Palkovits, P.P. Wasserscheid, Carbon Dioxide-Free Hydrogen Production with Integrated Hydrogen Separation and Storage, ChemSusChem. 10 (2017) 42–47.

[107] R. Subramanian, L.L. Williams, T.L. Vaughn, D. Zimmerle, J.R. Roscioli, S.C. Herndon, T.I. Yacovitch, C. Floerchinger, D.S. Tkacik, A.L. Mitchell, Methane emissions from natural gas compressor stations in the transmission and storage sector: Measurements and comparisons with the EPA greenhouse gas reporting program protocol, Environ. Sci. Technol. 49 (2015) 3252–3261.

[108] D. Saha, H.A. Grappe, A. Chakraborty, G. Orkoulas, Postextraction Separation, On-Board Storage, and Catalytic Conversion of Methane in Natural Gas: A Review, Chem. Rev. (2016).

[109] S.P. Cuellar-Bermudez, J.S. Garcia-Perez, B.E. Rittmann, R. Parra-Saldivar, Photosynthetic bioenergy utilizing CO 2: an approach on flue gases utilization for third generation biofuels, J. Clean. Prod. 98 (2015) 53–65.

[110] M. Agarwal, A. Dinker, Application of consolidate enzymatic system of Fusarium and Saccharomyces to enhance the production of ethanol from spent grain, J. Renew. Sustain. Energy. 5 (2013). doi:10.1063/1.4821518.

[111] Z. Xu, D.W. Sun, Z. Zhang, Z. Zhu, Research developments in methods to reduce carbon footprint of cooking operations: A review, Trends Food Sci. Technol. 44 (2015) 49–57.

[112] C. de Vries, M. Claeys, G. Schaub, Chemical energy storage in gaseous hydrocarbons via iron Fischer-Tropsch synthesis from H_2/CO_2-Kinetics, selectivity and process considerations, Catal. Today. 242 (2015) 184–192.

[113] L. Prasad, P. Muthukumar, Design and optimization of lab-scale sensible heat storage prototype for solar thermal power plant application, Sol. Energy. 97 (2013) 217–229. doi:10.1016/j.solener.2013.08.022.

[114] A. Castell, C. Sole, 11 – Design of latent heat storage systems using phase change materials (PCMs), Adv. Therm. Energy Storage Syst. Appl. A. (2015) 285–305.

[115] A. Eastman, S.U.S. Choi, S. Li, W. Yu, L.J. Thompson, Anomalously increased effective thermal conductivities of ethylene glycol-based nanofluids containing copper nanoparticles, Appl. Phys. 78 (2001) 718–724.

[116] B. Rufino, F. Boulch, M.-V. Coulet, G. Lacroix, R. Denoyel, Influence of particles size on thermal properties of aluminium powder, Acta Mater. 55 (2007) 2815–2827.

[117] E. Wasserman, L. Stixrude, R.E. Cohen, Thermal properties of iron at high pressures and temperatures, Phys. Rev. B. 27 (1996) 312–356.

[118] L. Gabriela, Seasonal Sensible Thermal Energy Storage Solutions, Leonardo Electron. J. Pract. Technol. (2011) 49–68.

[119] M.K.A. Sharif, A.A. Al-Abidi, S. Mat, K. Sopian, M.H. Ruslan, M.Y. Sulaiman, M.A.M. Rosli, No Title, Renew. Sustain. Energy Rev. 42 (2014) 557–568.

[120] E.M. Alawadhi, Thermal analysis of a building brick containing phase change material, Energy Build. 40 (2008) 351–357.

[121] H.H. Ozturk, A. Bascetincelik, Energy and Exergy Efficiency of a Packed-bed Heat Storage Unit for Greenhouse Heating, Biosyst. Eng. 86 (2003) 231–245.

[122] M. Inagaki, Y. Kaburagi, Y. Hishiyama, Thermal Management Material: Graphite, Adv. Eng. Mater. 16 (2014) 494–506.

[123] D.W. Hawes, D. Banu, D. Feldman, Latent heat storage in concrete. II, Sol. Energy Mater. 21 (1990) 61–80.

[124] E.C. Robertson, Thermal properties of rocks, 1988.

[125] A.A. El-Sebaii, M.R.I. Ramadan, S. Aboul-Enein, A.M. Khallaf, History of the solar ponds: a review study, Renew. Sustain. Energy Rev. 15 (2011) 3319–3325.

[126] V. Velmurugan, S. Pandiarajan, P. Guruparan, L.H. Subramanian, C.D. Prabaharan, K. Srithar, Integrated performance of stepped and single basin solar stills with mini solar pond, DES. 249 (2009) 902–909. doi:10.1016/j.desal.2009.06.070.

[127] M. Karakilcik, I. Dincer, M.A. Rosen, Performance investigation of a solar pond, Appl. Therm. Eng. 26 (2006) 727–735.

[128] R. Singh, S. Tundee, A. Akbarzadeh, Electric power generation from solar pond using combined thermosyphon and thermoelectric modules, Sol. Energy. 85 (2011) 371–378. doi:10.1016/j.solener.2010.11.012.

[129] M. Berkani, H. Sissaoui, A. Abdelli, M.K. A, G. Barker-Read, ScienceDirect Comparison of three solar ponds with different salts through bi-dimensional modeling, 116 (2015) 56–68. doi:10.1016/j.solener.2015.03.024.

[130] I. Bozkurt, S. Deniz, M. Karakilcik, I. Dincer, Performance Comparison of Sodium and Magnesium Chloride-Saturated Solar Ponds, Prog. Clean Energy. 2 (2015) 251–259.

[131] S. Tundee, P. Terdtoon, P. Sakulchangsatjatai, R. Singh, Heat extraction from salinity-gradient solar ponds using heat pipe heat exchangers, Sol. Energy. 84 (2010) 1706–1716. doi:10.1016/j.solener.2010.04.010.

[132] I. Bozkurt, M. Karakilcik, The daily performance of a solar pond integrated with solar collectors, Sol. Energy. 86 (2012) 1611–1620.

[133]] F. Suarez, J.A. Ruskowitz, S.W. Tyler, A.E. Childress, Renewable water: Direct contact membrane distillation coupled with solar ponds, Appl. Energy. 158 (2015) 532–539.

[134] G. Zanganeh, A. Pedretti, S. Zavattoni, M. Barbato, A. Steinfeld, Packed-bed thermal storage for concentrated solar power-Pilot-scale demonstration and industrial-scale design, Sol. Energy. 86 (2012) 3084–3098.

[135] G. Zanganeh, A. Pedretti, A. Haselbacher, A. Steinfeld, Design of packed bed thermal energy storage systems for high-temperature industrial process heat, Appl. Energy. 137 (2015) 812–822.

[136] H. Yuan, C. Lu, Z. Xu, Y. Ni, X. Lan, Mechanical and thermal properties of cement composite graphite for solar thermal storage materials, 86 (2012) 3227–3233. doi:10.1016/j.solener.2012.08.011.

[137] S. Kuravi, J. Trahan, D.Y. Goswami, M.M. Rahman, E.K. Stefanakos, Thermal energy storage technologies and systems for concentrating solar power plants, Prog. Energy Combust. Sci. 39 (2013) 285–319.

[138] I. Dincer, S. Dost, X. Li, Performance analyses of sensible heat storage systems for thermal applications, Fuel Energy Abstr. 38 (1997) 435. doi:10.1016/S0140-6701(97)82292-8.

[139] D. Laing, W.-D. Steinmann, R. Tamme, C. Richter, Solid media thermal storage for parabolic trough power plants, Sol. Energy. 80 (2006) 1283–1289. doi:10.1016/j.solener.2006.06.003.

[140] M. Esen, H. Esen, Experimental investigation of a two-phase closed thermosyphon solar water heater, Sol. Energy. 79 (2005) 459–468.

[141] A.F. Regin, S.C. Solanki, J.S. Saini, Heat transfer characteristics of thermal energy storage system using PCM capsules: A review, Renew. Sustain. Energy Rev. 12 (2008) 2438–2451. doi:10.1016/j.rser.2007.06.009.

[142] A. Abhat, Low temperature latent heat thermal energy storage: Heat storage materials, Sol. Energy. 30 (1983) 313–332. doi:10.1016/0038-092X(83)90186-X.

[143] F. Agyenim, N. Hewitt, P. Eames, M. Smyth, A review of materials, heat transfer and phase change problem formulation for latent heat thermal energy storage systems (LHTESS), Renew. Sustain. Energy Rev. 14 (2010) 615–628. doi:10.1016/j.rser.2009.10.015.

[144] T. Kousksou, A. Jamil, T. El Rhafiki, Y. Zeraouli, Paraffin wax mixtures as phase change materials, Sol. Energy Mater. Sol. Cells. 94 (2010) 2158–2165. doi:10.1016/j.solmat.2010.07.005.

[145] S. Himran, A. Suwono, G.A. Mansoori, Characterization of Alkanes and Paraffin Waxes for Application as Phase Change Energy Storage Medium, Energy Sources. 16 (1994) 117–128. doi:10.1080/00908319408909065.

[146] L. Yang, X. Xu, A renovated Hamilton–Crosser model for the effective thermal conductivity of CNTs nanofluids, Int. Commun. Heat Mass Transf. 81 (2017) 42–50. doi:http://dx.doi.org/10.1016/j.icheatmasstransfer.2016.12.010.

[147] A. Hammami, A.K. Mehrotra, Thermal behaviour of polymorphic n-alkanes: effect of cooling rate on the major transition temperatures, Fuel. 74 (1995) 96–101. doi:10.1016/0016-2361(94)P4338-3.

[148] H. Katsumi, M. Tominaga, M. Tajiri, S. Shimizu, Y. Sakazaki, T. Kinoshita, M. Okamoto, T. Kawayama, T. Hoshino, A case of lipoid pneumonia caused by inhalation of vaporized paraffin from burning candles, Respir. Med. Case Reports. 19 (2016) 166–168.

[149] A. Buck, B. Balluff, A. Voss, R. Langer, H. Zitzelsberger, M. Aichler, A. Walch, How Suitable is Matrix-Assisted Laser Desorption/Ionization-Time-of-Flight for Metabolite Imaging from Clinical Formalin-Fixed and Paraffin-Embedded Tissue Samples in Comparison to Matrix-Assisted Laser Desorption/Ionization-Fourier Transform Ion Cyclotro, Anal. Chem. 88 (2016) 5281–9. doi:10.1021/acs.analchem.6b00460.

[150] K.M. Zia, F. Zia, M. Ali, S. Rehman, M. Zuber, Lipid functionalized biopolymers: A review, Int. J. Biol. Macromol. 93 (2016) 1057–1068.

[151] K. Kaygusuz, A. Sari, Thermal energy storage system using a technical grade paraffin wax as latent heat energy storage material, Energy Sources. 27 (2005)

1535–1546. doi:10.1080/009083190914015.

[152] B. He, V. Martin, F. Setterwall, Phase transition temperature ranges and storage density of paraffin wax phase change materials, 29 (2004) 1785–1804. doi:10.1016/j.energy.2004.03.002.

[153] F. Goia, E. Boccaleri, Physical-chemical properties evolution and thermal properties reliability of a paraffin wax under solar radiation exposure in a real-scale PCM window system, Energy Build. 119 (2016) 41–50. doi:10.1016/j.enbuild.2016.03.007.

[154] M. Akgün, O. Aydin, K. Kaygusuz, Thermal energy storage performance of paraffin in a novel tube-in-shell system, Appl. Therm. Eng. 28 (2008) 405–413. doi:10.1016/j.applthermaleng.2007.05.013.

[155] A. Sharma, S.D. Sharma, D. Buddhi, Accelerated thermal cycle test of acetamide, stearic acid and paraffin wax for solar thermal latent heat storage applications, Energy Convers. Manag. 43 (2002) 1923–1930. doi:10.1016/S0196-8904(01)00131-5.

[156] . Nemeth, A. g. S. Nemeth, J. Toth, A. Fodor-Kardos, J. n. Gyenis, T. Feczko, Consolidated microcapsules with double alginate shell containing paraffin for latent heat storage, Sol. Energy Mater. Sol. Cells. 143 (2015) 397–405.

[157] M. Karkri, M. Lachheb, Z. Nógellová, B. Boh, B. Sumiga, M.A. Almaadeed, A. Fethi, I. Krupa, Thermal properties of phase-change materials based on high-density polyethylene filled with micro-encapsulated paraffin wax for thermal energy storage, Energy Build. 88 (2015) 144–152. doi:10.1016/j.enbuild.2014.11.061.

[158] S.A. Memon, H.Z. Cui, H. Zhang, F. Xing, Utilization of macro encapsulated phase change materials for the development of thermal energy storage and structural lightweight aggregate concrete, Appl. Energy. 139 (2015) 43–55. doi:10.1016/j.apenergy.2014.11.022.

[159] N. Şahan, M. Fois, H. Paksoy, Improving thermal conductivity phase change materials - A study of paraffin nanomagnetite composites, Sol. Energy Mater. Sol. Cells. 137 (2015) 61–67. doi:10.1016/j.solmat.2015.01.027.

[160] Z. Wang, Z. Zhang, L. Jia, L. Yang, Paraffin and paraffin/aluminum foam composite phase change material heat storage experimental study based on thermal management of Li-ion battery, Appl. Therm. Eng. 78 (2015) 428–436. doi:10.1016/j.applthermaleng.2015.01.009.

[161] C. Wang, T. Lin, N. Li, H. Zheng, Heat transfer enhancement of phase change composite material: Copper foam/paraffin, Renew. Energy. 96 (2016) 960–965. doi:10.1016/j.renene.2016.04.039.

[162] A. Fethi, L. Mohamed, K. Mustapha, B. Ameurtarek, B.N. Sassi, Investigation of a graphite/paraffin phase change composite, Int. J. Therm. Sci. 88 (2015) 128–135. doi:10.1007/s10973-012-2218-5.

[163] M. Lachheb, K. Mustapha, A. Fethi, B.N. Sassi, F. Magali, S. Patrik, Thermal properties measurement and heat storage analysis of paraffin/graphite composite phase change material, Compos. Part B Eng. 66 (2014) 518–525. doi:10.1016/j.compositesb.2014.05.011.

[164] W. Mhike, W.W. Focke, J.P. Mofokeng, A.S. Luyt, Thermochimica Acta Thermally conductive phase-change materials for energy storage based on low-density polyethylene , soft Fischer – Tropsch wax and graphite, Thermochim. Acta. 527 (2012) 75–82. doi:10.1016/j.tca.2011.10.008.

[165] A. Sari, A. Karaipekli, Thermal conductivity and latent heat thermal energy storage characteristics of paraffin/expanded graphite composite as phase change material, Appl. Therm. Eng. 27 (2007) 1271–1277. doi:10.1016/j.applthermaleng.2006.11.004.

[166] J. Wang, H. Xie, Z. Guo, L. Guan, Y. Li, Improved thermal properties of paraffin wax by the addition of TiO_2 nanoparticles, Appl. Therm. Eng. 73 (2014) 1541–1547. doi:10.1016/j.applthermaleng.2014.05.078.

[167] S. Kim, L.T. Drzal, High latent heat storage and high thermal conductive phase change materials using exfoliated graphite nanoplatelets, Sol. Energy Mater. Sol. Cells. 93 (2009) 136–142. doi:10.1016/j.solmat.2008.09.010.

[168] P. Sobolciaka, M. Karkric, Al-Maadeeda, Krupab, Mariam, Igor, Thermal characterization of phase change materials based on linear low-density

polyethylene, paraffin wax and expanded graphite, Renew. Energy. 88 (2016) 372–382.

[169] Y. Lv, W. Zhou, W. Jin, Experimental and numerical study on thermal energy storage of polyethylene glycol/expanded graphite composite phase change material, (2016) 242–252.

[170] J. Wang, H. Xie, Z. Xin, Thermal properties of paraffin based composites containing multi-walled carbon nanotubes, Thermochim. Acta. 488 (2009) 39–42. doi:10.1016/j.tca.2009.01.022.

[171] M. Nourania, N. Hamdamia, J. Keramata, A. Mohebc, Mohammad Shahedia, Thermal behavior of paraffin-nano-Al2O3 stabilized by sodium stearoyl lactylate as a stable phase change material with high thermal conductivity, Renew. Energy. 88 (2016) 474–482.

[172] J.Y.G. C.J. Ho, Preparation and thermophysical properties of nanoparticle-in-paraffin emulsion as phase change materia, Int. Commun. Heat Mass Transf. 36 (2009) 467–470.

[173] L.-W. Fana, X. Fanga, X. Wanga, Y. Zenga, Y.-Q. Xiaoa, Z.-T. Yua, X. Xuc, Y.-C. Hua, K.-F. Cenb, Effects of various carbon nanofillers on the thermal conductivity and energy storage properties of paraffin-based nanocomposite phase change materials, Appl. Energy. 110 (2013) 163–172.

[174] C.J. Ho, J.Y. Gao, An experimental study on melting heat transfer of paraffin dispersed with Al_2O_3 nanoparticles in a vertical enclosure, Int. J. Heat Mass Transf. 62 (2013) 2–8.

[175] G. Raza, Y. Shi, Y. Deng, Expanded graphite as thermal conductivity enhancer for paraffin wax being used in thermal energy storage systems, 2016 13th Int. Bhurban Conf. Appl. Sci. Technol. (2016) 1–12. doi:10.1109/IBCAST.2016.7429846.

[176] Y. Cui, C. Liu, S. Hu, Xun Yu, The experimental exploration of carbon nanofiber and carbon nanotube additives on thermal behavior of phase change materials, Sol. Energy Mater. Sol. Cells. 95 (2011) 1208–1212.

[177] Z. Zhang, X. Fang, Study on paraffin/expanded graphite composite phase change thermal energy storage material, Energy Convers. Manag. 47 (2006) 303–310.

[178] J.M. Marína, B. Zalbaa, L.F. Cabezab, H. Mehlingc, Improvement of a thermal energy storage using plates with paraffin–graphite composite, Int. J. Heat Mass Transf. 48 (2005) 2561–2570.

[179] X. Xiao, P. Zhang, M. Li, Preparation and thermal characterization of paraffin/metal foam composite phase change material, Appl. Energy. 112 (2013) 1357–1366.

[180] A.A. Madhumathi, B.M.C. Sundarraja, Experimental study of passive cooling of building facade using phase change materials to increase thermal comfort in buildings in hot humid areas, Int. J. Energy Environ. 3 (2012) 739–748.

[181] T.M.I.M. R.K. Sharma, P. Ganesan, V.V. Tyagi, Accelerated thermal cycle and chemical stability testing of polyethylene glycol (PEG) 6000 for solar thermal energy storage, Sol. Energy Mater. Sol. Cells. 147 (2016) 235–239.

[182] C. Liang, X. Lingling, S. Hongbo, Z. Zhibin, Microencapsulation of butyl stearate as a phase change material by interfacial polycondensation in a polyurea system, Energy Convers. Manag. 50 (2009) 723–729. doi:10.1016/j.enconman.2008.09.044.

[183] J. Zuo, W. Li, L. Weng, Thermal performance of caprylic acid/1-dodecanol eutectic mixture as phase change material (PCM), Energy Build. 43 (2011) 207–210. doi:10.1016/j.enbuild.2010.09.008.

[184] H. He, P. Zhao, Q. Yue, B. Gao, D. Yue, Q. Li, A novel polynary fatty acid/sludge ceramsite composite phase change materials and its applications in building energy conservation, Renew. Energy. 76 (2015) 45–52. doi:10.1016/j.renene.2014.11.001.

[185] A. Sari, K. Kaygusuz, Thermal performance of palmitic acid as a phase change energy storage material, Energy Convers. Manag. 43 (2002) 863–876. doi:10.1016/S0196-8904(01)00071-1.

[186] G. Fang, H. Li, Z. Chen, X. Liu, Preparation and properties of palmitic acid/SiO2 composites with flame retardant as thermal energy storage materials, Sol. Energy Mater. Sol. Cells. 95 (2011) 1875–1881. doi:10.1016/j.solmat.2011.02.010.

[187] M. Mehrali, S.T. Latibari, M. Mehrali, T.M. Indra Mahlia, H.S. Cornelis Metselaar, M.S. Naghavi, E. Sadeghinezhad, A.R. Akhiani, Preparation and characterization of palmitic acid/graphene nanoplatelets composite with remarkable thermal conductivity as a novel shape-stabilized phase change material, Appl. Therm. Eng. 61 (2013) 633–640. doi:10.1016/j.applthermaleng.2013.08.035.

[188] A. Sari, A. Karaipekli, Preparation, thermal properties and thermal reliability of palmitic acid/expanded graphite composite as form-stable PCM for thermal energy storage, Sol. Energy Mater. Sol. Cells. 93 (2009) 571–576. doi:10.1016/j.solmat.2008.11.057.

[189] A. Sari, A. Karaipekli, K. Kaygusuz, Capric acid and myristic acid for latent heat thermal energy storage, Energy Sources, Part A Recover. Util. Environ. Eff. 30 (2008) 1498–1507. doi:10.1080/15567030701436362.

[190] Y. Konuklu, M. Unal, H.O. Paksoy, Microencapsulation of caprylic acid with different wall materials as phase change material for thermal energy storage, Sol. Energy Mater. Sol. Cells. 120 (2014) 536–542. doi:10.1016/j.solmat.2013.09.035.

[191] A. Karaipekli, A. Sari, K. Kaygusuz, Thermal conductivity improvement of stearic acid using expanded graphite and carbon fiber for energy storage applications, Renew. Energy. 32 (2007) 2201–2210. doi:10.1016/j.renene.2006.11.011.

[192] G. Fang, H. Li, Z. Chen, X. Liu, Preparation and characterization of stearic acid/expanded graphite composites as thermal energy storage materials, Energy. 35 (2010) 4622–4626. doi:10.1016/j.energy.2010.09.046.

[193] C. Alkan, A. Sari, Fatty acid/poly(methyl methacrylate) (PMMA) blends as form-stable phase change materials for latent heat thermal energy storage, Sol.

Energy. 82 (2008) 118–124. doi:10.1016/j.solener.2007.07.001.

[194] X. Li, H. Wei, X. Lin, X. Xie, Preparation of stearic acid/modified expanded vermiculite composite phase change material with simultaneously enhanced thermal conductivity and latent heat, Sol. Energy Mater. Sol. Cells. 155 (2016) 9–13. doi:10.1016/j.solmat.2016.04.057.

[195] A. Sari, K. Kaygusuz, Thermal performance of myristic acid as a phase change material for energy storage application, Renew. Energy. 24 (2001) 303–317. doi:10.1016/S0960-1481(00)00167-1.

[196] R. Wen, Z. Huang, Y. Huang, X. Zhang, X. Min, M. Fang, Y. Liu, X. Wu, Synthesis and characterization of lauric acid/expanded vermiculite as form-stabilized thermal energy storage materials, Energy Build. 116 (2016) 677–683. doi:10.1016/j.enbuild.2016.01.023.

[197] W. Wang, X. Yang, Y. Fang, J. Ding, J. Yan, Preparation and thermal properties of polyethylene glycol/expanded graphite blends for energy storage, Appl. Energy. 86 (2009) 1479–1483. doi:10.1016/j.apenergy.2008.12.004.

[198] Y. Wang, T.D. Xia, H.X. Feng, H. Zhang, Stearic acid/polymethylmethacrylate composite as form-stable phase change materials for latent heat thermal energy storage, Renew. Energy. 36 (2011) 1814–1820. doi:10.1016/j.renene.2010.12.022.

[199] R.K. Sharma, P. Ganesan, V. V. Tyagi, Long-term thermal and chemical reliability study of different organic phase change materials for thermal energy storage applications, J. Therm. Anal. Calorim. 124 (2016) 1357–1366. doi:10.1007/s10973-016-5281-5.

[200] Y. Tang, Y. Jia, G. Alva, X. Huang, G. Fang, Synthesis, characterization and properties of palmitic acid/high density polyethylene/graphene nanoplatelets composites as form-stable phase change materials, Sol. Energy Mater. Sol. Cells. 155 (2016) 421–429. doi:10.1016/j.solmat.2016.06.049.

[201] X. Jiang, Y. Rui, G. Chen, Improved Properties of Cotton by Atmospheric Pressure Plasma Polymerization Deposition of Sericin, J Vinyl Addit. Technol. 21 (2009) 129–133. doi:10.1002/vnl.

[202] A. Karaipekli, A. Biçer, A. Sarı, V.V. Tyagi, Thermal characteristics of expanded perlite/paraffin composite phase change material with enhanced thermal conductivity using carbon nanotubes, Energy Convers. Manag. 134 (2017) 373–381. doi:10.1016/j.enconman.2016.12.053.

[203] S. Wu, T.X. Li, T. Yan, Y.J. Dai, R.Z. Wang, High performance form-stable expanded graphite/stearic acid composite phase change material for modular thermal energy storage, Int. J. Heat Mass Transf. 102 (2016) 733–744.

[204] A. Sari, C. Alkan, A. Karaipekli, O. Uzun, Microencapsulated n-octacosane as phase change material for thermal energy storage, Sol. Energy. 83 (2009) 1757–1763. doi:10.1016/j.solener.2009.05.008.

[205] Z. Zhang, G. Shi, S. Wang, X. Fang, X. Liu, Thermal energy storage cement mortar containing n-octadecane/expanded graphite composite phase change material, Renew. Energy. 50 (2013) 670–675. doi:10.1016/j.renene.2012.08.024.

[206] L. Shilei, Z. Neng, F. Guohui, Eutectic mixtures of capric acid and lauric acid applied in building wallboards for heat energy storage, Energy Build. 38 (2006) 708–711. doi:10.1016/j.enbuild.2005.10.006.

[207] A. Sarı, H. Sarı, A. Önal, Thermal properties and thermal reliability of eutectic mixtures of some fatty acids as latent heat storage materials, Energy Convers. Manag. 45 (2004) 365–376. doi:10.1016/S0196-8904(03)00154-7.

[208] A. Sari, Eutectic mixtures of some fatty acids for low temperature solar heating applications: Thermal properties and thermal reliability, Appl. Therm. Eng. 25 (2005) 2100–2107. doi:10.1016/j.applthermaleng.2005.01.010.

[209] A. Sari, Eutectic mixtures of some fatty acids for latent heat storage: Thermal properties and thermal reliability with respect to thermal cycling, Energy Convers. Manag. 47 (2006) 1207–1221. doi:10.1016/j.enconman.2005.07.005.

[210] G. Baran, A. Sari, Phase change and heat transfer characteristics of a eutectic mixture of palmitic and stearic acids as PCM in a latent heat storage system, Energy Convers. Manag. 44 (2003) 3227–3246.

[211] A. Sari, Thermal reliability test of some fatty acids as PCMs used for solar thermal latent heat storage applications, Energy Convers. Manag. 44 (2003) 2277–2287. doi:10.1016/S0196-8904(02)00251-0.

[212] Ahmet Sarı, A. Karaipekli, Preparation and thermal properties of capric acid/palmitic acid eutectic mixture as a phase change energy storage material, Mater. Lett. 62 (2008) 903–906.

[213] K. Tunçbilek, A. Sari, S. Tarhan, G. Ergüneş, K. Kaygusuz, Lauric and palmitic acids eutectic mixture as latent heat storage material for low temperature heating applications, Energy. 30 (2005) 677–692. doi:10.1016/j.energy.2004.05.017.

[214] H. Fauzi, H.S.C. Metselaar, T.M.I. Mahlia, M. Silakhori, H. Nur, Phase change material: Optimizing the thermal properties and thermal conductivity of myristic acid/palmitic acid eutectic mixture with acid-based surfactants, Appl. Therm. Eng. 60 (2013) 261–265. doi:10.1016/j.applthermaleng.2013.06.050.

[215] H. Fauzi, H.S.C. Metselaar, T.M.I. Mahlia, M. Silakhori, H.C. Ong, Thermal characteristic reliability of fatty acid binary mixtures as phase change materials (PCMs) for thermal energy storage applications, Appl. Therm. Eng. 80 (2015) 127–131.

[216] A. Karaipekli, A. Sarı, Capric–myristic acid/expanded perlite composite as form-stable phase change material for latent heat thermal energy storage, Renew. Energy. 33 (2008) 2599–2605.

[217] L. Wang, Duo Meng, Fatty acid eutectic/polymethyl methacrylate composite as form-stable phase change material for thermal energy storage, Appl. Energy. 87 (2010) 2660–2665.

[218] A.S. Ali Karaipekli, Capric–myristic acid/vermiculite composite as form-stable phase change material for thermal energy storage, Sol. Energy. 83 (2009) 323–332.

[219] N. Zhang, Y. Yuan, X. Wang, X. Cao, X. Yang, S. Hu, Preparation and characterization of lauric-myristic-palmitic acid ternary eutectic mixtures/expanded graphite composite phase change material for thermal

energy storage, Chem. Eng. J. 231 (2013) 214–219. doi:10.1016/j.cej.2013.07.008.

[220] C. Jiao, B. Ji, D. Fang, Preparation and properties of lauric acid-stearic acid/expanded perlite composite as phase change materials for thermal energy storage, Mater. Lett. 67 (2012) 352–354. doi:10.1016/j.matlet.2011.09.099.

[221] H. Zhang, X. Gao, C. Chen, T. Xu, Y. Fang, Z. Zhang, A capric-palmitic-stearic acid ternary eutectic mixture/expanded graphite composite phase change material for thermal energy storage, Compos. Part A Appl. Sci. Manuf. 87 (2016) 138–145. doi:10.1016/j.compositesa.2016.04.024.

[222] Y. Tang, G. Alva, X. Huang, D. Su, L. Liu, G. Fang, Thermal properties and morphologies of MA-SA eutectics/CNTs as composite PCMs in thermal energy storage, Energy Build. 127 (2016) 603–610. doi:10.1016/j.enbuild.2016.06.031.

[223] M. Li, Z. Wu, H. Kao, Study on preparation and thermal properties of binary fatty acid/diatomite shape-stabilized phase change materials, Sol. Energy Mater. Sol. Cells. 95 (2011) 2412–2416. doi:10.1016/j.solmat.2011.04.017.

[224] M. Li, Z. Wu, H. Kao, Study on preparation, structure and thermal energy storage property of capric-palmitic acid/attapulgite composite phase change materials, Appl. Energy. 88 (2011) 3125–3132. doi:10.1016/j.apenergy.2011.02.030.

[225] H. Fauzi, H.S.C. Metselaar, T.M.I. Mahlia, H. Chyuan Ong, Nasruddin, H.M. Khanlou, Preparation and thermal characteristics of eutectic fatty acids/Shorea javanica composite for thermal energy storage, Appl. Therm. Eng. 100 (2016) 62–67. doi:10.1016/j.applthermaleng.2016.01.146.

[226] X. Tang, B. Zhu, M. Xu, W. Zhang, Z. Yang, Y. Zhang, G. Yin, D. He, H. Wei, X. Zhai, Shape-stabilized phase change materials based on fatty acid eutectics/expanded graphite composites for thermal storage, Energy Build. 109 (2015) 353–360. doi:10.1016/j.enbuild.2015.09.074.

[227] X. Yang, Y. Yuan, N. Zhang, X. Cao, C. Liu, Preparation and properties of myristic-palmitic-stearic acid/expanded graphite composites as phase change

materials for energy storage, Sol. Energy. 99 (2014) 259–266. doi:10.1016/j.solener.2013.11.021.

[228] M.A. Jackson, F.J. Eller, Isolation of long-chain aliphatic alcohols from beeswax using lipase-catalyzed methanolysis in supercritical carbon dioxide, J. Supercrit. Fluids. 37 (2006) 173–177. doi:10.1016/j.supflu.2005.08.008.

[229] A.A. Attama, B.C. Schicke, C.C. Müller-Goymann, Further characterization of theobroma oil-beeswax admixtures as lipid matrices for improved drug delivery systems, Eur. J. Pharm. Biopharm. 64 (2006) 294–306. doi:10.1016/j.ejpb.2006.06.010.

[230] S. Kheradmandnia, E. Vasheghani-Farahani, M. Nosrati, F. Atyabi, Preparation and characterization of ketoprofen-loaded solid lipid nanoparticles made from beeswax and carnauba wax, Nanomedicine Nanotechnology, Biol. Med. 6 (2010) 753–759. doi:10.1016/j.nano.2010.06.003.

[231] R. Buchwald, M.D. Breed, A.R. Greenberg, The thermal properties of beeswaxes: unexpected findings, J. Exp. Biol. 211 (2007) 121–127. doi:10.1242/jeb.007583.

[232] M.E. Hossain, M.I. Khan, C. Ketata, and M.R. Islam, comparative pathway analysis of paraffin wax and beeswax for industrial applications, J. Charact. Dev. Nov. Mater. 1 (2010) 1–13.

[233] V. V. Tyagi, A.K. Pandey, R. Kothari, S.K. Tyagi, Thermodynamics and performance evaluation of encapsulated PCM-based energy storage systems for heating application in building, J. Therm. Anal. Calorim. 115 (2014) 915–924. doi:10.1007/s10973-013-3215-z.

[234] A.A. El-Sebaii, S. Al-Heniti, F. Al-Agel, A.A. Al-Ghamdi, F. Al-Marzouki, One thousand thermal cycles of magnesium chloride hexahydrate as a promising PCM for indoor solar cooking, Energy Convers. Manag. 52 (2011) 1771–1777. doi:10.1016/j.enconman.2010.10.043.

[235] S. Canbazoglu, a Sahinaslan, a Ekmekyapar, Y. Aksoya, F. Akarsu, Enhancement of solar thermal energy storage performance using sodium thiosulfate pentahydrate of a conventional solar water-heating system, Energy

Build. 37 (2005) 235–242. doi:10.1016/j.enbuild.2004.06.016.

[236] C. Martin, T. Bauer, H. Müller-Steinhagen, An experimental study of a non-eutectic mixture of KNO_3 and $NaNO_3$ with a melting range for thermal energy storage, Appl. Therm. Eng. 56 (2013) 159–166. doi:10.1016/j.applthermaleng.2013.03.008.

[237] A.G. Fernández, S. Ushak, H. Galleguillos, F.J. Pérez, Thermal characterisation of an innovative quaternary molten nitrate mixture for energy storage in CSP plants, Sol. Energy Mater. Sol. Cells. 132 (2015) 172–177. doi:10.1016/j.solmat.2014.08.020.

[238] R.I. Olivares, W. Edwards, $LiNO_3$-$NaNO_3$-KNO_3 salt for thermal energy storage: Thermal stability evaluation in different atmospheres, Thermochim. Acta. 560 (2013) 34–42. doi:10.1016/j.tca.2013.02.029.

[239] H.T. Zhang, Y.J. Zhao, J.L. Li, L.J. Shi, M. Wang, Preparation and Heat Transfer/Thermal Storage Properties of High-Temperature Molten Nitrate Salts, Mater. Sci. Forum. 814 (2015) 60–64. doi:10.4028/www.scientific.net/MSF.814.60.

[240] Y. Jiang, F. Bruno, A. Sa, S. Li, A new phase change material for high temperature thermal energy storage, (2017) 1–6.

[241] X. Wei, M. Song, W. Wang, J. Ding, J. Yang, Design and thermal properties of a novel ternary chloride eutectics for high-temperature solar energy storage, Appl. Energy. 156 (2015) 306–310. doi:10.1016/j.apenergy.2015.07.022.

[242] P. Li, E. Molina, K. Wang, X. Xu, G. Dehghani, A. Kohli, Q. Hao, M.H. Kassaee, S.M. Jeter, A.S. Teja, Thermal and Transport Properties of NaCl–KCl–$ZnCl_2$ Eutectic Salts for New Generation High-Temperature Heat-Transfer Fluids, J. Sol. Energy Eng. 138 (2016) 54501. doi:10.1115/1.4033793.

[243] T. Wang, D. Mantha, R.G. Reddy, Novel high thermal stability LiF-Na_2CO_3-K_2CO_3 eutectic ternary system for thermal energy storage applications, Sol. Energy Mater. Sol. Cells. 140 (2015) 366–375. doi:10.1016/j.solmat.2015.04.033.

[244] J. Lopez, Z. Acem, E. Palomo Del Barrio, $KNO_3/NaNO_3$- Graphite materials for thermal energy storage at high temperature: Part II. - Phase transition properties, Appl. Therm. Eng. 30 (2010) 1586–1593. doi:10.1016/j.applthermaleng.2010.03.014.

[245] L. Ye, C. Tang, Y. Chen, S. Yang, M. Tang, The thermal physical properties and stability of the eutectic composition in a Na_2CO_3-NaCl binary system, Thermochim. Acta. 596 (2014) 14–20. doi:10.1016/j.tca.2014.07.002.

[246] K. Posern, C. Kaps, Calorimetric studies of thermochemical heat storage materials based on mixtures of $MgSO_4$ and $MgCl_2$, Thermochim. Acta. 502 (2010) 73–76. doi:10.1016/j.tca.2010.02.009.

[247] Z. Huang, X. Gao, T. Xu, Y. Fang, Z. Zhang, Thermal property measurement and heat storage analysis of $LiNO_3$/KCl - expanded graphite composite phase change material, Appl. Energy. 115 (2014) 265–271. doi:10.1016/j.apenergy.2013.11.019.

[248] L. Zhong, X. Zhang, Y. Luan, G. Wang, Y. Feng, D. Feng, Preparation and thermal properties of porous heterogeneous composite phase change materials based on molten salts/expanded graphite, Sol. Energy. 107 (2014) 63–73. doi:10.1016/j.solener.2014.05.019.

[249] H. Tian, W. Wang, J. Ding, X. Wei, C. Huang, Preparation of binary eutectic chloride/expanded graphite as high-temperature thermal energy storage materials, Sol. Energy Mater. Sol. Cells. 149 (2016) 187–194. doi:10.1016/j.solmat.2015.12.038.

[250] R. Li, J. Zhu, W. Zhou, X. Cheng, Y. Li, Thermal compatibility of Sodium Nitrate/Expanded Perlite composite phase change materials, Appl. Therm. Eng. 103 (2016) 452–458. doi:10.1016/j.applthermaleng.2016.03.108.

[251] P.D. Myers, T.E. Alam, R. Kamal, D.Y. Goswami, E. Stefanakos, Nitrate salts doped with CuO nanoparticles for thermal energy storage with improved heat transfer, Appl. Energy. 165 (2016) 225–233. doi:10.1016/j.apenergy.2015.11.045.

[252] D. Shin, D. Banerjee, Specific heat of nanofluids synthesized by dispersing

alumina nanoparticles in alkali salt eutectic, Int. J. Heat Mass Transf. 74 (2014) 210–214. doi:10.1016/j.ijheatmasstransfer.2014.02.066.

[253] D. Shin, D. Banerjee, Enhancement of specific heat capacity of high-temperature silica-nanofluids synthesized in alkali chloride salt eutectics for solar thermal-energy storage applications, Int. J. Heat Mass Transf. 54 (2011) 1064–1070. doi:10.1016/j.ijheatmasstransfer.2010.11.017.

[254] M. Chieruzzi, A. Miliozzi, T. Crescenzi, L. Torre, J.M. Kenny, A New Phase Change Material Based on Potassium Nitrate with Silica and Alumina Nanoparticles for Thermal Energy Storage, Nanoscale Res Lett. 10 (2015) 984. doi:10.1186/s11671-015-0984-2.

[255] C. Liu, D. Groulx, Experimental study of the phase change heat transfer inside a horizontal cylindrical latent heat energy storage system, Int. J. Therm. Sci. 82 (2014) 100–110.

[256] R.E. Murray, D. Groulx, Experimental study of the phase change and energy characteristics inside a cylindrical latent heat energy storage system: Part 2 simultaneous charging and discharging, Renew. Energy. 63 (2014) 724–734. doi:10.1016/j.renene.2013.10.004.

[257] S.P. Jesumathy, M. Udayakumar, S. Suresh, S. Jegadheeswaran, An experimental study on heat transfer characteristics of paraffin wax in horizontal double pipe heat latent heat storage unit, J. Taiwan Inst. Chem. Eng. 45 (2014) 1298–1306. doi:10.1016/j.jtice.2014.03.007.

[258] S. Lorente, A. Bejan, J.L. Niu, Phase change heat storage in an enclosure with vertical pipe in the center, Int. J. Heat Mass Transf. 72 (2014) 329–335. doi:10.1016/j.ijheatmasstransfer.2014.01.021.

[259] S. Mat, A.A. Al-Abidi, K. Sopian, M.Y. Sulaiman, A.T. Mohammad, Enhance heat transfer for PCM melting in triplex tube with internal-external fins, Energy Convers. Manag. 74 (2013) 223–236. doi:10.1016/j.enconman.2013.05.003.

[260] M. Rahimi, A.A. Ranjbar, D.D. Ganji, K. Sedighi, M.J. Hosseini, R. Bahrampoury, Analysis of geometrical and operational parameters of PCM in a fin and tube heat exchanger, Int. Commun. Heat Mass Transf. 53 (2014) 109–

115. doi:10.1016/j.icheatmasstransfer.2014.02.025.

[261] Y.L. Shabtay, J.R.H. Black, Compact hot water storage systems combining copper tube with high conductivity graphite and phase change materials, Energy Procedia. 48 (2014) 423–430. doi:10.1016/j.egypro.2014.02.049.

[262] M. Johnson, M. Fiss, T. Klemm, M. Eck, Test and analysis of a flat plate latent heat storage design, Energy Procedia. 57 (2014) 662–671. doi:10.1016/j.egypro.2014.10.221.

[263] M. Liu, M. Belusko, N.H. Steven Tay, F. Bruno, Impact of the heat transfer fluid in a flat plate phase change thermal storage unit for concentrated solar tower plants, Sol. Energy. 101 (2014) 220–231. doi:10.1016/j.solener.2013.12.030.

[264] N. Soares, A.R. Gaspar, P. Santos, J.J. Costa, Experimental study of the heat transfer through a vertical stack of rectangular cavities filled with phase change materials, Appl. Energy. 142 (2015) 192–205. doi:10.1016/j.apenergy.2014.12.034.

[265] H. Shokouhmand, B. Kamkari, Experimental investigation on melting heat transfer characteristics of lauric acid in a rectangular thermal storage unit, Exp. Therm. Fluid Sci. 50 (2013) 201–222. doi:10.1016/j.expthermflusci.2013.06.010.

[266] D. Cano, C. Funéz, L. Rodriguez, J.L. Valverde, L. Sanchez-Silva, Experimental investigation of a thermal storage system using phase change materials, Appl. Therm. Eng. 107 (2016) 264–270. doi:10.1016/j.applthermaleng.2016.06.169.

[267] Z. Khan, Z. Khan, K. Tabeshf, Parametric investigations to enhance thermal performance of paraffin through a novel geometrical configuration of shell and tube latent thermal storage system, Energy Convers. Manag. 127 (2016) 355–365. doi:10.1016/j.enconman.2016.09.030.

[268] E. Zambolin, D. Del Col, Experimental analysis of thermal performance of flat plate and evacuated tube solar collectors in stationary standard and daily conditions, Sol. Energy. 84 (2010) 1382–1396.

doi:10.1016/j.solener.2010.04.020.

[269] H. Shabgard, T.L. Bergman, N. Sharifi, A. Faghri, High temperature latent heat thermal energy storage using heat pipes, Int. J. Heat Mass Transf. 53 (2010) 2979–2988. doi:10.1016/j.ijheatmasstransfer.2010.03.035.

[270] F. Agyenim, P. Eames, M. Smyth, Heat transfer enhancement in medium temperature thermal energy storage system using a multitube heat transfer array, Renew. Energy. 35 (2010) 198–207. doi:10.1016/j.renene.2009.03.010.

[271] M. Bechiri, K. Mansouri, Analytical solution of heat transfer in a shell-and-tube latent thermal energy storage system, Renew. Energy. 74 (2015) 825–838. doi:10.1016/j.renene.2014.09.010.

[272] S. Lorente, A. Bejan, J.L. Niu, Constructal design of latent thermal energy storage with vertical spiral heaters, Int. J. Heat Mass Transf. 81 (2015) 283–288. doi:10.1016/j.ijheatmasstransfer.2014.09.077.

[273] T. Pirasaci, D.Y. Goswami, Influence of design on performance of a latent heat storage system for a direct steam generation power plant, Appl. Energy. 162 (2016) 644–652. doi:10.1016/j.apenergy.2015.10.105.

[274] H. Niyas, S. Prasad, P. Muthukumar, Performance investigation of a lab–scale latent heat storage prototype – Numerical results, Energy Convers. Manag. 135 (2017) 188–199. doi:10.1016/j.enconman.2016.12.075.

[275] M. Aadmi, M. Karkri, M. El Hammouti, Heat transfer characteristics of thermal energy storage of a composite phase change materials: Numerical and experimental investigations, Energy. 72 (2014) 381–392. doi:10.1016/j.energy.2014.05.050.

[276] H. Mousa, A.M. Gujarathi, Modeling and analysis the productivity of solar desalination units with phase change materials, Renew. Energy. 95 (2016) 225–232. doi:10.1016/j.renene.2016.04.013.

[277] A. Revesz, I. Chaer, J. Thompson, M. Mavroulidou, M. Gunn, G. Maidment, Ground source heat pumps and their interactions with underground railway tunnels in an urban environment: A review, Appl. Therm. Eng. 93 (2016) 147–

154. doi:10.1016/j.applthermaleng.2015.09.011.

[278] A. Fopah-Lele, F. Kuznik, T. Osterland, W.K.L. Ruck, Thermal synthesis of a thermochemical heat storage with heat exchanger optimization, Appl. Therm. Eng. 101 (2016) 669–677. doi:10.1016/j.applthermaleng.2015.12.103.

[279] Y. Allouche, S. Varga, C. Bouden, A.C. Oliveira, Validation of a CFD model for the simulation of heat transfer in a tubes-in-tank PCM storage unit, Renew. Energy. 89 (2016) 371–379. doi:10.1016/j.renene.2015.12.038.

[280] J.L. Zeng, J. Gan, F.R. Zhu, S.B. Yu, Z.L. Xiao, W.P. Yan, L. Zhu, Z.Q. Liu, L.X. Sun, Z. Cao, Tetradecanol/expanded graphite composite form-stable phase change material for thermal energy storage, Sol. Energy Mater. Sol. Cells. 127 (2014) 122–128. doi:10.1016/j.solmat.2014.04.015.

[281] S. Kakaç, A. Pramuanjaroenkij, Review of convective heat transfer enhancement with nanofluids, Int. J. Heat Mass Transf. 52 (2009) 3187–3196. doi:10.1016/j.ijheatmasstransfer.2009.02.006.

[282] J. Albadr, S. Tayal, M. Alasadi, Heat transfer through heat exchanger using Al2O3 nanofluid at different concentrations, Case Stud. Therm. Eng. 1 (2013) 38–44. doi:10.1016/j.csite.2013.08.004.

[283] M.R. Salimpour, Heat transfer coefficients of shell and coiled tube heat exchangers, Exp. Therm. Fluid Sci. 33 (2009) 203–207. doi:10.1016/j.expthermflusci.2008.07.015.

[284] D.G. Prabhanjan, T.J. Rennie, G.S.V. Raghavan, Natural convection heat transfer from helical coiled tubes, Int. J. Therm. Sci. 43 (2004) 359–365. doi:10.1016/j.ijthermalsci.2003.08.005.

[285] A. Yasmin, J.J. Luo, I.M. Daniel, Processing of expanded graphite reinforced polymer nanocomposites, Compos. Sci. Technol. 66 (2006) 1179–1186. doi:10.1016/j.compscitech.2005.10.014.

[286] G. Zheng, J. Wu, W. Wang, C. Pan, Characterizations of expanded graphite/polymer composites prepared by in situ polymerization, Carbon N. Y. 42 (2004) 2839–2847. doi:10.1016/j.carbon.2004.06.029.

[287] M. Zhao, P. Liu, Adsorption of methylene blue from aqueous solutions by modified expanded graphite powder, Desalination. 249 (2009) 331–336. doi:10.1016/j.desal.2009.01.037.

[288] Z. Sun, Y. Zhang, S. Zheng, Y. Park, R.L. Frost, Preparation and thermal energy storage properties of paraffin/calcined diatomite composites as form-stable phase change materials, Thermochim. Acta. 558 (2013) 16–21. doi:10.1016/j.tca.2013.02.005.

[289] S. Patel, D.R. Nelson, a G. Gibbs, Chemical and physical analyses of wax ester properties., J. Insect Sci. 1 (2001) 4. doi:10.1093/jis/1.1.4.

[290] N.M. Ranjha, H. Khan, S. Naseem, Encapsulation and characterization of controlled release flurbiprofen loaded microspheres using beeswax as an encapsulating agent, J. Mater. Sci. Mater. Med. 21 (2010) 1621–1630. doi:10.1007/s10856-010-4034-4.

[291] W. Luo, T. Li, C. Wang, F. Huang, Discovery of Beeswax as binding agent on a 6th-century BC Chinese Turquoise-inlaid Bronze sword, J. Archaeol. Sci. 39 (2012) 1227–1237. doi:10.1016/j.jas.2011.12.035.

[292] L. Xia, P. Zhang, R.Z. Wang, Preparation and thermal characterization of expanded graphite/paraffin composite phase change material, Carbon N. Y. 48 (2010) 2538–2548. doi:10.1016/j.carbon.2010.03.030.

[293] B.S.V.S.R. Krishna, prediction of pressure drop in helical coil with single phase flow of non-newtonian fluid introduction :, (2012) 31–36.

[294] M. Avci, M.Y. Yazici, Experimental study of thermal energy storage characteristics of a paraffin in a horizontal tube-in-shell storage unit, Energy Convers. Manag. 73 (2013) 271–277. doi:10.1016/j.enconman.2013.04.030.

[295] D. Mei, B. Zhang, R. Liu, Y. Zhang, J. Liu, Preparation of capric acid/halloysite nanotube composite as form-stable phase change material for thermal energy storage, Sol. Energy Mater. Sol. Cells. 95 (2011) 2772–2777. doi:10.1016/j.solmat.2011.05.024.

[296] G.J. Suppes, M.J. Goff, S. Lopes, Latent heat characteristics of fatty acid

derivatives pursuant phase change material applications, Chem. Eng. Sci. 58 (2003) 1751–1763. doi:10.1016/S0009-2509(03)00006-X.

[297] X. Wang, X. Xu, S.U. S. Choi, Thermal Conductivity of Nanoparticle - Fluid Mixture, J. Thermophys. Heat Transf. 13 (1999) 474–480. doi:10.2514/2.6486.

[298] H. Kwak, D. Shin, D. Banerjee, Es2010- Heat Transfer Fluid Based Nanofluid for Solar Thermal Energy, (2010) 1–5.

[299] M. Chieruzzi, G.F. Cerritelli, A. Miliozzi, J.M. Kenny, Effect of nanoparticles on heat capacity of nanofluids based on molten salts as PCM for thermal energy storage., Nanoscale Res. Lett. 8 (2013) 448. doi:10.1186/1556-276X-8-448.

[300] Z. Zhang, N. Zhang, J. Peng, X. Fang, X. Gao, Y. Fang, Preparation and thermal energy storage properties of paraffin/expanded graphite composite phase change material, Appl. Energy. 91 (2012) 426–431. doi:10.1016/j.apenergy.2011.10.014.

[301] M.J. Hosseini, A.A. Ranjbar, K. Sedighi, M. Rahimi, A combined experimental and computational study on the melting behavior of a medium temperature phase change storage material inside shell and tube heat exchanger, Int. Commun. Heat Mass Transf. 39 (2012) 1416–1424. doi:10.1016/j.icheatmasstransfer.2012.07.028.

[302] M.K. Rathod, J. Banerjee, Experimental investigations on latent heat storage unit using paraffin wax as phase change material, Exp. Heat Transf. 27 (2014) 40–55. doi:10.1080/08916152.2012.719065.

[303] S. Wu, G. Fang, X. Liu, Dynamic discharging characteristics simulation on solar heat storage system with spherical capsules using paraffin as heat storage material, Renew. Energy. 36 (2011) 1190–1195. doi:10.1016/j.renene.2010.10.012.

[304] Y. Özonur, M. Mazman, H.Ö. Paksoy, H. Evliya, Microencapsulation of coco fatty acid mixture for thermal energy storage with phase change material, Int. J. Energy Res. 30 (2006) 741–749. doi:10.1002/er.1177.

Thesis

ORIGINALITY REPORT

4%	2%	5%	2%
SIMILARITY INDEX	INTERNET SOURCES	PUBLICATIONS	STUDENT PAPERS

PRIMARY SOURCES

1	Submitted to University of Cape Town Student Paper	1%
2	Sharma, R.K., P. Ganesan, V.V. Tyagi, H.S.C. Metselaar, and S.C. Sandaran. "Developments in organic solid–liquid phase change materials and their applications in thermal energy storage", Energy Conversion and Management, 2015. Publication	1%
3	Pielichowska, Kinga, and Krzysztof Pielichowski. "Phase change materials for thermal energy storage", Progress in Materials Science, 2014. Publication	1%
4	Zhang, P., X. Xiao, and Z.W. Ma. "A review of the composite phase change materials: Fabrication, characterization, mathematical modeling and application to performance enhancement", Applied Energy, 2016. Publication	1%

APPENDIX

Calculation of Efficiency and heat transfer coefficient for thermal storage unit

1) Efficiency of thermal storage unit

a) At the flow rate of 0.5 LPM and 80°C

Q_a = Heat available for thermal storage = Δt x $\dot{m}$ x C_{pw} $\Sigma\Delta T$

Δt = 15 min, $\Sigma\Delta T$ = 220K (as observed from data table), C_p = 4.196 kJ/kg.K, $\dot{m}$ = 0.5 LPM

Therefore, Q_a = 6.923 MJ

Heat available in terms of power = $\frac{6.923\ MJ}{1650\ min\ x\ 60\ s}$ = 69.92 W

Amount of heat required by beeswax to reach the charge completely

$$Q_w = m_w [C_{ps} (T_m - T_i) + L + C_{pl}(T_f - T_m)]$$

Given, m_w = 18 kg, C_{ps} = 2.6 kJ/kg.K, C_{pl} = 3 kJ/kg.K T_m = 59.8 °C, T_i = 35 °C, L = 214 kJ/Kg, T_f = 75 °C

Q_w = 5.833 MJ

Efficiency of thermal storage unit, $\eta = \frac{Q_w}{Q_a}$ = 5.833 MJ/6.923 MJ = 84.25%.

2.) Internal heat transfer cofficient

Internal heat transfer coefficient was calculated by correlation:

$$Nu_i = 0.152\ D_e^{0.431}\ Pr^{1.06}\ \gamma^{-0.277}$$

v = velocity of fluid calculated as = flow rate/cross section area of tube = $\frac{\dot{m}}{\pi r_i^2}$ = 0.5 x 10^{-3} (m^3)/60(s) x 3.14 x $(4)^2$ x 10^{-6} (m^2) = 0.165 m/s.

d_i = 8 mm

μ = 0.355 x 10^{-3} N s m^{-2} at 80 °C.

ρ = 971.8 kg/m^3 at 80 °C

k = 0.670 W/m.K

Reynold's number = $R_e = \frac{\rho v d_i}{\mu}$ = (971.8 x 0.165 x 8 x 10^{-3}) / 0.355 x 10^{-3} = 3613.45 ≈ 3613

where, Rc = 55.3 mm

Dean number $D_e = R_e \left(\frac{d_i}{2R_c}\right)^{0.5}$ = 971.70 ≈ 972

Dimensionless pitch $\gamma = b/2\pi R_c$ = 0.086

Prandlt number = Pr = $\mu \frac{C_p}{k}$ = 2.22

Therefore, $Nu_i = 0.152\ D_e^{0.431} P_r^{1.06} \gamma^{-0.277}$ = 0.152 $(972)^{0.431}(2.22)^{1.06}(0.086)^{-0.277}$

$$Nu_i = 13.54$$

Now, $Nu_i = \frac{h_i d_i}{k} = \frac{h_i\ x\ 8\ x\ 10^{-3}(m)}{0.670\ (\frac{W}{m}.K)}$ = 13.54

Therefore, $h_i = \frac{13.54\ x\ 0.670}{8\ x\ 10^{-3}}$ = 1133.97 ≈ 1134

3) External heat transfer coefficient:

Using following correlation given below h_o can be calculated –

$Nu_o = 0.381\ (Ra_o)^{0.293}$ (2)

R_a = Gr. Pr

Where Gr_r calculated as, $Gr = \frac{g\beta\Delta T D^3}{V^2}$

Therefore,

Gr = 2624.890

Pr = $\mu \frac{C_p}{k}$ where u for beeswax = 4.8 x 10^{-3} Ns/m^2

Therefore Pr = 49.56

R_a = Gr x Pr = 2624.890 x 49.56 = 1.3 x 10^5

Now,

$Nu_o = 0.381\ (Ra_o)^{0.293}$

$Nu_o = 0.381\ (1.3 \times 10^5)^{0.293} = 12.05$

$Nu_o = h_o d_o / k$

Therefore, $h_o =$ 386.78 W/mk

Calculation of thermal conductivities of heat transfer coefficient

1) Thermal conductivity of EG/water suspension

Concentration = 0.05 wt. % at 80 °C

Hamilton-crosser equation :

$$\frac{K_{eff}}{K_f} = \frac{K_p+(n-1)K_f-(n-1)\emptyset(K_f-K_p)}{K_p+(n-1)K_f+\emptyset(K_f-K_p)}$$

For expanded graphite n = 3/ψ = 6 (where ψ = 0.5 for graphite)

Kp = thermal conductivity of solute (graphite) = 97 W/m.K

Kf = thermal conductivity of base fluid (water at 80 °C) = 0.670 W/m.K

∅ = mass fraction of solute = 0.0107

Keff = effective thermal conductivity of solution

Therefore,

$$\frac{K_{eff}}{0.670} = \frac{97+(6-1)0.670-(6-1).01074(0.670-97)}{97+(6-1)0.670+0.01074(0.670-97)}$$

K_{eff} = 0.711 W/m.k

1) Uncertainity analysis in measurement of temperature

The total uncertainity in temperature measurement is the quadratic sum of three component

a) Maxiumu uncertainity provided by manufacturer = 0.1%

Therefore, $\frac{\Delta T}{T}$ = 0.1 %, which gives ΔT_1 = 0.353 K

b) Maximum uncertainity in measurement of temperature

= 3 x standard deviation of calibration curve fit =ΔT_2= 3 x 0.6535 = 1.96 K

c) Maximum uncertainity in average estimation of 10 readings

ΔT_3 = 3 x 0.01 = 0.03

Total uncertainity in tempartaure measurement = $\Delta T = \sqrt{\Delta T_1^2 + \Delta T_2^2 + \Delta T_3^2}$

Which gives $\Delta T = 1.99\ K$

Therefore $\Delta T/T$ = 0.5%.

Calculation of latent heat from DSC curve (Instrument Calculations) :

Heat flow in sample = ΔQ (mW), mass of sample on DSC pan = m(g), Rate of heating = τ (K/sec)

Therefore, the latent heat of material = $\frac{\Delta Q}{1000 \times m \times \tau}$ (kJ/g.s)

Calculation of critical Reynold's number for Helical coil :

For helical coil the critical Reynold's number is given by the relation :

$Rec = 2100(1 + 12(d/D)^{1/2})$

Where, Rec = Critical Reynold's number for helical coil, d = Diameter of tube, D = Diameter of helical coil,

Since, d = 9 mm, D = 110.6 mm. Therefore , $Rec = 2100\ (1+ 12(9/110.6)^{1/2}) = 9289$

BIOGRAPHY

Abhay Dinker

Address: P27, Krishna vihar colony Pratap Nagar, Jaipur- 302011, Rajasthan

Email: dinkerabhay@hotmail.com

Ph: +91-9785074291
+91-9007775250

Career Objective

To work with a reputed institution that will provide me a good platform to utilize my teaching, research & administration skills and will help me to grow my career.

Work Experience

Designation: Assistant system engineer (13 September 2012 – 27 September 2013)
Department: SAP ABAP
Organization: IBM Kolkata

Specialization Area(s)

Heat transfer, Renewable energy, Thermal energy storage, Storage materials and characterization, Modeling and Simulation, Biotechnology

Academic Background

Year	Qualification	College/School	University/Board	%/CGPA
2013-2017	Ph. D (submitted)	Department of Chemical Engineering	MNIT Jaipur	8
2012	M. Tech	Department of Chemical Engineering	MNIT Jaipur	8.27
2010	B. Tech	Department of Biotechnology	IASE University	77.4%
2004	XII	Air Force School, Jaipur	C.B.S.E.	70.2%
2002	X	Air Force School, Jaipur	C.B.S.E.	67.8%

Award(s) and Achievement(s)

- Secured 2nd Rank in B. Tech batch at university level.
- Member of Air force School Orchestra from 2006-2012.
- Member of School Basketball team.
- Worked for Help Age India Foundation as fund raiser.

Professional Skills

- One year teaching experience (tutorial sessions and practical lab as teaching assistantship during Ph.D. course).
- Thorough understanding of the subject with an ability to convey the same to the students.
- Computer based modeling, simulation and control techniques used in the chemical Industries via COMSOL.
- Profound knowledge of fundamental development languages such as PERL, BIOPERL, SAP ABAP.
- Well equipped with the techniques of biotechnology and chemical engineering.
- Good communication and comprehension abilities.

Conferences, Workshops, Short Term Projects and Training (Attended/ Organized)

1. One year project work on *Optimization of bioethanol production from brewer's spent grain using mixed fungal cultures* at Birla institute of scientific research and Malaviya national institute of Technology Jaipur.

2. Six months project on *Production of Magnetic Nanoparticles embedded in polystyrene microspheres and their application for oil removal from waste water* at Malaviya National Institute of Technology Jaipur.

3. Two months industrial training at SAB MILLER India, Rochees Brewery, Neemrana, Alwar, Rajasthan.

4. One month training on *Quantitative analysis of ibucomb* at Scortis Healthcare, Elcon drugs and formulations, Bindayka industrial area, Jaipur, Rajasthan.

5. One month training on *Molecular biological techniques and their applications* at Chemind Biosolutions, Sodala Jaipur Rajasthan.

6. One month training on *Quality control in dairy* at Saras Diary, JLN Marg Jaipur.

7. National workshop on *Genome Data Analysis* at Bioinformatics Sub-center, Devi Ahilya University, Indore.

8. National conference on *All India Seminar on Nanotechnology and its Application-2011,* organized by Arya College of Engineering, Kukas Jaipur (9-10 July 2011).

9. Conference on *International Conference on Green Chemistry-2011*, at Hotel Fortune Bella casa, Jaipur. Organized by Department of Chemistry, School of chemical sciences and Pharmacy, Central University of Rajasthan, Kishangarh. Ajmer, Rajasthan (7-9 December 2011).

10. Conference on *Technical Advancements in Chemical and Environment Engineering-2012*, at Birla Institute of Technology and Sciences, Pilani, Rajasthan (23-24 March 2012).

11. Conference on *Recent Advances in Bioenergy Research-2013, at* Sardar Swarn Singh National Institute of Renewable Energy, Kapurthala, Punjab (22-24 November 2013).

12. Workshop on *International Workshop on Green Initiatives Energy, Environment and Health-2013,* New Delhi.

13. Conference on *2nd International Conference on Emerging Technologies : Micro to Nano*, at Manipal University, Jaipur (24-25 October 2015).

Journal Publication(s)

1. **Dinker**, A. Agarwal, M. and Agarwal, G.D. "Experimental assessment on thermal storage performance of beeswax in helical tube embedded storage unit",*Applied Thermal Engineering,* volume 111, pp. 358-368 doi: 10.1016/j.applthermaleng.2016.09.128.

2. **Dinker,** A., Agarwal, M. and Agarwal, G.D. "Heat storage materials, geometry and applications: A review**",** *Journal of Energy Institute***,** Elsevier publication, doi:10.1016/j.joei.2015.10.002, *In press*.

3. **Dinker,** A., Agarwal, M. and Agarwal, G.D. "Preparation, characterization and performance study of beeswax/expanded graphite composite as thermal storage material", *Experimental heat transfer*, Taylor and Francis publications doi:10.1080/08916152.2016.1185198.

4. Agarwal, M. and **Dinker,** A. "Application of consolidate enzymatic system of Fusarium and Saccharomyces to enhance the production of ethanol from spent grain" (2013), *Journal of Renewable and Sustainable Energy,* 5, doi: 10.1063/1.48.

5. **Dinker** A., Agarwal, M. and Agarwal, G.D. "Thermal conductivity enhancement of stearic acid using expanded graphite for low temperature thermal storage", International Journal of Engineering Science and Innovative Technology, Volume :3/2014.

6. Agarwal, M., Patel, D. and **Dinker,** A. "Optimization of Manganese Removal from Water Using Response Surface Methodology", Iranian Journal of Science and Technology, Transactions A: Science, volume 40, issue 6, pp 63-73 doi: 10.1007/s40995-016-0013-z.

7. **Dinker A**., Agarwal, M. and Agarwal, G.D. "Performance study of beeswax/expanded graphite composite for thermal energy storage in a shell and tube unit" *Renewable Energy,* Elsevier publication (communicated)

Conference Proceeding(s)

1. **Dinker**, A., Agarwal, M. and Agarwal, G.D. "Preparation of expanded graphite and stearic acid composite for the low temperature thermal storage" *Proceedings of 67th Annual Session of IIChE and Indo-Japnese Symposium"* Jointly organized by Chandigarh Regional Center, IIChE and Dr, SSB University Institute of Chemical Engineering & Technology, Chandigarh, December 27-30, 2014.

2. **Dinker**, A., Agarwal, M. and Agarwal, G.D. "Experimental Study on Thermal Performance of Beeswax as Thermal Storage Material" *proceedings of International Conference On Recent Trends In Engineering And Material Sciences (ICEMS-2016)* " Organized by Jaipur National University, Jaipur.

3. **Dinker**, A., Agarwal, M. and Agarwal, G.D**. "**Thermal performance analysis of beeswax as thermal storage material with different types of heat transfer fluids" *Proceedings of International Conference on Computational Technology (ICCT -2016).*

Membership (s) / Professional Affiliation (s)

S. No.	**Name of Institution/ Society**	**Grade of Membership**	**Date of Election**
1.	Indian Institute of Chemical Engineers	Life Associate Member (ID: LAM52066)	2 August 2015
2.	Indian Desalination Association	Life Member (ID: LM427)	6 January 2017

Extra Curricular

- Member of Air Force School basketball team.
- Member of Air Force School orchestra team.
- Directed Award winning plays and add made shows at university level.
- Worked with Help Age India for collection of credits.

Declaration

I hereby declare that the above-mentioned information is correct up to my knowledge and I bear the responsibility for the correctness of the above-mentioned particulars.

Date: 26/08/2017
Place: Jaipur **Abhay Dinker**

Journal of the Energy Institute xxx (2015) 1–11

Contents lists available at ScienceDirect

Journal of the Energy Institute

journal homepage: http://www.journals.elsevier.com/journal-of-the-energy-institute

Heat storage materials, geometry and applications: A review

Abhay Dinker [a], Madhu Agarwal [a, *], G.D. Agarwal [b]

[a] Department of Chemical Engineering, Malaviya National Institute of Technology, Jaipur, India
[b] Department of Mechanical Engineering, Malaviya National Institute of Technology, Jaipur, India

ARTICLE INFO

Article history:
Received 1 June 2015
Received in revised form
6 October 2015
Accepted 6 October 2015
Available online xxx

Keywords:
Phase change materials
Expanded graphite
Latent heat storage
Thermal cycling
Thermal storage system

ABSTRACT

This paper reviews various kinds of heat storage materials, their composites and applications investigated over the last two decades. It was found that sensible heat storage systems are bulkier in size as compared to the latent heat storage systems. Latent heat storage system using phase change materials (PCMs) stores energy at high density in isothermal way. Various geometries of PCM containers used for enhancement of heat transfer area, materials used for the construction of PCM containers and their interaction with heat storage materials are studied. The choice of storage material depends on the desired temperature range, application of thermal storage unit and size of thermal storage system. Low temperature heat storage system uses organic phase change materials while inorganic phase change materials are best suited for high temperature heat storage. Heat transfer within the PCM can be enhanced by preparing composite of high thermal conductivity as well as by altering the geometrical design like addition of fins, use of straight and helical tubes etc. Shell and tube configurations were mostly used for thermal storage systems. Heat transfer enhancement using PCM composite is a promising approach as it reduces cost and bulkiness to the system.

1. Introduction

Energy storage techniques is one of the major concerns of the present century due to shortage of conventional nonrenewable sources of energy, increased environmental pollution, increased gap between energy supply and demand, and non-uniform distribution of renewable energy sources like solar energy, wind energy, geothermal energy and energy from ocean currents. Energy recovery systems also encountered with the problem of utilization and availability of energy at different time intervals and hence require energy storage systems for uninterrupted power supply [1,2]. Present energy storage systems relies on electrochemical energy in which Li ion batteries have shown their great potential and acquired a large portion of energy storage market as compare to conventional lead acid batteries [3]. The major advantage of using batteries is high energy density storage while the disadvantage is environmental pollution caused during their disposal [4].

Another form of energy storage includes sensible heat storage or latent heat storage. Sensible heat storage system is based on the temperature of the material, its weight, its heat capacity [5] and these systems are bulkier in size require more space. Compare to the sensible energy storage systems latent heat storage systems are attractive in nature due to compact size and high energy density. Latent heat storage systems stores heat as latent heat during change in the phase of material from solid to liquid or liquid to vapor and vice versa [6]. Amount of energy stored by latent heat energy system is more as compared to the sensible energy system as former one not only retain heat as latent heat but also as sensible heat which get absorbed when the temperature of the material rise up to its melting point. The materials used in latent heat storage systems are known as Phase Change Materials (PCMs) which also explains its nature during their application [7]. Depending on the chemical nature these PCMs are categorized as organic and inorganic materials. Selection of material depends on the application and temperature range of heat storage unit. The major disadvantage associated with phase change materials is their poor thermal conductivity hence various modification have been tried to enhance the material properties using composites prepared from phase change materials and materials with high thermal conductivity [8,9].

* Corresponding author. Tel.: +91 0141 2713498 (Office), +91 9413349429 (Mobile).
E-mail addresses: madhunaresh@gmail.com, magarwal.chem@mnit.ac.in (M. Agarwal).

http://dx.doi.org/10.1016/j.joei.2015.10.002
1743-9671/

Various experimental and numerical works related to heat storage devices were reviewed. These heat storage units were cylindrical shell type with single concentric [10,11] and multiple tubes for HTF flow [12], Rectangular shell with multiple tubes for HTF flow [13], Triplex tube with PCM in between two sided HTF flow [14] etc. Some work also involved addition of longitudinal and axial fins to enhance thermal conductivity by providing more surface area that promotes enhanced heat transfer by conduction [15–17].

This paper reviewed various heat storage materials, geometry and performance of heat storage units. Sensible heat storage units found to be having bulkier size as compared to latent heat storage units. Various kinds of composites with improved thermal properties were investigated for optimum storage of heat. These materials enhanced the amount of heat stored by the system at small volumes. Geometrical designs of different heat storage units were reviewed to find out the suitable design for optimum transfer of heat.

2. Sensible heat storage systems

Heat storage by increasing the temperature of the material known as sensible heat storage. Materials used for an efficient sensible heat storage system should have high specific heat capacity, long term stability in terms of thermal cycling and should be compatible to the container material in which storage takes place [18]. A variety of materials have been used in the past for sensible heat storage systems classified as liquid heat storage materials and solid heat storage materials [19]. A list of different materials used for sensible heat storage along with their properties is presented in Table 1 and these materials include metals like aluminium, copper, lead etc. [20–22]. These materials comprise high thermal conductivity and hence reduce charging and discharging time although they are also having low heat capacity, high density and high cost that make system expensive to use. Some building materials were also studied as sensible heat storage materials and they are used to build temperature controlled building or energy efficient building [23–27]. It is observed that water is a good sensible heat storage media due to its high thermal conductivity and cheap availability [28,29]. However due to its high vapor pressure water as heat storage material requires insulation and pressure withstanding container for operation at high temperature. Heat storage can be achieved either in fresh water using water storage tank or by employing solar pond which is based on the principle of thermal stratification [30]. Solar water tanks usually fabricated with a variety of materials like steel, concrete, aluminum, fiber glass and lined with insulator at the inner side so to avoid the heat loss through the wall. Solar pond provides an efficient and cheap method to store solar energy at low temperature. Some salts used for solar ponds are magnesium chloride and sodium chloride. Thermal stratification can be easily achieved in solar pond using different concentration of salts at the different layers of water with maximum temperature at bottom part of the pond where the sun radiation get absorbed. Solar ponds are also easy to handle in terms of removal of water without disturbing the other layers of the pond [31].

Another liquid used to store sensible heat include molten salts, petroleum based oils, and molten metals. Petroleum based oils have low thermal capacities as compare to that of water but due to low vapor pressure these are some good options as sensible heat storage medium.

Various systems related to sensible heat storage have been used for the study in past few decades and these are listed in Table 2. Metals as sensible heat storage provide high thermal conductivity and stores heat in less time as compared to the nonmetals [5]. Although use of metals as sensible heat storage material enhances cost and weight of the system. Various building materials were also investigated to store sensible heat with the aim to reduce cost by reducing investment in heating and cooling devices in the buildings [32–35]. Sensible heating storage materials with high heat capacity need to be developed in order to reduce system volume. Researchers also tried to combine sensible heat storage systems with latent heat storage system to increase the overall efficiency of heat storage system [36]. Application of sensible heat storage materials need to be studied based on the geographical distribution of solar radiation so as to optimize green energy storage in the field and development of energy storage materials for bulidings.

3. Latent heat storage systems

Latent heat storage systems absorb and release heat when a material undergoes phase change from solid to liquid and liquid to vapor and these materials are referred as phase change materials [37]. PCM stores heat 5 to 14 times as compared to sensible heat storage materials at constant temperature [38]. To store sufficient latent heat phase change materials should have high latent heat of fusion, high specific heat, high thermal conductivity and small volume change during phase change, little or no sub-cooling. These materials should be chemically stable after repeating thermal cycles and should be non-poisonous, non-corrosive, non-inflammable and should be available on large scale at lower price [39].

Table1
Sensible heat storage materials and their thermal properties at 20 °C.

Material	Thermal capacity (kJ/kg K)	Thermal conductivity (W. m/K)	Density (kg/m$^{3)}$	Energy density (kJ/m$^{3)}$	References
Aluminium	0.945	238.4	2700	2551.50	[21]
Copper	0.419	372	8300	3477.70	[20]
Iron	0.465	59.3	7850	3650.25	[22]
Lead	0.131	35.25	11340	1485.54	[22]
Brick	0.840	0.5	1800	1512	[23]
Concrete	0.879	1.279	2200	1933.80	[24]
Granite	0.892	2.9	2750	2453	[26]
Graphite	0.609	155	2200	13339.80	[25]
Limestone	0.741	2.2	2500	1852.50	[27]
Sandstone	0.710	1.8	2200	1562	[27]
Water	4.183	0.609	998.3	4175.88	[27]

Please cite this article in press as: A. Dinker, et al., Heat storage materials, geometry and applications: A review, Journal of the Energy Institute (2015), http://dx.doi.org/10.1016/j.joei.2015.10.002

Table 2
Different sensible heat storage systems.

Geometrical configuration	Materials	Parameters investigated	Findings	References
Cylindrical configuration with embedded charging tubes	Concrete, cast steel, cast iron	Charging time, energy storage rate, charging energy efficiency.	1 Charging time was reduced to 35.48% with four fins assembly and to 41.41% with six fins assembly. 2 Increased flow rate of heat transfer fluid reduce charging time in cast iron and cast steel as compare to concrete.	[5]
Packed bed configuration	Rocks for sensible part and mixture of fluoride salts encapsulated in AISI 316 for latent heat part	1D heat transfer model was formulated for the sensible and latent heat sections of TES considering separate fluid, solid and molten phases.	Outflow temperature was stabilized by using PCM on top with 1.33% of total storage volume is sufficient to accomplish stabilization as compare to 4.4% of total energy stored as latent heat energy.	[40]
Packed bed with spheres of Egyptian clay	Egyptian clay	Bed length, particle diameter and mass flow rate	Optimized parameters was 2.1 m for bed length, 0.019 m for particle diameter and 900 kg/h for mass flow rate.	[41]
Packed pebble bed with oil	Rock and oil	Axial temperature distribution with variable electrical heating was studied. Simulation was performed using Schumann model	Large deviation was found in axial temperature distribution between experimental and modeled values due to unaccounted heat loss. A modified Schumann model was implemented to reduce the gaps.	[33]
Cement composite graphite paste	Graphite and cement	Effect of water/cement ratio and graphite on comprehensive strength, thermal conductivity and volume heat capacity were studied	Increasing graphite with decrease in water content improves thermal properties of composite however it decreases the comprehensive strength of composite material and vice versa.	[35]
Concrete modules	High temperature concrete	Composition of concrete modules with its chemical and physical properties were studied.	This study provides guidelines and listed associated restrictions regarding use of high temperature concrete for thermal storage.	[34]

3.1. Classification of phase change material

Phase change materials on the basis of their chemical composition can be classified as organic and inorganic phase change materials [42]. Organic phase change materials are made of hydrocarbons and include paraffin's, fatty alcohols, fatty acids and waxes. Inorganic phase change materials include molten salts, salt hydrates and metallic. Another class of phase change materials includes eutectic mixtures of organic-inorganic, inorganic–inorganic and organic–organic compounds [19,43].

3.2. Thermal properties of phase change material

Selection of right phase change material for thermal storage application is an important part where range of parameters need to be investigated. These parameters include a desired melting point depending on the type of application, desired latent heat of fusion/vaporization, thermal conductivity and stability of material towards thermal cycling [44–46]. The important criterion for choosing a phase change material is that its melting point should lie in the range for desired application. Organic phase change materials have low melting temperature range and employed for low temperature thermal energy storage systems. Rauaolut et al. [47] used a low temperature thermal energy storage system consisting of paraffin wax as phase change material to control temperature of room. The storage system depends on thermal gap between night time and daytime outdoor air temperature to refresh indoor air using molten phase of paraffin. Bruno et al. [48] used PCM with melting point 10 °C inside the tubes of thermal storage unit coupled with ice based system and found that about 13.5% energy recovered by the system which was further enhanced by heat transfer optimization. Similarly inorganic phase change materials lie in the high temperature melting point range and used for high temperature thermal storage like in CSP (Concentrated Solar Plant) [49], thermocline storage material [50] etc.

Table 3 represents thermal properties of some organic and inorganic PCM are used in different applications for latent heat storage. Organic compounds like paraffin, fatty acids, and fatty alcohols have low melting point (10°C–60 °C) and used for low temperature domestic thermal storage. Paraffins are straight chain hydrocarbons and possess desirable properties like high heat of fusion, low vapor pressure, chemical inertness, self-nucleation with no phase segregation. The melting point of paraffin's varies with the number of carbon atoms in the chain. Technical grade paraffin's are cheaper as compared to pure paraffin. Fatty acids are good organic phase change material to store thermal energy at low temperature range also they have high heat of fusion with no super cooling comparable to paraffin wax and salt hydrates [37,51,52]. Fatty acids are stable and reliable in terms of their thermal properties [53]. Sari et al. [54] studied the thermal storage performance of palmitic acid in a tube-in-tube type heat exchanger and reported heat storage efficiency of 53.3%. They also observed that inlet fluid temperature and flow rate does not have any significant effect on the melting time of PCM. However, it was found that melting time had been reduced considerably by placing the tube containing PCM in horizontal position rather than a vertical position. Konukulu et al. [55] prepared microcapsules of capric acids with different shell materials for their use as thermal storage materials. They found that microcapsules with UF shell (E:Tween 40) were found to be stable and hence suitable for thermal storage applications.

Eutectic mixtures of organic and inorganic materials is again matter of interest for past research programs to develop mixtures with desirable melting point, high thermal capacity with no or little super cooling effect. Inorganic eutectic mixtures are suitable for high

Please cite this article in press as: A. Dinker, et al., Heat storage materials, geometry and applications: A review, Journal of the Energy Institute (2015), http://dx.doi.org/10.1016/j.joei.2015.10.002

Table 3
Phase change materials used for latent heat storage.

PCMs	Type	Melting point (°C)	Heat of fusion (kJ/kg)	Thermal conductivity (W/m.K)	References
Paraffin wax (C_{13}–C_{18})	Organic	32	251	0.214	[7,52]
Polyglycol E600	Organic	22	127.2	0.189	[56]
Vinyl stearate	Organic	29	122	0.25	[43]
Butyl stearate	Organic	19	140	0.21	[57,58]
1-Dodecanol	Organic	26	200	0.169	[52,59]
n-Octadecane	Organic	28	243.5	0.148	[60]
Palmitic acid	Organic	57.8	185.4	0.162	[54]
Capric acid	Organic	32	152.7	0.153	[61]
Caprylic acid	Organic	16	148	0.149	[55]
Propyl palmitate	Organic	10	186	n.a	[52]
KNO_3/$NaNO_3$	Inorganic	220	100.7	0.56	[67]
$CaCl_2.6H_2O$	Inorganic hydrates	29	187	0.53	[52]
$LiNO_3$/KNO_3/$NaNO_3$	Inorganic eutectic mixture	121	310	0.52	[62]
a) KNO_3–$LiNO_3$ b) KNO_3/$NaNO_3$/$LiNO_3$ Etuectic mixtures	Inorganic eutectic mixtures	124	155	0.58	[63,64]
$LiNO_3$/$CaNO_3$ With solar salts $NaNO_3$ and KNO_3	Inorganic	130	276	0.56	[65]
KNO_3/$NaNO_3$ (30%/70%)	Inorganic Non eutectic mixture	260	305	0.54	[51]
Capric acid (65.12%) and lauric acid (34.88%)	Organic eutectic mixture	19.67	126	0.21	[113]
Polymethylmethacrylate (PMMA)/ capric-stearic acid mixture	Organic eutectic mixture	21.37	116.25	0.15	[66]

temperature thermal storage systems like concentrated solar thermal plant (CSP), while organic eutectics are suitable for low temperature thermal storage like maintaining building temperature. Shilei et al. (2006) studied the eutectic mixture of capric acid and lauric acid for its use in building material and found that these phase change wallboards did not show any variation in melting point and latent heat after 360 thermal cycles and therefore can be used for building energy conservation. Various composition of nitrate salts of potassium, sodium, calcium and lithium were tried by researchers to obtained suitable mixture having desired melting point and latent heat for the purpose of thermal storage [62–64,67]. Sari et al. [66] prepared polymethylmethacrylate (PMMA)/capric-stearic acids eutectic mixture (C-SEM) micro/nanocapsules for latent heat storage using emulsion polymerization technique. With uniform shape these microcapsules had melting temperature of 21.37 °C with latent heat equal to 116.25 kJ/kg can be used as part of building material for temperature control, however, real world applications of these microcapsules are still need to investigate. All the materials (Table 3) need to be investigated both at microscopic and macroscopic level in order to enhance their thermal property so as to make them useful for commercial application.

3.3. Composites of phase change material

Although phase change materials have been used in wide range of applications to trap heat but they have poor thermal conductivity. Combination of phase change materials with materials of high thermal conductivity attracted the interest of the researchers to use them for various applications. Table 4 shows different composites prepared from organic phase change materials. The materials used to enhance the thermal conductivity of PCMs should have high thermal conductivity, resistant to chemical reaction and should be compatible both with phase change material and material of the container.

Thermal conductivity of pure paraffin is 0.216 W/m.K which increases its melting time and increases the charging time of thermal storage system which can be improved further by adding materials of high thermal conductivity to the paraffin wax. Sahan et al. [68] added nanomagnetite/nanoparticles of magnetite with high thermal conductivity 9.1 W/m.K to enhance the thermal conductivity of paraffin by providing metallic surface area for heat transfer and it is a costlier component which also adds weight to the system. TiO_2 nanoparticles (Harikrishnan et al., 2013) were used with paraffin wax as well as stearic acid to enhance their thermal conductivity. Aluminium foam (218 W/m.K) was also used to enhance thermal conductivity of paraffin [69]. Enhanced thermal conductivity was due to conduction through the aluminum foam as compared to the natural convection. Addition of metal foams or their nano forms will enhance the thermal conductivity but they also added weight to the system and increased the cost of the thermal storage system. Composites of fatty acids and their eutectic mixtures were prepared and tested for thermal storage [53].Zhang et al. [70] prepared a foam stable composite by incorporating ternary eutectic mixture of lauric acid-palmitic acid-stearic acid (55 wt%) in expanded perlite. The composite had low melting point (31.8 °C) and good latent heat (81.5 kJ/kg) and found to be thermally stable even after 1000 thermal cycles and proved to be a potential energy storage material. The application of this composite as building material component still needs to be investigated. Similarly [107] prepared a composite from eutectic mixture of lauric-myristic-stearic acid and expanded graphite (12:1 w/w) with low melting point (29.05 °C) and good latent heat (137 kJ/kg) for low temperature storage applications. They found improved thermal conductivity of eutectic mixture due to addition of expanded graphite and the composite was thermally stable even after 1000 thermal cycles. Yang et al. [72] also prepared composite from eutectic mixture of myristic-palmitic-stearic acid and expanded graphite for thermal storage with a melting point of 41.64 °C and latent heat of 153.5 kJ/kg suitable for solar thermal storage application. Some other composites were also prepared from eutectic mixtures of fatty acids and expanded graphite such as composite of capric-myristic-palmitic acid eutectic mixture with expanded graphite (13:1) [53] and composite of palmitic-stearic acid eutectic mixture with expanded graphite (13:1) [73]. Their corresponding melting points were 18.61 °C and 53.89 °C and latent heats were 128.2 kJ/kg and 166.27 kJ/kg respectively. Zhang et al. [73] prepared composites of palmitic-stearic acid eutectic mixture and carbon nanotubes (with 5 wt% to 8 wt%). Results showed that thermal

Please cite this article in press as: A. Dinker, et al., Heat storage materials, geometry and applications: A review, Journal of the Energy Institute (2015), http://dx.doi.org/10.1016/j.joei.2015.10.002

Table 4
Composites of organic phase change materials.

Composite	Thermal conductivity (W/m.K)	Observation	Reference
Paraffin wax (80% wt.) with nano magnetite (20% wt.)	0.40	Addition of 20% nanomagnetite enhanced the thermal conductivity of paraffin by 67%. Use of 10% nanomagnetite increased the cost of composite by 20%.	[68]
1 Liquid paraffin/aluminium foam 2 Solid paraffin/aluminum foam	1 46.04 2 46.12	Thermal conductivity of PCM composite increased up to 218 times more as compared to the pure paraffin with 26% drop in heat fluxes.	[69]
Paraffin (80% wt.)/graphite (20% wt.in form of foam, fibers and fins)	0.972	Heat flow much rapidly in porous graphite foam as compared to fin and fiber configuration. More temperature was enhanced using fin configuration as compared to foam and fibers for the same time.	[74]
1 Paraffin (80% wt.)/waste graphite (20% wt.) 2 Paraffin (80% wt.)/SFG75 (Timrex powder) (20% wt.)	1 0.428 2 0.906	91% enhancement in thermal conductivity of paraffin was observed with waste graphite as compared to 300% enhancement by fresh graphite	[75]
1Paraffin (90% wt.)/expanded graphite (10% wt.) 2 Paraffin (90% wt.)/graphite (10% wt.)	1 0.938 2 0.561	Expanded graphite enhanced thermal conductivity of paraffin by 300% while graphite enhanced the thermal conductivity by 150% as compared to pure paraffin.	[76]
Paraffin with expanded graphite (2% wt., 4% wt., 7% wt. and 10% wt.)	0.29, 0.51, 0.68, 0.81 respectively	Thermal conductivity of paraffin increased with increase in graphite content with no leakage up to 10% wt. of graphite.	[77]
Paraffin with TiO_2 (1%–4% wt.)	0.7	With increase in TiO_2 loading phase change temperature increases with decrease in latent heat capacity. Thermal conductivity of composite increases with increase in TiO_2 loading upto 3%.	[78]
Eutectic mixture of lauric-palmitic-stearic acid/perlite	0.44	Composite was found to be thermally stable after 1000 cycles and well suited as building material for temperature control.	[73]
Eutectic mixture of lauric-myristic-stearic acid/expanded graphite (12:1 w/w) composite	–	Addition of expanded graphite enhanced the thermal conductivity of lauric-stearic-myristic acid eutectic mixture. Thermal stability results showed that the mixture was stable after 1000 thermal cycles	[71]
Eutectic mixture of myristic-palmitic-stearic acid/expanded graphite (13:1 w/w) composite	–	Results showed that myristic-palmitic-stearic acid has proper phase change temperature, high latent heat and good thermal conductivity. Prepared composite was also found to be thermally stable and reliable in terms of solar energy storage.	[72]
Eutectic mixture of capric-myristic-palmitic acid/expanded graphite (13:1 w/w)	3.67	Results showed the composite achieved a good thermal conductivity after addition of expanded graphite which enhanced the energy storage and release rate. Also composite was found to be thermally stable after large number of repeating thermal cycles.	[79]
Eutectic mixture of palmitic acid –stearic acid/expanded graphite (13 w/w)	2.51	Thermal conductivity of the composite rose significantly which enhanced the heat storage and release rates. Composite was thermally stable and suitable for latent heat storage.	[70]
Eutectic mixure of lauric-palmitic-stearic acid/Carbon nanotubes (CNTs, 5%–8% w/w)	0.316–0.341	Thermal conductivity of the system enhanced with the mass percentage of the added carbon nanotubes. Addition of CNTs increased the heat transfer rate while decreased the amount of heat storage.	[80]
Stearic acid with TiO_2 nano-fluid (0.3% wt.) loading	0.3	Thermal conductivity of the system increases with increase in the TiO_2 percentage with optimum value at 0.3% wt. after which reduction in latent heat was observed.	[114]
Stearic acid and silica fumes	–	Form stable composite without leakage of stearic acid forms at 1:0.9	[81]
Stearic acid with polymethylmethacrylate	–	PMMA support stearic acid which enhanced heat transfer in phase change material.	[81]
a) Stearic acid with expanded graphite (90% wt.:10% wt.) b) Stearic acid with carbon fiber Both tested for different weight percentage (90% wt.: 10% wt.)	1. 1.1 2. 0.9	Thermal conductivities of PCM increases linearly with increase in weight percentage of graphite. With decrease in latent heat of the composite.	[82]
Eutectic mixture of lauric acid-stearic acid (7:3 by weight)/ expanded perlite	–	Melting temperature and latent heat hardly varies after 1000 thermal cycle. Expanded perlite provides a good material for support to PCM to prepare an ideal material for thermal storage application	[83]

(*continued on next page*)

Please cite this article in press as: A. Dinker, et al., Heat storage materials, geometry and applications: A review, Journal of the Energy Institute (2015), http://dx.doi.org/10.1016/j.joei.2015.10.002

Table 4 (*continued*)

Composite	Thermal conductivity (W/m.K)	Observation	Reference
Palmitic acid (80% wt.)/expanded graphite (20% wt.)	0.60	Thermal conductivity of composite is 2.5 times more than thermal conductivity of pure PA.	[109]
1 Capric acid (60% wt.)/hallosyte nanotube (40% wt.) 2 Capric acid (60%)/hallosyte nanotube (35% wt.)/ graphite (5% wt.)	1. 0.479 2. 0.758	Capric acid/hallosyte nanotube composite was formed with 60% of capric acid without leakage. Graphite was used as additive to enhance the thermal conductivity of the composite	[84]
Eutectic mixture of myristic acid/palmitic acid (70% wt.:30% wt.) with 5% wt. sodium myristate.	0.242	Addition of surfactant enhanced the thermal conductivity of fatty acids with increased latent heat of fusion	[85]
Plamitic acid (92% wt.)/graphene nanoplates (8% wt.)	2.11	Graphene nanoparticle s provide more surface for the heat transfer and hence provide 8 times more thermal conductivity then pure palmitate.	[86]
Ternary eutectic mixture of lauric acid/myristic acid/ palmitic acid (55.24% wt.:29.74% wt.:15.02% wt.) with expanded graphite, ratio of ternary mixture to EG is (18:1)	1.67	Ternary mixture of fatty acids stores without leakage at mass ration of (18:1) with EG and distributed uniformly in the porous structure of expanded graphite.	[87]
Capric-myristic acid (50% wt.)/expanded perlite composite (40% wt.)/expanded graphite (10% wt.)	0.076	CA–MA eutectic mixture (0.048 W/m.K) absorbed in the porous structure of perlite and enhanced the thermal conductivity of composite by 60%.	[88]

conductivities of composite PCMs increased by 20.2% (for 5 wt%), 26.2% (for 6 wt%), 26.2% (for 7 wt%) and 29.7% (for 8 wt%) respectively with the addition of carbon nanotubes. It was observed that thermal release rate of composite had increased with addition of carbon nanotubes but heat storage capacity has been decreased. Composites prepared from eutectic mixture of fatty acids can be used as low temperature thermal storage building material. However, low thermal conductivity and high cost of fatty acids make their use limited on commercial scale. Some other low cost materials with high thermal conductivity were also tested with organic compounds to improve thermal properties of material, these materials include carbon materials, graphite [74,75], expanded graphite [76,77], expanded perlite [82], hallosyte nanotube [84], and graphene nano plates [86]. All these are lightweight materials with high thermal conductivity used to improve thermal conductivity without adding weight to the system. Composite not only enhance the thermal property of phase change material but also enhance the thermal storage capacity of the material by providing more surface area for the absorption of phase change material. Composites studied here are not new material in their chemical nature but just the mixture of two different materials. The study of organic composites needs to be done on extensive scale in order to broaden its application area in domestic application and as building wall materials.

As discussed inorganic materials like salts and their eutectic and non-eutectic mixtures were suitable for their high temperature thermal storage. The disadvantages of inorganic PCM were low thermal conductivity, corrosion to the container wall, and high cost in terms of installation and operation which drew the attention of researchers to develop composites of high thermal conductivity. Material used to prepare composite should have high thermal conductivity, resistance to chemical reactions, lighter in weight and it should be compatible with the wall of the container as well as with the PCM. Table 5 listed various composites of inorganic PCM, their eutectic and non-eutectic

Table 5
Composite of inorganic phase change materials.

S. No.	Inorganic composite	Thermal conductivity (W/m.K)	Observation	References
1	KNO_3/$NaNO_3$-graphite composite (80% wt./20% wt.)	20	Molten salts also having low conductivity. Thermal conductivity is 20 W/m.K.	[67]
2	Non eutectic mixture KNO_3 (30% wt.)/$NaNO_3$ (70%)	0.5	Salt mixture provide wide range of temperature range between 220 and 260 °C for melting and freezing cycle	[51]
3	Lithium carbonate and sodium carbonate/ceramic/ carbon materials (10%)	4.3	Using eutectic mixture of sodium and lithium carbonate on skeleton on magnesium carbonate	[51]
4	Na_2CO_3/MgO composite with added multiwall carbon nanotubes (0.5% wt.)	1.13	Material without added carbon nanotubes showed good thermal stability but poor thermal conductivity.	[89]
5	Cylindrical model of paraffin and porous graphite matrix were studied.	Radial 27.3 Axial 5.3	Increased in graphite content directly proportional to thermal conductivity of composite.	[90]
6	Attapulgite granulate impregnate with the mixture of $MgSO_4$ (20% wt.) and $MgCl_2$ (80% wt.)	–	Hat of absorption increases with increase in the amount of $MgCl_2$ due to increase sorption of water in highly concentrated salt solution	[64]
7	$LiNO_3$/KCl (70% wt.)-expanded graphite	15	Presence of EG decrease the latent heat of the composite. Composite with higher density increases the thermal conductivity of the composite.	[91]
8.	LiF-NaF-KF (46.5% wt.,,/11.5% wt./42% wt.)	0.92	Salt mixture used to study effect of corrosion on metals. Addition of Ni-201 to alloy reduces the chances of corrosion.	[92]

Please cite this article in press as: A. Dinker, et al., Heat storage materials, geometry and applications: A review, Journal of the Energy Institute (2015), http://dx.doi.org/10.1016/j.joei.2015.10.002

mixtures for the purpose of high temperature thermal storage. Various composites of inorganic materials were prepared with materials of high thermal conductivity like graphite [67], expanded graphite [90], and multiwall carbon nanotubes [89] etc. and were used to enhanced the thermal conductivity of salts.

4. Geometry of thermal storage systems

For optimum heat storage system selection of PCM and geometry of heat storage unit plays crucial part. Type of PCM for a particular heat storage unit is based on its melting point while geometry of heat storage system drives the heat transfer. Different geometrical designs of thermal storage unit studied are shown in Fig. 1which includes cylindrical/rectangular heat.

storage unit with HTF (Heat Transfer Fluid) passing through single tube, multiple tubes and triplex tube heat transfer unit with HTF flowing through center and outer of phase change material. In some geometrical arrangements fins were integrated with the tubes to provide more surface area for heat transfer. However addition of fins reduces the amount of PCM in the storage unit and hence reduced overall heat capacity of the system. Material used for PCM container should be well insulated from outside and it should not show any reaction with the phase change material filled inside the container.

Applications, geometry and materials used for heat storage unit are presented in Table 6. Liu et al. [71] studied heat transfer effect in a horizontal acrylic cylindrical container with single copper tube having longitudinal and axial fins as shown in Fig. 1(e) to enhance the heat transfer. It is observed that with increase in heat transfer fluid temperature melting time decreases while there is little effect of variation in flow rate especially when convective heat flow becomes dominant. Study on vertical cylindrical heat storage unit with different arrangement of tubes showed similar effects.

In another study by [93] heat transfer fluid passed through the center and outer part of phase change material (known as triplex tube heat exchanger unit) to reduce charging time of heat storage and found that such assembly led to the heat loss from the outer surface of the unit if it was not properly insulated and therefore not very attractive for heat storage application.

Rectangular shell and tube assembly studied by [94] to consider the effect of fins, fluid flow rate and inlet temperature. Fins were employed to enhance heat transfer so as to reduce the charging time. Results of the study showed that increase in flow rate reduced melting time. Flat plate latent heat storage systems were designed, studied and found that it provides better flexibility in application and insertion of heat enhancement structures [71,95].

5. Corrosion of containers

Containers used for handling phase change materials are operated under different conditions and subjected to variable temperatures which led to the rapid corrosion of the container material if not chosen properly. Ferrer et al. [96] studied the corrosion effect for four different PCMs (one inorganic mixture, one ester, and two fatty acids eutectics) on five different metals (aluminium, copper, carbon steel,

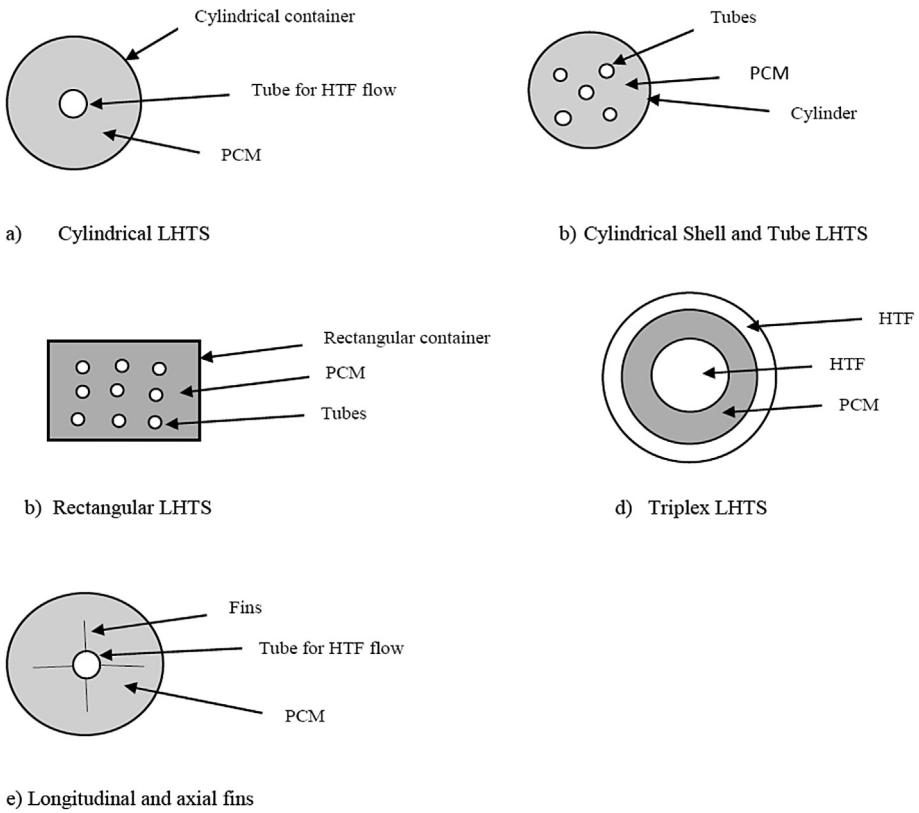

Fig. 1. Geometrical design of various thermal storage unit.

Please cite this article in press as: A. Dinker, et al., Heat storage materials, geometry and applications: A review, Journal of the Energy Institute (2015), http://dx.doi.org/10.1016/j.joei.2015.10.002

Table 6
Different geometrical designs of thermal storage unit.

Geometry and container material	PCM used	Parameters studied	Observations	References
Horizontal cylinder of acrylic plastic with copper pipe containing longitudinal and angular fins	Dodecanoic acid	Effect of inlet temperature and flow rate of HTF, configuration of fins	Both fin arrangement conduction is dominant followed by convection, high inlet temperature reduces melting time, flow rate did not have considerable effect on melting profile of PCM	[97]
Vertical cylindrical of acrylic plastic with two copper pipe connected to longitudinal fins	Dodecanoic acid	Simultaneous charging and discharging rates	Simultaneous heat transfer limited by solid PCM between two pipes, high flow rate of cold HTF allows better heat recovery. Uncertainty in input energy and energy recovery is large.	[98]
Double tube heat storage container with outer tube made of steel for PCM storage while inner tube of brass for flow of HTF	Paraffin wax	Effect of increasing inlet temperature and mass flow rate on charging and discharging process of PCM	Heat flow rate increase by 25% and 11% during melting and solidification on increase and decrease of HTF temperature by 2 °C. Increase in 4 °C of temperature of inlet water reduce the melting time by 31%.	[99]
Vertically arranged cylindrical enclosure with vertical pipe along its axis	Paraffin wax	Analysis of PCM melting process with natural convection, duration of melting followed by time dependent numerical simulations.	Numerical simulation validated the features predicted by theory.	[100]
Cylindrical shell and tube type with inner copper tube for HTF flow and outer shell part made of polypropylene	Paraffin wax	Melting profile of paraffin wax were studied at different values of eccentricity i.e. e = 10 mm, 20 mm and 30 mm.	Melting process dominated by conduction followed by convection and more enhanced in upper part of shell. 67% decrease in melting time was observed in case of eccentric geometry = 30 mm than concentric geometry.	[101]
Triplex tube heat exchanger with outer, inner and middle tubes made of copper with PCM filled between the inner tube and middle tube while HTF flows between the middle tube and outer tube.	RT82	Heat enhancement techniques were studied using inside outside tube, effect of fin length on enhancement technique were studied.	No considerable effect on melting rate of PCM in both the three enhancement techniques. Complete melting was reduced to 43.3% as compare to TTHX without fin.	[93]
Fin and Tube Heat exchanger with space between the rectangular shell and between the fins filled with PCM	R35	Flow rate, Inlet temperature of HTF and effect of fin pitch on charging and discharging process.	Increasing flow rate from 0.2 L/min to 0.4 L/min at temperature 60 °C showed significant change in PCM melting time while further increase in flow rate reduces it. Melting time also reduces on increasing fin pitch.	[94]
Studied two systems 1 Shell and tube type with copper tube embedded along with aluminium fins (PCM-HX). 2 Embedded copper tube in the highly conductive graphite-wax composite	PT43 wax	Comparison of technology to enhance the thermal conductivity of wax was studied, economics of system, charging discharging time, inlet and outlet temperature of HTF were also studied.	PCM HX and Copper tube in composite both performed well in their operations. PCM-HX only occupies 38% of water storage volume as compare to the copper tube based unit. The PCM unit can store 5 times more energy than water in useful range 40°C −52 °C.	[102]
Flat plate latent heat storage. HTF flow in the chamber between the flat carbon steel.	Mobiltherm 603 Thermal conductivity (0.122 W/K)	Temperature gradients, flow rates and insertion of heat transfer structures	Insertion of various heat transfer structures provide phase change discharge time between 2 and 8 h. Flat plate's collector offers wide range of flexibility with HTF, insertion of heat transfer enhancement structure.	[103]
Flat plate latent heat storage unit with flat slabs of phase change material.	Carbonate salts (solar salts), liquid sodium, air, CO_2 and steam	Comparison between liquid and gaseous HTF, heat transfer characteristics between the slabs, heat transfer rates and liquid fraction profiles were studied	Liquid sodium delivers maximum 99.4% electrical energy to grid relative to the ideal cases. Solar salts achieved 93.6% of electricity delivered while air, CO_2 and steam delivers 87.9% and 91.3% of electricity delivered.	[71]
Vertical stacks of rectangular cavities filled with PCM	1 Rubitherm RT28HC 2 Micronal DS5001X (Microencapsulated PCM)	Time required for melting and solidification was studied, control temperature value on hot surface of test sample and period of thermal regulation was studied.	Microencapsulated PCM (Micronal DS5001X) accelerated the charging process with no thermal stratification. Control temperature regulation and thermal regulation period both reduced in microencapsulated form. Sub cooling effect cannot be neglected in case of free PCM	[95]
Rectangular container with one wall made up of aluminium alloy. Holes were dig from the aluminium plate side to allow water to pass through the wall as HTF.	Lauric acid	Melt fraction, temporal heat storage, heat transfer characteristics.	Melting initiated by conduction followed by convection. In liquid state of PCM stratification of temperature occurs led to depression of convection.	[104]

Please cite this article in press as: A. Dinker, et al., Heat storage materials, geometry and applications: A review, Journal of the Energy Institute (2015), http://dx.doi.org/10.1016/j.joei.2015.10.002

stainless steel-304 and -316). Result indicated that aluminium containers showed faster corrosion with inorganic salt mixture and hence caution must be taken while selecting aluminium for PCM containers. Copper showed lower corrosion rate of 6–10 mg/cm^2 yr with the fatty acids formulations and can be used for PCM containers. Stainless steel showed great corrosion resistance of 0–1 mg/cm^2 yr and was the best available material for PCM containers.

Morreno et al. [115] carried out similar study with two metals (i.e. copper and aluminium) and two metal alloy (stainless steel 316 and carbon steel) and selected eleven types of salt mixtures out of which 5 were used for cooling application while 6 PCMs were used for heating applications. The corrosion rate of PCM containers were evaluated after 1 week, 4 week and 12 week. Result of the study showed that thin stainless steel alloy lining should be used with stainless steel and aluminium while later one was suitable only for selected PCM. It was also found that commercial PCM C10 was suitable to encapsulate in stainless steel and aluminium and PCMs used for heating application should be stored in stainless steel container.

In addition to metals and alloys, polymers were also used as container material for phase change material. Oro et al. [105] made comparison between four metals (copper, aluminium, stainless steel and carbon steel) and polymers (polypropylene), High Density Poly Ethylene (HDPE), polyethylene terephthalate and polystyrene. These container materials were tested with four commercial PCM and five developed PCM and observed that carbon steel and copper must be avoided in any situation due to their high reactivity towards corrosion. Aluminium was also not recommended due to the creation of pits on its surface. Stainless steel 316 was well suited material for PCM containers due to its resistivity towards corrosion. Polymer containers did not show any effect on the appearance and weight of the samples. Also there were no pitting, precipitation and bubble formation and hence they are compatible with PCMs.

The studies show that out of the range of selected metals stainless steel was the best available material for PCM container. Polymers are also good choice for phase change materials as they do not show any reactivity with the phase change material as well as they are resistant towards pitting, bubbling and precipitation etc.

6. Conclusion

There are various types of sensible and latent heat systems, their storage materials and their geometrical designs available. Sensible heat storage systems were simple in designs, easy to maintain but bulkier in size. Latent heat systems were found to be more suitable for thermal storage due to their high energy storage density and quasi thermal nature of storage. The low melting point of organic PCMs made them suitable for low temperature applications like domestic water heating, cold storage, as building material etc. While inorganic PCMs due to their high melting point were suitable for high temperature storage application like concentrated solar plant. Low thermal conductivity of both organic and inorganic phase change material had limited their direct use at commercial scale. Composites of organic and inorganic PCMs were prepared with high thermal conductivity materials like graphite, carbon nanotubes, metal oxides, metallic nanoparticles etc. for their large scale application. Composites with expanded graphite and carbon nanotubes were preferred due to high thermal conductivity and low weight. Most of the composites used in thermal storage were mixture of two materials rather than any new substance.

There are different geometrical configurations such as cylindrical shell and tube, rectangular shell and tube, triplex and configurations with longitudinal and axial fins were used with PCMs for thermal storage applications. Addition of fins reduced the melting time of the PCM but it also reduced the amount of PCMs in the system due to space occupancy and hence reduced the overall efficiency of the system. The heat storage units either in cylindrical or rectangular geometry found to be more efficient in their horizontal position as compare to the vertical position. It was due to the presence of large air space above PCM in horizontal position which enhanced conduction heat transfer as compare to the vertical position. Most of the sensible heat storage units used for pre heating of water through solar pond, for pre heating and cooling of air using packed bed configuration, etc. While most of the latent heat storage systems were mostly used for pre heating of water, for pre heating and pre cooling of air, for storage of waste industrial heat and as building materials for temperature control etc. Most of the containers holding PCMs were made of steel and polymers. Corrosion effect of PCMs on container materials has been studied by various researchers. The stainless steel was considered best material for PCMs due to least corrosion at high temperature applications, while containers made up of polymers were good for low temperature applications.

References

[1] P. Li, Energy storage is the core of renewable energy technologies, Nanotechnol. Mag. 4 (2008) 3–18.
[2] S. Weitemeyer, D. Kleinhans, T. Vogt, C. Agert, Integration of renewable energy sources in future power systems: the role of storage, Renew. Energy 75 (2015) 14–20.
[3] B. Diouf, R. Pode, Potential of lithium-ion batteries in renewable energy, Renew. Energy 76 (2015) 375–380.
[4] A. Blumberga, L. Timma, F. Romagnoli, D. Blumberga, Dynamic modeling of a collection scheme of waste portable batteries for ecological and economic sustainability, J. Clean. Prod. 88 (2015) 224–233.
[5] L. Prasad, P. Muthukumar, Design and optimization of lab-scale sensible heat storage prototype for solar thermal power plant application, Sol. Energy 97 (2013).
[6] A. Castell, C. Solé, Design of latent heat storage systems using phase change materials (PCMs), Adv. Therm. Energy Storage Systems-Methods Appl. 11 (2015) 285–305.
[7] B. Zalba, J. Marin, L. Cabeza, H. Mehling, Review on thermal energy storage with phase change materials, heat transfer analysis and application, Appl. Therm. Eng. 23 (2003) 251–283.
[8] F. Agyenim, N. Hewitt, P. Eames, M. Smyth, A review of materials, heat transfer and phase change formulation for latent heat thermal energy storage systems(LHTESS), Renew. Sustain. Energy Rev. 14 (2014) 615–628.
[9] M.M. Farid, A.M. Khudhair, S.A.K. Razack, S. Al-Hallaj, A review on phase change energy storage: materials and applications, Energy Conservation Manag. 45 (2004) 1597–1615.
[10] M.J. Hosseini, M. Rahimi, R. Bahrampoury, Experimental and computational evolution of a shell and tube heat exchanger as a PCM thermal storage system, Int. Commun. Heat Mass Transf. 50 (2014) 128–136.
[11] H.A. Adine, H.E. Qarnia, Numerical analysis of the thermal behaviour of a shell-and-tube heat storage unit using phase change materials, Appl. Math. Model. 33 (2009) 2132–2144.
[12] M. Bechiri, K. Mansouri, Analytical solution of heat transfer in a shell-and-tube latent thermal energy storage system, Renew. Energy 74 (2015) 825–838.
[13] A. Khalifa, L. Tan, A. Date, A. Akbarzadeh, A numerical and experimental study of solidification around axially finned heat pipes for high temperature latent heat thermal energy storage units, Appl. Therm. Eng. 70 (1) (2014) 609–619.
[14] A.A. Al-Abidi, Sohif Mata, K.S., M.Y. Sulaiman, A.T. Mohammad, Experimental study of PCM melting in triplex tube thermal energy storage for liquid desiccant air conditioning system, Energy Build. 60 (2013) 270–279.
[15] A. Sciacovelli, F. Gagliardi, V. Verd, Maximization of performance of a PCM latent heat storage system with innovative fins, Appl. Energy 137 (2015) 707–715.

Please cite this article in press as: A. Dinker, et al., Heat storage materials, geometry and applications: A review, Journal of the Energy Institute (2015), http://dx.doi.org/10.1016/j.joei.2015.10.002

[16] F. Chabane, N. Moummi, S. Benramache, Experimental study of heat transfer and thermal performance with longitudinal fins of solar air heater, J. Adv. Res. 5 (2014) 183–192.
[17] A. Fudholi, K. Sopian, M.H. Ruslan, M.Y. Othman, Performance and cost benefits analysis of double-pass solar collector with and without fins, Energy Convers. Manag. 76 (2013) 8–19.
[18] S. Khare, M. Dell'Amico, C. Knight, S. McGarry, Selection of materials for high temperature sensible energy storage, Sol. Energy Mater. Sol. Cells 115 (2013) 114–122.
[19] S.M. Hasnain, Review on sustainable thermal energy storage technologies, Part I: heat storage materials and techniques, Energy Conservation Manag. 39 (1997) 1127–1138.
[20] A. Eastman, S.U.S. Choi, S. Li, W. Yu, L.J. Thompson, Anomalously increased effective thermal conductivities of ethylene glycol-based nanofluids containing copper nanoparticles, Appl. Phys. 78 (6) (2001) 718–724.
[21] B. Rufino, F. Boulc'h, M.-V. Coulet, G. Lacroix, R. Denoyel, Influence of particles size on thermal properties of aluminium powder, Acta Mater. 55 (8) (2007) 2815–2827.
[22] E. Wasserman, L. Stixrude, R.E. Cohen, Thermal properties of iron at high pressures and temperatures, Phys. Rev. B 27 (1996) 312–356.
[23] E.M. Alawadhi, Thermal analysis of a building brick containing phase change material, Energy Build. 40 (3) (2008) 351–357.
[24] D.W. Hawes, D. Banu, D. Feldman, Latent heat storage in concrete. II, Sol. Energy Mater. 21 (1) (1990) 61–80.
[25] M. Inagaki, Y. Kaburagi, Y. Hishiyama, Thermal management material: graphite, Adv. Eng. Mater. 16 (5) (2014) 494–506.
[26] H.H. Ozturk, A. Bascetincelik, Energy and exergy efficiency of a packed-bed heat storage unit for greenhouse heating, Biosyst. Eng. 86 (2) (2003) 231–245.
[27] E.C. Robertson, Thermal Properties of Rock, United States Department of Interior Geological Survey, Virginia, 1988.
[28] L. Gabriela, Seasonal sensible thermal energy storage solutions, Leonardo Electron. J. Pract. Technol. (2011) 49–68 (19).
[29] M.K.A. Sharif, A.A. Al-Abidi, S. Mat, K. Sopian, M.H. Ruslan, M.Y. Sulaiman, et al., Review of the application of phase change material for heating and domestic hot water systems, Renew. Sustain. Energy Rev. 42 (2014) 557–568.
[30] I. Bozkurt, M. Karakilcik, The effect of sunny area ratios on the thermal performance of solar ponds, Energy Convers. Manag. 91 (2015) 323–332.
[31] N. Malik, A. Date, J. Leblanc, A. Akbarzadeh, B. Meehan, Monitoring and maintaining the water clarity of salinity gradient solar ponds, Sol. Energy 85 (2011) 2987–2996.
[32] A.I. Fernandez, M. Martanez, M. Segarra, I. Martorell, L.F. Cabeza, Selection of materials with potential in sensible thermal energy storage, Sol. Energy Mater. Sol. Cells 94 (2010) 1723–1729.
[33] A. Mawire, M. McPherson, Experimental and simulated temperature distribution of an oil-pebble bed thermal energy storage system with a variable heat source, Appl. Therm. Eng. 29 (2009) 1086–1095.
[34] V.A. Salomoni, C.E. Majorana, G.M. Giannuzzi, A. Miliozzi, R.D. Maggio, F. Girardi, et al., Thermal storage of sensible heat using concrete modules in solar power plants, Sol. Energy 103 (2014) 303–315.
[35] H.-W. Yuan, C.-H. Lu, Z.-Z. Xu, Y.-R. Ni, X.-H. Lan, Mechanical and thermal properties of cement composite graphite for solar thermal storage materials, Sol. Energy 86 (2012) 3227–3233.
[36] N. Nallusamy, S. Sampath, R. Velraj, Experimental investigation on a combined sensible and latent heat storage system integrated with constant/varying (solar) heat sources, Renew. Energy 32 (2007) 1206–1227.
[37] S.D. Sharma, K. Sagara, Latent heat storage materials and systems: a review, Int. J. Green Energy 2 (1) (2007) 1–56.
[38] A. Abhat, Low temperature latent heat thermal energy storage: heat storage materials, Sol. Energy 30 (4) (1983) 313–332.
[39] A.F. Regin, S.C. Solanki, J.S. Saini, Heat transfer characteristics of thermal energy storage system using PCM capsules: a review, Renew. Sustain. Energy Rev. 12 (9) (2012) 2438–2458.
[40] G. Zanganeh, M. Commerford, A. Haselbacher, A. Pedretti, A. Steinfeld, Stabilization of the outflow temperature of a packed-bed thermal energy storage by combining rocks with phase change materials, Appl. Therm. Eng. 70 (2014) 316–320.
[41] A.S.A. Ammar, M.A. El-Osairy, A.A. Ghoneim, Comparison of measured and predicted performance of heat storage unit packed with spheres of a local material, Renew. Energy 2 (1) (1992) 73–76.
[42] A.M. Khudhair, M.M. Farid, A review on energy conservation in building applications with thermal storage by latent heat using phase change materials, Energy Convers. Manag. 45 (2004) 263–273.
[43] D. Zhou, C. Zhou, Y. Tian, Reviewon thermal storage with phase change materials(PCMs) in building applications, Appl. Energy 92 (2012) 593–605.
[44] J. Heier, C. Bales, V. Martin, Combining thermal energy storage with buildings – a review, Renew. Sustain. Energy Rev. 42 (2015) 1305–1325.
[45] A. Hesaraki, S. Holmberg, F. Haghighat, Seasonal thermal energy storage with heat pumps and low temperatures in building projects—a comparative review, Renew. Sustain. Energy Rev. 43 (2015) 1199–1213.
[46] D.N. Nkwetta, F. Haghighat, Thermal energy storage with phase change material—a state-of-the art review, Sustain. Cities Soc. 10 (2014) 87–100.
[47] F. Rouault, D. Bruneau, P. Sebastian, J. Lopez, Experimental investigation and modelling of a low temperature PCM thermal energy exchange and storage system, Energy Build. 83 (2014) 96–107.
[48] F. Bruno, N.H.S. Tay, M. Belusko, Minimising energy usage for domestic cooling with off-peak PCM storage, Energy Build. 76 (2014) 347–353.
[49] A.G. Ferandez, S. Ushak, H. Galleguillos, F.J.P. a, Thermal characterisation of an innovative quaternary molten nitrate mixture for energy storage in CSP plants, Sol. Energy Mater. Sol. Cells 132 (2015) 172–177.
[50] N. Calvet, J.C. Gomez, A. Faik, V.V. Roddatis, A. Meffre, G.C. Glatzmaier, et al., Compatibility of a post-industrial ceramic with nitrate molten salts for use as filler material in a thermocline storage system, Appl. Energy 109 (2013) 387–393.
[51] C. Martin, T. Bauer, H. Müller-Steinhagen, An experimental study of a non-eutectic mixture of KNO_3 and $NaNO_3$ with a melting range for thermal energy storage, Appl. Therm. Eng. 56 (2013) 159–166.
[52] V. Tyagi, D. Buddhi, PCM thermal energy storage in buildings: a state of art renewable sustainable energy review, Renew. Sustain. energy Rev. 11 (2007) 1146–1166.
[53] Y. Yuan, N. Zhang, W. Tao, X. Cao, Y. He, Fatty acids as phase change materials: a review, Renew. Sustain. Energy Rev. 29 (2014) 482–498.
[54] A. Sari, K. Kaygusuz, Thermal performance of palmitic acid as a phase change energy storage material, Energy Conversat. Manag. 43 (6) (2002) 863–876.
[55] Y. Konuklu, M. Unal, H.O. Paksoy, Microencapsulation of caprylic acid with different wall materials as phase change material for thermal energy storage, Sol. Energy Mater. Sol. Cells 120 (2014) 536–542.
[56] H. Mehling, L. Cabeza, Heat and Cold Storage with PCM. An up to Date Introduction into Basics and Applications, Springer, 2008.
[57] L. Cabeza, A. Castell, C. Barreneche, A.d. Gracia, A. Fernandez, Materials used as PCM in thermal energy storage in buildings: a review, Renew. Sustain Energy Rev. 15 (3) (2011) 1675–1695.
[58] C. Liang, X. Lingling, S. Hongbo, Z. Zhibin, Microencapsulation of butyl stearate as a phase change material by interfacial polycondensation in a polyurea system, Energy Convers. Manag. 50 (3) (2009) 723–729.
[59] D.R. Lide, CRC Handbook of Chemistry and Physics, Vol. 92, Taylor and Francis, Ohio, 2011.
[60] H. He, P. Zhao, Q. Yue, B. Gao, D. Yue, Q. Li, A novel polynary fatty acid/sludge ceramsite composite phase change materials and its applications in building energy conservation, Renew. Energy 76 (2015) 45–52.
[61] N.D.D. Crareto, T. Castagnaro, M.C. Costa, A.J.A. Meirelles, The binary (solid + liquid) phase diagrams of (caprylic or capric acid) + (1-octanol or 1-decanol), J. Chem. Thermodyn. 78 (2014) 99–108.
[62] R.I. Olivares, W. Edwards, $LiNO_3$–$NaNO_3$–KNO_3 salt for thermal energy storage: Thermal stability evaluation in different atmospheres, Thermochim. Acta 560 (2013) 34–42.
[63] A.E. Gheribi, J.A. Torres, P. Chartrand, Recommended values for the thermal conductivity of molten salts between the melting and boiling points, Sol. Energy Mater. Sol. Cells 126 (2014) 11–25.
[64] K. Posern, C. Kaps, Calorimetric studies of thermochemical heat storage materials based on mixtures of $MgSO_4$ and $MgCl_2$, Thermochim. Acta 502 (2010) 73–76.
[65] A.G. Fernández, S. Ushak, H. Galleguillos, F.J. Perez, Development of new molten salts with $LiNO_3$ and $Ca(NO_3)_2$ for energy storage in CSP plants, Appl. Energy 119 (2014) 131–140.
[66] A. Sari, C. Alkan, A.N. Ozcan, Synthesis and characterization of micro/nano capsules of PMMA/capric-stearic acid eutectic mixture for low temperature-thermal energy storage in buildings, Energy Build. 90 (2015) 106–113.
[67] Z. Acem, L. Jerome, P.D.B. Elena, KNO_3/$NaNO_3$ e graphite materials for thermal energy storage at high temperature: part-I elaboration methods and thermal properties, Appl. Therm. Eng. 30 (2010) 1580–1585.
[68] N. Şahan, M. Fois, Halime Paksoy, Improving thermal conductivity phase change materials—a study of paraffin nanomagnetite composites, Sol. Energy Mater. SolarCells 137 (2015) 61–67.
[69] Z. Wang, Z. Zhang, L. Jia, L. Yang, Paraffin and paraffin/aluminum foam composite phase change material heat storage experimental study based on thermal management of Li-ion battery, Appl. Therm. Eng. 78 (2015) 428–436.

Please cite this article in press as: A. Dinker, et al., Heat storage materials, geometry and applications: A review, Journal of the Energy Institute (2015), http://dx.doi.org/10.1016/j.joei.2015.10.002

[70] N. Zhang, Y. Yuan, Y. Yuan, T. Li, X. Cao, Lauric-palmitic-stearic acid/expanded perlite composite as form-stable phase change material: preparation and thermal properties, Energy Build. 82 (2014) 505–511.
[71] C. Liu, Y. Yuan, N. Zhang, X. Cao, X. Yang, A novel PCM of lauric-myristic-stearic acid/expanded graphite composite for thermal energy storage,, Mater. Lett. 120 (2014) 43–46.
[72] X. Yang, Y. Yuan, N. Zhang, X. Cao, C. Liu, Preparation and properties of myristic-palmitic-stearic acid/expanded graphite composites as phase change materials for energy storage, Sol. Energy 99 (2014) 259–266.
[73] N. Zhang, Y. Yuan, Y. Yuan, X. Cao, X. Yang, Effect of carbon nanotubes on the thermal behavior of palmitic-stearic acid eutectic mixtures as phase change materials for energy storage, Sol. Energy 110 (2014) 64–70.
[74] A. Fethi, L. Mohamed, K. Mustapha, B. ameurTarek, B.N. Sassi, Investigation of a graphite/paraffin phase change composite, Int. J. Therm. Sci. 88 (2015) 128–135.
[75] M. Lachheb, M. Karkri, F. Albouchi, S.B. Nasrallah, M. Fois, P. Sobolciak, Thermal properties measurement and heat storage analysis of paraffin/graphite composite phase change material, Compos. Part B 66 (2014) 518–525.
[76] W. Mhike, W.W. Focke, J.P. Mofokeng, A.S. Luyt, Thermally conductive phase-change materials for energy storage based on low-density polyethylene, soft Fischer–-Tropsch wax and graphite, Thermochim. Acta 527 (2012) 75–82.
[77] A. Sarı, A. Karaipekli, Thermal conductivity and latent heat thermal energy storage characteristics of paraffin/expanded graphite composite as phase change material, Appl. Therm. Eng. 27 (2007) 1271–1277.
[78] J. Wang, H. Xie, Z. Guo, L. Guan, Y. Li, Improved thermal properties of paraffin wax by the addition of TiO_2 nanoparticles, Appl. Therm. Eng. 73 (2014) 1541–1547.
[79] Y. Yuan, Y. Yuan, N. Zhang, Y. Du, X. Cao, Preparation and thermal characterization of capric-myristic-palmitic acid/expanded graphite composite as phase change material for energy storage, Mater. Lett. 125 (2014) 154–157.
[80] N. Zhang, Y. Yuan, Y. Du, X. Cao, Y. Yuan, Preparation and properties of palmitic-stearic acid eutectic mixture/expanded graphite composite as phase change material for energy storage, Energy 78 (2014) 950–956.
[81] Y. Wang, T.D. Xia, H.X. Feng, H. Zhang, Stearic acid/polymethylmethacrylate composite as form-stable phase change materials for latent heat thermal energy storage, Renew. Energy 36 (6) (2011) 1814–1820.
[82] A. Karaipekli, A. Sarı, Capric–myristic acid/expanded perlite composite as form-stable phase change material for latent heat thermal energy storage, Renew. Energy 33 (12) (2008) 2599–2605.
[83] C. Jiao, B. Ji, D. Fang, Preparation and properties of lauric acid–stearic acid/expanded perlite composite as phase change materials for thermal energy storage, Mater. Lett. 67 (1) (2012) 352–354.
[84] D. Mei, Bing Zhang, R. Liu, Y. Zhang, L. Jindun, Preparation of capricacid/halloysite nanotube composite as form-stable phase change material for thermal energy storage, Sol. EnergyMaterials&SolarCells 92 (2011) 2772–2777.
[85] H. Fauzi, H.S.C. Metselaar, T.M.I. Mahlia, M. Silakhori, H. Nur, Phase change material: optimizing the thermal properties and thermal conductivity of myristic acid/palmitic acid eutectic mixture with acid-based surfactants, Appl. Therm. Eng. 60 (1–2) (2013) 261–265.
[86] M. Mehrali, S.T. Latibari, M. Mehralia, T.M.I. Mahlia, H.S.C. Metselaar, M.S. Naghavi, et al., Preparation and characterization of palmitic acid/graphene nanoplatelets composite with remarkable thermal conductivity as a novel shape-stabilized phase change material, Appl. Therm. Eng. 61 (2) (2013) 633–640.
[87] N. Zhang, Y. Yuan, X. Wang, X. Cao, X. Yang, S. Hu, Preparation and characterization of lauric–myristic–palmitic acid ternary eutectic mixtures/expanded graphite composite phase change material for thermal energy storage, Chem. Eng. J. 231 (2013) 214–219.
[88] A. Karaipekli, A. Sarı, K. Kaygusuz, Thermal conductivity improvement of stearic acid using expanded graphite and carbon fiber for energy storage applications, Renew. Energy 32 (2007) 2201–2210.
[89] F. Ye, Z. Ge, Y. Ding, J. Yang, Multi-walled carbon nanotubes added to Na_2CO_3/MgO composites forthermal energy storage, Particuology 15 (2014) 56–60.
[90] A. Greco, X. Jiang, D. Cao, An investigation of lithium-ion battery thermal management using paraffin/porous-graphite-matrix composite, J. Power Sources 278 (2015) 50–68.
[91] Z. Huang, X. Gao, T. Xu, Y. Fang, Z. Zhang, Thermal property measurement and heat storage analysis of $LiNO_3$/KCl – expanded graphite composite phase change material, Appl. Energy 115 (2014) 265–271.
[92] L.C. Olson, J.W. Ambrosek, K. Sridharan, M.H. Anderson, T.R. Allen, Materials corrosion in molten LiF–NaF–KF salt, J. Fluor. Chem. 130 (2009) 67–73.
[93] S. Mat, A.A. Al-Abidi, K. Sopian, M.Y. S, A.T. Mohammada, Enhance heat transfer for PCM melting in triplex tube with internal–external fins, Energy Convers. Manag. 76 (2013) 223–236.
[94] M. Rahimi, A.A. Ranjbar, D.D. Ganji, K. Sedighi, M.J. Hosseini, R. Bahrampoury, Analysis of geometrical and operational parameters of PCM in a fin and tube heat exchanger, Int. Commun. Heat Mass Transf. 53 (2014) 109–115.
[95] N. Soares, A.R. Gaspar, P. Santos, J.J. Costa, Experimental study of the heat transfer through a vertical stack of rectangular cavities filled with phase change materials, Appl. Energy 142 (2015) 192–205.
[96] G. Ferrer, A. Sol, C. Barreneche, I. Martorell, L.F. Cabeza, Corrosion of metal containers for use in PCM energy storage, Renew. Energy 76 (2015) 465–469.
[97] C. Liu, D. Groulx, Experimental study of the phase change heat transfer inside a horizontal cylindrical latent heat energy storage system, Int. J. Therm. Sci. 82 (2014) 100–110.
[98] R.E. Murray, D. Groulx, Experimental study of the phase change and energy characteristics inside a cylindrical latent heat energy storage system: part 2 simultaneous charging and discharging, Renew. Energy 63 (2014) 724–734.
[99] S.P. Jesumathy, M. Udayakumar, S. Suresh, S. Jegadheeswaran, An experimental study on heat transfer characteristics of paraffin wax in horizontal double pipe heat latent heat storage unit, J. Taiwan Inst. Chem. Eng. 45 (2014) 1298–1306.
[100] S. Lorente, A. Bejan, J.L. Niu, Phase change heat storage in an enclosure with vertical pipe in the center, Int. J. Heat Mass Transf. 72 (2014) 329–335.
[101] M.Y. Yazıcı, M. Avcı, O. Aydın, M. Akgun, Effect of eccentricity on melting behavior of paraffin in a horizontal tube-in-shell storage unit: an experimental study, Sol. Energy 101 (2014) 291–298.
[102] Y.L. Shabtay, J.R.H. Black, Compact hot water storage systems combining copper tube with high conductivity graphite and phase change materials, Energy Procedia 48 (2014) 423–430.
[103] M. Johnson, M. Fiss, T. Klemm, M. Eck, Test and analysis of a flat plate latent heat storage design, Energy Procedia 57 (2014) 662–671.
[104] H. Shokouhmand, B. Kamkari, Experimental investigation on melting heat transfer characteristics of lauric acid in a rectangular thermal storage unit, Exp. Therm. Fluid Sci. 50 (2013) 201–212.
[105] E. Oro, L. Miro, C. Barreneche, I. Martorell, M.M. Farid, L.F. Cabeza, Corrosion of metal and polymer containers for use in PCM cold storage, Appl. Energy 109 (2013) 449–453.
[107] M. Liu, M. Belusko, N.H.S. Tay, F. Bruno, Impact of the heat transfer fluid in a flat plate phase change thermal storage unit for concentrated solar tower plants, Sol. Energy 101 (2014) 220–231.
[109] A. Sarı, Ali Karaipekli, Preparation, thermal properties and thermal reliability of palmitic acid/expanded graphite composite as form-stable PCM for thermal energy storage, Sol. EnergyMaterials&SolarCells 93 (2009) 571–576.
[113] L. Shilei, Z. Neng, F. Guohui, Eutectic mixtures of capric acid and lauric acid applied in building wallboards for heat energy storage, Energy Build. 38 (2006) 708–711.
[114] S. Harikrishnan, S. Magesh, S. Kalaiselvam, Preparation and thermal energy storage behaviour of stearic acid–TiO_2 nanofluids as a phase change material for solar heating systems, Thermochimica Acta 565 (2013) 137–145.
[115] P. Moreno, L. Miro, A. Sole, C. Barreneche, C. Sole, I. Martorell, L.F. Cabeza, Corrosion of metal and metal alloy containers in contact with phase change materials (PCM) for potential heating and cooling applications, Appl. Energy 125 (2014) 238–245.

Further reading

[106] T. Kousksou, A. Jamil, T.E. Rhafiki, Y. Zeraouli, Paraffin wax mixtures as phase change materials, Sol. Energy Mater. SolarCells 94 (2010) 2158–2165.
[108] P. Moreno, L. Miro, A. Sole, C. Barreneche, C. Sole, I. Martorell, et al., Corrosion of metal and metal alloy containers in contact with phase change materials (PCM) for potential heating and cooling applications, Appl. Energy 125 (2014) 238–245.
[110] A. Sharma, A. Shukla, C.R. Chen, S. Dwivedi, Development of phase change materials for building applications, Energy Build. 64 (2013) 403–407.
[111] P. Tatsidjodoung, N.L. Pierres, L. Luo, A review of potential materials for thermal energy storage in building applications, Renew. Sustain. Energy Rev. 18 (2013) 327–349.
[112] Z. Ge, F. Ye, H. Cao, G. Leng, Y. Qind, Y. Ding, Carbonate-salt-based composite materials for medium- and high-temperature thermal energy storage, Particuology (2013).

Please cite this article in press as: A. Dinker, et al., Heat storage materials, geometry and applications: A review, Journal of the Energy Institute (2015), http://dx.doi.org/10.1016/j.joei.2015.10.002

Taylor & Francis
Taylor & Francis Group

Experimental Heat Transfer

A Journal of Thermal Energy Generation, Transport, Storage, and Conversion

ISSN: 0891-6152 (Print) 1521-0480 (Online) Journal homepage: http://www.tandfonline.com/loi/ueht20

Preparation, characterization, and performance study of beeswax/expanded graphite composite as thermal storage material

A. Dinker, M. Agarwal & G. D. Agarwal

To cite this article: A. Dinker, M. Agarwal & G. D. Agarwal (2017) Preparation, characterization, and performance study of beeswax/expanded graphite composite as thermal storage material, Experimental Heat Transfer, 30:2, 139-150, DOI: 10.1080/08916152.2016.1185198

To link to this article: http://dx.doi.org/10.1080/08916152.2016.1185198

Accepted author version posted online: 24 May 2016.
Published online: 24 May 2016.

EXPERIMENTAL HEAT TRANSFER
2017, VOL. 30, NO. 2, 139–150
http://dx.doi.org/10.1080/08916152.2016.1185198

Taylor & Francis
Taylor & Francis Group

Preparation, characterization, and performance study of beeswax/expanded graphite composite as thermal storage material

A. Dinker,[a] M. Agarwal,[a] and G. D. Agarwal[b]

[a]Department of Chemical Engineering, Malaviya National Institute of Technology, Jaipur, Rajasthan, India; [b]Department of Mechanical Engineering, Malaviya National Institute of Technology, Jaipur, Rajasthan, India

ABSTRACT

In this study, beeswax as a new energy storage material and its composite with expanded graphite were prepared and characterized for their surface and thermal properties. Surface characterization showed no chemical interaction between beeswax and expanded graphite. The thermal conductivity of the composite was improved with 117% enhancement. The thermal performance of beeswax and its composite as a heat storage material was studied in a rectangular shell-and-tube thermal storage unit. The melting point of the composite remained almost same as that of beeswax; however, the melting time was reduced considerably, from 540 to 360 min with inlet water at 80°C and a 2-lpm flow rate.

ARTICLE HISTORY
Received 5 January 2016
Accepted 27 April 2016

KEYWORDS
beeswax; expanded graphite; composite storage material; latent heat storage; shell-and-tube storage unit

Introduction

Latent heat storage systems using phase change materials (PCMs) received great attention over the last few decades due to their high energy density, compact size, and wider area of applications. Selection of the proper PCM depends on various factors, such as melting point, thermal conductivity, latent heat, degree of super cooling, and chemical inertness [1–5].

Paraffin and fatty acids were most commonly used as organic PCMs by earlier researchers for various applications, such as domestic solar water heating, maintaining inner temperatures of buildings, and cooling applications, due to their low melting point, high latent heat, chemical inertness, etc. [6–10]. Paraffin was used for different solar thermal storage applications [11–15] and heat-recovery systems in pure or composite form [16, 17]. Similarly, fatty acids and their mixtures were also studied as PCMs for various domestic solar heating applications with good performance [18–21]; however, paraffin wax and fatty acids have low thermal conductivity, high cost of production, and unsustainability in terms of usage [22]. It is observed that in some cases, fatty acids cause allergic effects and thus require special handling [23–25].

Beeswax is a naturally occurring substance and it is a mixture of alkanes, alkenes, monoesters, diesters, hydroxymonoesters, and fatty acids. Thirty to 80% of beeswax consists of long-chained esters of palmitic, oleic, and tetracosanoic acid [26–29]. Beeswax has many applications, including the manufacturing of candles, preparation of sculptures, coating of jelly, pharmaceuticals, varnishes, and cosmetics [30]. Beeswax can be used as a PCM in place of paraffin and fatty acids because of its similar thermal properties for thermal storage applications along with low cost and easy availability, especially in Asian countries. Beeswax as a PCM has low melting temperature range (62°C–64°C), high latent heat, chemical inertness, thermal cyclic stability, and no phase segregation on heating [31]. Being a natural substance obtained directly from honeybees, the production cost for beeswax is quite low and provides a

CONTACT Dr. Mahdu Agarwal madhunaresh@gmail.com Department of Chemical Engineering, Malaviya National Institute of Technology, Jaipur, JLN Marg, Rajasthan, Jaipur, 302017, India.
Color versions of one or more of the figures in the article can be found online at www.tandfonline.com/ueht.

sustainable solution for thermal storage applications [22]. However, it has low thermal conductivity (0.298 W/m.K) and high charging and discharging time during melting and solidification. Many methods have been suggested in the literature to enhance the thermal conductivity of organic PCMs, such as addition of high thermal conductivity solid particles, including metal chips and nanoparticles [32–34], altering the geometrical structure of heat storage units by addition of fins [35–38], and the addition of expanded graphite [39–41] PCM impregnation [42, 43]. A critical review by Zhang et al. in 2016 [44] also revealed that composite PCMs can effectively improve the performance of thermal storage systems through enhancement of the thermal conductivity of PCMs. In this study, expanded graphite was used to enhance the thermal conductivity of beeswax, as expanded graphite is lighter in weight, possesses high thermal conductivity, and provides a larger surface area for heat transfer.

Surface characteristics of beeswax were analyzed using x-ray diffraction (XRD), scanning electron microscopy (SEM), and Fourier transform infrared (FTIR) spectroscopy. Thermal properties of beeswax were analyzed by differential scanning calorimetry (DSC) and thermal gravimetric analysis (TGA). Performance of thermal storage material was studied using a shell-and-tube heat storage unit with charging and discharging time. The selected heat storage material was filled in the shell, and hot water as the heat transfer fluid passed through the tube at the center of the unit. In the present study, beeswax has been tried as the new heat storage material, and its composite with expanded graphite was developed; the performance of these materials is studied experimentally.

Material and methods

Preparation of expanded graphite

Natural graphite (NG), with average particle size of 200 μm, was used to prepare the expanded graphite by forming an intercalated compound using chemical the oxidation method as proposed by Zeng et al. [45] with some modifications. NG (Ases Chemicals, Jodhpur, India), nitric acid of 65% concentration (Qualikems, Gujarat, India), glacial acetic acid with 99.5% concentration (Qualikems, Gujarat, India), and potassium per magnet (99% concentration; Qualikems, Gujarat, India) were obtained from local market and used for the development of expanded graphite in the present study. The preparation method involves mixing of NG with nitric acid (3 mL/g of NG), glacial acetic acid (3 mL/g of NG), and potassium per magnet (0.25 g/g of NG) in a beaker. This mixture was stirred on a hot plate magnetic stirrer (300-W model-Q19-A; Remi) at 45°C for 90 min to obtain the intercalated compound, i.e., expandable graphite. This was washed three times with distilled water and then dried overnight at 60°C in a digital oven (model-SHI-102; Shivam Instruments, Jaipur, India). Expanded graphite was then obtained by irradiation of the expandable graphite inside a microwave oven (model CE1031L; Samsung, Jaipur) at 900 W for 60 sec per 0.20 g sample mass. This finally developed expanded graphite (EG) was then stored in an airtight container for further use.

Preparation of beeswax/EG composite

Beeswax (Qualikems, Gujarat, India) was purchased from local market of Jaipur, India, and the beeswax composite was prepared by dispersing expanded graphite in molten beeswax. Ten percent expanded graphite was added to 90 wt% of molten beeswax at 70°C in a beaker and stirred for 1 h to ensure homogeneous dispersion of expanded graphite within the beeswax. The prepared composite was then allowed to cool to room temperature. Composites of beeswax with NG and expanded graphite were prepared in similar weight percentages, and thermal conductivity was measured using a thermal constants analyzer (model-TPS 500; Hot Disk, Jaipur) and compared.

Sample characterization

Surface characterization of samples was carried out using a scanning electron microscope (model Nova Nano FE-SEM 450; FEI, Jaipur), an x-ray diffractometer (model Xpert Pro; Pan Analytical, Jaipur), and

an FTIR spectroscope (model Spectrum 2; Perkin Elmer, Jaipur). For SEM analysis, no coating of samples was required as samples were conducting. XRD analysis was carried out at $2\theta = 90°C$, while the FTIR investigation was done for a wavelength range ($400-4{,}000\ cm^{-1}$). DSC (Make-Perkin Elmer, Jaipur) was used to analyze the thermal behavior of the samples and analysis was performed at constant heating rate of 10°C/min for temperature range of 10-300°C under constant stream of nitrogen. Thermal stability of samples was analyzed using TGA (model-STA 6000; Perkin Elmer, Jaipur) between temperature ranges of 25°C and 400°C.

Latent heat storage unit

A rectangular shell-and-tube type thermal storage unit (horizontal type) was developed to study the thermal storage characteristics of beeswax and the beeswax/expanded graphite composite. This unit was connected to a hot water tank stainless steel ((SS), 100 L) through a pump (1/2 HP), three valves (brass), and a rotameter (range 0 – 10 LPM; Star Flow, Jaipur), as shown in Figure 1. The heat storage unit (31 cm × 8.5 cm × 9.5 cm) was fabricated using plywood (0.25 cm thick) and lined internally with 1-cm-thick asbestos sheet to provide insulation. Hot water was passed through a straight copper tube (8-mm internal diameter, 0.5-mm wall thickness) located at the center of the unit. Calibrated K-type thermocouples (Ni-Al, accuracy ±0.3°C, range −200°C to 1,350°C) were used to measure the temperature of the storage material at nine points along with inlet and outlet temperatures of the hot water. The position of thermocouples within the thermal storage unit is shown in Figure 2. During experimentation, the inlet temperature and flow rate of hot water was kept constant at 80°C and 120 L/hr, respectively.

Uncertainty analysis

There may be some uncertainties in the experimental results. The uncertainty may be in the measurement of temperature by K-type thermocouples, flow rate by the rotameter, and in the thermal conductivity meter reading. These uncertainty values were ±0.5°C for thermocouples and ±2% for the

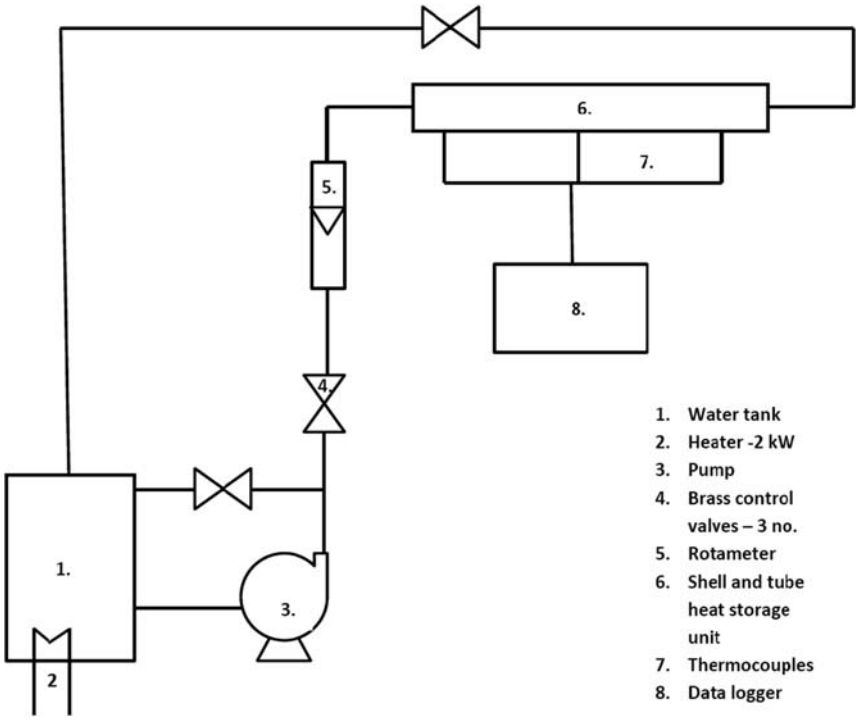

Figure 1. Schematic diagram of shell-and-tube type experimental set-up.

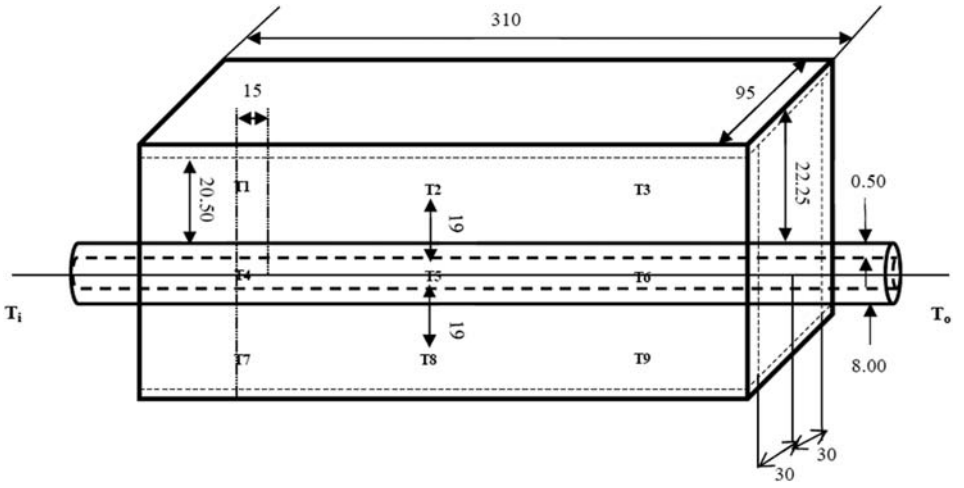

Figure 2. Thermocouple position in shell-and-tube heat storage unit. All dimensions are in mm.

rotameter as claimed by the manufacturers. The uncertainty in thermal conductivity measurement was ±4.06% as calculated by the methods explained in [46, 47].

Results and discussion

Sample thermal conductivity

Composites of beeswax with different NG and expanded graphite weight percentages were prepared to enhance the thermal conductivity of beeswax. The thermal conductivity of these samples were measured and plotted as shown in Figure 3. It was found that beeswax composites with expanded graphite had higher thermal conductivity compared to beeswax with NG; this may be due to the presence of a continuous matrix of expanded graphite throughout the beeswax that enhanced the heat flow through the composite (beeswax/expanded graphite), while in the other case (beeswax/NG composite), the discontinuous phase of NG leads to lower heat flow. It was noticed that composites of beeswax/NG were non-homogenous during the molten state due to settlement of the NG. The optimum weight percentage of expanded graphite was found to be 10%, as further addition of expanded graphite results in

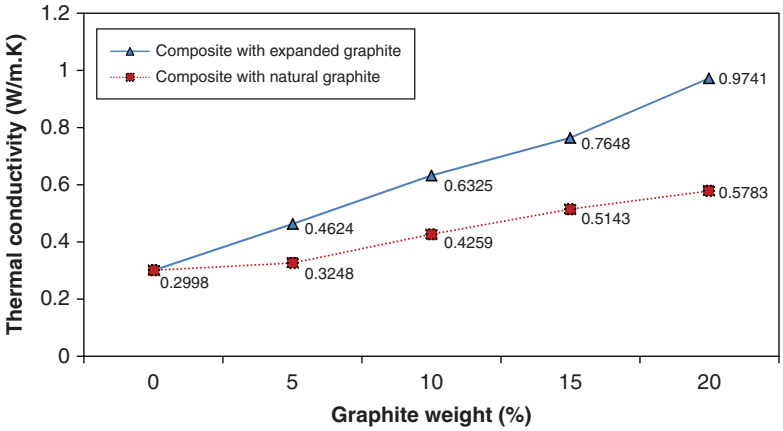

Figure 3. Plot between thermal conductivity and weight percentage of samples.

cracks in the composite that create air pockets and reduce the thermal conductivity. The specific heat of beeswax and its composite with expanded graphite is calculated as 2.6 and 3.0 kJ/kg K, respectively.

Microstructures of the samples

SEM images of NG, expanded graphite, and beeswax/expanded graphite composite is presented in Figure 4. The microstructure of NG particles is compact with less surface area due the absence of proper intra-layer separation and results in poor heat transfer. It is also observed that the high density of NG leads to its settlement during melting of the composite, and the beeswax/NG composite cannot be used for thermal storage applications. In the case of expanded graphite chemical oxidation with potassium, a permagnet generates a proper network of interconnected pores by separation of layers, as observable from Figure 4b, which increases the thermal contact area for beeswax; these interconnected pores provide a network of layers for better heat transfer and reduce the density of expanded graphite. Thus, light density expanded graphite forms a homogeneous mixture with beeswax, and a stable composite as heat storage material is obtained as shown in Figure 4c.

XRD patterns of beeswax, beeswax/expanded graphite composite, and expanded graphite are shown in Figure 5. The XRD pattern of the beeswax/expanded graphite composite showed low intensity peaks at $2\theta = 21°$, 23°, and 26° (d-spacing values 4.1185, 3.6997, and 3.3127, respectively). The peaks at $2\theta = 21°$ and 23° for beeswax (with d spacing values 4.1981 and 3.7805) are found to be similar to the peaks for composite material, and the peak at $2\theta = 26°$ (d spacing 3.947) is an extra peak generated due to the expanded graphite. The XRD pattern of beeswax/expanded graphite composite clearly shows that the composite formed is a mixture of two materials rather than formation of a new material by chemical conversion.

FTIR spectra of beeswax, beeswax/expanded graphite composite, and expanded graphite are depicted in Figure 6. The peak at a wavelength of 3,446 cm^{-1} for expanded graphite represents –O–H stretching, while the peak at 2,846 cm^{-1} represents a –C–H stretch, the alkane bonds present in the hexagonal structure of the graphite. The peak at 1,382 cm^{-1} represented the symmetric N–O stretch, which may be due to the presence of the nitro group, while the peak at 1,646 cm^{-1} represents –C ≡ C– stretch. FTIR spectra of beeswax show peaks at 2,922 and 2,852 cm^{-1}, the C–H stretch, i.e., the presence of alkane/hydrocarbons (HC) chain. Peaks at 1,742 cm^{-1} reflect the presence of ester, while peaks at 1,104 and 718 cm^{-1} represent alkene and amide groups. Similar FTIR spectra results for

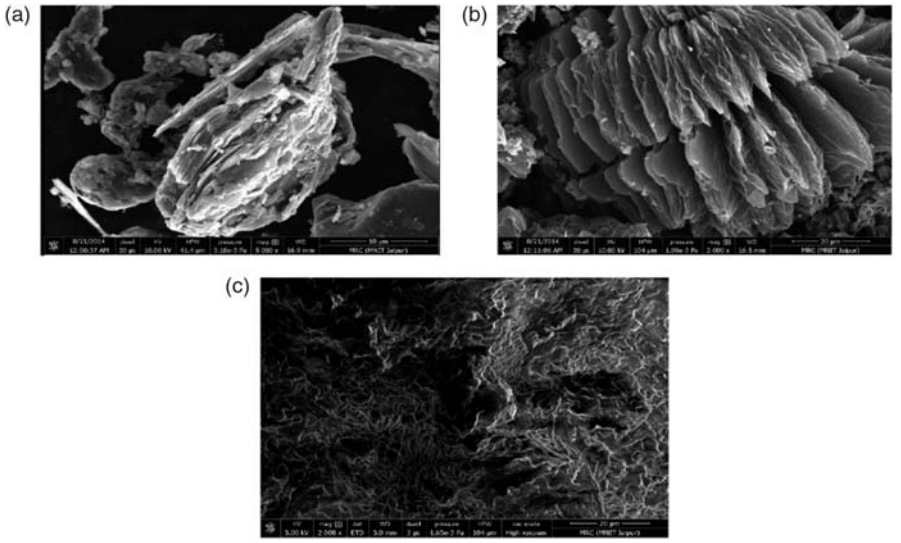

Figure 4. SEM images: (a) NG, (b) expanded graphite, and (c) composite.

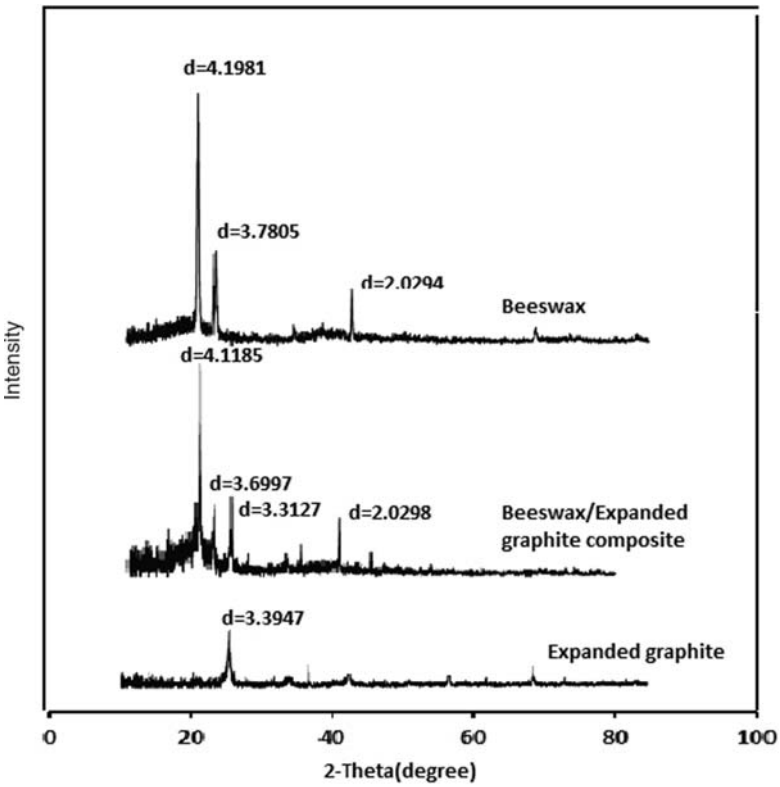

Figure 5. XRD pattern for beeswax, composite, and expanded graphite.

beeswax were also reported in [6, 48]. FTIR spectra of composite material are very similar to the FTIR spectra of beeswax due to merging of peaks of expanded graphite (3,446 and 2,916 cm^{-1}) within the peaks of composite (3,444 and 2,916 cm^{-1}). The absence of any new peak in the FTIR of composite material confirmed that the composite of beeswax and expanded graphite was just a combination of two materials rather than a chemically new material.

Thermal characterization of samples

DSC and TGA of the samples were carried out to evaluate their thermal properties. The DSC plot between heat flow and temperature for beeswax and beeswax/expanded graphite composite is shown in Figure 7, and it is observed that the peak obtained at 62.06°C for beeswax is due to the solid–liquid transactions. The DSC peak for beeswax/expanded graphite composite, however, shows a little reduction in the melting point of the composite from 62.06°C to 59.89°C. Latent heat for beeswax and its composite with expanded graphite is obtained from DSC as 214 and 201 kJ/kg, respectively. The TGA plot for beeswax and beeswax/expanded graphite is shown in Figure 8, and it is observed that there is no change in the weight of beeswax up to 388°C; after that, decreases may be due to the vaporization. The composite of beeswax/expanded graphite follows an almost similar pattern except a reduction in weight after 359°C; this may be due to enhanced thermal conductivity of the composite, which leads to its early vaporization.

Thermal energy storage performance evaluation

The thermal energy storage performance of beeswax and beeswax/expanded graphite composite is performed in a rectangular shell-and-tube heat storage unit. The shell part of this storage unit

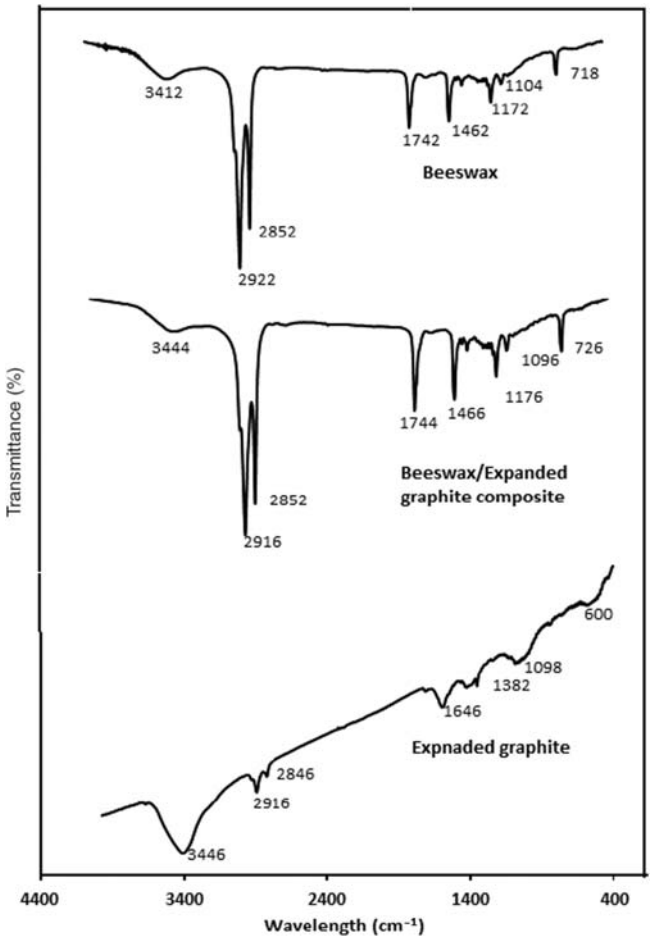

Figure 6. FTIR spectra of beeswax, composite, and expanded graphite.

contained beeswax as a PCM; hot water passed through the central copper tube, and nine temperatures at three axial locations were measured using calibrated K-type thermocouples along with hot water inlet and outlet temperatures. Figure 9 shows the temperature variation at the nine locations with time for beeswax and composite of beeswax/expanded graphite. It is observed that the time taken by beeswax to

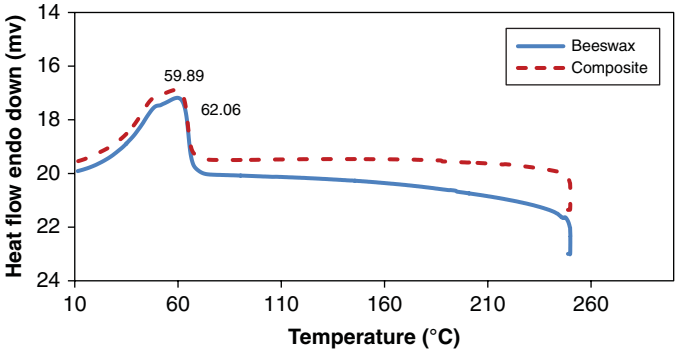

Figure 7. DSC plot for beeswax and composite.

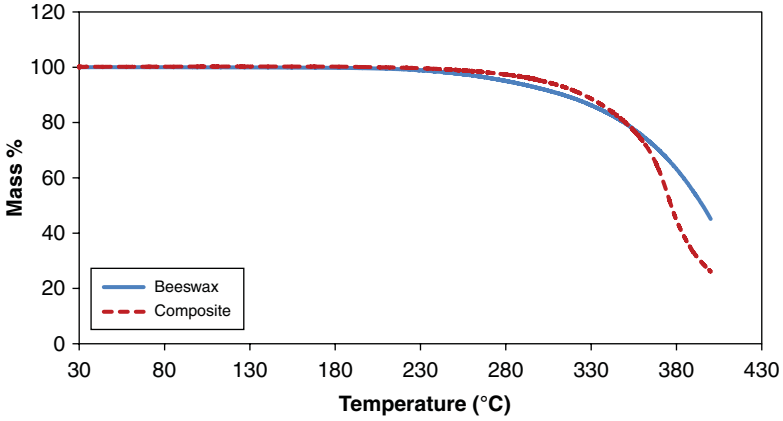

Figure 8. TGA plot for beeswax and composite.

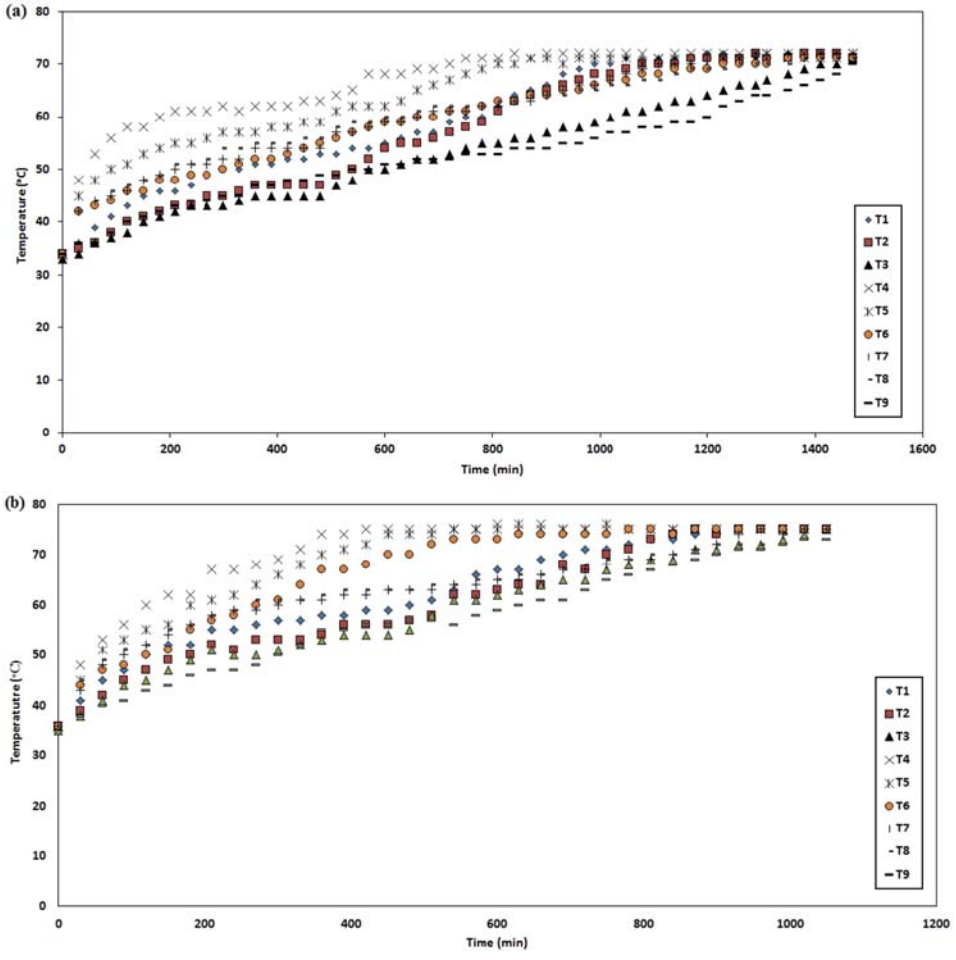

Figure 9. Temperature variation with time: (a) beeswax and (b) composite.

reach the melting point increases from the inlet (at point T4, 360 min), middle point (at point T5, 540 min), to the outlet (at point T6, 780 min) due to continuous reduction in temperature gradient between the hot water and beeswax. Similar patterns for reduction in melting time of the beeswax were observed for the axial points above (T1: 810 min, T2: 840 min, T3: 1,140 min) and below the tube (T7: 840 min, T8: 870 min, T9: 1,260 min). However, in the case of the composite of beeswax and expanded graphite, the melting time was reduced at all points along the axis (T4: 200 min, T5: 250 min, T6: 330 min) and parallel to the axis at the top (T1: 540 min, T2: 600 min, T3: 630 min) and bottom positions (T7: 450 min, T8: 480 min, T9: 720 min). After a certain time, the PCM in the shell reaches the same temperature at almost all points due to the convection effect. All nine thermocouples reached a constant temperature in 1,020 min in the case of the composite as compared to pure beeswax (1,430 min). The reduction in melting time in the case of the composite was due to enhanced thermal conductivity of beeswax due to the addition of expanded graphite.

The temperature rise with time at three locations along the vertical plane near the inlet of the tube for beeswax (Figure 10a) and for beeswax/expanded graphite composite (Figure 10b) is shown in Figure 10; it is observed that the temperature at the middle location (T4) of the heat transfer unit rose most rapidly compared to other locations, i.e., T1 and T7. This is due to the large temperature difference between the hot water and PCM at the middle location, which caused good heat condction, while in the upper and lower locations of the heat transfer unit, heat transferred through conduction followed by convection. It is also observed from Figure 10 that in both cases, the temperature at the lower location (T7) initially increased rapidly up to the melting point and then slowed down compared to the upper location (T1). During this process, the PCM melted first at the middle location and moved down to the lower location due to a gravitation effect, transferring heat and raising the temperature at

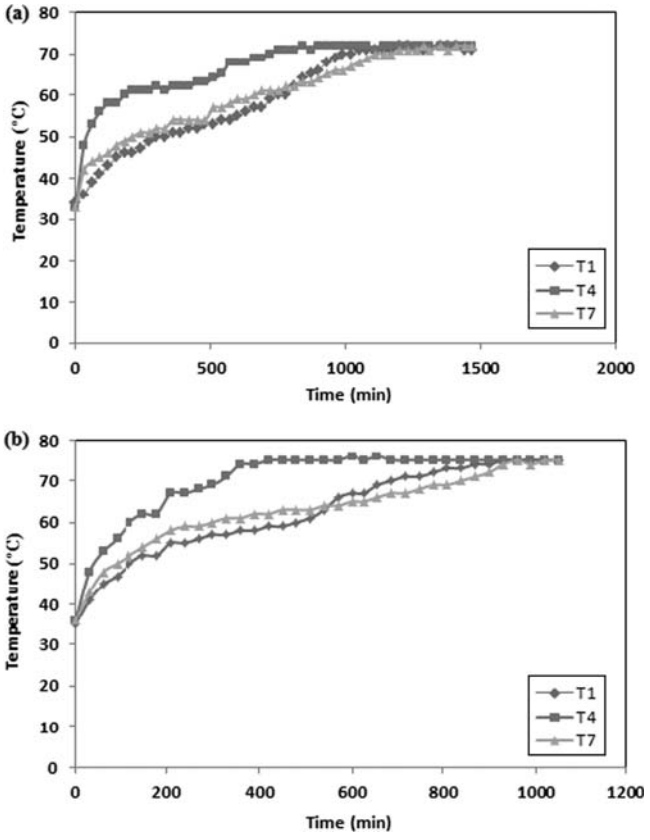

Figure 10. Temperature variation with time along vertical plane at inlet of tube: (a) beeswax and (b) composite.

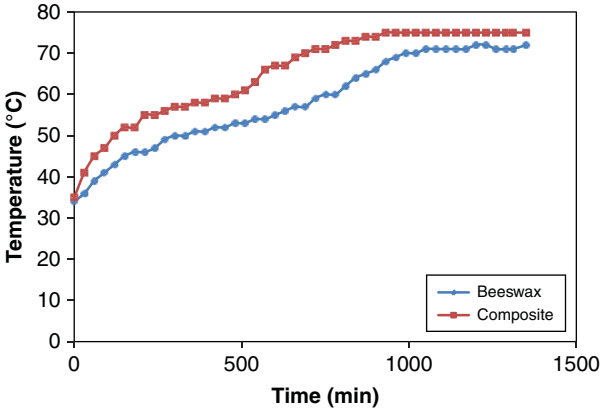

Figure 11. Temperature variations at top location (T1) of thermal storage unit.

the lower material. When the temperature of the lower material reaches the melting point, the convection heat transfer becomes dominant and forces the molten PCM to move upward of the unit. The temperature rise of the upper material in the unit is due to the combined effect of conduction from the middle location followed by convection from the middle and lower material of the unit. Along with conduction due to change in phase and density of beeswax (with temperature rise), natural convection plays an important role in heat transfer. With a rise in temperature at the middle part of the thermal storage unit, less dense melted beeswax started to move upward due to buoyancy, while a major part of it moved down due to a gravitational effect; it is responsible for the increased rate of heating in the lower part compared to the upper part of the thermal storage unit. As the beeswax in the bottom part melts completely, buoyancy forces along with convection current moved it to the upper part of the thermal storage unit to deliver more heat.

Temperature variation of PCM in the upper location (T1) of the thermal storage unit is shown in Figure 11 for beeswax and its composite. The time required to reach melting point is 800 min for beeswax; the temperature then further increases due to conduction and convection. However, in case of the composite material, the melting point was reached in less time, i.e., 540 min, due to the enhanced thermal conductivity of the composite material. It is also observed that time taken by the beeswax to attain a constant temperature of 72°C for complete material was 1,020 min compared to 900 min (for a constant temperature of 75°C) in the case of composite material. The reduction in charging time to reach constant temperature in whole composite material was due to the presence of an interconnected network of expanded graphite, which enhanced thermal conductivity.

Conclusion

Beeswax is a naturally available PCM that has lower thermal conductivity and requires more time to store thermal energy. The addition of expanded graphite to the beeswax enhances its thermal conductivity, and it is found that a 10% addition of EG in beeswax enhanced thermal conductivity from 0.29 to 0.63 W/m K (117% enhancement). The improvement in thermal conductivity of composite material reduced its melting time from 1,020 min (for pure beeswax) to 900 min.

SEM images of composite material showed that expanded graphite formed a continuous network within the beeswax and also that some beeswax got absorbed within the porous surface of the expanded graphite, which further enhanced the heat transfer through beeswax. XRD and FTIR analysis showed that the peaks appearing in beeswax/expanded graphite composite material were similar to the peaks observed in pure beeswax and expanded graphite, which clearly indicated that the prepared composite material was merely a mixture of two base materials rather than a new chemical compound. DSC analysis of composite material showed that the melting point of the composite was slightly lower than

that of pure beeswax. Thermal performance studies on storage material using a shell-and-tube type thermal storage unit showed that the time taken by composite material to store heat was 12% less compared to beeswax. The results of the present study show that the developed composite material from beeswax and 10% expanded graphite is a promising and reliable heat storage material for low-temperature thermal applications

Funding

This work was supported by MNIT Jaipur, India, as part of Ph.D. research and was funded by the same.

References

1. S. Wang, P. Qin, X. Fang, Z. Zhang, S. Wang, and X. Liu, A Novel Sebacic Acid/Expanded Graphite Composite Phase Change Material for Solar Thermal Medium-Temperature Applications, *Solar Energy*, vol. 99, pp. 283–290, 2014.
2. B. He and F. Setterwall, Technical Grade Paraffin Waxes as Phase Change Materials for Cool Thermal Storage and Cool Storage Systems Capital Cost Estimation, *Energy Convers. Manage.*, vol. 43, pp. 1709–1723, 2002.
3. M. Kenisarin and K. Mahkamov, Solar Energy Storage Using Phase Change Materials, *Renew. Sustain. Energy Rev.*, vol. 11, pp. 1913–1965, 2007.
4. A. Shukla, D. Buddhi, and R. L. Sawhney, Solar Water Heaters with Phase Change Material Thermal Energy Storage Medium: A Review, *Renew. Sustain. Energy Rev.*, vol. 13, pp. 2119–2125, 2009.
5. B. Zalba, B. M. J. Marin, L. F. Cabeza, and H. Mehling, Review on Thermal Energy Storage with Phase Change: Materials, Heat Transfer Analysis and Applications, *Appl. Thermal Eng.*, vol. 23, pp. 251–283, 2003.
6. Z. Sun, Y. Zhang, S. Zheng, Y. Park, and R. L. Frost, Preparation and Thermal Energy Storage Properties of Paraffin/Calcined Diatomite Composites as Form-Stable Phase Change Materials, *Thermochim. Acta*, vol. 558, pp. 16–21, 2013.
7. Z. Zhang, N. Zhang, J. Peng, X. Fang, X. Gao, and Y. Fang, Preparation and Thermal Energy Storage Properties of paraffin/Expanded Graphite Composite Phase Change Material, *Appl. Energy*, vol. 91, pp. 426–431, 2012.
8. A. Sariand and A. Karaipekli, Thermal Conductivity and Latent Heat Thermal Energy Storage Characteristics of Paraffin/Expanded Graphite Composite as Phase Change Material, *Appl. Therm. Eng.*, vol. 27, pp. 1271–1277, 2007.
9. M. K. Rathod and J. Banerjee, Experimental Investigations on latent Heat Storage Unit Using Paraffin Wax as Phase Change Material, *Exp. Heat Transf.*, vol. 27, pp. 40–55, 2014.
10. F. Trinquet, L. Karim, G. Lefebvre, and L. Royon, Mechanical Properties and Melting Heat Transfer Characteristics of Shape-Stabilized Paraffin Slurry, *Exp. Heat Transf.*, vol. 27, pp. 1–13, 2014.
11. A. Sharma, S. D. Sharma, and D. Buddhi, Accelerated Thermal Cycle Test of Acetamide, Stearic Acid and Paraffin Wax for Solar Thermal Latent Heat Storage Applications, *Energy Convers. Manage.*, vol. 43, pp. 1923–1930, 2002.
12. A. Sari, Form-Stable Paraffin/High Density Polyethylene Composites as Solid–Liquid Phase Change Material for Thermal Energy Storage: Preparation and Thermal Properties, *Energy Convers. Manage.*, vol. 45, pp. 2033–2042, 2004.
13. I. Al-Hinti, A. Al-Ghandoor, A. Maaly, I. A. Naqeera, Z. Al-Khateeb, and O. Al-Sheikh, Experimental Investigation on the Use of Water-Phase Change Material Storage in Conventional Solar Water Heating Systems, *Energy Convers. Manage.*, vol. 51, pp. 1735–1740, 2014.
14. S. O. Enibe, Performance of a Natural Circulation Solar Air Heating System with Phase Change Material Energy Storage, *Renew. Energy*, vol. 27, pp. 69–86, 2002.
15. A. Kurkulu, A. A. Zmerzi, and S. Bilgin, Thermal Performance of a Water-Phase Change Material Solar Collector, *Renew. Energy*, vol. 26, pp. 391–399, 2002.
16. Z. Gu, H. Liu, and Y. Li, Thermal Energy Recovery of air Conditioning System and Heat Recovery System Calculation and Phase Change Materials Development, *Appl. Therm. Eng.*, vol. 24, pp. 2511–2526, 2004.
17. N. Nallusamy, S. Sampath, and R. Velraj, Experimental Investigation on a Combined Sensible and Latent Heat Storage System Integrated with Constant/Varying (Solar) Heat Sources, *Renew. Energy*, vol. 32, pp. 1206–1227, 2007.
18. M. Mazman, L. F. Cabeza, H. Mehling, M. Nogues, H. Evliya, and H. A. Paksoy, Utilization of Phase Change Materials in Solar Domestic Hot Water Systems, *Renew. Energy*, vol. 34, pp. 1639–1643, 2009.
19. A. Sari and K. Kaygusuz, Thermal Performance of Myristic Acid as a Phase Change Material for Energy Storage Application, *Renew. Energy*, vol. 24, pp. 303–317, 2001.
20. D. Rozanna, T. G. Chuah, A. Salmiah, T. S. Y. Choong, and M. Sari, Fatty Acids as Phase Change Materials (PCMs) for Thermal Energy Storage: A Review, *Int. J. Green Energy*, vol. 1, pp. 495–513, 2005.
21. A. S. K. Kaygusuz, Thermal Energy Storage System Using Some Fatty Acids as Latent Heat Energy Storage Materials, *Energy Source*, vol. 23, pp. 275–285, 2001.

22. M. E. Hossain, M. I. Khan, C. Ketata, and M. R. Islam, Comparative Pathway Analysis of Paraffin Wax and Beeswax for Industrial Applications, *Int. J. Char. Develop. Novel Mat.*, vol. 1, pp. 1–13, 2010.
23. B. Zimnicka and A. Hacura, An Investigation of Molecular Structure and Dynamics of Crude Beeswax by Vibrational Spectroscopy, *Pol. J. Environ. Stud.*, vol. 15, pp. 112–114, 2006.
24. G. Baran and A. Sari, Phase Change and Heat Transfer Characteristics of a Eutectic Mixture of Palmitic and Stearic Acids as PCM in a Latent Heat Storage System, *Energy Convers. Manage.*, vol. 44, pp. 3227–3246, 2003.
25. K. Tuncbilek, A. Sari, S. Tarhan, G. Ergunes, and K. Kaygusuz, Lauric and Palmitic Acids Eutectic Mixture as Latent Heat Storage Material for Low Temperature Heating Applications, *Energy*, vol. 30, pp. 677–692, 2005.
26. X. Xiao, P. Zhang, and M. Li, Preparation and Thermal Characterization of Paraffin/Metal Foam Composite Phase Change Material, *Appl. Energy*, vol. 112, pp. 1357–1366, 2013.
27. M. A. Jackson and F. J. Eller, Isolation of Long-Chain Aliphatic Alcohols from Beeswax Using Lipase-Catalyzed Methanolysis in Supercritical Carbon Dioxide, *J. Supercrit. Fluids*, vol. 37, pp. 173–177, 2006.
28. R. Aichholz and E. Lorbee, Investigation of Combwax of Honeybees with High-Temperature Gas Chromatography and High-Temperature Gas Chromatography-Chemical Ionization Mass Spectrometry: I. High-Temperature Gas Chromatography, *J. Chromatogr. A*, vol. 855, pp. 601–615, 1999.
29. R. Aichholz and E. Lorbeer, Investigation of Combwax of Honeybees with High-Temperature Gas Chromatography and High-Temperature Gas Chromatography Chemical Ionization Mass Spectrometry: II: High-Temperature Gas Chromatography Chemical Ionization Mass Spectrometry, *J. Chromatogr. A*, vol. 883, pp. 75–88, 2000.
30. S. Bogdanov, S. Bogdanov, *The Beeswax Book*, Ch. 1, Beeswax: Properties, composition and control, pp. 1–18. Product Science, Sweden, 2009.
31. R. Buchwald, M. D. Breed, and A. R. Greenberg, The Thermal Properties of Beeswaxes: Unexpected Findings, *J. Exp. Biol.*, vol. 211, pp. 121–127, 2008.
32. S. Kim and L. T. Drzal, High Latent Heat Storage and High Thermal Conductive Phase Change Materials Using Exfoliated Graphite Nanoplatelets, *Sol. Energ. Mater. Solar Cells*, vol. 93, pp. 136–142, 2009.
33. L. Xia, P. Zhang, and R. Z. Wang, Preparation and Thermal Characterization of Expanded Graphite/Paraffin Composite Phase Change Material, *Carbon*, vol. 48, pp. 2538–2548, 2010.
34. X. Py, R. Olives, and S. Mauran, Paraffin/Porous-Graphite-Matrix Composite as a High and Constant Power Thermal Storage Material, *Int. J. Heat Mass Transf.*, vol. 44, pp. 2727–2737, 2001.
35. A. Castell, C. Sola, M. Medrano, J. Roca, L. F. Cabeza, and D. Garca, Natural Convection Heat Transfer Coefficients in Phase Change Material (PCM) Modules with External Vertical Fins, *Appl. Therm. Eng.*, vol. 28, pp. 1676–1686, 2008.
36. V. Shatikian, G. Ziskind, and R. Letan, Numerical Investigation of a PCM-Based Heat Sink with Internal Fins, *Int. J. Heat Mass Transf.*, vol. 48, pp. 3689–3706, 2005.
37. A. Yataganbaba and I. Kurtbas, Effect of Heating Position on Thermal Energy Storage in Cavity with/Without Open-Cell Metallic Foams, *Exp. Heat Transfer*, vol. 29, pp. 355–377, 2016.
38. R. Baby and C. Balaji, Network-Based Optimization of Thermal Performance of Phase Change Material-Based Finned Heat Sink—An Experimental Study, *Exp. Heat Transf.*, vol. 26, pp. 431–452, 2013.
39. X. Yang, Y. Yuan, N. Zhang, X. Cao, and C. Liu, Preparation and Properties of Myristic-Palmitic-Stearic Acid/Expanded Graphite Composites as Phase Change Materials for Energy Storage, *Solar Energy*, vol. 99, pp. 259–266, 2014.
40. Z. Zhang, G. Shi, S. Wang, X. Fang, and X. Liu, Thermal energy Storage Cement Mortar Containing n-Octadecane/Expanded Graphite Composite Phase Change Material, *Renew. Energy*, vol. 50, pp. 670–675, 2013.
41. D. Mei, B. Zhang, R. Liu, Y. Zhang, and J. Liu, Preparation of Capric Acid/Halloysite Nanotube Composite as Form-Stable Phase Change Material for Thermal Energy Storage, *Sol. Energy Mater. Solar Cells*, vol. 95, pp. 2772–2777, 2011.
42. A. Mills, M. Farid, J. R. Selman, and S. Al-Hallaj, Thermal Conductivity Enhancement of Phase Change Materials Using a Graphite Matrix, *Appl. Therm. Eng.*, vol. 26, pp. 1652–1661, 2006.
43. S. G. Jeong, J. Jeon, J. H. Lee, and S. Kim, Optimal Preparation of PCM/Diatomite Composites for Enhancing Thermal Properties, *Int. J. Heat Mass Transf.*, vol. 62, pp. 711–717, 2013.
44. P. Zhang, X. Xiao, and Z. W. Ma, A Review of the Composite Phase Change Materials: Fabrication, Characterization, Mathematical Modeling and Application to Performance Enhancement, *Appl. Energy*, vol. 165, pp. 472–510, 2016.
45. J. L. Zeng, J. Gan, F. R. Zhu, S. B. Yu, Z. L. Xiao, W. P. Yan, L. Zhu, Z. Q. Liu, L. X. Sun, and Z. Cao, Tetradecanol/Expanded Graphite Composite Form-Stable Phase Change Material for Thermal Energy Storage, *Solar Energy Mater. Solar Cells*, vol. 127, pp. 122–128, 2014.
46. X. Xiao, P. Zhang, and M. Li, Experimental and Numerical Study of Heat Transfer Performance of Nitrate/Expanded Graphite Composite PCM for Solar Energy Storage, *Energy Convers. Manage.*, vol. 105, pp. 272–284, 2015.
47. X. Xiao, P. Zhang, and M. Li, Effective Thermal Conductivity of Open-Cell Metal Foams Impregnated with Pure Paraffin for Latent Heat Storage, *Int. J. Therm. Sci.*, vol. 81, pp. 94–105, 2014.
48. S. Patel, D. R. Nelson, and A. G. Gibbs, Chemical and Physical Analyses of Wax Ester Properties, *J. Insect Sci.*, vol. 1, pp. 4–7, 2001.

Applied Thermal Engineering 111 (2017) 358–368

Contents lists available at ScienceDirect

Applied Thermal Engineering

journal homepage: www.elsevier.com/locate/apthermeng

Research Paper

Experimental assessment on thermal storage performance of beeswax in a helical tube embedded storage unit

Abhay Dinker [a], Madhu Agarwal [a,*], G.D. Agarwal [b]

[a] Department of Chemical Engineering, MNIT Jaipur, 302017, India
[b] Department of Mechanical Engineering, MNIT Jaipur, 302017, India

HIGHLIGHTS

- Beeswax has been introduced as natural phase change material.
- Beeswax was characterized for its thermal properties.
- Shell and tube type unit with embedded helical coil for thermal storage is proposed.
- Increase in inlet temperature of heat transfer fluid decreased charging time.
- Increase in flow rate of heat transfer fluid decreased efficiency of thermal storage unit.

ARTICLE INFO

Article history:
Received 2 June 2016
Revised 27 August 2016
Accepted 21 September 2016
Available online 22 September 2016

Keywords:
Beeswax
Phase change material
Latent heat storage
Thermal storage unit
Storage efficiency
Charging time

ABSTRACT

In the present study beeswax is considered as a natural latent heat storage material. A novel rectangular shell and tube type geometry is introduced as a thermal storage unit (TSU), in which copper helical coil carrying hot heat transfer fluid is embedded in the beeswax filled in rectangular shell. Thermal performance study of beeswax is carried out in a series of charging and discharging experiments with water as a heat transfer fluid (HTF). Temperature profiles along the axial and vertical direction of helical coil have been recorded by measuring nine temperatures to understand the mode of heat transfer within the beeswax. Effect of flow rates (0.25 LPM, 0.5 LPM, 0.75 LPM, 1.0 LPM) and inlet temperatures (60 °C, 70 °C, 80 °C) of HTF on charging time and thermal storage efficiency of beeswax is analyzed. It is observed that increase in fluid flow rate reduced the charging time and storage efficiency of the system, however increase in fluid inlet temperature increased the charging time of the system. Maximum efficiency of TSU during charging was 84% when HTF at 80 °C flows through TSU at 0.5 LPM. Results of the study prove beeswax as low cost and naturally available phase change material (PCM) performance wise better than conventional PCMs in lower temperature range.

1. Introduction

Our society is facing energy crisis due to rapidly depleting fossil fuels and environmental problems like global warming, climate change, loss of biodiversity, deforestation and ozone layer depletion. Studies revealed a sharp increase in greenhouse gases in environment. It is estimated that by the year 2400 there is about 5000 gigatonnes of carbon will be released in environment starting from industrial revolution keeping rates of fossil fuel consumption and carbon-sequestration constant [1]. Due to enhanced greenhouse effect average rise in temperature occurred globally at the rate of 0.15–0.20 °C [2,3]. Another concern with rise in greenhouse gases is the depletion of ozone layer led to increased environmental and health problems [4,5]. To address the above problems there is need of energy storage to reduce fossil fuel consumption and burden on environment. Renewable source of energy is intermittent in nature and dependent on weather conditions and therefore required some sort of energy storage systems like photo-voltaic systems [6–8], photovoltaic/thermal hybrid system, sensible energy storage through solar ponds [9,10], latent energy storage [11–13], concentrated solar plant [14,15] and hydrogen storage system [16–18].

Latent energy storage systems are one of the promising technologies available at present to meet world's energy crisis. These systems uses phase change material to store heat as latent heat of melting during their phase transition i.e. from solid to liquid.

* Corresponding author.
E-mail addresses: madhunaresh@gmail.com, magarwal.chem@mnit.ac.in (M. Agarwal).

http://dx.doi.org/10.1016/j.applthermaleng.2016.09.128
1359-4311/

Nomenclature

Dimensional variables

d_i	inner diameter of tube (m)
d_o	outer diameter of tube (m)
C_{ps}	heat capacity of solid (J kg^{-1} K^{-1})
C_{pl}	heat capacity of liquid (J kg^{-1} K^{-1})
T_w	wall temperature (K)
T_b	bulk temperature (K)
T_{out}	fluid outlet temperature (K)
T_{in}	fluid inlet temperature (K)
T_m	melting temperature (K)
T_i	initial temperature of PCM (K)
T_f	final temperature of PCM (K)
ΔT_m	least mean temperature difference (K)
$\dot{m}$	mass flow rate of HTF (kg s^{-1})
m_w	mass of PCM (kg)
ρ	density of water (kg m^{-3})
v	velocity (m s^{-1})
$\dot{Q}$	instantaneous energy (kJ/s)
Q_a	available energy (kJ)
Q_w	energy required by wax (kJ)
L	latent heat of fusion (kJ/kg)
U_o	overall heat transfer coefficient (W m^{-2} K^{-1})
h_i	internal heat transfer coefficient (W m^{-2} K^{-1})
h_o	external heat transfer coefficient (W m^{-2} K^{-1})
k	thermal conductivity (W m^{-1} K^{-1})
β	thermal expansion coefficient (K^{-1})
g	acceleration due to gravity (m s^{-2})
D_c	diameter of curvature (m)
L	length of tube (m)
b	pitch length (m)
A_s	total surface area of tube (m^{-2})
A_o	outer surface area of the coil (m^{-2})
A_i	inner surface area of the coil (m^{-2})

Dimensionless numbers

Nu_i	inside Nusselt number
Nu_o	outside Nusselt number
R_e	Reynolds number
D_e	Dean number
Pr	Prandlt number
γ	dimensionless pitch
Ra	Rayleigh number
Gr	Grashof number
N	total number of turns

Abbreviations

PCM	phase change material
HTF	heat transfer fluid
LPM	liter per minute
TSU	thermal storage unit

A latent heat storage system stores heat at a constant temperature and therefore has high energy storage density (5–10 times more as compared to sensible energy storage) [19]. High energy density, isothermal energy storage, low volume change, low vapor pressure, no super cooling and choice of temperature range are important properties of phase change materials for domestic and industrial applications like domestic solar water heater [20,21], temperature control of buildings [22] and electricity generation through concentrated solar power [23,24] respectively.

A variety of organic and inorganic phase change materials (PCMs) are available for the development of an efficient thermal energy storage system. Selection and use of an appropriate PCM is dependent on factors like melting point, stability after thermal cycles, toxicity and corrosive nature [25,26]. Inorganic phase change materials like sodium nitrate [27], sodium carbonate/lithium carbonate [28], sodium carbonate/sodium chloride binary mixture [29], lithium nitrate/potassium chloride mixture [30], Magnesium nitrate/magnesium chloride mixture [31], etc. with their high melting point temperature range are suitable for higher temperature heat storage applications like concentrated solar power plant [32,33], however, most of them are highly corrosive in nature [34,35] which reduces the life of thermal storage units and therefore needs special handling [34]. Organic phase change materials like Paraffin [14,36–38] and fatty acids [39–41] with low melting point range like paraffin, fatty acids, and fatty alcohols are commonly being used for lower temperature applications. These organic materials offer a wide possibility in solar thermal applications for heating water and for maintaining the indoor building temperatures [42]. Paraffin is the most commonly used PCM for lower temperature applications; however, being a derivative of petroleum product its production process involves the use of various toxic catalysts and follows the pathway where various byproducts of carcinogenic nature are produced [43] which make its promotion as promising PCM unsustainable for the environment. Fatty acids and their esters due to their higher cost of production are not recommendable for thermal energy storage applications [39]. These limitations of synthetic organic phase change materials restrict their use and demands for the identification and introduction of new phase change materials which are technically and economically feasible, easily available for different applications.

In this work natural beeswax is introduced as a new phase change material for latent heat storage. Beeswax is obtained from honey bees consisting of fatty acids (mainly palmitic acid, tetracosanoic acid and oleic acid), long chain of alkanes, monoesters (C_{24} to C_{34}), diesters, and hydroxyl-monoesters [44] and mainly used for making sculptures, candles and also in food and medical industries for surface coatings [45–49]. Beeswax also finds potential application in the field of drug delivery and proved more efficient as compared to other waxes in faster release of drugs [50,51]. Despite of its wide applications in the food, medical and other sectors the application of beeswax as thermal storage material is not reported much.

Natural beeswax is non-toxic, non-corrosive, having low melting point (60–68 °C), high latent heat of transition (145–395 kJ/kg) [52,53], small volume change, low vapor pressure and long term chemical stability almost similar to conventional paraffin [54,55]. Being a natural product its cost is quite less as compared to other organic materials and its production and degradation does not involve any toxic byproduct which makes it a sustainable product [56] and can be used in place of paraffin and other organic PCMs as latent heat storage material.

For an efficient thermal storage system an effective PCM as well as an efficient geometrical configuration is required for faster heat transfer. Various numerical and experimental thermal performance studies have been performed on shell and tube type thermal storage units using straight tube configuration for different organic PCMs [57–59]. These storage units are generally consisting of cylindrical shell encapsulating the PCM with straight tube carrying HTF. There are different geometries of shell and tube

configurations studied for thermal storage systems in the literature such as- single straight tube geometry [60,61], multiple straight tube geometry [62,63] and helical coil geometry [30,64,65]. However some studies have revealed that for the same volume of PCM used and same heat transfer area, rectangular shell configuration required lesser melting time as compared to the cylindrical shell configuration [66,67]. Some experimental and numerical work on helical tube based heat exchangers and thermal storage systems showed better efficiency and heat transfer as compared to straight tube geometry. This is due to higher heat transfer coefficient, generation of secondary flow by unbalanced centrifugal force and minimal axial dispersion [68,30,69]. Various works showed the advantages of using helical coil over straight tube for an effective heat transfer [70,71]. The use beeswax as thermal storage material with rectangular shell and helical coil type geometry is not available in the literature and studied in detail in the present paper.

Objective of this paper is to study thermal performance of natural beeswax in a rectangular shell and helical tube type thermal storage unit at different fluid flow rates and inlet temperatures. Thermo-fluidic phenomena of beeswax during charging process are studied, and efficiency and heat transfer coefficient of thermal storage system is analyzed.

2. Experimental methodology

2.1. Thermal analysis of beeswax

Beeswax (Make-CDH, India) obtained from local vendor is a natural product derived from honeybee. It is ecofriendly and having reasonably good latent heat over a small temperature range of 58–60 °C [72]. Melting and solidification properties of beeswax was measured using differential scanning calorimetry (DSC) (Make-Perkin Elmer), in which about 4 mg of beeswax was added in the alumina sample pan and placed in the instrument. Inert environment during the analysis was maintained by passing nitrogen gas at rate of 50 mL/min and melting characteristics were studied by heating the sample at a rate of 10 °C per minute up to the temperature of 250 °C. Linear baseline correction for alumina sample pan was performed before calculating latent heat for the samples. After complete melting of the beeswax, the sample was again cooled at the similar rate in order to study its solidification/cooling characteristics. In order to get deviation of instrument two samples of pure beeswax were tested under same experimental conditions. Fig. 1 shows the DSC result of beeswax (sample A and sample B) with peak at 42.3 °C representing the solid-solid phase transition in the beeswax while another peak at 59.8 °C showing solid-liquid phase transition occurred during melting. The melting and solidification temperature were found to be same for both the sample (sample A and sample B) with 2% deviation in heat flow. From DSC analysis melting point and freezing point of beeswax were found to be 59.8 ± 0.5 °C and 56.4 ± 0.5 °C respectively, while the latent heat of melting was measured as 214 kJ/kg for temperature range 30.8–68 °C.

Thermal gravimetric analysis of beeswax was carried out using TGA instrument (Make- Perkin Elmer, India). 25.61 mg of beeswax was added to ceramic crucible and placed within the instrument. An inert environment was maintained during the study using nitrogen gas at heating rate of 10 °C/min up to 400 °C. Fig. 2 depicts the graph for TGA analysis and no weight loss was observed up to 215 °C, with standard deviation of ±1.8% confirms its thermal stability up to this temperature. After 215 °C there is mass reduction

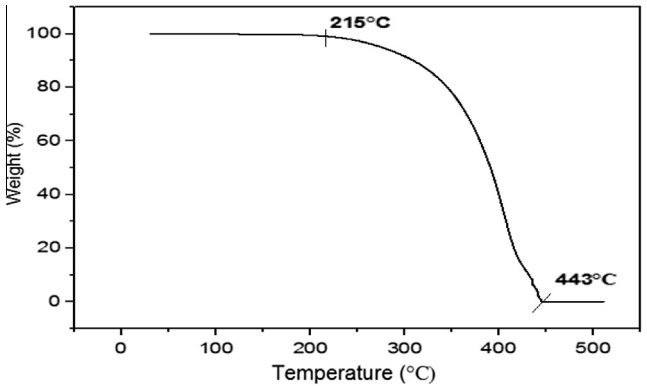

Fig. 2. TGA analysis of beeswax.

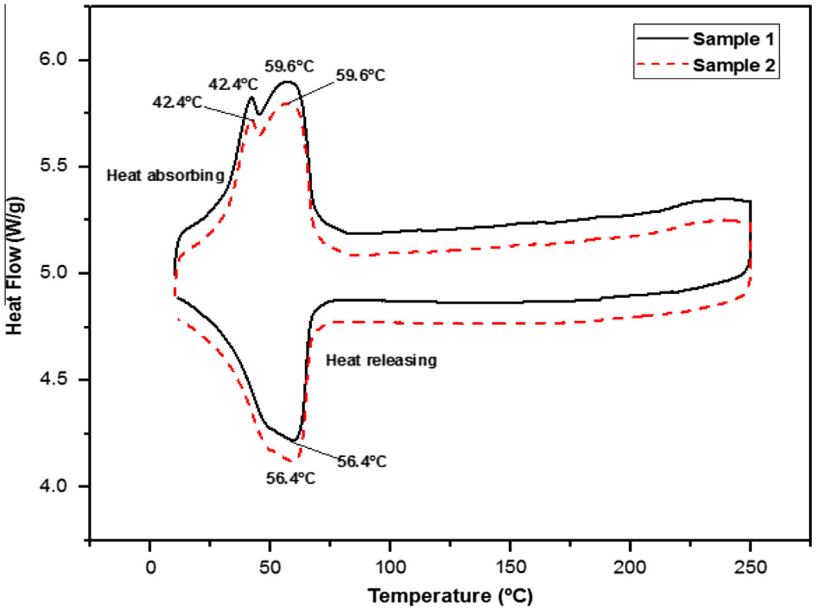

Fig. 1. DSC curves for beeswax.

of beeswax which may be due to vaporization of beeswax by degradation of hydrocarbons up to 443 °C where complete weight loss of beeswax was observed. Stability of beeswax makes it suitable for domestic and solar applications in the temperature range of 60–90 °C. Thermal conductivity of beeswax was measured using benchtop thermal constant analyzer (Model-TPS 500, Make-Hotdisk). To test the thermal conductivity of beeswax 5 samples of beeswax were taken from bulk. These 5 samples were used to prepare 5 pellets (10 mm diameter and 4 mm thick) using pelletizer. Each pellet is then tested with Kapton sensor within TPS instrument to measure its thermal conductivity. The final thermal conductivity of beeswax is then determined by taking average value of these 5 samples. Thermal conductivity of beeswax was observed as 0.299 ± 4% W/m K at room temperature while thermal conductivity of liquid beeswax was found to be 0.30 ± 4% W/m K at its melting point.

2.2. Geometry of TSU

A rectangular shell and helical tube type thermal storage unit (Fig. 3) is developed to experimentally study the thermal storage performance of beeswax. The rectangular shell (610 mm × 360 mm × 450 mm) of thermal storage unit is made up of teak wood (20 mm thick, k = 0.12–0.04 W/m K) having low thermal conductivity [73] and inner side of the shell is well insulated by the thermocol (25 mm thick, k = 0.033 W/m K) [74] followed by insulation layer of asbestos (10 mm thick, k = 0.08 W/m K) to avoid any heat loss from PCM to the ambient air. A helical coil having 13 turns of copper tube (I.D. = 8 mm, O.D. = 9 mm) with pitch of 3 cm and coil diameter of 110.6 mm is passing through the center of the shell. TSU in a loop (Fig. 3) comprising of a hot water tank made of stainless steel (capacity 100 L) with embedded electric heater (2 kW, Make- Bajaj India), glass rotameter (0.25 LPM–1 LPM), a centrifugal pump (1/2 hp, Make – Crompton, India) and brass valves. Nine k-type thermocouples (Ni-Cr based) with accuracy of ±0.2 °C (Fig. 4) are placed along vertical and axial positions at equal distances embedded within PCM inside thermal storage. Two more two thermocouples are placed at the inlet and outlet of the TSU in order to study variation in temperature during charging and discharging cycle. Fig. 5 represents the picture of actual setup and Fig. 6 showing the picture of inner part of TSU before and after filling beeswax. Geometry of helical coil is defined by some other parameters as:

(a) Curvature ratio - a dimensionless parameter of the coil defined as the ratio of inner diameter of the tube to coil diameter, $\delta = \frac{d_i}{2R_c}$
(b) Non-dimensional pitch, $\gamma = b/2\pi R_c$
(c) Reynolds number, $R_e = \frac{\rho v d_i}{\mu}$

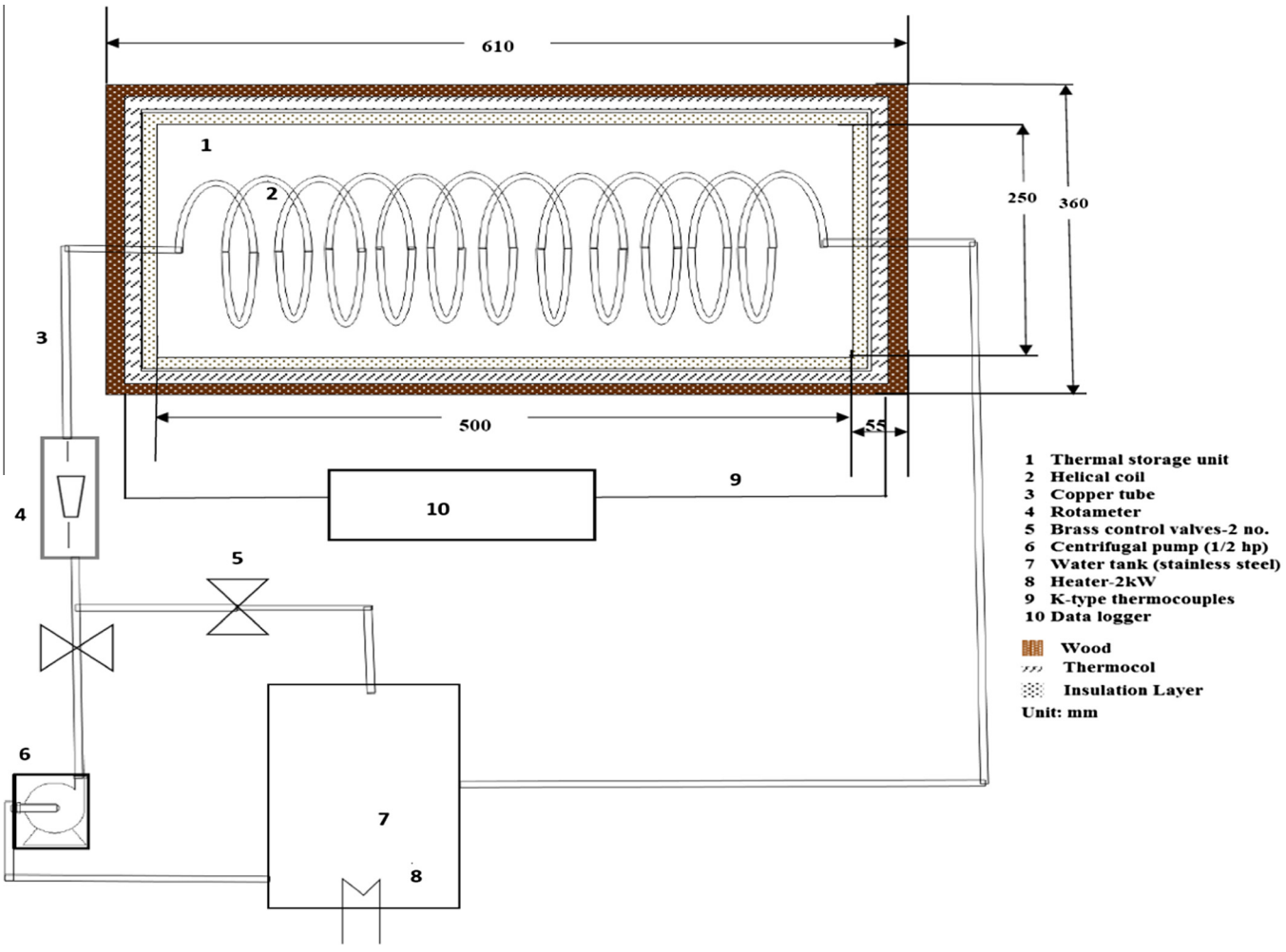

Fig. 3. Schematic diagram of shell and tube type thermal storage unit.

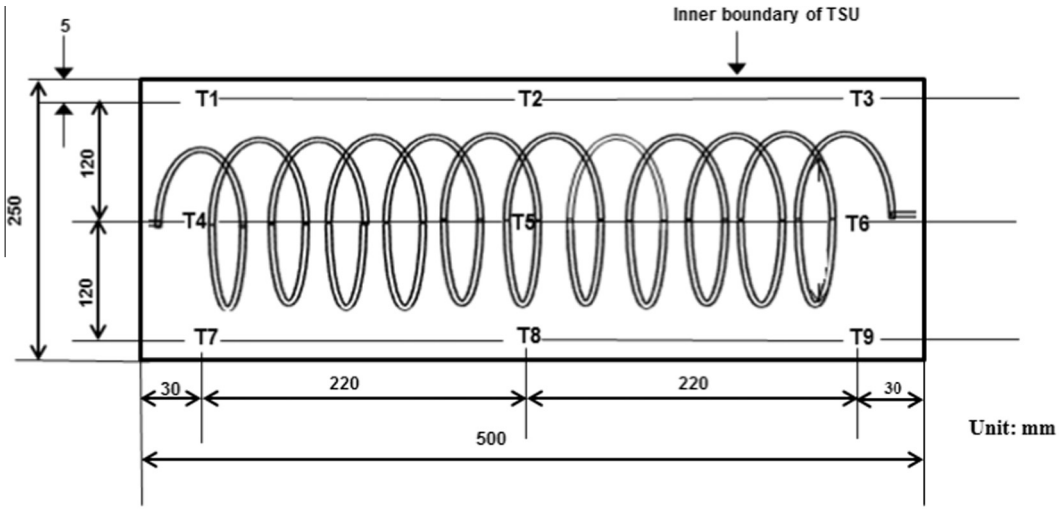

Fig. 4. Position of nine thermocouples inside PCM.

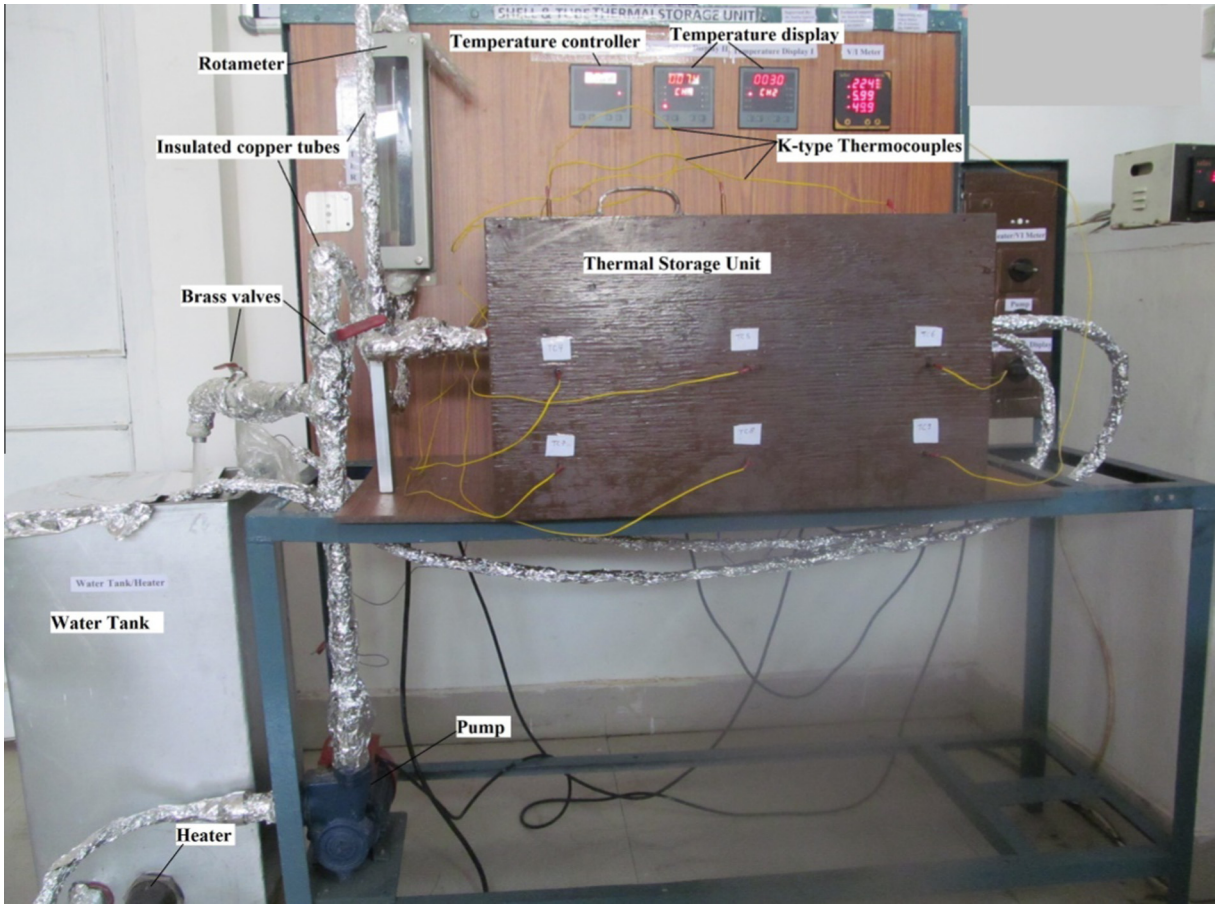

Fig. 5. Experimental setup for thermal storage study.

(d) Dean number, $D_e = R_e\left(\frac{d_i}{2R_c}\right)^{0.5}$

2.3. Experimental procedure

Thermal performance of beeswax as PCM is studied by obtaining melting and solidification profile of beeswax during the experimental study. In the beginning of experiment PCM storage container i.e. rectangular shell is filled with 18 kg of molten beeswax for homogenous distribution within the unit and to avoid trapping of any air pockets in PCM matrix. Plain tap water is used as HTF (for passing through the helical tube) and heated electrically in water tank, maintained at constant temperature by digital temperature controller. The HTF is circulated by centrifugal pump in the closed loop. Effect of three different inlet temperatures of HTF (60 °C, 70 °C, 80 °C) and four fluid flow rates (0.25 LPM, 0.5

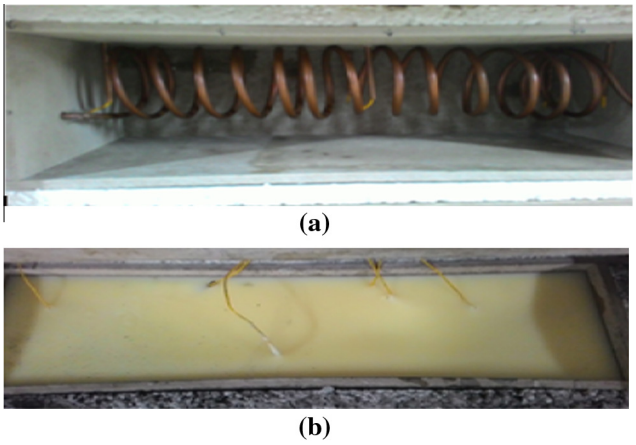

Fig. 6. Inside view of TSU (a) without beeswax and (b) with beeswax.

LPM, 0.75 LPM, 1 LPM) are considered for studying charging profile of beeswax. Charging of PCM was initiated by passing hot fluid through the coil embedded in the beeswax until all the nine thermocouples reached to constant maximum temperature and just after the completion of charging process TSU is discharged by passing cold water at 20 °C through the unit.

2.4. Efficiency of thermal storage unit

Energy stored in the thermal storage unit is calculated as the cumulative of instantaneous heat transfer from HTF to PCM [65] considering no heat losses from TSU. Inlet and outlet temperatures of HTF were recorded by data logger at an interval of every 15 min.

Table 1
Selected experimental parameters for the experimental study.

Charging/discharging experiment	Flow rates (LPM)	Inlet temperature of HTF (°C)
Repeatable charging experiment	0.5 ± 0.01	80 ± 0.2
Charging experiment	0.5	60 ± 0.2
Charging experiment	0.5	70 ± 0.2
Charging experiment	Variable: 0.25, 0.5, 0.75 and 1.0	80 ± 0.2
Discharging experiment	0.5	20 ± 0.2

$\dot{Q}$ is the instantaneous energy available for storage in the PCM from HTF is expressed as:

$$\dot{Q} = \dot{m}C_P(T_{in} - T_{out}) \quad (1)$$

Therefore, total energy available (Q_a) for charging is the cumulative of instantaneous energy is defined as:

$$Q_a = \dot{m}\{C_p\Sigma(T_{in} - T_{out})\}.\Delta t \quad (2)$$

Total energy stored (Q_w) by PCM during the charging process is:

$$Q_w = m_w\left[C_{ps}(T_m - T_i) + L + C_{pl}(T_f - T_m)\right] \quad (3)$$

Thermal storage efficiency of beeswax is,

$$\eta = \frac{Q_w}{Q_a} \quad (4)$$

2.5. Heat transfer coefficient

Overall heat transfer coefficient between the coil and beeswax is calculated as:

$$U_o = \frac{Q_a}{A_s\Delta T_{mean}} \quad (5)$$

ΔT_{mean} = Log mean temperature difference = $\frac{(T_{in}-T_b)-(T_{out}-T_b)}{\ln\frac{(T_{in}-T_b)}{(T_{out}-T_b)}}$

Overall heat transfer coefficient in terms of internal and external heat transfer coefficient is represented as:

$$\frac{1}{U_o} = \frac{A_o}{A_i h_i} + \frac{A_o \ln\frac{d_o}{d_i}}{2\pi kL} + \frac{1}{h_o} \quad (6)$$

Nussle number correlation for calculation of heat transfer between HTF and copper helical tube is expressed as [75]:

$$Nu_i = 0.152 D_e^{0.431} P_r^{1.06} \gamma^{-0.277} \quad (7)$$

This correlation is applicable for tube side heat transfer for constant temperature boundary conditions i.e. constant HTF inlet temperature and low dean number (D_e < 3000).

For the determination of external heat transfer coefficient (h_o) between copper tube and beeswax following correlation is used:

$$Nu_o = 0.381(Ra)^{0.293} \quad (8)$$

where $Ra = Gr.Pr$.

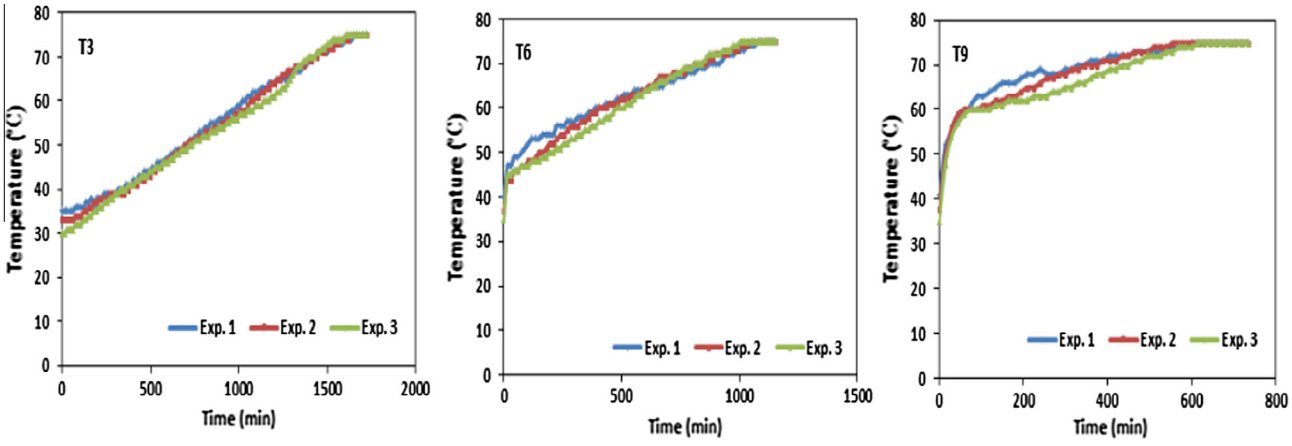

Fig. 7. Temperature variation measured at three different positions of thermocouples.

3. Results and discussion

3.1. Repeatability

In the beginning of experimental study in order to ensure repeatability of data each experiment was performed three times at fixed selected parameters as shown in Table 1. The temperature variation of PCM with time at three different positions of thermocouples (T3, T6, and T9) along the vertical line in middle of TSU were obtained and analyzed.

Similar results were obtained during initial three experiments (Exp. 1, Exp. 2 and Exp. 3) for given set of parameters (0.5 LPM flow rate and 80 °C initial fluid temperatures) as shown in Fig. 7, which confirmed the repeatability of the data. Then experiments were conducted for different sets of parameters to get the data at different positions of thermocouples within PCM for studying the melting and solidification profiles.

3.2. Effect of flow rate

The effect of four different flow rates i.e. 0.25 LPM, 0.50 LPM, 0.75 LPM and 1 LPM on charging time of beeswax at constant inlet temperature of HTF at 80 °C is studied and temperature of nine thermocouples (T1-T9) is recorded with time as shown in Fig. 8. Charging time of a phase change material is defined as the time at which temperature of all the thermocouples reached to a constant value, which decreased at increased flow rate. At flow rate of 0.25 LPM, 0.50 LPM, 0.75 LPM and 1 LPM charging time found to be 1810 min, 1650 min, 1640 and 1635 min respectively at position T3. The decrease in charging time with increase in flow rate may be due to more enthalpy carried by the HTF at higher flow rates. Increase in HTF flow rate showed almost similar pattern for beeswax charging at all the nine thermocouples (T1-T9) location due to symmetrical geometrical design of thermal storage system. A plot between flow rate and thermal storage efficiency is

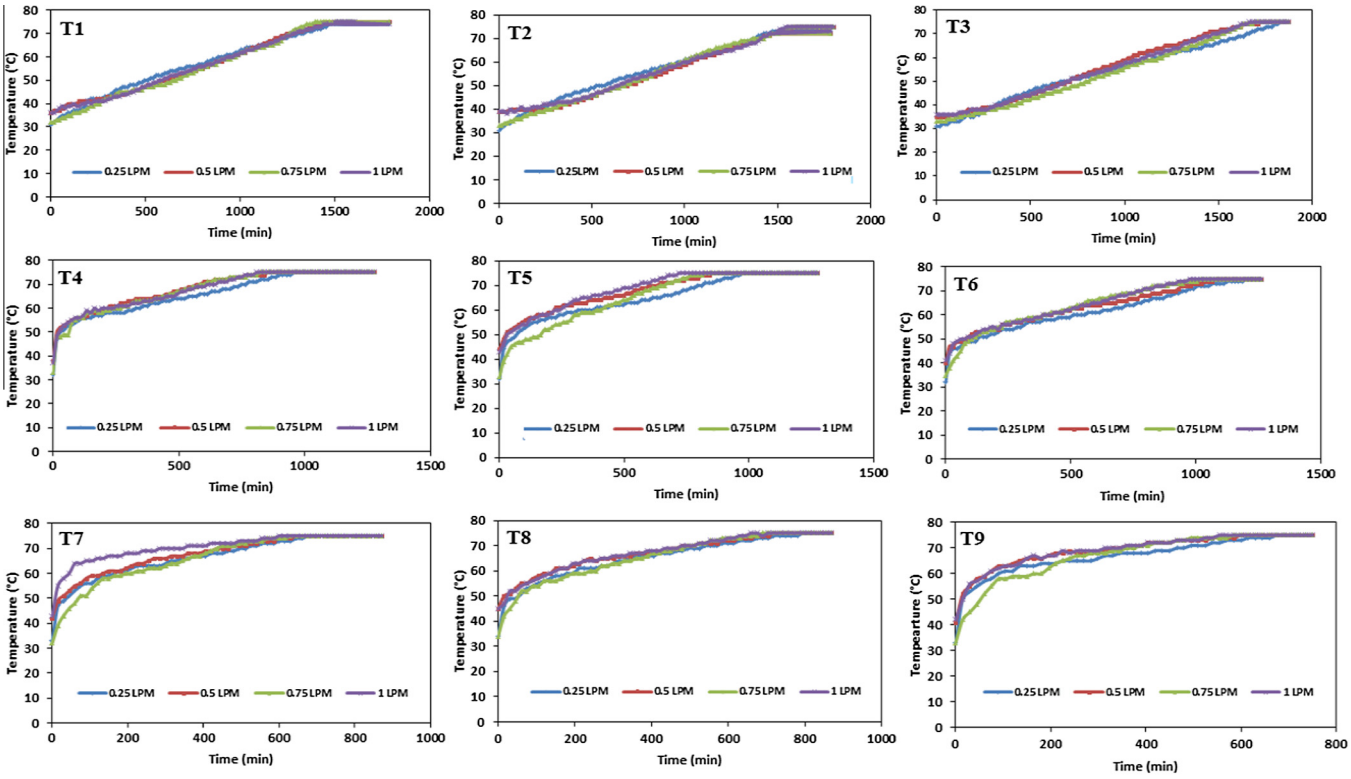

Fig. 8. Temperature variation in PCM at different flow rates.

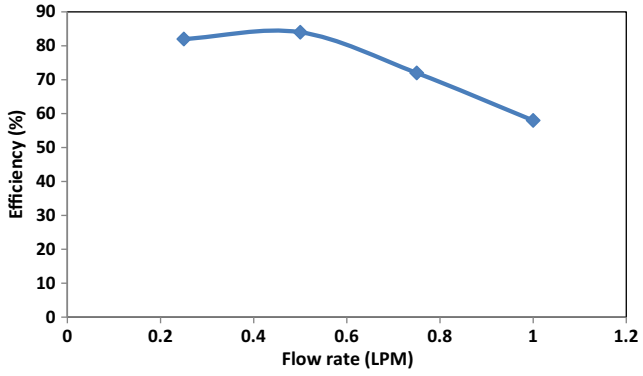

Fig. 9. Effect of flow rate of HTF on efficiency of TSU.

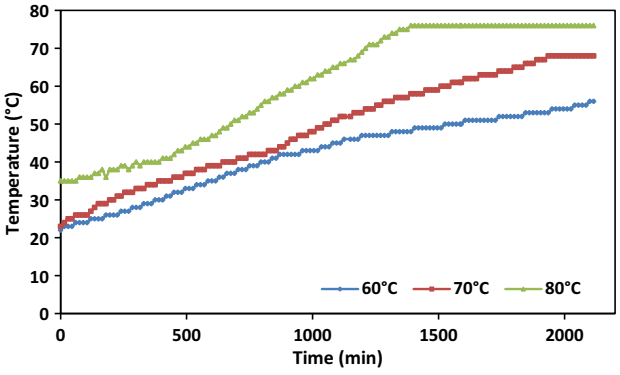

Fig. 10. Charging time at three inlet temperatures.

shown in Fig. 9 and 84% thermal storage efficiency is observed at 0.5 LPM, which decreases with increase in flow rate after 0.5 LPM flow rate. However, at lower flow rate of 0.25 LPM the efficiency of system observed was 82%, slightly less than 0.5 LPM may be due to difficulties in maintaining such a low flow rate due to large coil diameter. Therefore the flow rate below 0.5 LPM is not considered in further study. Thus at higher flow rates reduction in charging time and decrease in efficiency of TSU is observed due to more power needed to pump the heat transfer fluid.

3.3. Effect of inlet temperature

Fig. 10 shows the effect of inlet temperature of heat transfer fluid on charging time of beeswax at position T3. The choice of HTF inlet temperature was based on the availability of temperature from domestic solar water heater which is up to 80 °C and in the present study three temperatures (60 °C, 70 °C and 80 °C) were considered. Charging time of 2115 min, 1935 min and 1390 min was obtained at 60 °C, 70 °C and 80 °C respectively. Minimum charging time was observed at 80 °C due to large temperature difference between the HTF and PCM which enhanced the heat transfer.

3.4. Temperature profile during melting

Temperature profile of beeswax was studied during melting process at fluid flow rate of 0.5 LPM and at 80 °C inlet temperature of heat transfer fluid. This temperature variation of beeswax with time was studied at all nine positions of thermocouples placed along the axial and vertical direction as shown in Fig. 11. As hot HTF is passing through helical coil from left to right so melting process begins at the left end of TSU i.e. T1, T4, T7 as compared to right end, with smaller charging time on the left side beeswax. The melting pattern was found to be similar for thermocouple positions along the axis at the middle position of coil and below the coil as shown in Fig. 11(b) and (c) respectively.

It is also observed that time taken by beeswax to reach the melting point at bottom (T7) of the thermal storage unit was smallest as compared to the middle (T4) and top thermocouples (T1) and in the beginning heat transfer between HTF and beeswax is through conduction. Since, thermocouples at positon T1 and T7 are quite close to helical coil as compared to thermocouple at position T4, thus melting at T1 and T7 begins earlier as compared to position T4 through conductive heat transfer. The molten beeswax moves downward due to gravitational effect and transfers heat to the bottom part of the thermal storage unit which leads to faster rise in the temperature of the bottom beeswax. Then molten beeswax from bottom part starts moving up due to bouncy effect which causes additional heat transfer to beeswax at position T4 and T1 due to convection along with conduction through solid beeswax. The mode of heat transfer and melting pattern are similar for all three vertical planes. Thus there are two dimensional movements in the PCM in rectangular TSU i.e. from left to right and bottom to top.

3.5. Solidification pattern of beeswax

Once all the nine thermocouples reach to saturation temperature in the beeswax then solidification pattern is studied by observing temperature variation in the beeswax. For this solidification study i.e. discharging of thermal storage unit cold water is passed through helical coil from left to right in exactly same manner immediately after the charging process. During discharging process water coming out of the TSU is collected in a water tank and used again and again in a closed circuit for estimating amount of the heat collected during discharging. Fig. 12 shows the temperature profile of beeswax for horizontal and vertical planes using inlet water temperature of 20 °C at the flow rate of 0.5 LPM.

Solidification time is almost same horizontally for all the thermocouples. The solidification peak for beeswax in TSU was obtained at 58 °C and for beeswax sample it is 56.4 °C through DSC analysis. Similar to the charging process solidification starts first at the bottom part and moves upwards up to the top part of TSU, which shows that natural convection plays a little role during the discharging process of beeswax. During solidification process since water is initially available at 20 °C and maximum temperature difference is available between beeswax and water so in the beginning beeswax temperature drops suddenly and then at a slower rate due to temperature rise of the water being circulated through the helical coil in a close circuit.

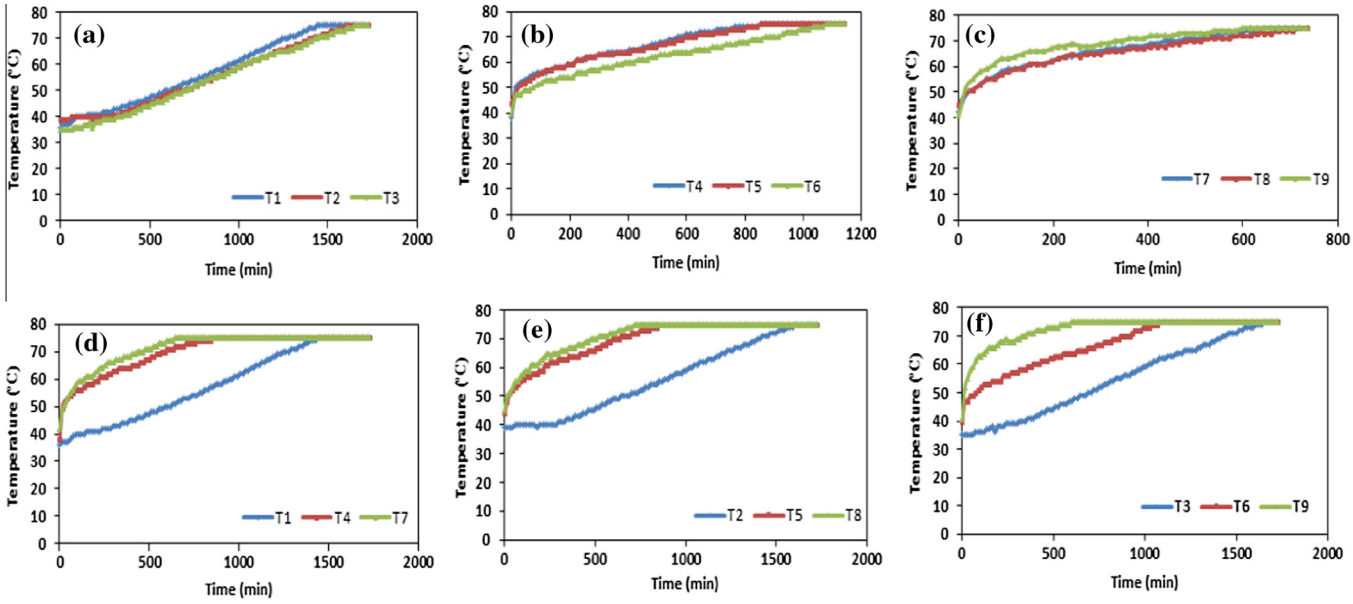

Fig. 11. Horizontal and vertical temperature profile in beeswax.

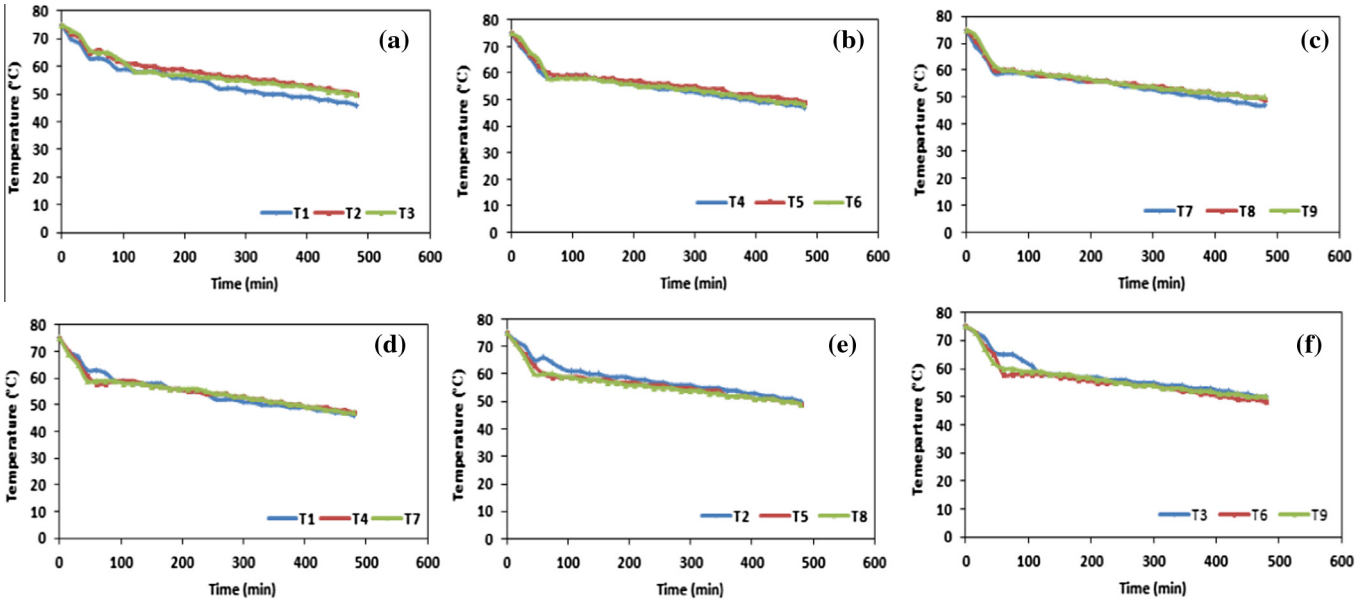

Fig. 12. Temperature profiles during discharging process.

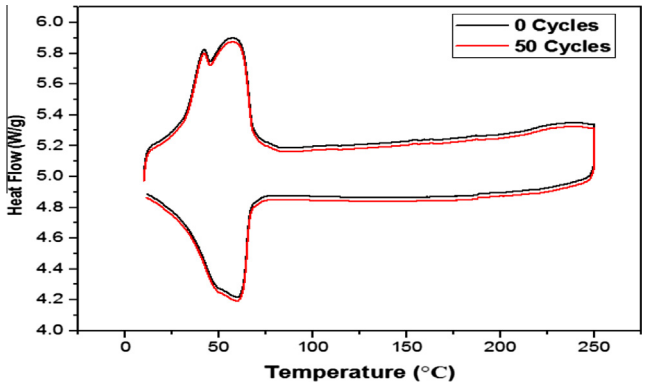

Fig. 13. DSC curves of beeswax before and after thermal cycles.

3.6. Energy storage efficiency of beeswax

Total energy stored (Q_w) by 18 kg of beeswax used in the thermal storage unit when beeswax is heated from 30 °C to 75 °C for inlet HTF temperature of 80 °C, at flow rate of 0.5 LPM is 6.382 MJ, when all the nine thermocouples reached to the saturation temperature of 75 °C. Total energy available (Q_a) for charging beeswax in TSU was found to be 8.127 MJ with energy efficiency of 84%. With flow rates of 0.25 LPM and 1 LPM at 80 °C storage efficiency was found to be 82% and 58% respectively. Since TSU was properly insulated with three layers of insulation so heat losses from the unit were negligible and not considered for efficiency calculation of TSU. From this it is observed that at flow rate of 0.5 LPM and 80 °C HTF inlet temperature systems reaches the maximum efficiency of energy storage. Thermal stability of beeswax was tested by DSC analysis after 50 thermal cycles. Fig. 13 showed the DSC result of beeswax before and after 50 cycles of charging and discharging. It was observed that after 50 thermal cycles melting point of beeswax was changed from 59.8 °C to 59.2 °C, while no variation was observed in solidification temperature. From this study beeswax as PCM in proposed TSU is found to be more efficient (84%) as compared to other PCMs like Paraffin wax, stearic acid, palmitic acid, and myristic acid having efficiency of 40.4%, 50.3, 53.3%, and 54% respectively in their heat storage units [76–78].

4. Conclusion

Natural beeswax obtained from honeybees is studied as a new phase change material for low temperature thermal storage in place of synthetic organic PCM in rectangular shell and tube type TSU. Thermal properties of beeswax are similar to paraffin and it is non-toxic, sustainable and cheaper as compared to other organic PCM's. Melting point and solidification point of beeswax found to be 59.6 °C respectively from DSC analysis which makes it suitable for low temperature application. TGA showed no weight loss of beeswax up to 215 °C, hence thermally stable up to this temperature. Four fluid flow rates and three inlet fluid temperatures were considered, which affect charging time of beeswax and efficiency of TSU. Charging time and efficiency were the minimum at the highest flow rate of 1 LPM, and maximum efficiency of TSU is obtained at 0.5 LPM. However, flow rate below 0.5 LPM is difficult to maintain in the system due to large coil diameter, therefore to ignore errors in result this flow rate has not been considered. Increase in inlet fluid temperature from 60 °C to 80 °C reduced charging time from 2115 min to 1390 min. At the flow rate of 0.5 LPM and inlet fluid temperature of 80 °C efficiency of TSU found to be 84%. Study shows can be efficiently used as a suitable natural phase change material for lower temperature thermal storage and can find wide applications such as solar air heater, solar water heater, and temperature controlled buildings.

Acknowledgement

This work was supported by MNIT Jaipur, India as part of the Ph. D. research and funded by the same.

References

[1] J.C. Zachos, G.R. Dickens, R.E. Zeebe, An early Cenozoic perspective on greenhouse warming and carbon-cycle dynamics, Nature 451 (2008) 279–283.
[2] R. Lal, Global potential of soil carbon sequestration to mitigate the greenhouse effect, Crit. Rev. Plant Sci. 22 (2003) 151–184.
[3] M. Carlowicz, World of Change: Global Temperatures: Feature Articles, 2010.

[4] R. Falkner, Business Power and Conflict in International Environmental Politics, Palgrave Macmillan, 2008.
[5] V. Papadimitriou, Prospective primary teachers' understanding of climate change, greenhouse effect, and ozone layer depletion, J. Sci. Educ. Technol. 13 (2004) 299–307.
[6] T. Khatib, A. Mohamed, K. Sopian, A review of photovoltaic systems size optimization techniques, Renew. Sustain. Energy Rev. 22 (2013) 454–465.
[7] A.S. Joshi, I. Dincer, B.V. Reddy, Performance analysis of photovoltaic systems: a review, Renew. Sustain. Energy Rev. 13 (2009) 1884–1897.
[8] T.T. Chow, A review on photovoltaic/thermal hybrid solar technology, Appl. Energy 87 (2010) 365–379.
[9] V. Velmurugan, K. Srithar, Prospects and scopes of solar pond: a detailed review, Renew. Sustain. Energy Rev. 12 (2008) 2253–2263.
[10] A.E. Kabeel, S.A. El-Agouz, Review of researches and developments on solar stills, Desalination 276 (2011) 1–12.
[11] N. Nallusamy, S. Sampath, R. Velraj, Experimental investigation on a combined sensible and latent heat storage system integrated with constant/varying (solar) heat sources, Renew. Energy 32 (2007) 1206–1227.
[12] A. Koca, H.F. Oztop, T. Koyun, Y. Varol, Energy and exergy analysis of a latent heat storage system with phase change material for a solar collector, Renew. Energy 33 (2008) 567–574.
[13] S.D. Sharma, K. Sagara, Latent heat storage materials and systems: a review, Int. J. Green Energy 2 (2005) 1–56.
[14] Z. Zhang, N. Zhang, J. Peng, X. Fang, X. Gao, Y. Fang, Preparation and thermal energy storage properties of paraffin/expanded graphite composite phase change material, Appl. Energy 91 (2012) 426–431.
[15] O. Behar, A. Khellaf, K. Mohammedi, A review of studies on central receiver solar thermal power plants, Renew. Sustain. Energy Rev. 23 (2013) 12–39.
[16] B. Sakintuna, F. Lamari-Darkrim, M. Hirscher, Metal hydride materials for solid hydrogen storage: a review, Int. J. Hydrogen Energy 32 (2007) 1121–1140.
[17] L.H. Rude, T.K. Nielsen, D.B. Ravnsbaek, U. Boesenberg, M.B. Ley, B. Richter, L.M. Arnbjerg, M. Dornheim, Y. Filinchuk, F. Besenbacher, Tailoring properties of borohydrides for hydrogen storage: a review, Phys. Status Solidi (a) 208 (2011) 1754–1773.
[18] F.L. Darkrim, P. Malbrunot, G.P. Tartaglia, Review of hydrogen storage by adsorption in carbon nanotubes, Int. J. Hydrogen Energy 27 (2002) 193–202.
[19] B. Zalba, J.M. Marín, L.F. Cabeza, H. Mehling, Review on thermal energy storage with phase change: materials, heat transfer analysis and applications, Appl. Therm. Eng. 23 (2003) 251–283.
[20] A. Shukla, D. Buddhi, R.L. Sawhney, Solar water heaters with phase change material thermal energy storage medium: a review, Renew. Sustain. Energy Rev. 13 (2009) 2119–2125.
[21] T. Kousksou, P. Bruel, G. Cherreau, V. Leoussoff, T. El Rhafiki, PCM storage for solar DHW: from an unfulfilled promise to a real benefit, Sol. Energy 85 (2011) 2033–2040.
[22] A. Castell, I. Martorell, M. Medrano, G. Perez, L.F. Cabeza, Experimental study of using PCM in brick constructive solutions for passive cooling, Energy Build. 42 (2010) 534–540.
[23] S. Kuravi, J. Trahan, D.Y. Goswami, M.M. Rahman, E.K. Stefanakos, Thermal energy storage technologies and systems for concentrating solar power plants, Prog. Energy Combust. Sci. 39 (2013) 285–319.
[24] K. Nithyanandam, R. Pitchumani, A. Mathur, Analysis of a latent thermocline storage system with encapsulated phase change materials for concentrating solar power, Appl. Energy 113 (2014) 1446–1460.
[25] A.M. Khudhair, M.M. Farid, A review on energy conservation in building applications with thermal storage by latent heat using phase change materials, Energy Convers. Manage. 45 (2004) 263–275.
[26] A. Dinker, M. Agarwal, G.D. Agarwal, Heat storage materials, geometry and applications: a review, J. Energy Inst. (2015).
[27] T. Bauer, L. Dorte, K. Ulrike, T. Rainer, Sodium nitrate for high temperature latent heat storage, 2009.
[28] Z. Ge, F. Ye, H. Cao, G. Leng, Y. Qin, Y. Ding, Carbonate-salt-based composite materials for medium-and high-temperature thermal energy storage, Particuology 15 (2013) 77–81.
[29] L. Ye, C. Tang, Y. Chen, S. Yang, M. Tang, The thermal physical properties and stability of the eutectic composition in a Na_2CO_3–NaCl binary system, Thermochim. Acta 596 (2014) 14–20.
[30] M.J. Huang, P.C. Eames, S. McCormack, P. Griffiths, N.J. Hewitt, Microencapsulated phase change slurries for thermal energy storage in a residential solar energy system, Renew. Energy 36 (2011) 2932–2939.
[31] K. Nagano, K. Ogawa, T. Mochida, K. Hayashi, H. Ogoshi, Performance of heat charge/discharge of magnesium nitrate hexahydrate and magnesium chloride hexahydrate mixture to a single vertical tube for a latent heat storage system, Appl. Therm. Eng. 24 (2004) 209–220.
[32] V. Piemonte, M. De Falco, P. Tarquini, A. Giaconia, Life cycle assessment of a high temperature molten salt concentrated solar power plant, Comput. Aided Chem. Eng. 28 (2011) 1063–1068.
[33] D. Barlev, R. Vidu, P. Stroeve, Innovation in concentrated solar power, Sol. Energy Mater. Sol. Cells 95 (2011) 2703–2725.
[34] S. Guillot, A. Faik, A. Rakhmatullin, J. Lambert, E. Veron, P. Echegut, C. Bessada, N. Calvet, X. Py, Corrosion effects between molten salts and thermal storage material for concentrated solar power plants, Appl. Energy 94 (2012) 174–181.
[35] C.K. Ho, B.D. Iverson, Review of high-temperature central receiver designs for concentrating solar power, Renew. Sustain. Energy Rev. 29 (2014) 835–846.
[36] T. Kousksou, A. Jamil, T. El Rhafiki, Y. Zeraouli, Paraffin wax mixtures as phase change materials, Sol. Energy Mater. Sol. Cells 94 (2010) 2158–2165.
[37] X. Xiao, P. Zhang, M. Li, Preparation and thermal characterization of paraffin/metal foam composite phase change material, Appl. Energy 112 (2013) 1357–1366.
[38] Z. Sun, Y. Zhang, S. Zheng, Y. Park, R.L. Frost, Preparation and thermal energy storage properties of paraffin/calcined diatomite composites as form-stable phase change materials, Thermochim. Acta 558 (2013) 16–21.
[39] C. Alkan, A. Sari, Fatty acid/poly (methyl methacrylate)(PMMA) blends as form-stable phase change materials for latent heat thermal energy storage, Sol. Energy 82 (2008) 118–124.
[40] L. Wang, D. Meng, Fatty acid eutectic/polymethyl methacrylate composite as form-stable phase change material for thermal energy storage, Appl. Energy 87 (2010) 2660–2665.
[41] L. Shilei, Z. Neng, F. Guohui, Eutectic mixtures of capric acid and lauric acid applied in building wallboards for heat energy storage, Energy Build. 38 (2006) 708–711.
[42] F. Agyenim, N. Hewitt, P. Eames, M. Smyth, A review of materials, heat transfer and phase change problem formulation for latent heat thermal energy storage systems (LHTESS), Renew. Sustain. Energy Rev. 14 (2010) 615–628.
[43] J.S. Buchanan, The chemistry of olefins production by ZSM-5 addition to catalytic cracking units, Catal. Today 55 (2000) 207–212.
[44] M.A. Jackson, F.J. Eller, Isolation of long-chain aliphatic alcohols from beeswax using lipase-catalyzed methanolysis in supercritical carbon dioxide, J. Supercrit. Fluids 37 (2006) 173–177.
[45] N.S. Al-Waili, Topical application of natural honey, beeswax and olive oil mixture for atopic dermatitis or psoriasis: partially controlled, single-blinded study, Complement. Ther. Med. 11 (2003) 226–234.
[46] C. Ghidelli, E. Sanchis, C.R. Argudo, M. Mateos, M.A. del Rio, M.B. Perez-Gago, Application of soy protein-beeswax edible coating with antioxidants: effect reducing enzymatic browning of fresh-cut eggplants, VI International Postharvest Symposium, vol. 877, 2009, pp. 591–596.
[47] E. Velickova, E. Winkelhausen, S. Kuzmanova, V.D. Alves, M. MoldÃ£o-Martins, Impact of chitosan-beeswax edible coatings on the quality of fresh strawberries (Fragaria ananassa cv Camarosa) under commercial storage conditions, LWT-Food, Sci. Technol. 52 (2013) 80–92.
[48] F.r. Yilmaz, E. Dagdemir, The effects of beeswax coating on quality of Kashar cheese during ripening, Int. J. Food Sci. Technol. 47 (2012) 2582–2589.
[49] A. Martinez-Abad, J.M. Lagaron, M.J. Ocio, Antimicrobial beeswax coated polylactide films with silver control release capacity, Int. J. Food Microbiol. 174 (2014) 39–46.
[50] A.A. Attama, B.C. Schicke, C.C. Muller-Goymann, Further characterization of theobroma oil-beeswax admixtures as lipid matrices for improved drug delivery systems, Eur. J. Pharm. Biopharm. 64 (2006) 294–306.
[51] S. Kheradmandnia, E. Vasheghani-Farahani, M. Nosrati, F. Atyabi, Preparation and characterization of ketoprofen-loaded solid lipid nanoparticles made from beeswax and carnauba wax, Nanomed.: Nanotechnol., Biol. Med. 6 (2010) 753–759.
[52] S. Sinaringati, N. Putra, M. Amin, F. Afriyanti, The Utilization of Paraffin and Beeswax as Heat Energy Storage in Infant Incubator, 2006.
[53] N. Putra, E. Prawiro, M. Amin, Thermal properties of Beeswax/CuO nano-phase-change material used for thermal energy storage, Int. J. Technol. 7 (2016) 244–253.
[54] R. Buchwald, M.D. Breed, A.R. Greenberg, The thermal properties of beeswaxes: unexpected findings, J. Exp. Biol. 211 (2008) 121–127.
[55] A. Sharma, V.V. Tyagi, C.R. Chen, D. Buddhi, Review on thermal energy storage with phase change materials and applications, Renew. Sustain. Energy Rev. 13 (2009) 318–345.
[56] M.E. Hossain, M.I. Khan, C. Ketata, M.R. Islam, Comparative pathway analysis of paraffin wax and beeswax for industrial applications, Int. J. Charact. Dev. Novel Mater. 1 (2010) 1–13.
[57] H.A. Adine, H. El Qarnia, Numerical analysis of the thermal behaviour of a shell-and-tube heat storage unit using phase change materials, Appl. Math. Model. 33 (2009) 2132–2144.
[58] R.E. Murray, D. Groulx, Experimental study of the phase change and energy characteristics inside a cylindrical latent heat energy storage system: Part 1 consecutive charging and discharging, Renew. Energy 62 (2013) 571–581.
[59] S.P. Jesumathy, M. Udayakumar, S. Suresh, S. Jegadheeswaran, An experimental study on heat transfer characteristics of paraffin wax in horizontal double pipe heat latent heat storage unit, J. Taiwan Inst. Chem. Eng. 45 (2014) 1298–1306.
[60] M. Avci, M.Y. Yazici, Experimental study of thermal energy storage characteristics of a paraffin in a horizontal tube-in-shell storage unit, Energy Convers. Manage. 73 (2013) 271–277.
[61] M.J. Hosseini, M. Rahimi, R. Bahrampoury, Experimental and computational evolution of a shell and tube heat exchanger as a PCM thermal storage system, Int. Commun. Heat Mass Transf. 50 (2014) 128–136.
[62] M. Bechiri, K. Mansouri, Analytical solution of heat transfer in a shell-and-tube latent thermal energy storage system, Renew. Energy 74 (2015) 825–838.
[63] C. Liu, D. Groulx, Experimental study of the phase change heat transfer inside a horizontal cylindrical latent heat energy storage system, Int. J. Therm. Sci. 82 (2014) 100–110.
[64] Y. Li, H. Qiao, H. Dong, J. Hu, Heat transfer performance of phase change heat storage with helical coil structure, in: Power and Energy Engineering Conference, IEEE, Asia-Pacific, 2009, pp. 1–4, APPEEC 2009.
[65] M. Kabbara, D. Groulx, A. Joseph, Experimental study of a latent heat storage unit with a helical coil heat exchanger, in: CSME International Congress 2014, Toronto, Canada, 2014.

[66] B. Zivkovic, I. Fujii, An analysis of isothermal phase change of phase change material within rectangular and cylindrical containers, Sol. Energy 70 (2001) 51–61.
[67] M.J. Hosseini, A.A. Ranjbar, K. Sedighi, M. Rahimi, A combined experimental and computational study on the melting behavior of a medium temperature phase change storage material inside shell and tube heat exchanger, Int. Commun. Heat Mass Transfer 39 (2012) 1416–1424.
[68] D.G. Prabhanjan, T.J. Rennie, G.S.V. Raghavan, Natural convection heat transfer from helical coiled tubes, Int. J. Therm. Sci. 43 (2004) 359–365.
[69] T.H. Ko, K. Ting, Entropy generation and thermodynamic optimization of fully developed laminar convection in a helical coil, Int. Commun. Heat Mass Transf. 32 (2005) 214–223.
[70] S. Ali, Pressure drop correlations for flow through regular helical coil tubes, Fluid Dyn. Res. 28 (2001) 295–310.
[71] M.A. Akhavan-Behabadi, M.F. Pakdaman, M. Ghazvini, Experimental investigation on the convective heat transfer of nanofluid flow inside vertical helically coiled tubes under uniform wall temperature condition, Int. Commun. Heat Mass Transf. 39 (2012) 556–564.
[72] A. Dinker, M. Agarwal, G.D. Agarwal, Preparation, characterization and performance study of beeswax/expanded graphite composite as thermal storage material, Exp. Heat Transf. (2016).
[73] S.V. Glass, S.L. Zelinka, Moisture relations and physical properties of wood (2010).
[74] N.S. Thakur, J.S. Saini, S.C. Solanki, Heat transfer and friction factor correlations for packed bed solar air heater for a low porosity system, Sol. Energy 74 (2003) 319–329.
[75] M.R. Salimpour, Heat transfer coefficients of shell and coiled tube heat exchangers, Exp. Therm. Fluid Sci. 33 (2009) 203–207.
[76] H.H. Ozturk, Experimental evaluation of energy and exergy efficiency of a seasonal latent heat storage system for greenhouse heating, Energy Convers. Manage. 46 (2005) 1523–1542.
[77] A.S.K. Kaygusuz, Thermal energy storage system using some fatty acids as latent heat energy storage materials, Energy Sourc. 23 (2001) 275–285.
[78] A. Sari, K. Kaygusuz, Thermal performance of myristic acid as a phase change material for energy storage application, Renew. Energy 24 (2001) 303–317.